

Nucleic Acid Measurements for Antibiotic
Susceptibility Testing and Early Detection of
SARS-CoV-2

Thesis by
Emily Sue Savela

In Partial Fulfillment of the Requirements for
the Degree of
Doctor of Philosophy

The Caltech logo, featuring the word "Caltech" in a bold, orange, sans-serif font, centered within a light yellow rectangular background.

CALIFORNIA INSTITUTE OF TECHNOLOGY
Pasadena, California

2022
(Defended October 22, 2021)

© 2022

Emily Sue Savelle
ORCID: 0000-0001-9614-4276

ACKNOWLEDGEMENTS

I would first like to thank my thesis committee Dr. Niles Pierce, Dr. Dianne K. Newman, Dr. Jared R. Leadbetter, and Dr. Rustem F. Ismagilov. Thank you all for challenging me to grow professionally and intellectually throughout the years and to find a balance of building collaborations with my colleagues and taking ownership over my own accomplishments. Dr. Niles Pierce, thank you for setting a high standard of research excellence and for your help and suggestions in my thesis work. Dr. Dianne K Newman, I appreciate your attention to detail, your perspective and insightful questions, and for your encouragement for scientific and professional development. Dr. Jared R. Leadbetter, I have always appreciated your advice to step back from the lab work and gain perspective of the big picture. Thank you for your insight into the challenges of working with microorganisms from clinical samples as they compare to environmental samples.

I want to give a special thanks to my advisor, Rustem. Thank you for your mentorship over the years. In your group I have had the chance to grow as a researcher and have learned how to design robust, reproducible, and question-driven experiments. I have been challenged to solve not only scientific, but logistical problems and am grateful for the opportunities to work on such exciting projects throughout my years in this lab. Thank you for challenging me to work outside of my comfort zone.

To my colleagues and close collaborators of the *N. gonorrhoeae* AST team, Dr. Nathan G. Schoepp, Matthew Cooper, Dr. Justin C. Rolando, Dr. Olusegun Soge (S.O.), and Dr. Jeffrey D. Klausner.

Nathan, I'd like to thank you for your mentorship and guidance for me as a junior graduate student when I had joined the AST project. You taught me so much about experimental design, and careful and skeptical data analysis, and your mentorship, helped me find my voice as a scientist.

Matt, you have been such an incredible colleague over the years. I have appreciated how your approaches to scientific problem solving are different than mine. Conversations with

you helped improve my experimental designs, often by you helping simplify the number of variables I wanted to test. I am so proud to see the progress you have made as a graduate student and cannot wait to see all you accomplish in your career. I'd also like to thank you for being such a hard worker, for being so in sync with me while we were running parallel experiments that I have handed you a piece of paper and a pipette, and you executed the experiment I had written up with mere minutes of notice. I'd like to give you a special shout out specifically for wearing so much glitter when I wanted to enter a Halloween costume contest in 2019. It was worth it, if you remember, as they had to make a special category to congratulate us on the creativity of that costume; I am pretty sure there is still glitter on both of our desks in the office 2 years later.

Justin, thank you for helping us execute the high-level analysis with digital LAMP on a quick turnaround, which added so much to the gonorrhea paper. I am so glad we had the chance to collaborate on this aspect of the project and for your encouragement through the years. S.O., after all of your help with the early stages of planning, I am so grateful to have met you in person during the ISSTDR/IUSTI 2019 conference. Thank you and your laboratory for processing each *N. gonorrhoeae* culture from the isolated clinical sample colonies. Lastly, thank you Dr. Klausner, for sharing your expertise in *N. gonorrhoeae* testing and for coordinating and providing oversight of the clinical sample collection at the AIDS Healthcare Foundation (AHF).

To my colleagues and close collaborators of the COVID-19 community study team, I am so proud to have worked on a team with everyone on the COVID-19 study. With the added challenges of working remotely and under strict COVID-19 guidelines while in the laboratory, I am so grateful to have worked with such a supportive team.

Study administrator Natasha Shelby, and study coordinators Jessica Reyes, Noah Schlenker, and Hannah Davich, I am in awe of the dedication and hard work that you did during such a stressful and unpredictable time in the pandemic. Thank you for taking the extra step with each of our study participants to make sure they had the empathy, help, and care from your

team. I was always so happy to hear about the participants who were encouraged to contribute to scientific research.

The dedication of my colleagues on the lab team Alex Winnett, Anna Romano, Michael Porter, Alyssa Carter, and Matt Cooper was a huge reason why this project was able to succeed. With the amount of lab work, it wouldn't have been possible without the division of labor. Alex and Anna, I would like to thank you for your help in making the swab and saliva comparison paper happen on such a short amount of time.

The data processing team, Reid Akana, Jenny Ji, and Jacob Barlow is thanked for their work in establishing each phase of the database, corrections, and data entry, Reid and Jacob especially, for helping the team think through all of the possible metadata and associations we would want to record before any samples arrived in the lab. Jenny, thank you for your dedication and quick turnaround on entering and processing the symptom data. The data visualization benefitted so much from your eyes and time. I'm so impressed that you were able to work so hard on these figure panels and your other contributions to this study while being a full time student.

Collaborations with the AIDS Healthcare Foundation (AHF) and the Pasadena Public Health Department. To the incredible staff at AHF, including Adam Sukhija-Cohen, Sherrelle Banks, Matt Santos, and Yancy Granados for their technical assistance with the clinical study and patient enrollment, and for graciously allowing us to setup a satellite lab in your BSL-2 lab so we could process the samples quickly. Sherrelle, thank you for going above and beyond with your efforts and thoroughness in patient enrollment, and for your enthusiastic support for the work we were doing. To Dr. Ying-Ying Goh, Dr. Matthew Feaster, and Colten Tognazzini, and everyone else at the Pasadena Public Health Department, thank you for your hard work and dedication to your work during the pandemic. Thank you for going above and beyond in your role during the pandemic response and for aiding in the study design and participant enrollment for our lab's household transmission study.

Professional mentors throughout my career, Dr. Natasha Shelby, Dr. Lauriane Quenee, Dr. Kurt Halverson, and Dr. Jason Bjork.

Tasha, you have inspired me and helped me throughout my graduate school career in the Ismagilov lab. You are the glue that holds our group together and have such a gift with words and science that you have elevated the telling of each scientific story that I have worked on in this lab. You are one of the hardest workers I know, and I only hope to emulate your dedication, positivity, and enthusiasm for science as I move on to my next career steps. Thank you for being such a great collaborator and professional mentor to me over the years.

Lauriane, you have been such an incredible role model, both scientifically and professionally. I have learned so much from you about not only biosafety, risk assessments, and how to write SOPs, but how to be a better communicator and to think critically about experimental design and controls. Thank you for the last-minute calls and safety questions I have brought your way as our research projects continued to escalate in risks throughout my time in the Ismagilov lab. In particular, thank you for your incredible intuition for having us invest in several MAXAIR CAPR respirators when we were starting up the COVID project. This saved us so much headache, literal and figurative, as the projects scaled and we had extensive hours of work spent in those respirators.

I am so grateful for the professional mentorship and encouragement from Kurt and Jason at the 3M Corporate Research Materials Laboratory (CRML) Biomaterials Laboratory during my undergraduate research internships. You both played a huge role in helping me find my research voice and to realize how much creativity and exploration there is in the world of research. As someone who has many artistic and creative outlets, it was an incredible experience to see how much overlap there is with the scientific method. The lab culture you have is something so special and was a huge motivator for me to apply to graduate school. Thank you for your encouragement and support, specifically, to aim my sights high, to not be intimidated by big name universities, and for writing me letters of recommendation for my graduate school applications.

Each rotation student and mentee I have had the chance to work with and mentor through their lab rotations. Thank you for your contributions to the spinoff ideas and projects we were pursuing at the time. Alex Winnett, thank you for helping drive some of the accessibility questions forward during your time as a rotation student on the beta lactam ASTs in the group. Bryan Gerber, thank you for your enthusiasm and help with testing the potential of mechanical and enzymatic enhancers. Kevin Winzey, thank you for your time in this lab as a technician, for being such a sponge for learning new information and for your help processing all of the DNA and RNA isolated from the *N. gonorrhoeae* clinical samples. Zack Fouladian, thank you for the help on researching RNA isolation protocols in development for the quantification of RNA from the clinical urine samples. Heyun Li, thank you for taking the first steps in the goals for quantifying bacterial small RNAs. Yutian Li, I greatly appreciate your dedication and hard work during your time as a rotation student during the first few months of the pandemic in 2020 and help studying the potential for small RNA sequencing and helping me find excitement for the project while we were waiting to get back into the lab. Your patience and weekly check-ins together helped me stay grounded and find purpose in our work even when we didn't even know when we would be allowed back into the lab to test any of these ideas. Matt Cooper, I've already spent some words above thanking you, especially for your dedication and helping make the AHF study happen. I am so glad you ended up joining the group for your PhD and I'm so proud of how far you have come as a scientist, a researcher, and a leader in the group.

The entire Ismagilov lab, past, present, and future members. Past and present members for setting up the foundations of the lab which made thesis projects like mine possible. In particular, to Jacob Barlow, Matt Cooper, Mary Arrastia, Asher Preska Steinberg, and Anna Romano, thank you for each of the lunchtime conversations, for being sounding boards for early experimental design and data analysis, and for the encouragement when experiments did not go as planned. I feel so lucky to have worked with such amazing researchers in my time here.

My family. I do not have sufficient words to describe the overwhelming love and support I've had from my family my entire life. I'd like to give the biggest "Thank You" to my parents Amy and Gordy Savela for always prioritizing education and encouraging all of my creative projects since I was a little kid. I would not be where I am today without the way education and creative pursuits were encouraged in our household growing up. You have both inspired me so much in life and my career and am grateful for your unwavering support and interest in my studies. Thank you for guiding me through the processes of applying to colleges and for the encouragement to pursue an advanced degree. To my siblings, Angie and Stewart, thank you for your endless patience in listening to me ramble about the experiments and cool science that I have gotten to learn. I have learned that I don't have much of a filter when I get excited to talk about my work and I am aware of how exhausting it must have been to be on the other sides of these conversations. You have both been such amazing friends throughout the years and I appreciate how you've both been sounding boards for when things have not gone according to plan.

Friends and support system

To Anita, I am so lucky to have found you. Finding time to connect and find joy in the little things in life with you has made all the difference in navigating the challenges of the pandemic, pandemic research, and finding a balance in all things. Thank you for your unwavering support and encouragement through some of the most challenging parts of my PhD. Thank you for making me smile and laugh every single day and for helping me become a better communicator in all aspects of life.

The COVID-19 pandemic added so many challenges to life and work (before and after we were running the community study). Thank you to Sarah Simon for being my quarantine bubble roommate. I don't know how I would have been able to keep track of time without our Friday dinners throughout 2020 and early 2021. As someone who was living alone, the in-person interactions were the tiniest bit of normalcy we got and were so vital to maintaining my mental health during the pandemic (especially during the pre-vaccination months).

Many thanks to the yarn shop Wollhaus, specifically Ulli, Kathi, and Betty, for making sure I would never run out of knitting projects. Special shout outs to Becky Tyler-Rickon, Lauren Tyler, Liza Bernstein, Ben Beky, Jen Maynulet, and Kirsten Hansen, for always encouraging me to stop by the weekly zoom calls no matter how busy my research was. You have helped me find work-life balance, helped me to gain perspective for things that are going on outside of graduate school, given me so many incredible book recommendations, and for always supporting my creative and academic takings-on. I appreciate how much closer we have had the chance to become during the months of the pandemic.

To the unsung heroes that made this work possible behind the scenes, thank you. To each of the couriers from Apollo Couriers, Inc. who drove participant samples to the laboratory at all days of the week and hours of the evenings from the greater LA area, especially during rush hours. Thank you for your patience with navigating Caltech's campus to find us and deliver these samples. I would also like to give a shout out to all of the contact tracers who work in the public health space of STI transmission and pandemic responses. You have played such an important role helping people get access to diagnostic testing, treatments, and reducing the spread of infectious diseases. Finally, I would like to thank each of our hundreds of study participants who donated their time and samples during a stressful time in your lives (at the AHF free clinic or while quarantining at home with your family and housemates during the early months of the pandemic). Thank you for the time you spent contributing to these scientific studies and making our work possible.

ABSTRACT

Nucleic-acid-amplification tests (NAATs) are widely used in microbial detection both in environmental characterization and human diagnostics. NAATs offer highly sensitive and specific detection of target molecules among the noise of complex samples. This thesis covers two important applications of nucleic-acid quantification techniques in human clinical samples. First, I co-developed a new phenotypic antibiotic susceptibility test that uses species-specific DNA detection to detect bacterial cell-wall damage following incubation with beta-lactam antibiotics. Second, I helped compile a longitudinal dataset of SARS-CoV-2 viral loads during a community-based COVID-19 study run by the Ismagilov Lab through October 2020 – April 2021 in the greater Los Angeles County area, USA. Sensitive and specific nucleic-acid tests allowed for robust detection of pathogenic microbes in both these applications. Designing and implementing NAATs for these applications required consideration of biological constraints of the microorganisms, molecular stability over the time of quantification, and the practical constraints of acquiring and transporting samples. Continued innovation of NAAT technologies will be critical to contain present and future pandemics and empower medical professionals with data to inform treatment options.

PUBLISHED CONTENT AND CONTRIBUTIONS

Chapter II: Emily S. Savela[†], Nathan G. Schoepp[†], Justin C. Rolando, Jeffrey D. Klausner, Olusegun O. Soge, and Rustem F. Ismagilov. 2020. “Surfactant-enhanced DNA accessibility to nuclease accelerates phenotypic β -lactam antibiotic susceptibility testing of *Neisseria gonorrhoeae*.” PLoS Biology. 18(3):e3000651. doi: 10.1371/journal.pbio.3000651

This chapter describes the design of a novel phenotypic antibiotic susceptibility test for *Neisseria gonorrhoeae* and the beta-lactam class of antibiotics and the results of a pilot test using clinical urine samples from infected patients. The method, nuclease-accessibility antibiotic susceptibility test (nuc-aAST) utilizes a DNase digestion of accessible bacterial DNA as a readout for damage to the cell wall by 15-30 minutes of antibiotic incubation. This method for measuring DNA accessibility changes with such short antibiotic incubations is made possible with the addition of a surfactant-based enhancement step after the antibiotics to selectively damage the already damaged cells. The nuc-aAST was further adapted to clinical urine samples.

ESS performed initial testing of osmotic, autolysis, and surfactant enhancers. ESS optimized sample handling prior to ABX exposure. ESS performed and analyzed enhancer testing and nuc-aAST experiments (Figs. 2-3, 2-4, 2-6), and assisted in performing digital LAMP experiments (Fig. 2-6). ESS performed data analysis and selected optimal conditions for nucaAST. ESS was a major contributor in selecting the readout metric of percent accessibility. ESS led experimental work and data analysis with clinical urine samples (Fig. 2-5d, 2-6e), and performed the experiments for the isolate replicates for (Fig. 2-5d). ESS contributed to writing the manuscript and figure design, created Fig. 2-5. and wrote the Methods section.

NGS guided initial testing of enhancers and developed two-step nuc-aAST workflow. NGS selected and performed initial screening of surfactant enhancers NGS optimized sample handling during ABX exposure. NGS performed and analyzed no-enhancer time course experiments (Fig. 2-2). NGS was a minor contributor in selecting the readout metric of

percentage accessibility. NGS designed LAMP primers and contributed to the optimization of LAMP conditions for digital LAMP experiments (Fig. 2-6). NGS wrote the manuscript and created Figures 2-1, 2-2, 2-3, 2-4, and 2-6.

MMC performed experimental work and data analysis on the clinical urine samples (Fig. 2-5). MMC assisted in collecting the data for fig 2-4. MMC contributed to writing the Methods section.

JCR optimized digital LAMP conditions, and performed and analyzed all digital LAMP experiments for Fig. 2-6.

OOS provided isolates and guided discussion on gold-standard AST, and current treatment practices, and performed gold-standard agar dilution AST for Ng.

JDK coordinated and provided oversight of clinical-sample collection at AHF, provided technical assistance to AHF staff, and guided the selection of eligibility criteria for patient recruitment.

Chapter III: Emily S. Savela[†], Alexander Winnett[†], Anna E. Romano[†], Michael K. Porter, Natasha Shelby, Reid Akana, Jenny Ji, Matthew M. Cooper, Noah W. Schlenker, Jessica A. Reyes, Alyssa M. Carter, Jacob T. Barlow, Colten Tognazzini, Matthew Feaster, Ying-Ying Goh, Rustem F. Ismagilov. 2021. "Quantitative SARS-CoV-2 viral-load curves in paired saliva and nasal swabs inform appropriate respiratory sampling site and analytical test sensitivity required for earliest viral detection." doi:10.1101/2021.04.02.21254771

This chapter describes the expansion of the community based COVID-19 study implemented in Appendix B to obtain viral load curves for paired saliva and nasal-swab samples. Results show the importance of both anatomical sample type and diagnostic test limit of detection (LOD) for detecting SARS-CoV-2 in human samples during early infection. Quantitation of the SARS-CoV-2 viral loads in both sample types shows the importance of selecting diagnostic tests with low LOD in cases where viral load trajectories rise slowly, and low-sensitivity tests may miss detection during the early days.

Author contributions are listed alphabetically by last name.

Reid Akana (RA) assisted in literature analysis with ES, MKP, AW, MC; collaborated with AW in creating digital participant symptom surveys; assisted with data quality control/curation with JJ, NWS, NS; collaborated with ES, JJ to write data analysis/visualization code; created current laboratory information management system (LIMS) for specimen logging and tracking. Creation of iOS application for sample logging/tracking. Configured a SQL database for data storage. Created an Apache server and websites to view study data. Configured FTPS server to catalog PCR data. Wrote a Python package to access study data. Worked with ES, AW, AR to implement logic that prioritized specimen extraction order. Collaborated with ES, MKP, AW, AR in analyzing RNA stability. Created supplementary figures 3-3B and 3-3C.

Jacob T. Barlow (JTB) created initial specimen tracking database to aid in specimen logging and tracking. Maintenance of database and implementation of corrections. Feedback on manuscript draft.

Alyssa M. Carter (AMC) received and logged specimens, and performed sample QC. Prepared reagents for and assisted with RNA extractions. Performed RT-qPCR and analyzed RT-qPCR data for both time series and screening experiments. Performed some of the initial experiments that assessed RNA stability in nasal swab samples.

Matthew M. Cooper (MMC) collaborated with AW, MF, NS, YG, RFI, on study design and recruitment strategies. Co-wrote initial IRB protocol and informed consent with AW and NS; assisted in the writing of the enrollment questionnaire; developed laboratory sample processing workflow for saliva with AW and AER; performed sample processing on subset of samples; funding acquisition; collaborated with AR to write data processing/visualization code for observing household transmission events for active study participants. Contributor to the design of the calibration curve for saliva LOD experiments.

Matthew Feaster (MF) co-investigator; collaborated with AW, MMC, NS, YG, RFI on study design and recruitment strategies; provided guidance and expertise on SARS-CoV-2 epidemiology and local trends.

Ying-Ying Goh (YYG) co-investigator; collaborated with AW, MMC, NS, MF, RFI on study design and recruitment strategies; provided guidance and expertise on SARS-CoV-2 epidemiology and local trends.

Rustem F. Ismagilov (RFI) co-investigator; collaborated with AW, MMC, NS, MF, YYG on study design and recruitment strategies; provided leadership, technical guidance, oversight, and was responsible for obtaining funding for the study. Jenny Ji (JJ): Contributed to study design and study organization and implementation with NS and JAR; co-wrote enrollment questionnaire with NS and AW. Major contributor to curation of participant symptom data. Provided quality control of participant data with RA, NS, NWS. Major contributor to the symptom data analysis and visualization shown in Fig. 3-2.

Michael K. Porter (MKP) performed specimen logging and QC, RNA extractions, RT-qPCR, data processing. Performed data acquisition and analysis for and made Figure S1 with AW. Prepared participant sample collection materials and helped with supplies acquisition. Assisted in literature analysis with ES, RA, AW.

Jessica A. Reyes (JAR) study coordinator; collaborated with NS, AW, NWS, and RFI on recruitment strategies, translated study materials into Spanish, co-wrote informational sheets with AW and NS; created instructional videos for participants; enrolled and maintained study participants with NS and NWS.

Anna E. Romano (AER) developed laboratory swab sample processing workflow with ES. Optimized extraction and ddPCR protocols working with vendor scientists. Created budgets and managed, planned, and purchased reagents and supplies; developed and validated method for RT-qPCR and RT-digital droplet PCR analysis for saliva & swab samples with MMC, and AW. Performed specimen logging and QC, RNA extractions, RT-qPCR and RT-

digital droplet PCR; Design of saliva calibration curve experiment. Analyzed ddPCR data for participant and calibration curve data included in Figure 1. Interpretation of sequence data with AW. Prepared Figure 3-1 and SI Figure 3-S2 with ES and AW; Collaborated with ES and RA to generate and curate data for RNA stability analysis. Managing logistics for the expansion of the BSL-2+ lab space with ESS. Edited manuscript.

Emily S. Savelle (ESS) coordinated the laboratory team and division of lab work, coordinated lab schedules to ensure completion of time-sensitive analyses of participant samples while complying with COVID-19 lab occupancy restrictions and biosafety requirements. Performed initial nasal-swab workflow validation experiments with AER. Major contributor to workflow validation, methods, biosafety SOPs, and sample storage. Developed a plan for, and executed, the long term sample storage for efficient, safe, storage. Performed specimen logging and QC, RNA extractions, RT-qPCR, data processing, and conducted biosafety training. Performed the data curation and data analysis for Figure 3-2. Made Figure 3-2. Minor contributor to symptoms data analysis and visualization with JJ and RA for Figure 3-2. Experimental design and RNA extractions of the samples, to Figure 3-1A and minor contributor to Figure S2A with AER. Managing logistics for the expansion of the BSL-2+ lab space with AER and biohazardous waste pickups. Collaborated with ES, RA, and AW to generate data for and curated data set to assess viral RNA stability (Fig. 3-S3). Prepared Fig. 3-S4. Co-wrote the manuscript. Verified the underlying data with AW.

Noah W. Schlenker (NWS) study coordinator; collaborated with NS, AW, JAR, and RFI on recruitment strategies; enrolled and maintained study participants with NS and JAR; study-data quality control, curation and archiving with RA, JJ, and NS. Natasha Shelby (NS): Study administrator; collaborated with AW, MMC, RFI, YG, MF on initial study design and recruitment strategies; co-wrote IRB protocol and informed consent with AW and MMC; co-wrote enrollment questionnaire with AW and JJ; co-wrote participant informational sheets with AW and JAR; enrolled and maintained study participants with JAR and NWS; study-data quality control, curation and archiving with RA, JJ, and NWS; reagents and

supplies acquisition; assembled Table 3-S1; managed citations and reference library; co-wrote and edited the manuscript.

Colten Tognazzini (CT) coordinated the recruitment efforts at PPHD with case investigators and contact tracers; provided guidance and expertise on SARS-CoV-2 epidemiology and local trends.

Alexander Winnett (AW) collaborated with MMC, NS, RFI, YG, MF on initial study design and recruitment strategies; co-wrote IRB protocol and informed consent with MMC and NS; co-wrote enrollment questionnaire with NS and JJ; co-wrote participant informational sheets with NS and JAR and digital survey; developed and validated methods for saliva and nasal-swab sample collection; developed and validated methods for RT-qPCR and RT-digital droplet PCR analysis for saliva and swab samples with AER, ESS, MMC; reagents and supplies acquisition; funding acquisition; developed laboratory sample processing workflow with AER, ESS, and MMC; performed specimen logging and QC, nucleic acid extraction, RT-qPCR, data processing – including experimental data generation for saliva calibration curve (Fig. 3-1, Fig. 3-S2) designed with MMC and AER, establishment of nasal swab limit of detection (Fig. 3-S1), and viral load timeseries data (Fig. 3-2) with ESS, AER, MKP, and AMC; interpreted sequencing data with AER; analyzed viral load timeseries data to visualize trends (Fig. 3-3, Fig. 3-S4) with ESS; generated, analyzed and visualized data to assess degradation of viral RNA in saliva and nasal swab samples with RA, ESS, and AER (Fig. 3-S3); literature analysis with RA, ESS, and MKP; co-wrote sections of the manuscript outlined by ESS and RFI, edited the manuscript. Verified the underlying data with ESS.

Appendix A: Nathan G. Schoepp, Eric J. Liaw, Alexander Winnett, Emily S. Savelle, Omai B. Garner, and Rustem F. Ismagilov. 2020. “Differential DNA Accessibility to Polymerase during Nucleic Acid Amplification Enables 30-minute phenotypic β -lactam Antibiotic Susceptibility testing of Carbapenem-resistant Enterobacteriaceae.” *PLoS Biology*. 18(3):e3000652. doi: 10.1371/journal.pbio.3000652.

This chapter describes a complementary assay to the nuclease-accessibility phenotypic antibiotic susceptibility test (nuc-aAST) shown in chapter II. The methods were designed in parallel and this polymerase-accessibility phenotypic AST (pol-aAST) utilizes a similar, but different, method to measure nucleic acids that are made accessible to enzymes after cell wall damage by beta-lactam antibiotics. In the pol-aAST, polymerases are used to amplify accessible nucleic acids using loop mediated isothermal amplification (LAMP). Design of the assay and the pilot test in clinical samples are shown in this chapter.

NGS, EJM, AW, ESS, and RFI contributed to conceiving the method, revising the manuscript, and interpretation of experimental results.

NGS developed the sample handling workflow and performed all experiments for comparison of amplification methods, validation, and timed sample-to-answer experiments. NGS was the major contributor to manuscript preparation and prepared all figures.

EJM performed filtration experiments, reviewed relevant medical literature, and contributed to manuscript writing.

NGS and AW tested clinical samples using the modified workflow.

ESS performed early experimental work to link beta-lactam exposure to differential nucleic acid readout, analyzed data from validation experiments, and developed TTPD metrics.

OBG provided clinical guidance on the selection of clinical isolates and clinical samples and coordinated and provided oversight of clinical-sample collection at UCLA, including technical assistance to UCLA staff. RFI supervised and guided the project, and helped compose the manuscript.

RFI supervised and guided the project, and helped compose the manuscript.

Appendix B: Alexander Winnett*, Matthew M. Cooper*, Natasha Shelby*, Anna E. Romano, Jessica A. Reyes, Jenny Ji, Michael K. Porter, Emily S. Savelle, Jacob T. Barlow,

Reid Akana, Colten Tognazzini, Matthew Feaster, Ying-Ying Goh, Rustem F. Ismagilov. 2020. "SARS-CoV-2 Viral Load in Saliva Rises Gradually and to Moderate Levels in Some Humans." medRxiv. <https://doi.org/10.1101/2020.12.09.20239467>

This chapter describes the implementation of a community-based COVID-19 study in Los Angeles. Longitudinally-collected saliva samples were self-collected by an index case and their three household contacts. Using highly-sensitive nucleic-acid quantification, viral load curves were plotted over time (twice daily for two weeks) for each individual to observe the changes in viral load in the early infection of the household contacts.

Author contributions are listed below.

AW collaborated with MMC, NS, RFI, YG, MF on initial study design and recruitment strategies; co-wrote IRB protocol and informed consent with MMC and NS; co-wrote enrollment questionnaire with NS and JJ; co-wrote participant informational sheets with NS and JAR; reagents and supplies acquisition; funding acquisition; assisted in sample logging system implementation with JTB; developed laboratory sample processing workflow with AER and MMC; performed nucleic acid extraction, and RT-qPCR; co-wrote and edited the manuscript; prepared Figure B-1, Figure B-S1 with RA, Figure B-S2, Table B-S1 with NS, JAR and JJ, and Table B-S2.

MMC collaborated with AW, NS, RFI, YG, MF on initial study design and recruitment strategies; co-wrote IRB protocol and informed consent with AW and NS; assisted in the writing of the enrollment questionnaire; developed laboratory sample processing workflow with AW and AER; contributed to the analyses of the RT-qPCR and RT-ddPCR data; validated the LOD of the assay; funding acquisition; co-wrote and edited the manuscript.

NS study administrator; collaborated with AW, MMC, RFI, YG, MF on initial study design and recruitment strategies; co-wrote IRB protocol and informed consent with AW and MMC; co-wrote enrollment questionnaire with AW and JJ; co-wrote participant informational

sheets with AW and JAR; enrolled and maintained study participants with JAR; reagents and supplies acquisition; co-wrote and edited the manuscript.

AER developed laboratory sample processing workflow with AW and MMC; reagents and supplies acquisition; developed and validated method for RT-qPCR and RT-digital droplet PCR analysis of extracted saliva samples; performed RT-qPCR and RT-digital droplet PCR;

JAR study coordinator; collaborated with NS, AW, RFI on recruitment strategies, translated study materials into Spanish, co-wrote informational sheets with AW and NS, enrolled and maintained study participants with NS.

JJ contributed to study design and study organization and implementation with NS and JAR; co-wrote enrollment questionnaire with NS and AW. Provided quality control and curation of participant data.

MP prepared participant sample collection materials, helped with supplies acquisition, and performed sample processing (RT-qPCR).

ES major contributor to biosafety SOPs and setting up lab workflow. Conducted biosafety training. Organized and coordinated lab work for the team. Performed sample processing including specimen logging and RT-qPCR. Minor contributor to validation of LOD of the assay.

JTB created specimen tracking database to aid in specimen logging and tracking.

RA provided literature review and processed data used in Figure S1.

CT coordinated the recruitment efforts at PPHD with case investigators and contact tracers.

MF co-investigator; collaborated with AW, MMC, NS, YG, RFI on study design and recruitment strategies; provided guidance and expertise on SARS-CoV-2 epidemiology and local trends.

YG co-investigator; collaborated with AW, MMC, NS, MF, RFI on study design and recruitment strategies; provided guidance and expertise on SARS-CoV-2 epidemiology and local trends.

TABLE OF CONTENTS

Acknowledgements	iii
Abstract	x
Published Content and Contributions.....	xi
Table of Contents.....	xxi
List of Illustrations and/or Tables	xxiii
Chapter I: AN OVERVIEW.....	1
References	5
Chapter II: NUCLEASE-ACCESSIBILITY ANTIBIOTIC SUSCEPTIBILITY TEST FOR NEISSERIA GONORRHOEAE.....	7
Abstract	7
Introduction.....	8
Results.....	11
Discussion.....	27
Methods	30
References.....	38
Acknowledgements	47
Supplementary Materials.....	47
Chapter III: SARS-COV-2 VIRAL LOAD IN LONGITUDINALLY COLLECTED SALIVA AND NASAL SWABS	60
Abstract	60
Introduction.....	61
Results.....	65
Limitations	74
Conclusions.....	75
Methods	79
Data Availability.....	82
Competing Interests Statement	82
Funding	82
Acknowledgements	82
References.....	83
Supplemental Information.....	90
Appendix A: POLYMERASE-ACCESSIBILITY ANTIBIOTIC SUSCEPTIBILITY TEST FOR CARBAPENEM-RESISTANT ENTEROBACTERIACEAE	102
Abstract	102
Introduction.....	103
Results.....	105

Discussion.....	114
Methods	119
References.....	124
Acknowledgements	132
Supplementary Materials.....	133
Appendix B: QUANTIFICATION OF SARS-COV-2 VIRAL LOAD IN LONGITUDINALLY COLLECTED SALIVA SAMPLES	135
One Sentence Summary	135
Abstract.....	135
Introduction.....	136
Methods	138
Results and Discussion.....	141
Data Availability.....	145
Competing Interests Statement	145
Funding	145
Acknowledgements	145
References.....	146
Supplemental Information.....	149
Appendix C: ABBREVIATIONS.....	154

LIST OF ILLUSTRATIONS AND/OR TABLES

<i>Number</i>	<i>Page</i>
1. Figure 1-1: <i>Neisseria gonorrhoeae</i> clinical collaboration with the AIDS Healthcare Foundation (AHF) sample screening workflow.....	3
2. Figure 1-2: COVID-19 community study human specimen screening workflow	4
3. Figure 1-3: COVID-19 community study SARS-CoV-2 RNA viral load time series workflow.....	5
4. Figure 2-1: The nuc-aAST workflow shown for a sample containing a β -lactam susceptible pathogen	12
5. Figure 2-2: Percentage accessibility of DNA over time using the nuc-aAST without the addition of an enhancing step	13
6. Figure 2-3: Selection of enhancers	16
7. Figure 2-4: Validation of nuc-aAST using clinical isolates.....	18
8. Figure 2-5: Pilot nuc-aAST with clinical urine samples.....	20
9. Figure 2-6: The nuc-aAST workflow for contrived and clinical urine samples with each step timed	23
10. Figure 2-S1: DNase is properly inactivated by extraction and heat treatment steps used in this work.....	49
11. Figure 2-S2: DNase I remains active in clinical urine samples	49
12. Figure 2-S3: The nuc-aAST using clinical isolates separated by minimum inhibitory concentration (MIC).....	50
13. Figure 2-S4: Receiver operating characteristic (ROC) curves	51
14. Table 2-S1: <i>Neisseria gonorrhoeae</i> isolates used in this study.....	52
15. Table 2-S2: Percentage lysis of <i>Neisseria gonorrhoeae</i> cells after 5 min exposure to an enhancer	53

16. Table 2-S3: The percentage of <i>Neisseria gonorrhoeae</i> DNA accessible after a 15-min antibiotic (ABX) exposure (1 µg/mL) followed by a 5-min exposure to an enhancer.....	53
17. Table 2-S4: The percentage of <i>Neisseria gonorrhoeae</i> DNA accessible after a 15- or 30-min exposure to an antibiotic (ABX) and 5 min enhancement with CHAPS	53
18. Table 2-S5: The results of nuc-aAST with a dLAMP readout using contrived samples with <i>Neisseria gonorrhoeae</i> (Ng) isolates and clinical urine samples positive for Ng	54
19. Table 2-S6: Nuc-aAST data for clinical urine samples and isolates from the samples	55
20. Table 2-S7: Nuc-aAST summary of samples and isolates from the samples	55
21. Table 2-S8: DNase I inactivation data.....	55
22. Table 2-S9: DNA digestion of the lambda spike-in	56
23. Table 2-S10: Percentage accessibility of DNA over time without an enhancer	57
24. Table 2-S11: Each biological replicate nuc-aAST of Ng DNA accessible after a 15-min exposure to an antibiotic (ABX) and 5 min enhancement with CHAPS	58
25. Table 2-S12: Each biological replicate nuc-aAST of Ng DNA accessible after a 30-min exposure to an antibiotic (ABX) and 5 min enhancement with CHAPS	58
26. Table 2-S13: A representative subset of fluorescence values from a digital LAMP antibiotic-susceptibility test (AST) run on a susceptible <i>N. gonorrhoeae</i> isolate in the control (no antibiotic) treatment	58
27. Table 2-S14: A representative subset of fluorescence values from a digital LAMP antibiotic-susceptibility test (AST) run on a susceptible <i>N. gonorrhoeae</i> isolate in the treated (penicillin) treatment.....	58

28. Table 2-S15: A representative subset of fluorescence values from a digital LAMP antibiotic-susceptibility test (AST) run on a resistant <i>N. gonorrhoeae</i> isolate in the control (no antibiotic) treatment	58
29. Table 2-S16: A representative subset of fluorescence values from a digital LAMP antibiotic-susceptibility test (AST) run on a resistant <i>N. gonorrhoeae</i> isolate in the treated (penicillin) treatment.....	59
30. Figure 3-1: SARS-CoV-2 viral load quantification for nasal-swab and saliva specimens from positive participants measured with RT-ddPCR and RT-qPCR	66
31. Figure 3-2: Symptoms and SARS-CoV-2 viral loads in paired saliva and nasal-swab samples of seven participants who became SARS-CoV-2 positive during study participation.....	68
32. Figure 3-3: Summary of Diagnostic Insights from Study Participants who became infected with SARS-CoV-2 while enrolled in the study.....	73
33. Figure 3-S1: Limit of detection of saliva and nasal-swab RT-qPCR assays used in this study.....	90
34. Figure 3-S2: Calibration curve of SARS-CoV-2 inactivated particles to establish viral load conversion equations.....	91
35. Figure 3-S3: SARS-CoV-2 RNA stability over time in Spectrum SDNA-1000 buffer at 4 °C	92
36. Figure 3-S4: Predicted impact of SARS-CoV-2 RNA stability on viral loads shown in Fig. 5-2	93
37. Table 3-S1: Study participant demographic data	94
38. Fig A-1: Overview of the polymerase-accessibility AST (pol-aAST) shown for susceptible (S) and resistant (R) samples exposed to β -lactams.....	106
39. Fig A-2: The pol-aAST requires non-lytic amplification conditions	108
40. Fig A-3: Percentage of DNA released following antibiotic exposure.....	109

41. Fig A-4: Validation of the pol-aAST method using control (ctrl) and antibiotic-treated (+ABX) aliquots.....	110
42. Fig A-5: Validation of the pol-aAST method using lysed control (lc) and antibiotic-treated (+ABX) aliquots.....	111
43. Fig A-6: Timed sample-to-answer pol-aAST using contrived urine samples spiked with either E. coli (Ec) or Klebsiella pneumoniae (Kp).....	113
44. Fig A-7: Pilot testing of pol-aAST with clinical UTI samples with a modified protocol	114
45. Fig A-S1: Validation of pol-aAST TTPDCT method using ampicillin	133
46. Table A-S1: Clinical isolates used in this study.....	133
47. Table A-S2: Clinical urine samples from patients with urinary tract infections (UTI) used in this study	133
48. Table A-S3: Raw data and calculated error for all pol-aASTs performed using clinical isolates. Cqs.....	134
49. Table A-S4: Raw data and calculated error for all pol-aASTs performed using clinical UTI samples	134
50. Table A-S5: Raw data for amplification curves shown in Fig 2	134
51. Table A-S6: Raw data for percentage of DNA release shown in Fig 3...	134
52. Fig B-1: Quantified SARS-CoV-2 saliva viral load after transmission between household contacts relative to detection limits of rapid tests.....	144
53. Table B-S1: Pertinent Demographic and Health Information for Study Participants	149
54. Fig B-S1: Re-analysis of Select Data from Kissler et al. (2020).....	150
55. Fig B-S2. Human RNase P Ct values and SARS-CoV-2 viral load measurements from RT-qPCR for all household contacts	151
56. Table B-S2. Summary of Reported Limits of Detection (LOD) for Rapid Point of Care SARS-CoV-2 Antigen Tests	152

Chapter 1

AN OVERVIEW

Public health measures reducing the spread of antibiotic resistance and global pandemics depend on diagnostics. In many parts of the world, antibiotics for sexually transmitted infections (STIs) such as gonorrhea or urinary tract infections (UTIs) are prescribed empirically (based only on the presence of symptoms) because point-of-care (POC) diagnostic tests do not exist. Prescribing antibiotics without a diagnosis is one of the contributing factors to the rise of antibiotic resistance¹. In the examples detailed in chapters II-V of this doctoral thesis, the need for innovation of new diagnostic tests and implementation strategies are explained. Improving diagnostics that detect phenotypic antibiotic susceptibility has the potential to empower physicians to make evidence-based prescription of antibiotics and would ultimately reduce the further development of antibiotic resistance. Robust diagnostic strategies for infections that are often transmitted during the asymptomatic or pre-symptomatic period of infection (common with both gonorrhea² and COVID-19³) would help reduce community spread^{1,3}.

There is a critical demand for rapid, sensitive, and specific diagnostic tests for early diagnosis of STIs, UTIs, COVID-19, and other infectious diseases. Nucleic acid amplification tests (NAATs) are a powerful tool⁴⁻⁵, as they enable detection of a targeted nucleic acid sequence within the complex background of host and commensal organisms that are commonly found in human samples. Through innovation of new diagnostic assays for rapid AST and evaluation of existing diagnostic test sensitivities for early detections of SARS-CoV-2 during a pandemic, NAATs are an important tool for diagnostic surveillance.

Another key theme of my doctoral work is the design of diagnostics around the biological and practical constraints of clinical samples. Considering the constraints posed by the clinical samples and clinical settings are critical for the translation of the assay to real-world settings with real samples. Identifying and working around these variables is not always obvious and required detailed control experiments to identify. After variables of sample stability (*e.g.* viable CFUs and RNA stability in samples) were identified, adaptations to workflows to reduce the impact of these parameters on the downstream assays and quantification.

My doctoral thesis addresses two main themes of diagnostic relevance: phenotypic antibiotic susceptibility tests (AST) and SARS-CoV-2 diagnostics for early detection. Throughout these chapters, I document my contributions to each field through assay design, clinical pilot tests, and a community study. Chapter II describes the design of a diagnostic test for phenotypic antibiotic susceptibility of the gram-negative bacterium *N. gonorrhoeae* to the beta-lactam class of antibiotics. Each novel AST design uses nucleic acids to determine if the cell is intact or damaged, making the nucleic acids accessible to enzymes. I co-lead the design of the nuclease-accessibility assay and led the pilot test and the evaluation of performance in clinical urine samples in Chapter II. For the complementary assay described in Appendix A, I was a contributing author who aided in the early experimental work to link beta-lactam exposure to nucleic acid differences and to test the translatability to different antibiotics. Chapter III and Appendix B detail the implementation of a community-based COVID-19 household transmission study to quantify viral load of SARS-CoV-2 in self-collected human samples. I contributed to the setup of the laboratory workflow detailed in Appendix B and I co-lead the comparison study between saliva and anterior nares nasal swabs detailed in Chapter III.

Chapter II describes a phenotypic nuclease-accessibility AST designed for *Neisseria gonorrhoeae* (NG) and beta-lactam antibiotics. Nucleic acids made accessible by cell wall damage to the antibiotic exposure and surfactant enhancer are digested by an exogenously added DNase. The difference between the control and antibiotic-treated incubations are used to calculate percentage accessibility.

Initially, the design parameters for clinical relevance were focused around the timing and simplicity of the assay. The challenges posed by NG include doubling time, difficulty to establish log phase cultures in liquid media⁶ and tendency to autolyse⁷⁻¹⁰. Beta-lactam antibiotics add the additional challenges of slower antibiotic kinetics, with kill-curves on the order of hours¹¹⁻¹² and no direct effects on the nucleic acids of the cells¹³. The accessibility AST (aAST) was designed under these challenges with the constraints of a short-as-possible antibiotic exposure tying to a detectable change on the host nucleic acids. The methods developed and tested here show sum-of-steps shorter than the doubling time of the microbe, which in best-case conditions is 1-2 hours in liquid culture depending on some chemical and physical constraints¹⁴⁻¹⁶.

Through the pilot test and collaboration with the AIDS Healthcare Foundation (AHF) we obtained and tested urine samples from symptomatic individuals who were undergoing gold-

standard identification testing prior to starting antibiotic treatment. Therefore, it was unknown for our team whether or not the urine samples were positive or negative for *N. gonorrhoeae*. The workflow steps performed on each sample included identification with real-time loop-mediated isothermal amplification (LAMP), characterization or urinalysis, and plating on selective agar for gold standard assessment (Fig. 1-1). Some modifications were made to the nuclease-accessibility assay to translate to the added complexity of working from bacteria in urine instead of a log-phase culture of an isolate in the lab.

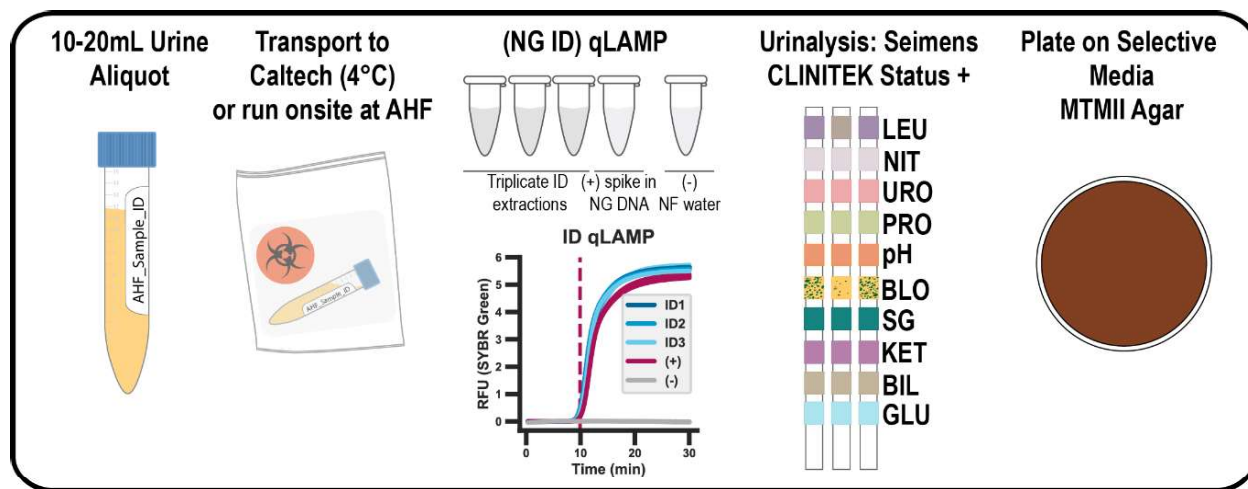


Fig 1-1: *Neisseria gonorrhoeae* clinical collaboration with the AIDS Healthcare Foundation (AHF) sample screening workflow. Participants self-collected urine samples and an AHF technician prepared a 10-20 mL aliquot for our lab's processing. The samples were transported by a medical courier for characterization of *N. gonorrhoeae* identification (NG ID). DNA, urinalysis and selective plating. Urinalysis characterizes presence of leukocyte esterase (LEU), nitrite (NIT), urobilinogen (URO), protein (PRO), blood (BLO), specific gravity (SG), ketone (KET), bilirubin (BIL), and glucose (GLU).

Appendix A details the design of a polymerase-accessibility AST designed more broadly for carbapenem-resistant Enterobacteriaceae (CRE) and the beta-lactam class of antibiotics. This assay was developed in clinical isolates and pilot tested with clinical urinary tract infection (UTI) clinical samples.

While there are some similarities, the assay design in Appendix A is distinct from Chapter II. There are similarities in inspiration and methods, however the biological differences between microorganisms such as doubling times, sample types, and bacterial loads, each of the accessibility assays may not be directly adaptable to new microorganism and antibiotic pairings. For example, *N. gonorrhoeae* can utilize extracellular DNA in biofilm formation and uptake¹⁷. Extracellular nucleic acids would be a challenge for a direct-to-LAMP accessibility AST with *N. gonorrhoeae*. Phenotypic

assays will likely require such species-specific design in order to correctly characterize the antibiotic responses when the microbial biology can vary between organisms.

Appendix B shows the implementation of a community-based COVID-19 study in the greater Los Angeles County area, CA, USA, in collaboration with the Pasadena Public Health Department. This study was launched in September 2020 during the first year of the COVID-19 pandemic and I contributed to the team by establishing biosafety standard operating procedures (SOPs), safety training, coordinated the distribution of the lab work for the team, contributed to validation of the assay LOD, and logged and processed specimens. This chapter details a case study of one household, showing how viral load curves of early infection can inform the diagnostic sensitivity required for SARS-CoV-2 diagnostic surveillance testing strategies.

Chapter III describes the expansion of the community based COVID-19 study implemented in Appendix A to include more than one sample type and scaling in the number of participants enrolled at a given time. I co-lead a project of the COVID-19 study that set out to compare SARS-CoV-2 viral loads in participant-collected saliva and anterior-nares nasal-swab samples. Knowledge of viral load curves throughout the entire infection course (beginning at earliest detectable viral loads) is necessary to design diagnostic strategies for early detection of infection to reduce the community spread during a pandemic. Results showed the importance of both anatomical sample type and diagnostic test LOD for detecting SARS-CoV-2 in human samples during early infection.

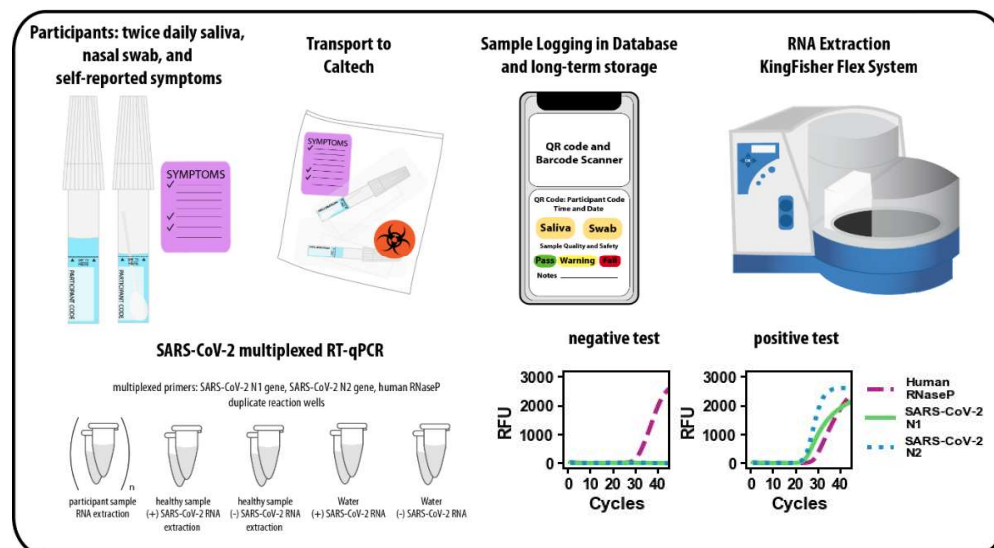


Fig 1-2: COVID-19 community study human specimen screening workflow. Participants collect saliva and anterior nares nasal swabs twice daily with self-reported symptom cards. The de-identified samples are transported to Caltech with a courier. Lab team members inspect and log sample and symptom cards to the database. Samples are screened for SARS-CoV-2 at regular intervals with the CDC 2019–Novel Coronavirus (2019-nCoV) Real-Time RT-PCR Diagnostic Panel¹⁸ (see Chapter V Methods for details).

Similar to the challenges with the AHF collaboration in Chapter II, each sample that was delivered to the lab was unknown to be positive or negative for SARS-CoV-2, and was screened for sample quality, safety, and SARS-CoV-2 positivity. Participants self-reported symptoms with each sample (Fig 1-2). As the study grew from what is outlined in Appendix B, we validated the additional sample type of nasal swabs and translated the manual extraction protocols to an automated liquid handler (Fig 1-2 KingFisher Flex System) to scale-up the number RNA extractions and numbers of samples processed. Samples were archived at -80°C (Fig 1-3) with all metadata, symptoms, and SARS-CoV-2 multiplexed PCR data to serve as a sample bank for ongoing COVID-19 projects.

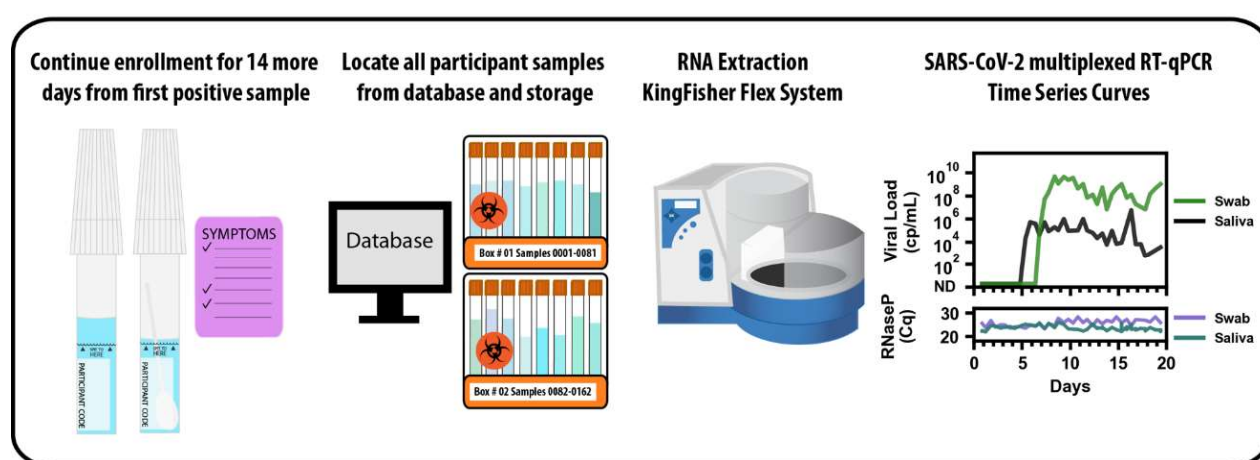


Fig 1-3: COVID-19 community study SARS-CoV-2 RNA viral load time series workflow. Each of the participant samples are collected and logged into the database for 14 days after the first positive sample (either saliva or nasal swab) by the screening methods. When a series of samples are to be quantified as a longitudinally collected time series, the samples are then retrieved from the archived storage boxes and processed with the RNA extraction with the MagMax Viral Pathogen I Nucleic Acid Isolation kit on the Thermo Fisher Scientific KingFisher Flex 96 instrument and purified RNA is run with the CDC 2019-Novel Coronavirus (2019-nCoV) Real-Time RT-PCR Diagnostic Panel¹⁸ (see Chapter V Methods for details).

REFERENCES

1. CDC. *Antibiotic Resistance Threats in the United States 2019*. <<https://www.cdc.gov/drugresistance/pdf/threats-report/2019-ar-threats-report-508.pdf>> (2019).
2. M. Unemo and Shafer, W.M. 2014. "Antimicrobial resistance in *Neisseria gonorrhoeae* in the 21st century: past, evolution, and future." *Clin Microbiol Rev.* 27: 587-613.
3. Johansson, M. A. *et al.* SARS-CoV-2 Transmission From People Without COVID-19 Symptoms. *JAMA Network Open* 4, e2035057-e2035057 (2021).
4. CDC. *Nucleic Acid Amplification Tests (NAATs)*, <<https://www.cdc.gov/coronavirus/2019-ncov/lab/naats.html>> (2021).

5. CDC. *Recommendations for the Laboratory-Based Detection of Chlamydia trachomatis and Neisseria gonorrhoeae -2014*. <<https://www.cdc.gov/mmwr/preview/mmwrhtml/rr6302a1.htm>>(2014).
6. M.A.G. Jeremy James Wade. 2007. "A fully defined, clear and protein-free liquid medium permitting dense growth of *Neisseria gonorrhoeae* from very low inocula." *FEMS Microbiology Letters*. 273: 35-37.
7. D.L. Garcia and Dillard, J.P. 2006. "AmiC functions as an N-acetylmuramyl-L-alanine amidase necessary for cell separation and can promote autolysis in *Neisseria gonorrhoeae*." *Journal of Bacteriology*. 188: 7211-7221.
8. B.H. Hebel and Young, F.E. 1975. "Autolysis of *Neisseria gonorrhoeae*." *J Bacteriol*. 122: 385-392. PMC246068.
9. L.G.B. Theodor Elmors, Gunnar D. Bloom. 1976. "Autolysis of *Neisseria Gonorrhoeae*." *Journal of Bacteriology*. 126: 969-976.
10. L.G.B. Theodor Elmors, Gunnar D. Bloom. 1976. "Brit. J. vener. Dis." 52:
11. A. Tomasz. 1979. "The mechanism of the irreversible antimicrobial effects of penicillins: how the beta-lactam antibiotics kill and lyse bacteria." *Annual review of microbiology*. 33: 113-137.
12. M.U. Sunniva Foerster, Lucy J. Hathaway, Nicola Low, Christain L. Althaus. 2016. "Time-kill curve analysis and pharmacodynamic modelling for in vitro evaluation of antimicrobials against *Neisseria gonorrhoeae*." *BMC Microbiol*. 16:
13. M.A. Kohanski, Dwyer, D.J. and Collins, J.J. 2010. "How antibiotics kill bacteria: from targets to networks." *Nat Rev Micro*. 8: 423-435.
14. Morse SA, Hebel BH. Effect of pH on the growth and glucose metabolism of *Neisseria gonorrhoeae*. *Infect Immun*. 1978;21(1):87-95.
15. Tobiason DM, Seifert HS. The obligate human pathogen, *Neisseria gonorrhoeae*, is polyploid. *PLoS Biol*. 2006;4(6):1069-78. doi: 10.1371/journal.pbio.0040185.
16. Wade JJ, Graver MA. A fully defined, clear and protein-free liquid medium permitting dense growth of *Neisseria gonorrhoeae* from very low inocula. *FEMS Microbiol Lett*. 2007;273(1):35-7. doi: 10.1111/j.1574-6968.2007.00776.x.
17. S.S. Maria Zweig, Andrea Koerdt, Katja Siewering, Claus Sternberg, Kai Thormann, Sonja-Verena Albers, Søren Molin, Chris van der Does. 2014. "Secreted single-stranded DNA is involved in the initial phase of biofilm formation by *Neisseria gonorrhoeae*." *Environmental Microbiology* 16: 1040-1052.
18. FDA. *CDC 2019-Novel Coronavirus (2019-nCoV) Real-Time RT-PCR Diagnostic Panel (EUA)*, <<https://www.fda.gov/media/134922/download>> (2020).

Chapter 2

NUCLEASE-ACCESSIBILITY ANTIBIOTIC SUSCEPTIBILITY TEST FOR NEISSERIA GONORRHOEAE

Emily S. Savela[†], Nathan G. Schoepp[†], Justin C. Rolando, Jeffrey D. Klausner, Olusegun O. Soge, and Rustem F. Ismagilov. 2020. “Surfactant-enhanced DNA accessibility to nuclease accelerates phenotypic β -lactam antibiotic susceptibility testing of *Neisseria gonorrhoeae*.” PLoS Biology. 18(3):e3000651. doi: 10.1371/journal.pbio.3000651

ABSTRACT

Rapid antimicrobial susceptibility testing (AST) for *Neisseria gonorrhoeae* (*Ng*) is critically needed to counter widespread antibiotic resistance. Detection of nucleic acids in genotypic AST can be rapid but it has not been successful for β -lactams (the largest antibiotic class used to treat *Ng*). Rapid phenotypic AST for *Ng* is challenged by the pathogen’s slow doubling time and the lack of methods to quickly quantify the pathogen’s response to β -lactams. Here, we asked two questions: (i) Is it possible to use nucleic acid quantification to measure the β -lactam susceptibility phenotype of *Ng* very rapidly, using antibiotic-exposure times much shorter than the 1-2 hour doubling time of *Ng*? (ii) Would such short-term antibiotic exposures predict the antibiotic resistance profile of *Ng* measured by plate growth assays over multiple days? To answer these questions, we devised an innovative approach for performing a rapid phenotypic AST that measures DNA accessibility to exogenous nucleases after exposure to β -lactams (termed nuc-aAST, nuclease-accessibility AST). We showed that DNA in antibiotic-susceptible cells has increased accessibility upon exposure to β -lactams, and that a judiciously chosen surfactant permeabilized the outer membrane and enhanced this effect. We tested penicillin, cefixime, and ceftriaxone and found good agreement between the results of the nuc-aAST after 15-30 min of antibiotic exposure and the results of the gold-standard culture-based AST measured over days. These results provide a new pathway toward developing a critically needed phenotypic AST for *Ng* and additional global-health threats.

Keywords: antibiotic resistance, sexually transmitted infection, diagnostics, antibiotic susceptibility test

INTRODUCTION

Gonorrhea, caused by *Neisseria gonorrhoeae* (*Ng*), is the second most common notifiable sexually transmitted infection (STI) in the U.S. [1] and the third most common STI globally. Gonorrhea affects 86,900,000 people each year worldwide [2]. Untreated *Ng* infections can lead to pelvic inflammatory disease, infertility, ectopic pregnancy, and neonatal blindness [3], and have a significant financial burden on healthcare systems [4]. Antibiotic resistance in *Ng* emerged quickly and continues to spread unchecked because there is no rapid antibiotic susceptibility test (AST) to guide treatment. The Centers for Disease Control and Prevention (CDC) estimates that almost half (550,000) of the 1.14 million new *Ng* infections reported are antibiotic-resistant [5]. Lacking a rapid AST, clinicians are limited to making empiric prescriptions as recommended by the CDC [6] or World Health Organization (WHO) [7]. When resistance to a particular antibiotic exceeds 5%, treatment guidelines are updated and the recommended treatment protocol is escalated to the next line of antibiotic [8,9]. As a result, *Ng* strains continue to evolve resistance, even to the last-line treatment (dual treatment with azithromycin/ceftriaxone) [10-12]. The global prevalence and spread of resistant *Ng* infections has led the CDC to place *Ng* in its highest (“urgent”) category of antimicrobial-resistant pathogen threats [13] and the WHO to label *Ng* as a high-priority pathogen [14]. Despite the threat of untreatable *Ng* [15] and an international call for rapid diagnostics [16-18], no phenotypic AST currently exists that can be performed rapidly enough for the point of care (POC).

Successful and timely treatment of *Ng* infections while still considering antibiotic stewardship requires two sequential steps to be performed at the POC. First, an identification (ID) test is run on the patient’s sample (typically urine or swab) to confirm that the patient is infected with *Ng*. Then, an AST must be run on the sample to determine whether the infecting strain of *Ng* is susceptible to the available ABX, so that the correct treatment can be prescribed. The health crisis associated with antibiotic-resistant infections is internationally recognized [19], and substantial efforts (both academic [20-22] and commercial [23,24]) are making great progress toward shortening the time required to identify *Ng* infections. However, there is no published path toward development of a rapid phenotypic AST for *Ng*, especially for beta-lactam antibiotics. Thus, even with swift diagnosis of an *Ng* infection, prescription of the correct antibiotics at the POC will remain bottlenecked by the lack of a rapid AST.

AST methods are either genotypic or phenotypic. Genotypic methods predict resistance by screening for the presence of known resistance genes, whereas phenotypic methods determine susceptibility and resistance by directly measuring an organism's response to an antibiotic. Rapid genotypic methods exist for select antibiotic classes such as quinolones [25,26], but the diverse mechanisms of resistance present in *Ng* would require highly multiplexed assays for most other antibiotic classes [27,28], including β -lactams [29,30], which are the largest class of ABX for *Ng*. For example, hundreds of β -lactamase genes are known [31], and new resistance genes continue to emerge, making it challenging to design a comprehensive genotypic AST, even for a single organism. Only phenotypic AST methods provide the ability to directly detect resistance, and susceptibility, regardless of the antibiotic's mechanism of action. The current gold-standard AST for *Ng* is agar dilution, a phenotypic method that takes many days and is only performed in a small number of reference laboratories [32]. Efforts have been made to shorten the total assay time of culture-based techniques [33-35], but these methods still rely on multiple cell divisions and thus require many hours due to the slow doubling time (1-2 h) of *Ng*. The doubling time of *Ng* is impacted by many factors including, pH [36], temperature [37], initial cell concentration, media, and isolate [38]. Although differences in conditions are straightforward to control in experiments with clinical isolates, the effects of variable growth time will be much greater when considering the unknown composition in clinical samples, which can have great variability, particularly in bacterial load and pH.

A phenotypic AST rapid enough for the POC would be paradigm-shifting for *Ng* [39] because it would provide the correct timely treatment of infections, significantly reduce disease burden, and improve global surveillance efforts [40-42]. Until a POC diagnostic is developed for *Ng*, empiric prescribing of the last-line dual antibiotic therapy of azithromycin/ceftriaxone will likely continue, as it has in the U.S. over the last five years [43]. Likewise, if informed antibiotic prescriptions cannot be made, resistance will continue to spread, at which point no currently available ABXs will be recommended for treatment of *Ng*. Importantly, a rapid, phenotypic AST would greatly increase treatment options because if clinicians know which ABX will be efficacious for each infection, they can once again treat with ABX that are not prescribed in the current (empiric-based) system because of the risk of resistance. For example, even though cefixime (CFM) is no longer used as a first-line therapy for *Ng*, up to 95% of infections in the U.S. are still susceptible to

CFM [1,44]. Similarly, up to 77% of *Ng* infections are susceptible to TET [1]. Therefore, having a POC AST could enable clinicians to once again safely prescribe CFM and other antibiotics [45]. Several recent cases of *Ng* infections resistant to azithromycin [46,47], or the currently recommended combination of ceftriaxone/azithromycin [10,12] were detected after treatment was administered, highlighting the critical need for faster diagnostics.

For an *Ng* AST to inform treatment decisions at the POC, the total assay time to determine phenotypic susceptibility must be greatly decreased [48-50]. Quantification of pathogen-specific nucleic acid (NA) concentrations has shown major promise for the rapid determination of susceptibility phenotype [51-54]. These methods rely on comparing the NA concentrations of control and antibiotic-treated samples, and thus work well for rapidly dividing organisms and for ABX that directly affect NA replication. NA-based phenotypic AST methods also benefit from the high sensitivity of NA amplification, and fast isothermal amplification techniques have led to short total assay times [51]. For example, by measuring the concentration of *E. coli* DNA, we have shown that the antibiotic-exposure step for phenotypic AST can be shortened to 15 min [55]. We also were able to achieve a phenotypic AST with a 10-min antibiotic exposure time in *Ng* by measuring changes in RNA concentration after exposure to ciprofloxacin, which directly inhibits DNA replication and downstream translation [56]. However, for ABX that do not impact DNA replication or gene expression on short time scales, such as β -lactams, these NA-based AST techniques have proven difficult; the fastest published method for *Ng* still requires four hours of beta-lactam exposure [57]. Importantly, of the ABX prescribed for *Ng*, only one, ciprofloxacin [56], has been demonstrated to be compatible with this existing NA-based approach.

In this work, we asked two questions. (1) Is it possible to use nucleic acid quantification to measure beta-lactam susceptibility phenotype of *N. gonorrhoeae* very rapidly, using antibiotic exposure times (15-30 minutes) much shorter than the doubling time of *N. gonorrhoeae* (1-2 h)? (2) Would such short-term antibiotic exposures predict the antibiotic resistance profile of *N. gonorrhoeae* measured by plate growth assays over multiple days? To answer these questions, here we describe an innovation that enables a rapid, NA-based phenotypic AST for β -lactams, the largest class of ABX used to treat *Ng*. We hypothesized that cell wall damage caused by exposure to β -lactams could be exploited to determine phenotypic susceptibility faster than cell division. Our method, termed nuc-aAST (nuclease-accessibility AST), measures the accessibility of intracellular

Ng DNA to exogenously added nucleases after a short antibiotic exposure. We also wished to test whether the total time of the assay could be further decreased by including an enhancement step, defined as a condition that would lead to greater differences in DNA accessibility between resistant (R) and susceptible (S) samples.

We chose to validate this proof-of-concept nuc-aAST using three β -lactams, penicillin (PEN), cefixime (CFM), and ceftriaxone (CRO). Each of these three ABXs represent first-line treatments at different points in the history of *Ng* treatment [58,59]. Additionally, CRO, in combination with azithromycin, is the current recommended (and last-line) treatment for *Ng*. Determining susceptibility to CRO is thus relevant not only for treatment, but for surveillance efforts. Clinical urine samples were chosen (and urine was chosen as the as the matrix for contrived samples) because urine is one of the primary sample types used for *Ng* diagnosis, especially in males [6,59]. We chose to test only categorically S or R isolates, based on EUCAST breakpoints [60], because S and R isolates are more useful than intermediate isolates for gaining initial mechanistic insights into nuc-aAST, and because S and R are actionable calls in antibiotic-prescribing scenarios. Lastly, keeping in mind clinical utility, we timed each assay step to determine whether the nuc-aAST could yield a definitive susceptibility call within the time period of a patient's visit, which is usually less than an hour [49,50].

RESULTS

Design and rationale of the nuc-aAST

The nuc-aAST method measures differences in the accessibility of genomic DNA to an exogenous nuclease between control and treated samples following a short antibiotic (ABX) exposure. Like other NA-based AST methods, the nuc-aAST (Fig 2-1) relies on measuring changes in the quantity of pathogen-specific NAs in response to a treatment with ABX; however, the nuc-aAST differs from existing NA-based ASTs in three aspects. First, in nuc-aAST, exposure of cells to β -lactams is performed in the presence of a DNase enzyme to degrade any DNase-accessible NAs (Fig 2-1a). DNA is accessible to DNase if it is released from the cells upon cell lysis, or if the action of the antibiotic porates the cells and allows DNase to access the intracellular DNA. Second, in nuc-aAST, an enhancement step is introduced to increase accessibility of DNA in cells that have damaged or

compromised peptidoglycan caused by β -lactams; DNase is present and active during this enhancement step (Fig 2-1b). Third, in nuc-aAST, lysis of the sample is performed only after DNase has degraded all accessible DNA (Fig 2-1c). This lysis step also inactivates the DNase, so that the enzyme does not impact downstream quantification (Fig 2-S1). Following inactivation of DNase and lysis, DNA remaining in the sample is quantified and the percentage of accessible DNA is used to determine susceptibility (Fig 2-1d). The percentage of accessible DNA is quantified by subtracting the concentration of inaccessible DNA (DNA not digested) in the treated aliquot from the concentration of DNA in the control aliquot, and dividing this value by the concentration of DNA in the control. Measuring the percentage of accessible DNA is an NA-based metric that enables quantification of the damage to the cellular envelope induced by ABX targeting cell wall biosynthesis.

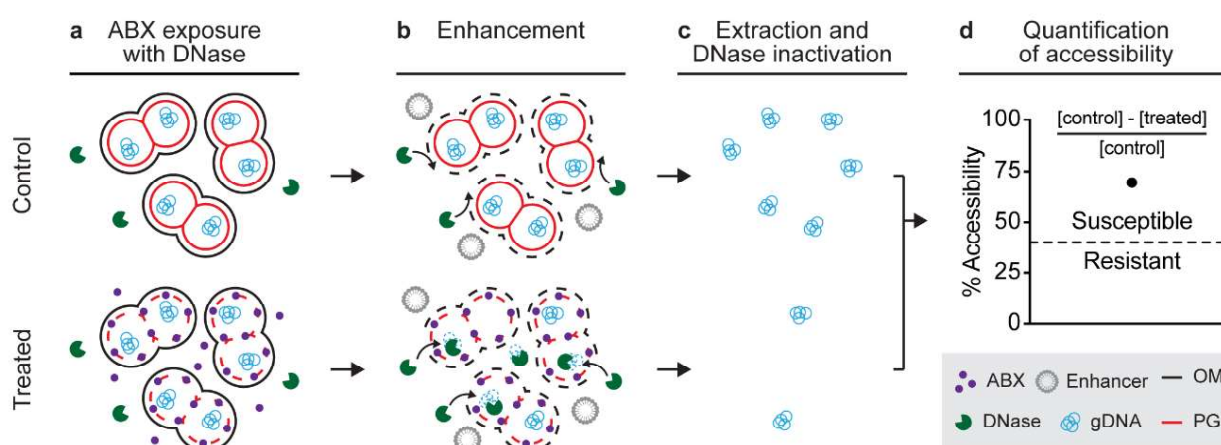


Fig 2-1. The nuc-aAST workflow shown for a sample containing a β -lactam susceptible pathogen. (a) A sample is split into control and treated aliquots; the treated aliquot is exposed to antibiotics (ABX) in the presence of DNase and any extracellular DNA is digested. ABX compromise peptidoglycan (PG) of cells in the treated aliquot. (b) Accessibility to nucleases is enhanced by the addition of an enhancer, which disrupts the outer membrane (OM). Genomic DNA becomes accessible and is degraded in the treated aliquot. Intact peptidoglycan in control samples (or in treated but resistant samples) prevents degradation. (c) Nucleic acids (NAs) are extracted, and DNase is inactivated. (d) Accessibility is quantified by measuring NA concentrations in the control and treated aliquots and dividing the amount of digested DNA by the amount in the control (to yield percentage accessibility). When the percentage accessibility is greater than the threshold (dashed line), the sample is categorized as susceptible.

β -lactams should primarily affect peptidoglycan [61], and should not have a major impact on the outer membrane, which serves as a structural element in Gram-negative bacteria [62]. Therefore, we expected the primary mechanism behind any increase in accessibility to be cell lysis as a result of exposure to β -lactams, leading to release of genomic DNA to the extracellular environment

containing DNase. Additionally, we hypothesized that autolysis, which has been observed as an active stress response in *Ng* [63,64], might accelerate changes in accessibility due to ABX exposure. We tested our hypotheses in a time-course experiment using two penicillin-susceptible (PEN-S) and two penicillin-resistant (PEN-R) *Ng* clinical isolates (Fig 2-2). We observed a significant difference in the percentage accessibility between susceptible and resistant isolates after 90 min of exposure. This is the shortest incubation time for an *Ng* AST with PEN to date, and faster than existing NA-based methods that rely on DNA replication [57]. However, the ideal length of an exposure step for an AST at the POC would be even shorter (15-30 min) to keep the entire workflow within the time period of a patient visit. Thus, we were compelled to further accelerate changes in accessibility of DNA to nuclease as a result of β -lactam exposure in susceptible samples.

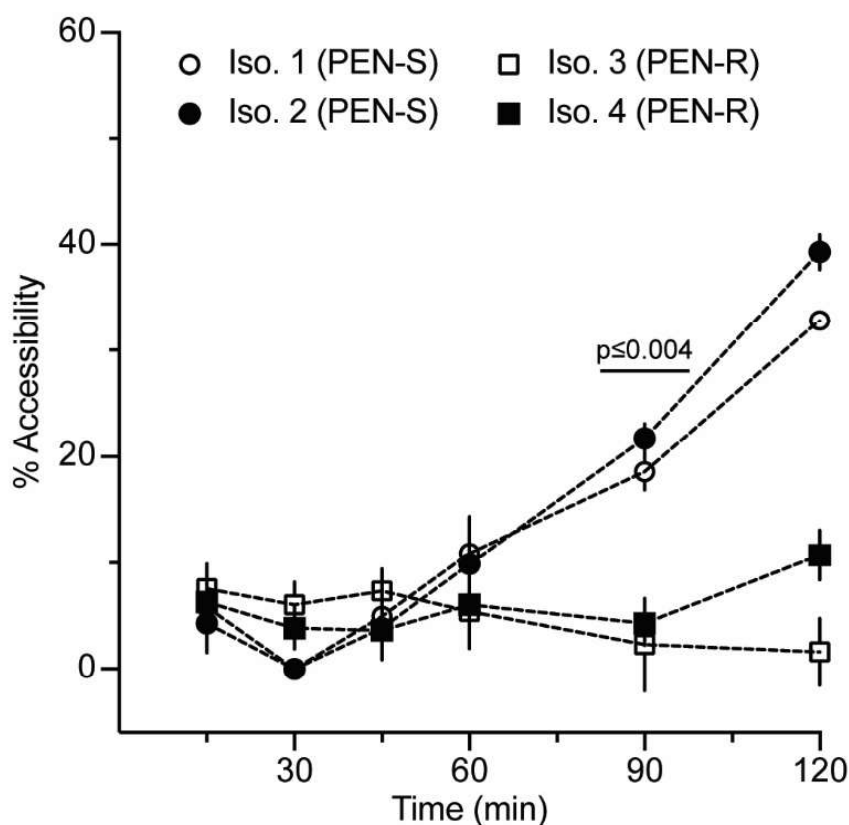


Fig 2-2. Percentage accessibility of DNA over time using the nuc-aAST without the addition of an enhancing step. Two penicillin-susceptible (PEN-S) and two penicillin-resistant (PEN-R) *Ng* isolates were exposed to penicillin in the presence of DNase I. DNA from the control and PEN-treated aliquots was extracted and quantified using qPCR at multiple time points to calculate percentage accessibility. Error bars represent the standard deviation of the PCR triplicates. Data are in Table 2-S10.

Enhancing changes in accessibility

We next hypothesized that the differences in DNA accessibility that we observed between susceptible and resistant isolates exposed to β -lactams could be enhanced using conditions that would increase the permeability of the cell envelope. In Gram-negative organisms like *Ng*, the outer membrane (OM) presents the first, and major, permeability barrier to macromolecules (e.g. nucleases and other enzymes) entering or exiting the cell, typically allowing only small molecules with molecular weights $< \sim 600$ Da to pass through [65,66]. The peptidoglycan, in contrast to the OM, is a looser barrier that has been estimated to allow macromolecules up to 50 kDa to pass through [67-69]. We thus suspected that if the OM could be compromised, damage to the peptidoglycan would result in immediate, measurable changes in accessibility of genomic DNA to DNase, both by allowing DNase to enter and by allowing DNA fragments to exit. Therefore, we hypothesized that we could compromise the OM using an “enhancer” to decrease total assay time.

The ideal enhancer would i) increase DNA accessibility to DNase in cells that have a compromised cell wall as a result of ABX exposure, ii) result in minimal lysis of healthy cells, iii) have a consistent effect on all *Ng* isolates and iv) have no effect on downstream extraction and quantification of NAs. With these parameters in mind, we chose to test hypo-osmotic stress, stimulated autolysis, and four classes of surfactants as potential enhancers.

Hypo-osmotic stress was chosen as a method to enhance lysis of cells with damaged or compromised cell walls because osmotic stress of varying degrees is known to increase release of intracellular contents in Gram-negative bacteria [70-72], although it has never been used to enhance accessibility in the context of AST. We exposed cells to hypo-osmotic conditions by diluting control and treated aliquots 20-fold in water with DNase I and 500 μ M CaCl₂, resulting in a ~ 244 mOsm/kg shift from the ABX exposure conditions. Autolysis was chosen as an enhancer with the rationale of leveraging an already existing stress response in *Ng* to enhance changes in accessibility. Autolysis is a natural stress response in *Ng*, and can be accelerated by incubation in high pH conditions (e.g. Tris, pH 8.5) [73,74]. We hypothesized that using autolysis as an enhancer might result in large changes in NA accessibility. Surfactants were chosen as potential enhancers as a targeted chemical means of disrupting the bacterial cell membrane. We chose a representative surfactant from each of the four major charge-based classes of surfactants to investigate whether surfactant charge might

lead to variability in their effectiveness due to natural variations in the OM of *Ng*. We tested the anionic surfactant sodium dodecyl sulfate (SDS), the cationic surfactant benzalkonium chloride (BAC), the non-ionic surfactant TERGITOL NP (TNP), and the zwitterionic surfactant 3-[(3-Cholamidopropyl)dimethylammonio]-1-propanesulfonate (CHAPS). Each of these surfactant classes, with the exception of zwitterionic surfactants, have been well-studied for their ability to compromise the integrity of the cell envelope [75], but none have been used in the context of AST, or to change DNA accessibility on such short time scales. We chose to include the less well-studied zwitterionic surfactant CHAPS based on the diverse interactions of zwitterionic solutes with the bacterial cell envelope [76].

We tested each potential enhancer with respect to i) the degree of lysis caused by incubation with the enhancer alone, ii) the ability to differentiate PEN-S and PEN-R isolates using an enhancement step after exposure to PEN, and iii) the ability to differentiate CRO-S and CRO-R isolates using an enhancement step after exposure to CRO, and iv) the ability to differentiate CFM-S and CFM-R isolates using an enhancement step after exposure to CFM. We chose to use PEN, CRO, and CFM because we expected that the degree of change in NA accessibility as a result of enhancement would depend on the type of β -lactam used during exposure. CRO, CFM, and PEN bind and inhibit a different profile of penicillin-binding proteins [45,77] and have different rates of killing [78], which we expected would lead to different effects depending on the enhancer. Each enhancer was tested using multiple isolates susceptible or resistant to either PEN, CRO, or CFM. All enhancers were tested using a 5-min enhancement step after 15 min of ABX exposure. Antibiotic-exposure and enhancement steps were performed separately to decouple their effects on the *Ng* isolates.

Enhancers were first tested for the degree of lysis caused by a 5-min incubation with the enhancer alone (Fig 2-3a-f). If the enhancement step lyses the majority of cells even without antibiotic exposure, then accessibility will increase in both control and treated aliquots, and any effect of the antibiotic will be diminished. We observed an average of < 50% lysis when testing all potential enhancers except BAC (Fig 2-3d), which showed an average of 91.6% lysis across all 12 isolates tested (See Table 2-S2 and Table 2-S3 for data).

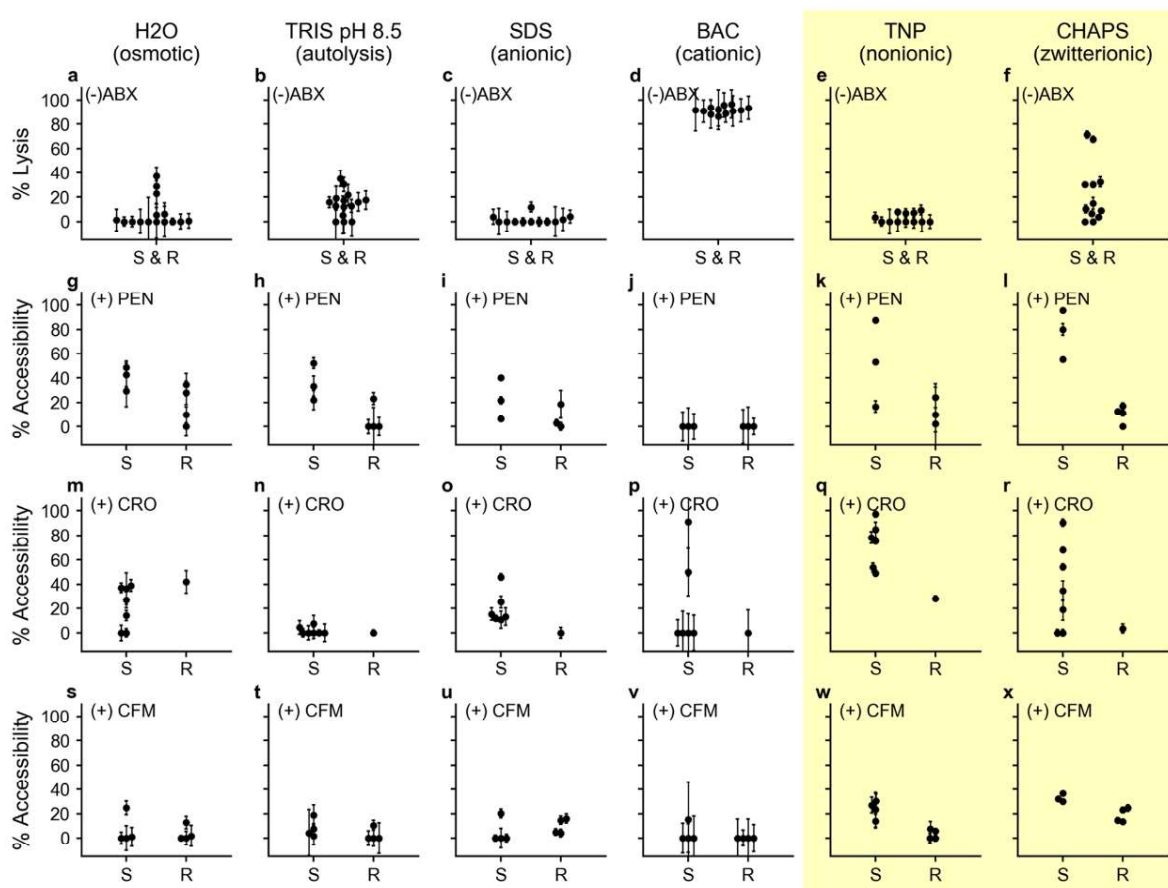


Fig 2-3. Selection of enhancers. Six enhancers were tested for percentage of cell lysis due to enhancer alone (prior to antibiotic exposure) (a-f); enhancement after 15-min exposure to penicillin (PEN) (g-l); enhancement after 15-min exposure to ceftriaxone (CRO) (m-r); and enhancement after 15-min exposure to cefixime (CFM) (s-x). Each point represents a clinical isolate run as a single experiment for that condition. All PCR was performed in technical triplicates with error bars representing the error in the PCR measurement propagated for the calculation of percentage lysis or percentage accessibility; all numerical values are available in Table 2-S2 and Table 2-S3. The yellow shading indicates the two enhancers (TNP and CHAPS) most promising for nuc-aAST. Data for (a-f) are in Table 2-S2 and (g-x) are in Table 2-S3.

We next measured the percentage accessibility when using each enhancer after a 15 min exposure to PEN. We evaluated the ability to differentiate PEN-S and PEN-R isolates based on the average percentage accessibility in S isolates (which we want to be large), the average percentage accessibility in R isolates (which we want to be small), and the magnitude of separation between those two values. Based on these criteria, Tris (Fig 2-3h), TNP (Fig 2-3k), and CHAPS (Fig 2-3l) were the most promising enhancers for differentiating PEN-S and PEN-R isolates after 15 min of exposure. However, we observed differences in accessibility in response to CRO and CFM compared with PEN depending on the enhancer used (Fig 3m-x). Among CFM-S isolates, the responses to

antibiotics and each enhancer were smaller than in PEN-S and CRO-S isolates. TNP and CHAPS were the only tested enhancers that enabled us to differentiate CRO-S and CRO-R responses (Fig 2-3w-x) after 15 min of CFM exposure. We were unable to observe consistently large changes in the seven tested CRO-S isolates using the other two ionic surfactants, SDS (Fig 2-3i,o) and BAC (Fig 2-3j,p), regardless of the ABX treatment. Following these tests, we chose CHAPS as the enhancer to use for validation of the nuc-aAST with clinical isolates because it resulted in low percentage lysis, large increases in DNA accessibility for PEN-S and CRO-S isolates following exposure, and only small increases in the DNA accessibility of PEN-R, CRO-R, and CFM-R isolates.

Validation using clinical isolates

To validate the nuc-aAST we performed 48 ASTs (with at least three biological replicates each) using 21 clinical isolates of *Ng* exposed individually to PEN, CFM, or CRO for 15 min. We then compared the categorical susceptibility determined using the nuc-aAST to the susceptibility determined using gold-standard agar dilution (Fig 2-4a-c). Receiver operating characteristic (ROC) plots [79] (Fig 2-S4) were created so that the area under the curve (AUC) could be calculated separately for each β -lactam tested. After 15 min of exposure we obtained an AUC of 1.000 (PEN), 0.875 (CFM), and 1.000 (CRO). The AUC is determined by scanning a threshold through the ROC plot and measuring the sensitivity and specificity at each theoretical threshold value. This scanning allows one to select the threshold that would differentiate susceptible and resistant organisms with the maximum sensitivity and specificity within the given dataset. For example, an AUC of 1.000 indicates there was a threshold value that perfectly separated susceptible (S) and resistant (R) categories. However, AUC measurements do not consider the experimental noise or the magnitude of separation between S and R samples and should be applied with care to datasets with limited numbers of measurements, such as ours. For example, in the case of CRO, the difference between the single CRO-R isolate that was available to us and the two CRO-S isolates with the lowest responses was small after 15 min of exposure. Therefore, setting the susceptibility threshold between them would be impractical, even though it would yield 100% categorical agreement. We therefore decided to set a single threshold for all three ABX at a more conservative 26.5% even though this threshold generates some errors in both the CFM and CRO measurements after 15 min of ABX exposure. This threshold was chosen because it generated the fewest number of errors with 15 min CFM exposure. The exact value is the average of the closest S and R isolate.

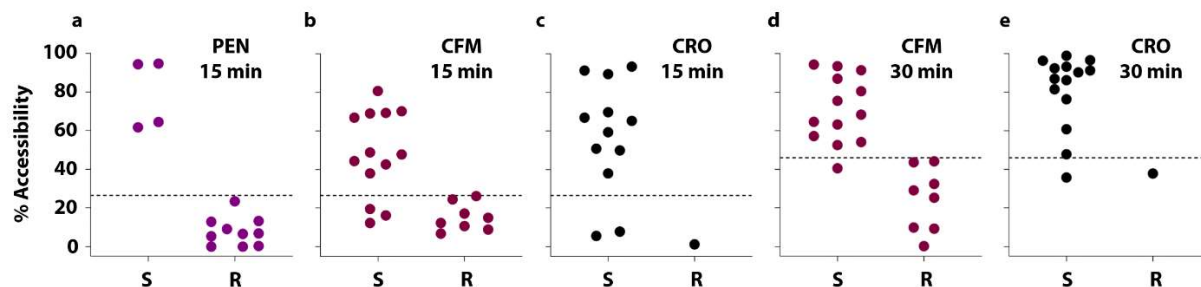


Fig 2-4. Validation of nuc-aAST using clinical isolates. (a-c) nuc-aAST results after 15 min of exposure to (a) penicillin (PEN), (b) cefixime (CFM), and (c) ceftriaxone (CRO). (d-e) nuc-aAST results after exposure to (d) CFM and (e) CRO for 30 min. Each point represents the average for a single isolate run in (at least) biological triplicate for that condition. All PCR was performed in technical triplicate. The dashed line represents the susceptibility threshold, which was set at 26.5% accessibility for 15-min exposures and 46% for 30-min exposures. Data plotted are in Table 2-S4; experimental data from individual replicates are detailed in Table 2-S11 and Table 2-S12.

We then hypothesized that the differences observed in the magnitude of the response of the susceptible isolates after 15 min of exposure to each antibiotic, including the errors observed when testing CFM and CRO, could be the result of differences in how fast each β -lactam affects *Ng* [78]. For example, a possible explanation for differences among isolates in their response to ABX could be phylogenetic differences [80-82]. If isolates differ in their response times, a longer exposure would result in larger average separation between S and R isolates and potentially better categorical agreement if the S isolates were less responsive as a result of a delayed response to antibiotic.

To test the hypothesis that there are inherent differences in isolate response time, we performed nuc-aAST using CFM and CRO with 30-min exposure times and, as predicted, we observed a larger average separation between S and R isolates and only a single error with each ABX. After 15 min of exposure to CFM and CRO, 77% and 83% of susceptible isolates, respectively, were classified as susceptible using nuc-aAST. After 30 min of exposure to CFM and CRO, 95% and 92% categorical agreement was obtained for CFM and CRO, respectively. The AUC for CFM and CRO after 30 min of exposure were 0.917 and 0.981, respectively (Fig 2-S4).

Pilot nuc-aAST tested directly on clinical urine samples

Our long-term goal, well beyond the scope of this paper, is to develop phenotypic AST assays and devices for clinical settings. As a proof-of-concept that our nuc-aAST method is aligned with that goal, we performed pilot nuc-aAST experiments directly on fresh clinical urine samples without a culturing step (see Methods). We note that a phenotypic *Ng* AST has never been successfully

performed directly on clinical samples by any method; the gold standard AST requires isolation of the pathogen and then the AST is performed on the isolate. At the time we began this pilot, it was unknown whether it would even be possible to obtain an AST result directly from a clinical sample without a culturing step. The stability and viability of *Ng* in urine samples has never been characterized, and to reduce the unknown variables, these proof-of-concept nuc-aAST were performed on fresh clinical samples. We set up a satellite lab at the AIDS Healthcare Foundation (AHF) clinic where samples were obtained. The nuc-aAST method depends on DNase I functionality, so we first ran control experiments with a spike-in of lambda DNA into three different urine samples to show that DNase I remained active under the conditions and time frame we are testing (data shown Fig 2-S2). All clinical urine samples reported herein were run immediately after collection (in all four samples, the sample handling began within 30 min of sample donation). Not all clinical samples were positive or yielded AST results (some samples for negative for *Ng* and some could not be reliably quantified, see Methods for details). Six nuc-aASTs were obtained directly on four clinical urine samples; including four with PEN and two with CRO. All nuc-aAST experiments were performed with technical triplicates.

To perform nuc-aAST and gold-standard comparison, each clinical urine sample was divided into two parts, one part was used immediately to run the nuc-aAST and one part was cultured to obtain the isolates for the gold-standard culture-based AST. For the nuc-aAST (Fig 2-5a-b), clinical urine was first centrifuged to concentrate, then resuspended in culture media with saponin (to selectively lyse host cells) and DNase I (to clear free DNA from host and dead bacterial cells) for a 15-min incubation [83-85]. The suspension was centrifuged again and then resuspended in fresh GWM media. Next, the sample was exposed to ABX (PEN or CRO) or the control solution (NF water) for 30 min. Then, all samples were exposed to the enhancer TNP for 3-5 min. Quantification was performed with qPCR and the data analyzed as described in the Methods. The results from each experimental replicate are shown in Fig 2-5d.

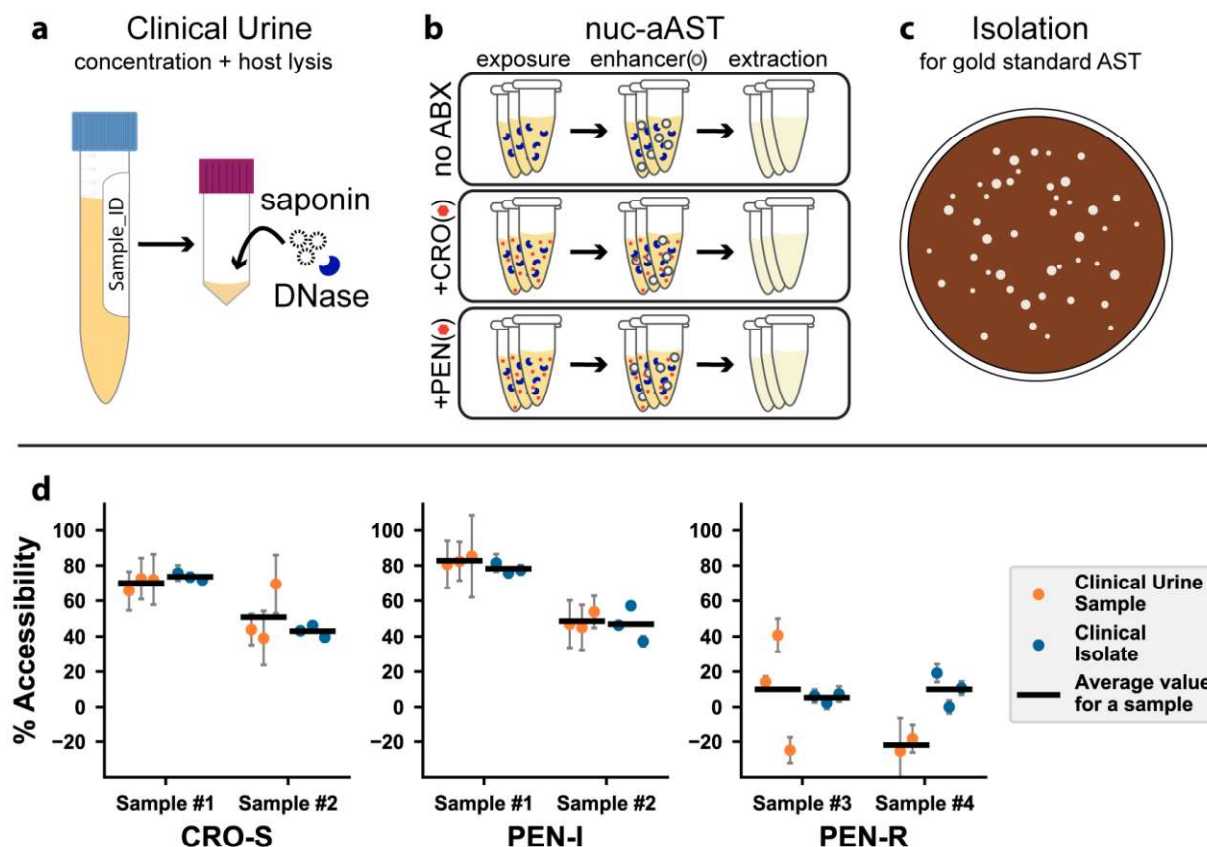


Fig 2-5. Pilot nuc-aAST with clinical urine samples. (a) Clinical urine samples were concentrated by a factor of 5 and incubated with DNase I and saponin for 15 min to lyse host cells and clear free DNA. (b) The nuc-aAST protocol was performed in technical triplicates with no antibiotic (no ABX), ceftriaxone (CRO), or penicillin (PEN). Each nuc-aAST consisted of a 30-min exposure to 1 $\mu\text{g}/\text{mL}$ CRO or PEN followed by a 3-5 min exposure to the enhancer TNP (see Methods for details). (c) Each clinical sample was isolated for gold-standard MIC testing and further experiments. (d) Results of six nuc-aASTs were performed directly on four clinical urine samples and susceptibility was determined (orange points). In parallel, isolates were prepared from these clinical samples and the results of the rapid nuc-aAST with clinical urine samples were compared to the same protocol with the prepared isolate (blue points). The means of the replicates are shown as horizontal lines (Table 2-S7). The minimum inhibitory concentration (MIC) was determined by the gold-standard method (MIC values are provided in Table 2-S1) and the category of susceptible “S”, intermediate “I”, or resistant “R” is shown on the x-axis. Error bars are the error in the PCR measurement propagated for the calculation of percentage lysis or percentage accessibility (Table 2-S6).

To perform the gold-standard culture-based AST, the second part of each of the four clinical urine samples was plated and subcultured on selective media and over the course of 3-5 days, isolates were prepared (details in “MIC testing and creation of clinical isolates” in the Methods). Gold-standard agar-dilution MIC testing was performed on these isolates and the resulting MICs are reported in Fig 2-5d and Table 2-S1. We emphasize that gold standard AST information was obtained days later after nuc-aAST experiments. The isolates from each of these four clinical urine samples were then handled identically to the urine samples, including saponin and DNase I

pretreatments, and the nuc-aAST was repeated. The results of the direct-from-sample nuc-aAST and the results of the nuc-aAST on the isolate from these clinical samples are reported in Fig 2-5d to compare the performance. The nuc-aAST results of the clinical urine sample and the isolate carried out with the same method gave comparable results; notably, the clinical data is (as expected) more variable among replicates which is partially the result of bacterial loads in the urine sample being lower than in the assay run on isolates. A milder nuc-aAST enhancer protocol was chosen for the fresh clinical samples, but when interpreting the data, we conservatively used the 46% threshold from the 30-min clinical isolate experiments shown in Fig 2-4 as a worst case scenario accessibility threshold. A threshold at 46% accessibility (Fig 2-4) correctly categorized all six ASTs from the fresh clinical samples (Table 2-S7) as antibiotic-resistant or not-antibiotic-resistant. When repeated with clinical isolates, the mean percentage accessibility response, for samples with signal above 0%, fell within 8% of mean percentage accessibility of the fresh samples. In follow-up studies a new accessibility threshold will be established with the optimized clinical sample protocol and enhancers.

The pilot nuc-aAST experiments with clinical samples were run with a slightly modified workflow compared with the isolates. For example, we used a slightly shorter enhancement step, and we used TNP instead of CHAPS as the enhancer to minimize background lysis of bacterial cells. Additionally, we only encountered penicillin-intermediate (PEN-I) *Ng* and penicillin-resistant (PEN-R) *Ng*. Because we are testing one concentration of antibiotics (1 $\mu\text{g}/\text{mL}$) in the nuc-aAST, which is above the MIC of the PEN-I *Ng* and below MIC of the PEN-R *Ng*, as expected PEN-I *Ng* gave a susceptible (or “not resistant,” NR) call and PEN-R *Ng* gave a resistant call.

Sum-of-steps total time using contrived urine samples

To make a more realistic measure of total assay time, we modified the extraction and quantification steps of the nuc-aAST. The exposure and enhancement steps were performed as described above, but NA quantification was performed using a rapid, chip-based, digital loop-mediated isothermal amplification (dLAMP) method, as described previously [86]. Additionally, we used a faster, single-step nucleic acid extraction method based on previous work [51]. Both modifications made the workflow faster. Additionally, the high precision of digital quantification allowed us to make a susceptibility call as soon as there was a significant difference between the concentration of NAs in the control and treated aliquots.

We measured total assay time based on the sum of the steps of the nuc-aAST using contrived urine samples. Contrived samples mimic clinical urine samples and allowed us to better evaluate how the assay would perform in a clinical setting compared with assays performed with isolates in media. Samples were created using two PEN-S and two PEN-R isolates; one of the two PEN-R isolates was positive for β -lactamase activity, which we included in order to have PEN-R isolates with different mechanisms of resistance. To perform the AST, samples were first split into control and treated aliquots, and incubated at 37 °C for 15 min. Next the samples were transferred to the enhancement step, and incubated for 5 min in the presence of CHAPS. Samples were then extracted as described above and dLAMP was performed in commercial chips [86]. Images were obtained in real time using a custom imaging system [87]. LAMP quantification was performed using an automated data-analysis workflow in MATLAB [86] in which images are automatically processed and positive wells counted based on a digitized mask created from the final image (Fig 2-6b). NA concentrations were used to determine percentage accessibility as soon as the measured NA concentrations in the susceptible sample became significantly different between the control and treated chips. All samples were tested in a total time (measured as the sum-of-steps) of 30 min and agreed with gold-standard agar dilution (Fig 2-6d). Performance of dLAMP was evaluated on extractions from clinical sample nuc-aAST experiments (Fig 2-6e). The extension of the dLAMP reaction is a result of low nucleic acid concentrations present in the clinical samples (data shown in Table 2- S5).

Here we described a new approach—nuc-aAST—to enable developing a critically needed rapid phenotypic AST for the globally-important pathogen *Neisseria gonorrhoeae*. We show that by measuring the change in the accessibility of DNA after 15 or 30 min β -lactam exposure, the nuc-aAST yields a phenotypic susceptibility readout in less than 1 hour, as opposed to the currently available methods which require hours to days. We further show that the nuc-aAST breaks the current speed limits for nucleic-acid-based phenotypic ASTs using β -lactams (which do not directly impact NAs) by using an innovative approach: coupling cell wall damage to NA readout. The nuc-aAST thus provides a new approach for designing rapid phenotypic ASTs with NA-based readouts for ABX that impact cell envelope integrity. Overall, we envision that leveraging the nuc-aAST and combining it with other creative biological and chemical insights will result in similarly innovative approaches for other important antibiotic classes for *Ng*, such as protein-biosynthesis inhibitors like

tetracycline and azithromycin. Existing NA-based approaches, such as those for ciprofloxacin [25,56], can also be combined alongside the nuc-aAST.

We found that phenotypic ASTs that use NA accessibility as a readout benefit from the use of a carefully chosen enhancer. Here, the enhancement step consisted of a surfactant (CHAPS) that

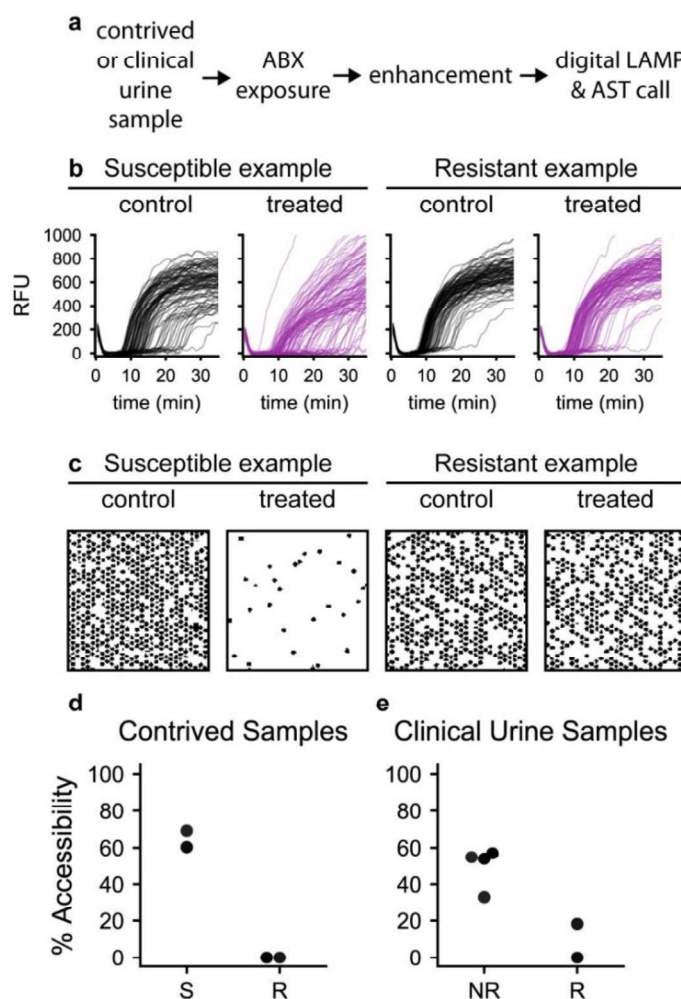


Fig 2-6. The nuc-aAST workflow for contrived and clinical urine samples with each step timed. (a) The nuc-aAST workflow times required for contrived samples are 15 min ABX exposure, 5 min enhancement, 2 min for DNA extraction, 8 min for dLAMP and AST call); timing for clinical urine samples include 30 min ABX exposure, 3-5 min enhancement, 10 min for extraction, and 20 min for dLAMP and AST call. (b) Amplification curves from which positive wells were determined and counted (a subset of 100 wells is shown for each microfluidic chip, 2-S1 – 2-S4 Data) (c) A 2 x 2 mm subsection of masks was created from chips used for performing dLAMP on control and antibiotic-treated aliquots of susceptible and resistant samples; as an illustration, each mask shows ~625 wells (out of ~20,000 total wells) after 10 min of amplification. Wells that showed amplification of *Ng* DNA appear black. (d) The percentage of accessible DNA was determined at earliest significance (7-8 min of amplification; see Methods and Table 2-S5) for two penicillin-

susceptible (S) and two penicillin-resistant (R) samples run using dLAMP (Table 2-S5). Each step was timed individually and the sum-of-steps of the assay was 30 min. (e) Percentage accessibility was determined after 20 min of dLAMP for a representative technical replicate for each of the six nuc-aAST performed directly on four clinical urine samples. Ceftriaxone-susceptible and penicillin-intermediate samples are plotted together as not-resistant (NR) (Table 2-S5; MICs are in Table 2-S1).

enabled detection of cell wall damage faster than cell division. Without the enhancement step, the cell envelope remains intact longer, so measurements of accessibility approximate the timescale of cell division (Fig 2-2), which, for fastidious organisms such as *Ng*, will be too slow for POC applications. Furthermore, on the timescales tested here, DNA release in susceptible, treated samples may in part be the result of β -lactams “porating” the cell wall or cell lysis as a result of stress. Cell wall turnover may also proceed even if cells are not actively dividing. In both cases, the enhancement step is critical to shorten the time required to detect a difference between control and antibiotic-treated samples. The increase in DNA accessibility in susceptible isolates will differ based on the combination of β -lactam used and enhancer, highlighting the importance of testing multiple β -lactams with the nuc-aAST. Of the surfactants tested as enhancers, the charge-neutral surfactants TNP and CHAPS gave better results than the ionic surfactants SDS and BAC, suggesting that charge may be an important factor when designing an effective enhancement step. We also anticipate organism-specific OM chemistry and general stress responses will play a role in determining which enhancers are optimal in other organisms.

We found that for PEN, susceptibility of *Ng* could be determined after just 15 min of exposure in all isolates tested (Fig 2-4a). However, for CFM and CRO, a small number of S isolates did not respond after 15 min of exposure but almost perfect categorical agreement was obtained after 30 min of exposure (Fig 2-4b-e) shown by ROC curve AUC of 0.917 for CRO at 30 min exposure and an AUC of 0.981 for CFM at 30 min exposure (Fig 2-S4d-e). We hypothesize that CFM and CRO required a longer exposure than PEN because of their differences in binding kinetics and rates of killing [77,78,88]. Despite these differences, an actionable susceptibility call (i.e. determining that a susceptible isolate is susceptible to a particular ABX and therefore can be treated with that ABX) could still be made for most isolates after 15 min of exposure. The errors yielded from the nuc-aAST at 15 min of ABX exposure would not result in ineffective treatment because these errors are from susceptible isolates (three CFM-S and two CRO-S) that were misidentified as resistant. We emphasize that in our isolate dataset, these errors are reduced to one CFM-S and one CRO-S isolate by extending ABX incubation time by just 15 min. One approach to balance reducing assay time

with minimizing errors is to perform two exposures in parallel for each ABX. The first exposure would be analyzed after 15 minutes. If a response is obtained indicating that the pathogen is susceptible (which should be the case for the majority of patients), the second exposure would be discarded. If no response or if an equivocal response is obtained, then the second exposure (after 30 min total) would be analyzed to provide the definitive susceptibility call. With this approach, the test would provide the answer after 15 min of ABX exposure for the majority of patients, and only a few patients would be delayed by the additional 15 min of ABX exposure.

Several limitations will need to be overcome in order to translate the nuc-aAST approach to an automated and distributable system. First, in this paper we used clinical isolates, contrived urine samples, and four clinical urine samples. Although contrived samples are a good proxy for clinical samples and are accepted by the U.S. Food and Drug Administration in certain cases [89], we also wished to perform a pilot experiment to demonstrate the nuc-aAST can work directly on fresh clinical samples. Our six nuc-aAST experiments gave good agreement with the ASTs that were run on isolates taken from the same samples (Figs 2-5 and 2-6). These pilot data suggest that the nuc-aAST can be adapted to work directly on clinical urine samples without the need for a culturing step, and can utilize existing digital LAMP techniques from crude lysate of a clinical sample. Because there is no rapid (20 min) point of care *Ng* identification test currently available, we had to run ASTs without knowing whether the samples are positive for *Ng*; as expected, not all clinical samples collected yielded interpretable AST data (see Methods). Further development will be needed to optimize the nuc-aAST for clinical use. Performing phenotypic AST on clinical samples is extremely challenging and has only been demonstrated a few times, many from clinical UTI samples [51,53,90,91]. This manuscript is a demonstration of a phenotypic AST used directly on *Ng* clinical samples. Many recent breakthroughs in phenotypic AST are initially reported without any validation with clinical samples; most papers use isolates [56,81], contrived samples [57,92-94] or positive blood cultures [95] instead of raw clinical samples. Second, future work should test more *Ng* isolates with diverse phylogeny [80-82] when they are made available to researchers and characterized, as well as test isolates with intermediate resistance to PEN, CFM, and CRO. These efforts could also aim to establish a correlation in the magnitude of nuc-aAST response and minimum inhibitory concentration (MIC) of ABX, which would provide even more detailed information at the POC. Third, in timing the sum-of-steps, we did not include handling time; future work should include

optimization of handling steps and timed sample-to-answer experiments. Finally, the nuc-aAST method will need to be translated to a POC device so that larger-scale clinical evaluations can be performed. Devices for multiplexed digital quantification [96-98] have been demonstrated and would be useful in performing nuc-aAST for multiple ABX in parallel.

We envision that nuc-aAST would be deployed in combination with two complementary technologies: (i) the pathogen ID technologies that are being developed by others [20,21,23,24] to identify *Ng*-positive samples that require an AST, and (ii) rapid genotypic and/or phenotypic ASTs that rely on NA readouts for other ABX used in the treatment of *Ng*, including fluoroquinolones (ciprofloxacin) [25,51,81] and protein synthesis inhibitors (tetracycline and azithromycin) [81]. Assuming these two complementary technologies are developed and validated, further development of nuc-aAST would provide the last—and we would argue the most challenging—piece needed for a complete rapid ID/AST workflow for *Ng* based on NA readout. We chose NA readout for the nuc-aAST for two reasons. First, NA readouts will enable easy integration with pathogen ID and other NA-based AST technologies. Second, NA readouts are organism-specific [51], and therefore should be effective even for mixed microbial populations potentially present in clinical samples (e.g., *Ng* in the presence of commensals or other pathogens).

Implementation of a rapid phenotypic AST would dramatically improve the antibiotic stewardship of *Ng* infections and therefore impact the health of people who are infected with *Ng*; currently, there are an estimated 78,000,000 global cases of *Ng* every year [99]. Furthermore, the nuc-aAST approach provides a framework for developing additional accessibility-based AST chemistries for other pathogens that pose global health threats but have been challenging for current phenotypic AST methods. For example, we have shown that quantifying NA accessibility to polymerases can be used to rapidly determine ABX susceptibility in Enterobacteriaceae [100]. Overall, this work highlights the diagnostic capabilities that can be attained by developing innovative NA-based assays for AST; further expansion and application of these approaches is critically needed to address the crisis posed by antibiotic-resistant bacteria.

DISCUSSION

Here we described a new approach—nuc-aAST—to enable developing a critically needed rapid phenotypic AST for the globally-important pathogen *Neisseria gonorrhoeae*. We show that by measuring the change in the accessibility of DNA after 15 or 30 min β -lactam exposure, the nuc-aAST yields a phenotypic susceptibility readout in less than 1 hour, as opposed to the currently available methods which require hours to days. We further show that the nuc-aAST breaks the current speed limits for nucleic-acid-based phenotypic ASTs using β -lactams (which do not directly impact NAs) by using an innovative approach: coupling cell wall damage to NA readout. The nuc-aAST thus provides a new approach for designing rapid phenotypic ASTs with NA-based readouts for ABX that impact cell envelope integrity. Overall, we envision that leveraging the nuc-aAST and combining it with other creative biological and chemical insights will result in similarly innovative approaches for other important antibiotic classes for *Ng*, such as protein-biosynthesis inhibitors like tetracycline and azithromycin. Existing NA-based approaches, such as those for ciprofloxacin [25,56], can also be combined alongside the nuc-aAST.

We found that phenotypic ASTs that use NA accessibility as a readout benefit from the use of a carefully chosen enhancer. Here, the enhancement step consisted of a surfactant (CHAPS) that enabled detection of cell wall damage faster than cell division. Without the enhancement step, the cell envelope remains intact longer, so measurements of accessibility approximate the timescale of cell division (Fig 2-2), which, for fastidious organisms such as *Ng*, will be too slow for POC applications. Furthermore, on the timescales tested here, DNA release in susceptible, treated samples may in part be the result of β -lactams “porating” the cell wall or cell lysis as a result of stress. Cell wall turnover may also proceed even if cells are not actively dividing. In both cases, the enhancement step is critical to shorten the time required to detect a difference between control and antibiotic-treated samples. The increase in DNA accessibility in susceptible isolates will differ based on the combination of β -lactam used and enhancer, highlighting the importance of testing multiple β -lactams with the nuc-aAST. Of the surfactants tested as enhancers, the charge-neutral surfactants TNP and CHAPS gave better results than the ionic surfactants SDS and BAC, suggesting that charge may be an important factor when designing an effective enhancement step. We also anticipate organism-specific OM chemistry and general stress responses will play a role in determining which enhancers are optimal in other organisms.

We found that for PEN, susceptibility of *Ng* could be determined after just 15 min of exposure in all isolates tested (Fig 2-4a). However, for CFM and CRO, a small number of S isolates did not respond after 15 min of exposure but almost perfect categorical agreement was obtained after 30 min of exposure (Fig 2-4b-e). We hypothesize that CFM and CRO required a longer exposure than PEN because of their differences in binding kinetics and rates of killing [77,78,88]. Despite these differences, an actionable susceptibility call (i.e. determining that a susceptible isolate is susceptible to a particular ABX and therefore can be treated with that ABX) could still be made for most isolates after 15 min of exposure. The errors yielded from the nuc-aAST at 15 min of ABX exposure would not result in ineffective treatment because these errors are from susceptible isolates (three CFM-S and two CRO-S) that were misidentified as resistant. We emphasize that in our isolate dataset, these errors are reduced to one CFM-S and one CRO-S isolate by extending ABX incubation time by just 15 min. One approach to balance reducing assay time with minimizing errors is to perform two exposures in parallel for each ABX. The first exposure would be analyzed after 15 minutes. If a response is obtained indicating that the pathogen is susceptible (which should be the case for the majority of patients), the second exposure would be discarded. If no response or if an equivocal response is obtained, then the second exposure (after 30 min total) would be analyzed to provide the definitive susceptibility call. With this approach, the test would provide the answer after 15 min of ABX exposure for the majority of patients, and only a few patients would be delayed by the additional 15 min of ABX exposure.

Several limitations will need to be overcome in order to translate the nuc-aAST approach to an automated and distributable system. First, in this paper we used clinical isolates, contrived urine samples, and four clinical urine samples. Although contrived samples are a good proxy for clinical samples and are accepted by the U.S. Food and Drug Administration in certain cases [89], we also wished to perform a pilot experiment to demonstrate the nuc-aAST can work directly on fresh clinical samples. Our six nuc-aAST experiments gave good agreement with the ASTs that were run on isolates taken from the same samples (Figs 2-5 and 2-6). These pilot data suggest that the nuc-aAST can be adapted to work directly on clinical urine samples without the need for a culturing step, and can utilize existing digital LAMP techniques from crude lysate of a clinical sample. Because there is no rapid (20 min) point of care *Ng* identification test currently available, we had to run ASTs without knowing whether the samples are positive for *Ng*; as expected, not all clinical samples

collected yielded interpretable AST data (see Methods). Further development will be needed to optimize the nuc-aAST for clinical use. Performing phenotypic AST on clinical samples is extremely challenging and has only been demonstrated a few times, many from clinical UTI samples [51,53,90,91]. This manuscript is a demonstration of a phenotypic AST used directly on *Ng* clinical samples. Many recent breakthroughs in phenotypic AST are initially reported without any validation with clinical samples; most papers use isolates [56,81], contrived samples [57,92-94] or positive blood cultures [95] instead of raw clinical samples. Second, future work should test more *Ng* isolates with diverse phylogeny [80-82] when they are made available to researchers and characterized, as well as test isolates with intermediate resistance to PEN, CFM, and CRO. These efforts could also aim to establish a correlation in the magnitude of nuc-aAST response and minimum inhibitory concentration (MIC) of ABX, which would provide even more detailed information at the POC. Third, in timing the sum-of-steps, we did not include handling time; future work should include optimization of handling steps and timed sample-to-answer experiments. Finally, the nuc-aAST method will need to be translated to a POC device so that larger-scale clinical evaluations can be performed. Devices for multiplexed digital quantification [96-98] have been demonstrated and would be useful in performing nuc-aAST for multiple ABX in parallel.

We envision that nuc-aAST would be deployed in combination with two complementary technologies: (i) the pathogen ID technologies that are being developed by others [20,21,23,24] to identify *Ng*-positive samples that require an AST, and (ii) rapid genotypic and/or phenotypic ASTs that rely on NA readouts for other ABX used in the treatment of *Ng*, including fluoroquinolones (ciprofloxacin) [25,51,81] and protein synthesis inhibitors (tetracycline and azithromycin) [81]. Assuming these two complementary technologies are developed and validated, further development of nuc-aAST would provide the last—and we would argue the most challenging—piece needed for a complete rapid ID/AST workflow for *Ng* based on NA readout. We chose NA readout for the nuc-aAST for two reasons. First, NA readouts will enable easy integration with pathogen ID and other NA-based AST technologies. Second, NA readouts are organism-specific [51], and therefore should be effective even for mixed microbial populations potentially present in clinical samples (e.g., *Ng* in the presence of commensals or other pathogens).

Implementation of a rapid phenotypic AST would dramatically improve the antibiotic stewardship of *Ng* infections and therefore impact the health of people who are infected with *Ng*;

currently, there are an estimated 78,000,000 global cases of *Ng* every year [99]. Furthermore, the nuc-aAST approach provides a framework for developing additional accessibility-based AST chemistries for other pathogens that pose global health threats but have been challenging for current phenotypic AST methods. For example, we have shown that quantifying NA accessibility to polymerases can be used to rapidly determine ABX susceptibility in Enterobacteriaceae [100]. Overall, this work highlights the diagnostic capabilities that can be attained by developing innovative NA-based assays for AST; further expansion and application of these approaches is critically needed to address the crisis posed by antibiotic-resistant bacteria.

METHODS

Ethics statement. Clinical urine samples were collected at the AIDS Healthcare Foundation (AHF) clinic under Caltech IRB #18-0865 from consented male patients symptomatic for *N. gonorrhoeae*.

Study Design. The objective of this study was to develop a rapid phenotypic AST for β -lactams based on DNA accessibility to nuclease for use with *Neisseria gonorrhoeae* (*Ng*). The key hypotheses of this work were: (i) following antibiotic exposure, DNA in susceptible cells would be more accessible to an exogenously added nuclease than DNA in resistant cells due to cell wall damage as a result of exposure to antibiotics, (ii) this difference would occur faster than cell division, and (iii) this difference in accessibility could be detected sooner if a surfactant enhancement step was included. To test the first two hypotheses, we performed an exposure timecourse using two penicillin-susceptible and two penicillin-resistant clinical isolates of *Ng*. To test the third hypothesis, we performed 48 nuc-aASTs using 21 clinical *Ng* isolates (exposed to ABX for 15 min) and 36 nuc-aASTs using 21 clinical *Ng* isolates (exposed to ABX for 30 min). We then compared the results to gold-standard agar dilution.

To calculate the sample size, the methods and Equation 5 from [101] were used as described previously [51]. Namely, we suspected that the specificity and sensitivity of the nuc-aAST method would be 95% with a desired margin of error of $\pm 10\%$. Under these conditions, 18.2 (or 19) samples must be tested with the nuc-aAST method and compared to the gold standard. For 15 min ABX exposures, we performed 29 ASTs with isolates susceptible to the ABX being tested, and 19 ASTs with isolates resistant to the ABX being tested.

Isolates and agar-dilution MIC testing. Isolates were provided by the University of Washington Neisseria Reference Laboratory and the Centers for Disease Control (CDC) Antibiotic Resistance Isolate Bank *Neisseria gonorrhoeae* panel (Table 2-S1). MICs of the CDC AR Isolate Bank are reported by the CDC [102], and MIC of all other isolates were determined by agar dilution according to the Clinical and Laboratory Standards Institute (CLSI) guidelines [103].

Reagents and culture media. BD BBL Chocolate II Agar prepared plated media (GC II Agar, with Hemoglobin and BD IsoVitaleX) was purchased from VWR International LLC (VWR, Radnor, PA, USA). Graver-Wade Medium (GWM) was prepared as described previously [38]. Cation-adjusted Mueller Hinton II Broth (MHB) (BD, Franklin Lakes, NJ, USA) was prepared according to manufacturer instructions. All sodium bicarbonate (NaHCO_3) (Sigma, St. Louis, MO, USA) and calcium chloride (CaCl_2) (Fisher Scientific, Hampton, NH, USA) stocks were dissolved in nuclease-free water (NF- H_2O) and sterilized using 0.2- μm filters. DNase I (2000 U/mL) was obtained from New England Biolabs (NEB; Ipswich, MA, USA). Normal urine from pooled human donors was purchased from Lee Biosolutions (Maryland Heights, MO, USA) and filtered through 0.2- μm filters before use.

Antibiotic stocks were prepared and stored as single-use aliquots at $-80\text{ }^\circ\text{C}$. Aliquots were thawed once and diluted in NF- H_2O before use. PEN (1 mg/mL) was prepared from penicillin G sodium salt (Sigma, St. Louis, MO, USA) in NF- H_2O . CRO (1 mg/mL) was prepared from ceftriaxone disodium salt hemi(heptahydrate) (Sigma) in NF- H_2O . CFM (5 mg/mL) was prepared from cefixime trihydrate (Sigma) in DMSO.

Unless otherwise noted, enhancer stock solutions were prepared in NF- H_2O and stored at room temperature. Tris buffer (500 mM; pH 8.5 at $37\text{ }^\circ\text{C}$) was prepared according to the Sigma buffer reference tables [104] using 0.2- μm filter sterilized stocks of 1 M Tris-HCl (Sigma) and 1 M Tris base (Fisher Scientific) prepared in milliQ H_2O . TNP HLB 13.1 (100 mM) was prepared by mixing 334 μL 100 mM Tergitol NP-9 (Sigma) + 666 μL 100 mM Tergitol NP-10 (Sigma). CHAPS (200 mM) was prepared from CHAPS solid powder (Sigma). 0.1% sodium dodecyl sulfate (SDS) was prepared by diluting 10% SDS (Invitrogen, Carlsbad, CA, USA). BAC (10%) was prepared from benzalkonium chloride solid powder (MP Biomedicals, Santa Ana, CA, USA).

Nucleic acid quantification. Quantitative PCR (qPCR) was performed using ssoFast EvaGreen Supermix (BioRad, Hercules, CA, USA) in 10 μ L reactions with 500 nM primers targeting the *Ng* 16S rRNA gene [105]. DNA template composed 10% of the reaction volume. Cycling conditions consisted of 3.0 min at 95 °C, followed by 35 cycles of 15 sec at 95 °C, 15 sec at 62 °C, and 20 sec at 72 °C. All qPCR was performed on either a Roche LightCycler 96 or BioRad CFX96 instrument. The C_q values obtained from qPCR are used to compute the percentage accessibility and percentage lysis as described in the equations below. Any negative percentages were set to 0 for plotting.

$$(1) \% \text{ Accessibility (control and treated)} = (1 - 2^{(c_{q\text{control}} - c_{q\text{treated}})}) \times 100$$

$$(2) \text{ PCR error \% Accessibility} = \sqrt{\left(\frac{\sigma_C}{\mu_C}\right)^2 + \left(\frac{\sigma_T}{\mu_T}\right)^2} \times 100$$

- $C = \text{linearized control } Cqs = 2^{C_{q\text{control}}}$
- $T = \text{linearized treated } Cqs = 2^{C_{q\text{treated}}}$
- $\sigma = \text{standard deviation}$
- $\mu = \text{mean}$

$$(3) \% \text{ Lysis (no enhancer and enhancer)} = (1 - 2^{(c_{q\text{no enhancer}} - c_{q\text{enhancer}})}) \times 100$$

$$(4) \text{ PCR error \% Lysis} = \sqrt{\left(\frac{\sigma_N}{\mu_N}\right)^2 + \left(\frac{\sigma_E}{\mu_E}\right)^2} \times 100$$

- $N = \text{linearized no enhancer } Cqs = 2^{C_{q\text{no enhancer}}}$
- $E = \text{linearized enhancer } Cqs = 2^{C_{q\text{enhancer}}}$
- $\sigma = \text{standard deviation}$
- $\mu = \text{mean}$

Droplet digital PCR (ddPCR) was performed using QX200 ddPCR Supermix for EvaGreen (BioRad, Hercules, CA, USA) with the same primers and primer concentrations used in qPCR. DNA template composed 10% of the reaction volume. Cycling conditions consisted of 5.0 min at 95 °C, followed by 40 cycles of 30 sec at 95 °C, 30 sec at 60 °C, and 30 sec at 72 °C, followed by a droplet stabilization step of 4 °C for 5 min, and 95 °C for 5 min. Calculations of percentage accessibility and percentage lysis for ddPCR are given the equations below, where λ represents template concentration in copies/ μ L. The template concentrations are used to compute percentage accessibility and percentage lysis as described in the equations below. Any negative percentages were set to 0 for all analyses.

$$(5) \% \text{ Accessibility (control and treated)} = \left(1 - \left(\frac{\lambda_{\text{treated}}}{\lambda_{\text{control}}}\right)\right) \times 100$$

$$(6) \% \text{ Lysis (no enhancer and enhancer)} = \left(1 - \left(\frac{\lambda_{\text{enhancer}}}{\lambda_{\text{no enhancer}}}\right)\right) \times 100$$

A dLAMP assay was performed using a previously published system [86]. The dLAMP mix consisted of 1 μL NEB Isothermal Amplification Buffer (200 mM Tris-HCl, 20 mM MgSO_4 , 500 mM KCl, 100 mM $(\text{NH}_4)_2\text{SO}_4$, 1% Tween 20, pH 8.8), 0.6 μL MgSO_4 , 0.5 μL BSA (20 mg/mL), 0.4 μL Syto-9 (50 μM , prepared within two weeks of use), 1.4 μL dNTPs (10 mM each), 0.5 μL 20X primer mix, 0.4 μL NEB Bst 2.0 WarmStart, 0.2 μL Ambion RNase cocktail, 4.0 μL $\text{NF-H}_2\text{O}$, and 1 μL of template. Primers were designed to target the *Ng* 16S gene, and screened as described previously [51]. Primer sequences used are as follows, with the final concentration in the amplification mix in parentheses: GCGGTGGATGATGTGGATT (forward outer primer, 0.2 μM), CCGGCAGTCTCATTAGAGTG (backward outer primer, 0.2 μM), CTCCTCCGTCTCCGGAGGATTCaaaaCGATGCAACGCGAAGAAC (forward inner primer, 1.6 μM), TCGTCAGCTCGTGTCTGAGATttttCCCAACCGAATGATGGCA (backward inner primer, 1.6 μM), CGCACATGTCAAACCAGG (forward loop primer, 0.4 μM), and GCAACGAGCGCAACCC (reverse loop primer, 0.4 μM). Equation 3 was used to compute percentage accessibility, where λ represents the template NA concentration in copies/ μL as measured by dLAMP.

***Ng* culture preparation.** Isolates were streaked from glycerol stocks stored at -80°C onto BD BBL Chocolate II Agar plates and incubated overnight in a 37°C incubator with 5% CO_2 . Isolates were then passed onto fresh BD BBL Chocolate II Agar plates and grown for 4-7 h at 37°C with 5% CO_2 . In all experiments, cells from plates passed 1-3 times were used. Several colonies were scraped and resuspended in 37°C GWM to generate a working suspension. Optical density at 600 nm (OD_{600}) was measured, and the working suspension was diluted to create a 2 mL working culture of OD_{600} 0.05 in GWM in 15 mL polypropylene culture tubes. Cultures were incubated, with 500 rpm shaking, at $37^\circ\text{C} + 5\% \text{CO}_2$ for 3-5 h prior to ABX exposure.

nuc-aAST time-course without enhancing step. Working cultures of *Ng* isolates were prepared as described in “*Ng* culture preparation.” Incubation at 37°C was performed in 100 μL reaction volumes in PCR tube strips on a BioRad C1000 Thermal Cycler. Treated samples consisted of 77.5

μL MHB, 2.5 μL NaHCO_3 (200 mM), 5 μL DNase I (2 U/ μL), 5 μL PEN (20 $\mu\text{g}/\text{mL}$), and 10 μL working *Ng* isolate culture. PEN was replaced with NF-H₂O in control samples. A 10 μL aliquot of each sample was extracted at 15, 30, 45, 60, 90, and 120 min and diluted 10X in QuickExtract DNA Extraction Solution (Lucigen, Middleton, WI, USA), then heated for 6 min at 65 °C followed by 4 min at 98 °C on a BioRad C1000 Thermal Cycler. All sample handling following antibiotic exposure was performed using a multichannel pipette; qPCR and calculation of % accessibility were performed as described above.

Enhancer use. Working cultures of *Ng* isolates were prepared as described in “*Ng* culture preparation.” Initial exposure was performed by incubating 100 μL control and treated samples at 37 °C in PCR tube strips on a BioRad C1000 Thermal Cycler. Treated samples consisted of 75 μL MHB, 5 μL NaHCO_3 (100 mM), 5 μL DNase I (2 U/ μL), 5 μL PEN or CRO (20 $\mu\text{g}/\text{mL}$), and 10 μL working *Ng* isolate culture. ABX were replaced with NF-H₂O in control samples. After 15 min of incubation, samples were vortexed and quick-spun, and aliquots of all samples were transferred to the enhancement step as described below. After the enhancement step, 5 or 10 μL of all samples were extracted by diluting 10X in QuickExtract DNA Extraction Solution (Lucigen) and heating for 6 min at 65 °C followed by 4 min at 98 °C on a BioRad C1000 Thermal Cycler. All sample handling following ABX exposure was performed using a multichannel pipette; qPCR and calculation of % accessibility was performed as described above.

Osmotic and autolytic enhancing steps were performed in 100 μL volumes. The osmotic enhancing step consisted of 89.75 μL NF-H₂O, 4.75 μL DNase I (2 U/ μL), 0.5 μL CaCl_2 (100 mM, 0.2- μM filtered), and 5 μL initial exposure samples. The autolytic enhancing step consisted of 75 μL NF-H₂O, 4.75 μL NaHCO_3 (100 mM, 0.2- μM filtered), 10 μL Tris pH 8.5 (500 mM), 4.75 μL DNase I (2 U/ μL), 0.5 μL CaCl_2 (100 mM), and 5 μL of the sample exposed to antibiotic.

All surfactant-enhancing steps were performed in 50 μL volumes with 25 of the 50 μL consisting of initial exposure samples. In the TNP enhancement step, the remaining 25 μL consisted of 1.25 μL DNase I (2 U/ μL), 1.25 μL NaHCO_3 (100 mM), 20 μL MHB, and 2.5 μL TNP (100 mM). In the CHAPS enhancement step, the remaining 25 μL consisted of 1.25 μL DNase I (2 U/ μL), 1.25 μL NaHCO_3 (100 mM), 20 μL MHB, and 2.5 μL CHAPS (200 mM). In the SDS and BAC

enhancement steps, the remaining 25 μL consisted of 1.25 μL DNase I (2 U/ μL), 1.25 μL NaHCO_3 (100 mM), 17.5 μL MHB, and either 5 μL SDS (1% w/v) or BAC (1% w/v), respectively.

Nuclease-accessibility AST validation. Working cultures were prepared, exposed to ABX, and enhancing steps performed as described for the CHAPS enhancement step in the “enhancer selection” section above. Extraction was performed as described above. Treated samples in the initial exposure step had a final concentration of 1.0 $\mu\text{g}/\text{mL}$ PEN, CFM, or CRO. Samples were excluded if the percentage lysis (equation 2) due to CHAPS was $> 75\%$. If the percentage lysis was negative, the value was set to zero before averaging. Three to thirteen biological replicates were performed for each isolate-antibiotic combination. Biological replicates included separate antibiotic exposure, control exposure, and no-enhancer controls.

Preparation of clinical sample suspensions. After initial urine collection by a patient, AHF research staff pipetted an 8–14 mL aliquot into a 15 mL conical tube. For each clinical sample, handling began within 30 min of the sample donation. A 1 mL aliquot of the clinical urine was centrifuged in a 2 mL screw-cap microcentrifuge tube (VWR) for 5 min at 1,000 x g (Eppendorf 5418). The supernatant was then immediately removed, and the pellets resuspended in GWM to generate a working suspension. Next, a 320 μL aliquot of the working suspension was added to a mixture of 40 μL 10X DNase I Reaction Buffer (NEB), 20 μL , DNase I (2000 U/mL) (NEB), and 20 μL Saponin (20% w/v; Cas#8047-15-2, TCI). The suspension was then vortexed, spun in a benchtop microcentrifuge at 2,000 x g for 2-3 sec (Labnet Spectrafuge Mini Microcentrifuge), and placed on a heat block (GeneMate Mini Dry Bath) at 37 $^{\circ}\text{C}$ for 15 min. Next, the suspension was vortexed and centrifuged for 5 min at 1,000 x g. The supernatant was removed, and the pellet resuspended in a mixture of equal volume and concentration of GWM, DNase I Reaction Buffer, and DNase I, as described above.

Clinical sample nuc-aAST. Suspensions of clinical urine samples were prepared as described above. All suspensions were generated, and the ABX-exposure step initiated within 90 min of sample donation. The initial ABX-exposure was performed by incubating 50 μL control and treated samples at 37 $^{\circ}\text{C}$ in PCR tube strips on a BioRad C1000 Thermal Cycler. Treated samples consisted of 48.8 μL of suspension and 1.25 μL aliquot of PEN or CRO (40 $\mu\text{g}/\text{mL}$). ABX were replaced with $\text{NF-H}_2\text{O}$ in control samples. After 30 min of incubation, samples were vortexed and quickly spun on a

benchtop microcentrifuge (Labnet) at 2,000 x g for 2-3 sec, and 2.7 μ L TNP (100 mM) was added to each sample for the enhancement step. Samples were then immediately vortexed, spun on a benchtop microcentrifuge (Labnet) at 2,000 x g for 2-3 sec, and incubated at 37 °C for 3-5 min. After the enhancement step, 20 μ L from each sample was extracted by diluting 5X in QuickExtract DNA Extraction Solution (Lucigen) and heating for 6 min at 65 °C followed by 4 min at 98 °C on a BioRad C1000 Thermal Cycler. All sample handling following ABX exposure was performed using a multichannel pipette; qPCR and calculation of percentage accessibility were performed as previously described, with the modification that the qPCR mix included 2 μ L of template per 10 μ L PCR reaction instead of 1 μ L template per 10 μ L reaction.

When processing the nucleic acid measurements, sample-inclusion criteria were as follows: samples must have had a 16S DNA concentration in the no-ABX control tube of less than a Cq of 29 (which translates to approximately 200 copies of 16S DNA/ μ L DNA extraction or 20 copies/ μ L in the PCR or LAMP reaction). ASTs from clinical samples with a negative percentage accessibility calculated to be less than -30% accessibility, or those with only one usable replicate out of three, were excluded from analysis.

MIC testing and creation of clinical isolates. While each of the clinical samples was being run with the nuc-aAST protocol, a 5-10 mL aliquot of the same clinical urine sample was packaged and transported on ice from AHF (Los Angeles, CA) to the laboratory at Caltech (Pasadena, CA). At the Caltech lab, a 50 μ L aliquot was plated onto *Neisseria*-selective media (Modified Thayer Martin II (MTMII) Agar; Fisher Scientific) and incubated for 24-72 h at 37 °C and 5% CO₂. Four individual colonies were sub-cultured onto a fresh MTMII agar plate and incubated for 8-48 h at 37 °C and 5% CO₂. The agar plates were parafilm-sealed, packaged, and shipped overnight via FedEx at ambient temperature for isolation and gold-standard (agar-dilution) MIC testing at the *Neisseria* Reference Laboratory in Seattle, WA. Agar-dilution MIC testing was performed as previously described.

Clinical sample nuc-aAST repeated with clinical isolates. After we prepared the clinical isolate and ran the gold-standard agar-dilution MIC test, the isolate was shipped back from the *Neisseria* Reference Laboratory (Seattle, WA) to the Caltech laboratory (Pasadena, CA). The isolate was then grown according to the methods for “*Ng* culture preparation” previously described. The experimental steps for “Clinical sample preparation” and “Clinical sample nuc-aAST” were repeated using the

cell suspension of the isolate instead of the urine sample. The data from these clinical isolates were then compared to the results of the nuc-aAST performed directly on the original clinical urine samples.

Timed sum-of-steps. Working cultures of *Ng* isolates used in Fig 4 were prepared as described in “*Ng* culture preparation” and 1.5 mL of the cultures were pelleted at 2500 g for 2.5 min and resuspended in 150 μ L normal human urine (Lee Biosciences) pre-warmed to 37 °C. Initial exposure was performed by incubating 100 μ L control and treated samples at 37 °C in PCR tube strips on a BioRad C1000 Thermal Cycler. Treated samples consisted of 65 μ L MHB, 5 μ L NaHCO₃ (100 mM), 5 μ L DNase I (2 U/ μ L), 5 μ L PEN (20 μ g/mL), and 20 μ L *Ng* isolate suspension in urine. NF-H₂O was used in place of PEN in control samples. A CHAPS enhancing step was performed as described above. After the enhancement step, a 20 μ L aliquot from each sample was extracted by diluting 5X in QuickExtract DNA Extraction Solution (Lucigen) and heated for 1 min at 65 °C followed by 1 min at 98 °C on a BioRad C1000 Thermal Cycler. All sample handling following ABX exposure was performed using a multichannel pipette. Amplification was then performed using qPCR, ddPCR, or dLAMP. Extractions were diluted 2.5X in NF-H₂O before use in dLAMP.

Osmolarity measurements. Osmolarity measurements were performed on a Model 3320 Osmometer (Advanced Instruments Inc., Norwood, MA, USA). The instrument was calibrated with reference standards (Advanced Instruments) prior to experiments. Samples identical to the antibiotic-exposure condition (i.e. media, nuclease, etc.) and samples identical to the osmotic enhancing condition were prepared and measured. The volume that would normally be comprised of *Ng* culture was replaced with media.

Statistical analysis. *P*-values for Fig 2 were calculated using GraphPad Prism 8.0 software from an unpaired, two-tailed t-test comparing the averages of the three replicates of each susceptible sample to each resistant sample. A significance value of 0.02 was used for statistical significance. ROC plots used for setting susceptibility thresholds in Fig 4 were created using GraphPad Prism 8.0 software. Sensitivity was defined as the proportion of gold-standard susceptible samples correctly identified as susceptible by the nuc-aAST. Specificity was defined as the proportion of gold-standard resistant samples correctly identified as resistant by the nuc-aAST. Statistical analyses for Fig 6, (dLAMP measurements) were performed as published previously [51,106]. As in our previous publication [51], the control and treated concentrations are compared as a ratio for statistical analysis.

$$(7) \text{ Concentration Ratio} = \frac{\lambda_{control}}{\lambda_{treated}}$$

This concentration ratio is transformed into a percentage change for visualization purposes, but the ratio is assessed for statistical significance. Poisson statistics were used to calculate the confidence interval of the NA concentration for each measurement. The error in the concentration ratio, a term used in the calculation of percentage accessibility, is calculated with standard-error propagation methods:

$$(8) \sigma_{ratio} = \sqrt{\left(\frac{\sigma_{\lambda_2}}{\lambda_1}\right)^2 + \left(\frac{\lambda_2 \cdot \sigma_{\lambda_1}}{\lambda_1^2}\right)^2}$$

A one-tailed Z-test, assuming a normal distribution, is used to calculate p -values for digital NA concentrations. A threshold value for significance is set as a ratio of 1.22, corresponding to a percentage accessibility of 18%.

$$(9) Z = \frac{\ln(l_{control}) - \ln(1.22 l_{treated})}{\sqrt{\sigma^2 \ln(\lambda_{control}) + \sigma^2 \ln(\lambda_{treated})}}$$

A significance value of 0.05 was used for statistical significance. The p -values to determine significance in dLAMP experiments were computed using Microsoft Excel's standard normal cumulative distribution function and Z-value.

REFERENCES

1. CDC. Sexually Transmitted Disease Surveillance 2017. Available from: <https://www.cdc.gov/std/stats17/default.htm>.
2. Rowley J, Vander Hoorn S, Korenromp E, Low N, Unemo M, Abu-Raddad L, et al. Chlamydia, gonorrhoea, trichomoniasis and syphilis: global prevalence and incidence estimates, 2016. Bull WHO. 2019;BLT.18.228486
3. Quillin SJ, Seifert HS. Neisseria gonorrhoeae host adaptation and pathogenesis. Nat Rev Microbiol. 2018;16(4):226-40. doi: 10.1038/nrmicro.2017.169.
4. Chesson HW, Kirkcaldy RD, Gift TL, Owusu-Edusei K, Jr., Weinstock HS. An Illustration of the Potential Health and Economic Benefits of Combating Antibiotic-Resistant Gonorrhoea. Sex Transm Dis. 2018;45(4):250-3. doi: 10.1097/OLQ.0000000000000725.

5. CDC. Antibiotic resistance threats in the United States. Centers for Disease Control and Prevention. 2019:114-. doi: CS239559-B.
6. CDC. Sexually Transmitted Diseases Treatment Guidelines: Morbidity and Mortality Weekly Report 2015 [cited June 5, 2015]. Available from: <https://www.cdc.gov/std/tg2015/tg-2015-print.pdf>.
7. WHO. WHO Guidelines for the treatment of Neisseria gonorrhoeae. 2016.
8. Newman LM, Moran JS, Workowski KA. Update on the management of gonorrhea in adults in the United States. Clin Infect Dis. 2007;44 Suppl 3:S84-101. doi: 10.1086/511422.
9. WHO. Antimicrobial Resistance in Neisseria gonorrhoeae. In: Tapsall J, editor. World Health Organization, Department of Communicable Disease Surveillance and Response 2001.
10. Fifer H, Natarajan U, Jones L, Alexander S, Hughes G, Golparian D, et al. Failure of Dual Antimicrobial Therapy in Treatment of Gonorrhea. N Engl J Med. 2016;374(25):2504-6. doi: 10.1056/NEJMc1512757.
11. Whiley DM, Jennison A, Pearson J, Lahra MM. Genetic characterisation of Neisseria gonorrhoeae resistant to both ceftriaxone and azithromycin. Lancet Infect Dis. 2018;18(7):717-8. doi: Doi 10.1016/S1473-3099(18)30340-2.
12. Eyre DW, Sanderson ND, Lord E, Regisford-Reimmer N, Chau K, Barker L, et al. Gonorrhoea treatment failure caused by a Neisseria gonorrhoeae strain with combined ceftriaxone and high-level azithromycin resistance, England, February 2018. Euro Surveill. 2018;23(27). doi: 10.2807/1560-7917.ES.2018.23.27.1800323.
13. CDC. Antibiotic Resistance Threats in the United States 2013 [December 3, 2018]. Available from: <https://www.cdc.gov/drugresistance/pdf/ar-threats-2013-508.pdf>.
14. WHO. Global Priority List of Antibiotic-resistant Bacteria to Guide Research, Discovery, and Development of New Antibiotics 2017 [December 3, 2018]. Available from: <https://www.who.int/medicines/publications/global-priority-list-antibiotic-resistant-bacteria/en/>.
15. Bolan GA, Sparling PF, Wasserheit JN. The emerging threat of untreatable gonococcal infection. N Engl J Med. 2012;366(6):485-7. doi: 10.1056/NEJMp1112456.
16. Wi T, Lahra MM, Ndowa F, Bala M, Dillon J-AR, Ramon-Pardo P, et al. Antimicrobial resistance in Neisseria gonorrhoeae: Global surveillance and a call for international collaborative action. PLoS Med. 2017;14(7):e1002344. doi: 10.1371/journal.pmed.1002344.
17. WHO. Global Action Plan to Control the Spread of and Impact of Antimicrobial Resistance in Neisseria gonorrhoeae. 2012.

18. Weston EJ, Wi T, Papp J. Strengthening Global Surveillance for Antimicrobial Drug-Resistant *Neisseria gonorrhoeae* through the Enhanced Gonococcal Antimicrobial Surveillance Program. *Emerg Infect Dis*. 2017;23(13). doi: 10.3201/eid2313.170443.
19. WHO. No time to wait: Securing the future from drug-resistant infections Report to the Secretary-General of the United Nations; 2019.
20. Rahimi F, Goire N, Guy R, Kaldor JM, Ward J, Nissen MD, et al. Direct urine polymerase chain reaction for chlamydia and gonorrhoea: a simple means of bringing high-throughput rapid testing to remote settings? *Sex Health*. 2013;10(4):299-304. doi: 10.1071/SH12108.
21. Cho S, Park TS, Nahapetian TG, Yoon JY. Smartphone-based, sensitive microPAD detection of urinary tract infection and gonorrhoea. *Biosens Bioelectron*. 2015;74:601-11. doi: 10.1016/j.bios.2015.07.014.
22. Gootenberg JS, Abudayyeh OO, Kellner MJ, Joung J, Collins JJ, Zhang F. Multiplexed and portable nucleic acid detection platform with Cas13, Cas12a, and Csm6. *Science*. 2018;360(6387):439-44. doi: 10.1126/science.aag0179.
23. binx. io system for clinical point of care 2018 [01/30/2018]. Available from: <https://mybinxhealth.com/clinical-poc/>.
24. Gaydos CA, Van Der Pol B, Jett-Goheen M, Barnes M, Quinn N, Clark C, et al. Performance of the Cepheid CT/NG Xpert Rapid PCR Test for Detection of *Chlamydia trachomatis* and *Neisseria gonorrhoeae*. *J Clin Microbiol*. 2013;51(6):1666-72. doi: 10.1128/JCM.03461-12.
25. Allan-Blitz LT, Wang X, Klausner JD. Wild-Type Gyrase A Genotype of *Neisseria gonorrhoeae* Predicts In Vitro Susceptibility to Ciprofloxacin: A Systematic Review of the Literature and Meta-Analysis. *Sex Transm Dis*. 2017;44(5):261-5. doi: 10.1097/OLQ.0000000000000591.
26. Li Z, Yokoi S, Kawamura Y, Maeda S, Ezaki T, Deguchi T. Rapid detection of quinolone resistance-associated *gyrA* mutations in *Neisseria gonorrhoeae* with a LightCycler. *J Infect Chemother*. 2002;8(2):145-50. doi: 10.1007/s101560200025.
27. Balashov S, Mordechai E, Adelson ME, Gyax SE. Multiplex bead suspension array for screening *Neisseria gonorrhoeae* antibiotic resistance genetic determinants in noncultured clinical samples. *J Mol Diagn*. 2013;15(1):116-29. doi: 10.1016/j.jmoldx.2012.08.005.
28. Dona V, Smid JH, Kasraian S, Egli-Gany D, Dost F, Imeri F, et al. Mismatch Amplification Mutation Assay-Based Real-Time PCR for Rapid Detection of *Neisseria gonorrhoeae* and Antimicrobial Resistance Determinants in Clinical Specimens. *J Clin Microbiol*. 2018;56(9). doi: 10.1128/JCM.00365-18.
29. Buckley C, Trembizki E, Donovan B, Chen M, Freeman K, Guy R, et al. Real-time PCR detection of *Neisseria gonorrhoeae* susceptibility to penicillin. *J Antimicrob Chemother*. 2016;71(11):3090-5. doi: 10.1093/jac/dkw291.

30. Wong LK, Hemarajata P, Soge OO, Humphries RM, Klausner JD. Real-Time PCR Targeting the penA Mosaic XXXIV Type for Prediction of Extended-Spectrum-Cephalosporin Susceptibility in Clinical *Neisseria gonorrhoeae* Isolates. *Antimicrob Agents Chemother.* 2017;61(11). doi: 10.1128/AAC.01339-17.
31. Davies J, Davies D. Origins and evolution of antibiotic resistance. *Microbiol Mol Biol Rev.* 2010;74(3):417-33. doi: 10.1128/MMBR.00016-10.
32. CDC. Agar Dilution Antimicrobial Susceptibility Testing 2013 [cited 2018 October 31]. Available from: <https://www.cdc.gov/std/gonorrhea/lab/agar.htm>.
33. Foerster S, Desilvestro V, Hathaway LJ, Althaus CL, Unemo M. A new rapid resazurin-based microdilution assay for antimicrobial susceptibility testing of *Neisseria gonorrhoeae*. *J Antimicrob Chemother.* 2017;72(7):1961-8. doi: 10.1093/jac/dkx113.
34. Singh V, Bala M, Kakran M, Ramesh V. Comparative assessment of CDS, CLSI disc diffusion and Etest techniques for antimicrobial susceptibility testing of *Neisseria gonorrhoeae*: a 6-year study. *BMJ Open.* 2012;2(4):e000969. doi: 10.1136/bmjopen-2012-000969.
35. Siedner MJ, Pandori M, Castro L, Barry P, Whittington WL, Liska S, et al. Real-time PCR assay for detection of quinolone-resistant *Neisseria gonorrhoeae* in urine samples. *J Clin Microbiol.* 2007;45(4):1250-4. doi: 10.1128/JCM.01909-06.
36. Morse SA, Hebel BH. Effect of pH on the growth and glucose metabolism of *Neisseria gonorrhoeae*. *Infect Immun.* 1978;21(1):87-95.
37. Tobiason DM, Seifert HS. The obligate human pathogen, *Neisseria gonorrhoeae*, is polyploid. *PLoS Biol.* 2006;4(6):1069-78. doi: 10.1371/journal.pbio.0040185.
38. Wade JJ, Graver MA. A fully defined, clear and protein-free liquid medium permitting dense growth of *Neisseria gonorrhoeae* from very low inocula. *FEMS Microbiol Lett.* 2007;273(1):35-7. doi: 10.1111/j.1574-6968.2007.00776.x.
39. Sadiq ST, Mazzaferri F, Unemo M. Rapid accurate point-of-care tests combining diagnostics and antimicrobial resistance prediction for *Neisseria gonorrhoeae* and *Mycoplasma genitalium*. *Sex Transm Infect.* 2017;93(S4):S65-S8. doi: 10.1136/sextrans-2016-053072.
40. Fingerhuth SM, Low N, Bonhoeffer S, Althaus CL. Detection of antibiotic resistance is essential for gonorrhoea point-of-care testing: a mathematical modelling study. *BMC Med.* 2017;15(1):142. doi: 10.1186/s12916-017-0881-x.
41. Tuite AR, Gift TL, Chesson HW, Hsu K, Salomon JA, Grad YH. Impact of Rapid Susceptibility Testing and Antibiotic Selection Strategy on the Emergence and Spread of Antibiotic Resistance in Gonorrhea. *J Infect Dis.* 2017;216(9):1141-9. doi: 10.1093/infdis/jix450.
42. Turner KM, Christensen H, Adams EJ, McAdams D, Fifer H, McDonnell A, et al. Analysis of the potential for point-of-care test to enable individualised treatment of infections caused by

antimicrobial-resistant and susceptible strains of *Neisseria gonorrhoeae*: a modelling study. *BMJ Open*. 2017;7(6):e015447. doi: 10.1136/bmjopen-2016-015447.

43. Kirkcaldy RD, Harvey A, Papp JR, Del Rio C, Soge OO, Holmes KK, et al. *Neisseria gonorrhoeae* Antimicrobial Susceptibility Surveillance - The Gonococcal Isolate Surveillance Project, 27 Sites, United States, 2014. *MMWR Surveill Summ*. 2016;65(7):1-19. doi: 10.15585/mmwr.ss6507a1.

44. Kirkcaldy RD, Bartoces MG, Soge OO, Riedel S, Kubin G, Del Rio C, et al. Antimicrobial Drug Prescription and *Neisseria gonorrhoeae* Susceptibility, United States, 2005-2013. *Emerg Infect Dis*. 2017;23(10):1657-63. doi: 10.3201/eid2310.170488.

45. Allen VG, Mitterni L, Seah C, Rebbapragada A, Martin IE, Lee C, et al. *Neisseria gonorrhoeae* treatment failure and susceptibility to cefixime in Toronto, Canada. *JAMA*. 2013;309(2):163-70. doi: 10.1001/jama.2012.176575.

46. Katz AR, Komeya AY, Kirkcaldy RD, Whelen AC, Soge OO, Papp JR, et al. Cluster of *Neisseria gonorrhoeae* Isolates With High-level Azithromycin Resistance and Decreased Ceftriaxone Susceptibility, Hawaii, 2016. *Clin Infect Dis*. 2017;65(6):918-23. doi: 10.1093/cid/cix485.

47. Papp JR, Abrams AJ, Nash E, Katz AR, Kirkcaldy RD, O'Connor NP, et al. Azithromycin Resistance and Decreased Ceftriaxone Susceptibility in *Neisseria gonorrhoeae*, Hawaii, USA. *Emerg Infect Dis*. 2017;23(5):830-2. doi: 10.3201/eid2305.170088.

48. Piddock LJ. Assess drug-resistance phenotypes, not just genotypes. *Nat Microbiol*. 2016;1(8):16120. doi: 10.1038/nmicrobiol.2016.120.

49. Hicks JM, Haeckel R, Price CP, Lewandrowski K, Wu AHB. Recommendations and opinions for the use of point-of-care testing for hospitals and primary care: summary of a 1999 symposium. *Clin Chim Acta*. 2001;303(1-2):1-17. doi: Doi 10.1016/S0009-8981(00)00400-9.

50. Marston HD, Dixon DM, Knisely JM, Palmore TN, Fauci AS. Antimicrobial Resistance. *JAMA*. 2016;316(11):1193-204. doi: 10.1001/jama.2016.11764.

51. Schoepp NG, Schlappi TS, Curtis MS, Butkovich SS, Miller S, Humphries RM, et al. Rapid pathogen-specific phenotypic antibiotic susceptibility testing using digital LAMP quantification in clinical samples. *Sci Transl Med*. 2017;9(410). doi: 10.1126/scitranslmed.aal3693.

52. Mezger A, Gullberg E, Goransson J, Zorzet A, Herthnek D, Tano E, et al. A general method for rapid determination of antibiotic susceptibility and species in bacterial infections. *J Clin Microbiol*. 2015;53(2):425-32. doi: 10.1128/JCM.02434-14.

53. Mach KE, Mohan R, Baron EJ, Shih MC, Gau V, Wong PK, et al. A biosensor platform for rapid antimicrobial susceptibility testing directly from clinical samples. *J Urol*. 2011;185(1):148-53. doi: 10.1016/j.juro.2010.09.022.

54. Halford C, Gonzalez R, Campuzano S, Hu B, Babbitt JT, Liu J, et al. Rapid antimicrobial susceptibility testing by sensitive detection of precursor rRNA using a novel electrochemical biosensing platform. *Antimicrob Agents Chemother*. 2013;57(2):936-43. doi: 10.1128/AAC.00615-12.
55. Schoepp NG, Khorosheva EM, Schlappi TS, Curtis MS, Humphries RM, Hindler JA, et al. Digital Quantification of DNA Replication and Chromosome Segregation Enables Determination of Antimicrobial Susceptibility after only 15 Minutes of Antibiotic Exposure. *Angew Chem Int Ed Engl*. 2016;55(33):9557-61. doi: 10.1002/anie.201602763.
56. Khazaei T, Barlow JT, Schoepp NG, Ismagilov RF. RNA markers enable phenotypic test of antibiotic susceptibility in *Neisseria gonorrhoeae* after 10 minutes of ciprofloxacin exposure. *Sci Rep*. 2018;8(1):11606. doi: 10.1038/s41598-018-29707-w.
57. Chen L, Shin DJ, Zheng S, Melendez JH, Gaydos CA, Wang T-H. Direct-qPCR Assay for Coupled Identification and Antimicrobial Susceptibility Testing of *Neisseria gonorrhoeae*. *ACS Infectious Diseases*. 2018;4(9):1377-84. doi: 10.1021/acsinfecdis.8b00104.
58. Unemo M, Shafer WM. Antimicrobial resistance in *Neisseria gonorrhoeae* in the 21st century: past, evolution, and future. *Clin Microbiol Rev*. 2014;27(3):587-613. doi: 10.1128/CMR.00010-14.
59. WHO. WHO Guidelines for the treatment of *Neisseria gonorrhoeae* 2016. Available from: <https://www.who.int/reproductivehealth/publications/rtis/gonorrhoea-treatment-guidelines/en/>.
60. EUCAST. European Committee on Antimicrobial Susceptibility Testing: Breakpoint Tables for Interpretation of MICs and Zone Diameters (ver. 7.1) 2017. Available from: http://www.eucast.org/clinical_breakpoints/.
61. Kohanski MA, Dwyer DJ, Collins JJ. How antibiotics kill bacteria: from targets to networks. *Nat Rev Microbiol*. 2010;8(6):423-35. doi: 10.1038/nrmicro2333.
62. Rojas ER, Billings G, Odermatt PD, Auer GK, Zhu L, Miguel A, et al. The outer membrane is an essential load-bearing element in Gram-negative bacteria. *Nature*. 2018;559(7715):617-21. doi: 10.1038/s41586-018-0344-3.
63. Wegener WS, Hebel BH, Morse SA. Cell envelope of *Neisseria gonorrhoeae*: penicillin enhancement of peptidoglycan hydrolysis. *Infect Immun*. 1977;18(3):717-25.
64. Dillard JP, Seifert HS. A peptidoglycan hydrolase similar to bacteriophage endolysins acts as an autolysin in *Neisseria gonorrhoeae*. *Mol Microbiol*. 1997;25(5):893-901. doi: DOI 10.1111/j.1365-2958.1997.mmi522.x.
65. Zgurskaya HI, Lopez CA, Gnanakaran S. Permeability Barrier of Gram-Negative Cell Envelopes and Approaches To Bypass It. *ACS Infect Dis*. 2015;1(11):512-22. doi: 10.1021/acsinfecdis.5b00097.

66. Silhavy TJ, Kahne D, Walker S. The bacterial cell envelope. *Cold Spring Harb Perspect Biol.* 2010;2(5):a000414. doi: 10.1101/cshperspect.a000414.
67. Demchick P, Koch AL. The permeability of the wall fabric of *Escherichia coli* and *Bacillus subtilis*. *J Bacteriol.* 1996;178(3):768-73.
68. Dijkstra AJ, Keck W. Peptidoglycan as a barrier to transenvelope transport. *J Bacteriol.* 1996;178(19):5555-62. doi: DOI 10.1128/jb.178.19.5555-5562.1996.
69. Pink D, Moeller J, Quinn B, Jericho M, Beveridge T. On the architecture of the gram-negative bacterial murein sacculus. *J Bacteriol.* 2000;182(20):5925-30.
70. Harrison ST. Bacterial cell disruption: a key unit operation in the recovery of intracellular products. *Biotechnol Adv.* 1991;9(2):217-40.
71. Vazquez-Laslop N, Lee H, Hu R, Neyfakh AA. Molecular sieve mechanism of selective release of cytoplasmic proteins by osmotically shocked *Escherichia coli*. *J Bacteriol.* 2001;183(8):2399-404. doi: 10.1128/JB.183.8.2399-2404.2001.
72. van den Bogaart G, Hermans N, Krasnikov V, Poolman B. Protein mobility and diffusive barriers in *Escherichia coli*: consequences of osmotic stress. *Mol Microbiol.* 2007;64(3):858-71. doi: 10.1111/j.1365-2958.2007.05705.x.
73. Hebeler BH, Young FE. Autolysis of *Neisseria gonorrhoeae*. *J Bacteriol.* 1975;122(2):385-92.
74. Wegener WS, Hebeler BH, Morse SA. Cell envelope of *Neisseria gonorrhoeae*: relationship between autolysis in buffer and the hydrolysis of peptidoglycan. *Infect Immun.* 1977;18(1):210-9.
75. Felix H. Permeabilized cells. *Anal Biochem.* 1982;120(2):211-34.
76. Nikaido H. Molecular basis of bacterial outer membrane permeability revisited. *Microbiol Mol Biol Rev.* 2003;67(4):593-656. doi: 0.1128/MMBR.67.4.593-656.2003.
77. Zhao S, Duncan M, Tomberg J, Davies C, Unemo M, Nicholas RA. Genetics of chromosomally mediated intermediate resistance to ceftriaxone and cefixime in *Neisseria gonorrhoeae*. *Antimicrob Agents Chemother.* 2009;53(9):3744-51. doi: 10.1128/AAC.00304-09.
78. Foerster S, Unemo M, Hathaway LJ, Low N, Althaus CL. Time-kill curve analysis and pharmacodynamic modelling for in vitro evaluation of antimicrobials against *Neisseria gonorrhoeae*. *BMC Microbiol.* 2016;16:216. doi: 10.1186/s12866-016-0838-9.
79. Zou KH, O'Malley AJ, Mauri L. Receiver-operating characteristic analysis for evaluating diagnostic tests and predictive models. *Circulation.* 2007;115(5):654-7. doi: 10.1161/CIRCULATIONAHA.105.594929.

80. Grad YH, Harris SR, Kirkcaldy RD, Green AG, Marks DS, Bentley SD, et al. Genomic Epidemiology of Gonococcal Resistance to Extended-Spectrum Cephalosporins, Macrolides, and Fluoroquinolones in the United States, 2000-2013. *J Infect Dis.* 2016;214(10):1579-87. doi: 10.1093/infdis/jiw420.
81. Wadsworth CB, Sater MRA, Bhattacharyya RP, Grad YH. Impact of Species Diversity on the Design of RNA-Based Diagnostics for Antibiotic Resistance in *Neisseria gonorrhoeae*. *Antimicrob Agents Chemother.* 2019;63(8):e00549-19. doi: 10.1128/AAC.00549-19.
82. Gianecini RA, Golparian D, Zittermann S, Litvik A, Gonzalez S, Oviedo C, et al. Genome-based epidemiology and antimicrobial resistance determinants of *Neisseria gonorrhoeae* isolates with decreased susceptibility and resistance to extended-spectrum cephalosporins in Argentina in 2011-16. *J Antimicrob Chemother.* 2019/03/02 ed2019.
83. Baumann E, Stoya G, Volkner A, Richter W, Lemke C, Linss W. Hemolysis of human erythrocytes with saponin affects the membrane structure. *Acta Histochem.* 2000;102(1):21-35. doi: 10.1078/0065-1281-00534.
84. Charalampous T, Kay GL, Richardson H, Aydin A, Baldan R, Jeanes C, et al. Nanopore metagenomics enables rapid clinical diagnosis of bacterial lower respiratory infection. *Nat Biotechnol.* 2019;37(7):783-92. doi: 10.1038/s41587-019-0156-5.
85. Murata-Kamiya N, Kikuchi K, Hayashi T, Higashi H, Hatakeyama M. *Helicobacter pylori* exploits host membrane phosphatidylserine for delivery, localization, and pathophysiological action of the CagA oncoprotein. *Cell Host Microbe.* 2010;7(5):399-411. doi: 10.1016/j.chom.2010.04.005.
86. Rolando JC, Jue E, Schoepp NG, Ismagilov RF. Real-Time, Digital LAMP with Commercial Microfluidic Chips Reveals the Interplay of Efficiency, Speed, and Background Amplification as a Function of Reaction Temperature and Time. *Anal Chem.* 2018. doi: 10.1021/acs.analchem.8b04324.
87. Selck DA, Ismagilov RF. Instrument for Real-Time Digital Nucleic Acid Amplification on Custom Microfluidic Devices. *PLoS One.* 2016;11(10):e0163060. doi: 10.1371/journal.pone.0163060.
88. Lee SG, Lee H, Jeong SH, Yong D, Chung GT, Lee YS, et al. Various penA mutations together with mtrR, porB and ponA mutations in *Neisseria gonorrhoeae* isolates with reduced susceptibility to cefixime or ceftriaxone. *J Antimicrob Chemother.* 2010;65(4):669-75. doi: 10.1093/jac/dkp505.
89. FDA. Evaluation of Automatic Class III Designation for T2Candida Panel and T2Dx Instrument. 2014.
90. Barczak AK, Gomez JE, Kaufmann BB, Hinson ER, Cosimi L, Borowsky ML, et al. RNA signatures allow rapid identification of pathogens and antibiotic susceptibilities. *Proc Natl Acad Sci U S A.* 2012;109(16):6217-22. doi: 10.1073/pnas.1119540109.

91. Avesar J, Rosenfeld D, Truman-Rosentsvit M, Ben-Arye T, Geffen Y, Bercovici M, et al. Rapid phenotypic antimicrobial susceptibility testing using nanoliter arrays. *Proceedings of the National Academy of Sciences*. 2017;114(29):E5787. doi: 10.1073/pnas.1703736114.
92. Liu T, Lu Y, Gau V, Liao JC, Wong PK. Rapid antimicrobial susceptibility testing with electrokinetics enhanced biosensors for diagnosis of acute bacterial infections. *Ann Biomed Eng*. 2014;42(11):2314-21. doi: 10.1007/s10439-014-1040-6.
93. Premasiri WR, Chen Y, Williamson PM, Bandarage DC, Pyles C, Ziegler LD. Rapid urinary tract infection diagnostics by surface-enhanced Raman spectroscopy (SERS): identification and antibiotic susceptibilities. *Anal Bioanal Chem*. 2017;409(11):3043-54. doi: 10.1007/s00216-017-0244-7.
94. Baltekin O, Boucharin A, Tano E, Andersson DI, Elf J. Antibiotic susceptibility testing in less than 30 min using direct single-cell imaging. *Proc Natl Acad Sci U S A*. 2017;114(34):9170-5. doi: 10.1073/pnas.1708558114.
95. Bhattacharyya RP, Bandyopadhyay N, Ma P, Son SS, Liu J, He LL, et al. Simultaneous detection of genotype and phenotype enables rapid and accurate antibiotic susceptibility determination. *Nat Med*. 2019;25(12):1858-64. doi: 10.1038/s41591-019-0650-9.
96. Li L, Du W, Ismagilov R. User-loaded SlipChip for equipment-free multiplexed nanoliter-scale experiments. *J Am Chem Soc*. 2010;132(1):106-11. doi: 10.1021/ja908555n.
97. Shen F, Du W, Davydova EK, Karymov MA, Pandey J, Ismagilov RF. Nanoliter multiplex PCR arrays on a SlipChip. *Anal Chem*. 2010;82(11):4606-12. doi: 10.1021/ac1007249.
98. Shen F, Sun B, Kreutz JE, Davydova EK, Du W, Reddy PL, et al. Multiplexed quantification of nucleic acids with large dynamic range using multivolume digital RT-PCR on a rotational SlipChip tested with HIV and hepatitis C viral load. *J Am Chem Soc*. 2011;133(44):17705-12. doi: 10.1021/ja2060116.
99. Newman L, Rowley J, Vander Hoorn S, Wijesooriya NS, Unemo M, Low N, et al. Global Estimates of the Prevalence and Incidence of Four Curable Sexually Transmitted Infections in 2012 Based on Systematic Review and Global Reporting. *PLoS One*. 2015;10(12):e0143304. doi: 10.1371/journal.pone.0143304.
100. Schoepp NG, Liaw EJ, Winnett A, Savela ES, Ismagilov RF. Differential Accessibility to Polymerase During Isothermal Nucleic Acid Amplification Enables 30-Minute Phenotypic Beta-lactam Antibiotic Susceptibility Testing of Carbapenem-resistant Enterobacteriaceae (CRE). *PLoS Biol*. 2020.
101. Banoo S, Bell D, Bossuyt P, Herring A, Mabey D, Poole F, et al. Evaluation of diagnostic tests for infectious diseases: general principles. *Nat Rev Microbiol*. 2006;4(9 Suppl):S21-31. doi: 10.1038/nrmicro1523.
102. CDC. CDC & FDA Antibiotic Resistance Isolate Bank: *Neisseria gonorrhoeae*. 2019.

103. CLSI. M100-S25 Performance Standards for Antimicrobial Susceptibility Testing. CLSI. 2015;35(3).

104. Sigma. Buffer Reference Center [01/17/19]. Available from: <https://www.sigmaaldrich.com/life-science/core-bioreagents/biological-buffers/learning-center/buffer-reference-center.html>.

105. Lee SR, Chung JM, Kim YG. Rapid one step detection of pathogenic bacteria in urine with sexually transmitted disease (STD) and prostatitis patient by multiplex PCR assay (mPCR). *J Microbiol.* 2007;45(5):453-9.

106. Kreutz JE, Munson T, Huynh T, Shen F, Du W, Ismagilov RF. Theoretical design and analysis of multivolume digital assays with wide dynamic range validated experimentally with microfluidic digital PCR. *Anal Chem.* 2011;83(21):8158-68. doi: 10.1021/ac201658s.

ACKNOWLEDGEMENTS

We thank Adam Sukhija-Cohen, Sherrelle Banks, Matt Santos, and Yancy Granados at the AIDS Healthcare Foundation for their technical assistance with the clinical study and patient enrollment. We thank Peera Hemarajata at the UCLA Clinical Microbiology Laboratory for providing isolates and for discussion of gold-standard practices. We also thank Natasha Shelby for help with writing and editing this manuscript.

SUPPLEMENTARY MATERIALS

Supplementary Methods

DNase I inactivation experiment. Incubations were performed in PCR tubes on a Bio-Rad C1000 Thermal Cycler. Samples including DNase I (Samples B-F in Fig 2-S1) consisted of 90 μ L MHB, 5 μ L NaHCO₃ (100 mM), and 5 μ L NEB DNase I (2000 U/mL). Nuclease-free water was used in place of DNase I in the control sample (Sample A in S1 Fig). After vortexing to mix, 5 μ L of each suspension was added to 45 μ L QuickExtract DNA Extraction Solution (Lucigen). Samples A and B were heated at 65 °C for 6 min and 98 °C for 4 min. Sample C was heated at 65 °C for 4 min and 98 °C for 3 min. Sample D was heated at 65 °C for 3 min and 98 °C for 2 min. Sample E was heated at 65 °C for 2 min and 98 °C for 1 min. Sample F was heated at 65 °C for 1 min and 98 °C for 1 min. After each heating step was completed, the samples were placed on an ice block. DNase I

activity was tested by adding 15 μL of a spike-in control of *Ng* DNA (1/20 dilution of stock Cq 19, expected concentration in PCR in this experiment to be a Cq of 23.3) to 15 μL of the Samples A-F in PCR tubes, samples were heated to 37 $^{\circ}\text{C}$ for 5 min, and then the samples were quantified in qPCR, as described in the main methods section.

DNA digestion of the lambda spike-in. Seven or eight 1.25 mL aliquots of clinical urine samples were centrifuged in 2 mL microcentrifuge tubes (VWR) for 5 min at 1,000 x g (Eppendorf 5418R). Pellets were re-suspended in 250 μL GWM containing a lambda DNA spike-in (see below for preparation). All working suspensions were then pooled together. To generate the (+) DNase I controls, 320 μL aliquots of the working suspensions were added to 40 μL 10X DNase I Reaction Buffer (NEB), 20 μL DNase I (2,000 U/mL) (NEB), and 20 μL nuclease-free water. Nuclease-free water was used in place of DNase I in the (-) DNase I control sample. Suspensions were then vortexed, quickly spun on a benchtop microcentrifuge (Labnet) at 2,000 x g for 2-3 sec, and incubated at 37 $^{\circ}\text{C}$ for 15 min on a heat block (ThermoScientific Digital Shaking Drybath). Suspensions were then removed from the heat block, vortexed, and spun on a benchtop microcentrifuge (Labnet) at 2,000 x g for 2-3 sec. After mixing, 20 μL of each suspension was added to 80 μL QuickExtract DNA Extraction Solution (Lucigen). Samples were heated at 65 $^{\circ}\text{C}$ for 6 min and 98 $^{\circ}\text{C}$ for 4 min on a BioRad C1000 Thermal Cycler. DNase I activity was tested by subtracting the concentration of lambda DNA in the (-) DNase I control from the concentration in the (+) DNase I control tube. Quantification of DNA was done with qPCR (Roche, LightCycler 96) as described in the main methods. As in the clinical nuc-aAST, we used 2 μL of template per 10 μL qPCR reaction.

The lambda DNA spike-in was prepared as follows. 12.5 μL lambda phage DNA (7.1×10^5 copies/ μL , as quantified with ddPCR) (QX200, Bio-Rad) in 0.5X TE Buffer was mixed with 1238 μL Graver-Wade Medium (GWM).

Supplementary Tables and Figures

Provided below. Any table that is longer than 1 page has a link to download from the Supporting Information section of the published paper.

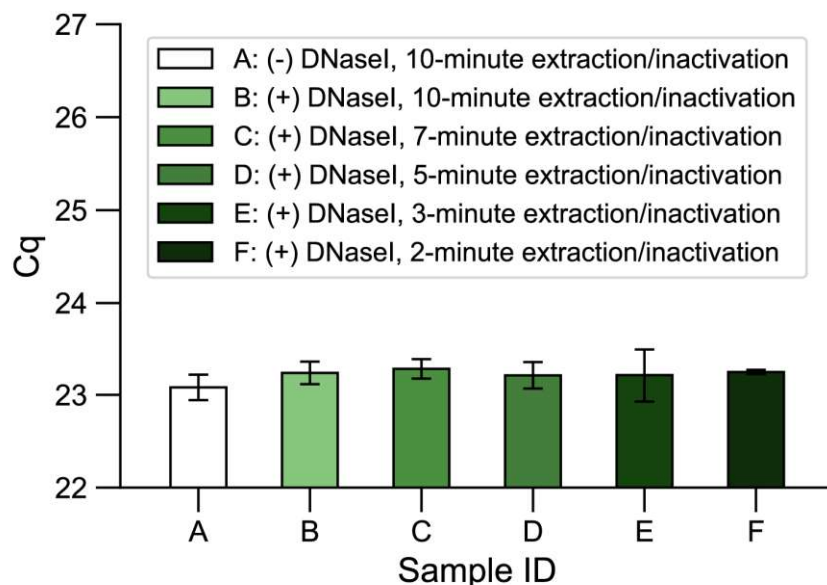


Fig 2-S1. DNase is properly inactivated by extraction and heat treatment steps used in this work (see Methods for details). After extraction/inactivation, *Neisseria gonorrhoeae* (Ng) DNA was spiked into the extractions containing the inactivated DNase I and incubated at 37 °C. The Ng DNA was not degraded, confirming the inactivation of the DNase I enzyme. The concentration of DNase I, the composition of the incubations, and the extraction conditions were all performed under the same conditions as the ASTs. Error bars are 98% confidence intervals for three PCR replicates [55]. Data are in S8 Table.

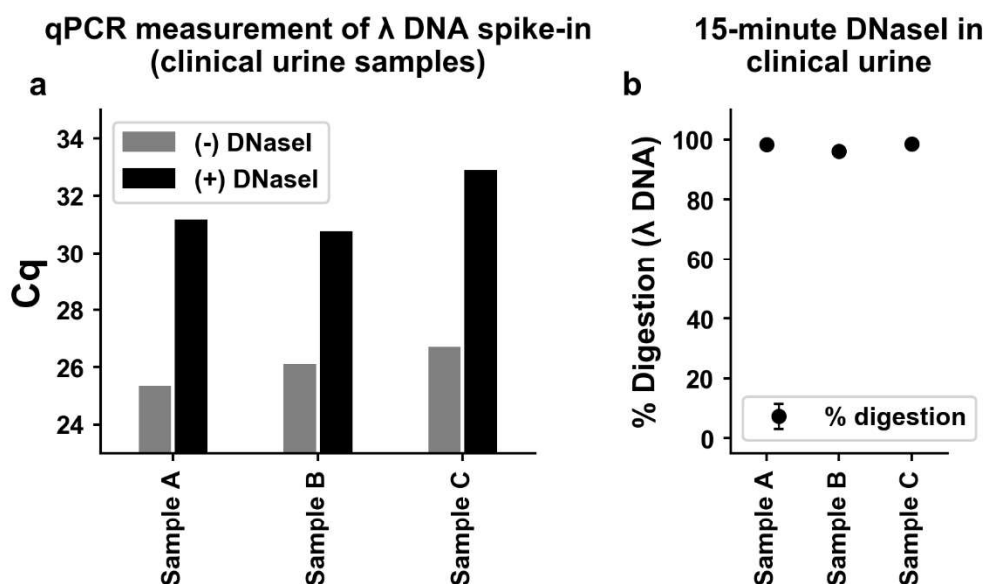


Fig 2-S2 DNase I remains active in clinical urine samples. (a) The qPCR results for the lambda DNA spike-in for three different urine samples. **(b)** Percentage of DNA digested calculated from qPCR results with the same equations used previously (see Methods) to calculate percentage lysis. Data are in Table 2-S9.

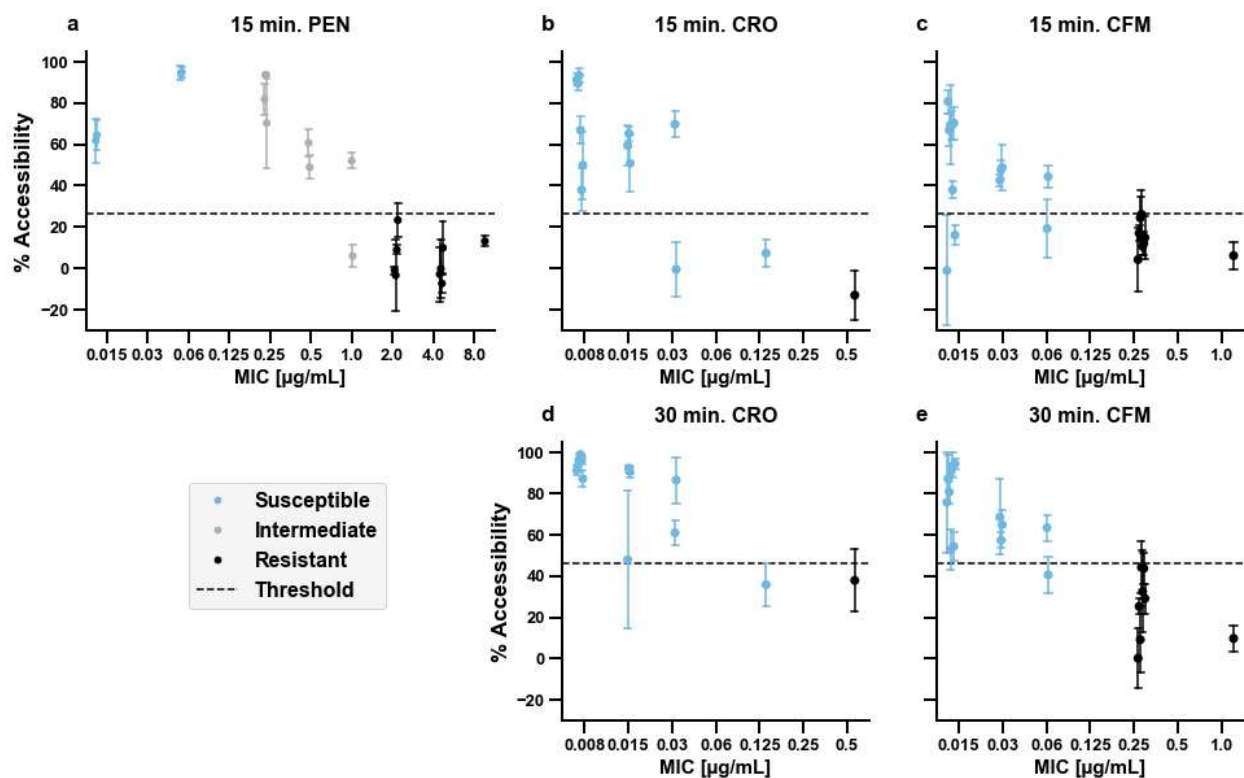


Fig 2-S3 The nuc-aAST using clinical isolates separated by minimum inhibitory concentration (MIC). (a-c) Results of nuc-aAST after 15 min of exposure to (a) penicillin (PEN), (b) cefixime (CFM), or (c) ceftriaxone (CRO). (d-e) nuc-aAST results after exposure to (d) CFM or (e) CRO for 30 min. Each point represents the average for a single isolate run in (at least) biological triplicate for that condition; error bars represent the standard deviation from the biological replicates. All PCR assays were performed in technical triplicate. The dashed line represents the susceptibility threshold, which was set at 26.5% accessibility for 15-min exposures and 46% for 30-min exposures. Data are also plotted in Fig 2-4. (Data plotted here are in Table 2-S4; experimental data from individual replicates are in Table 2-S11 and Table 2-S12; MICs are in Table 2-S1).

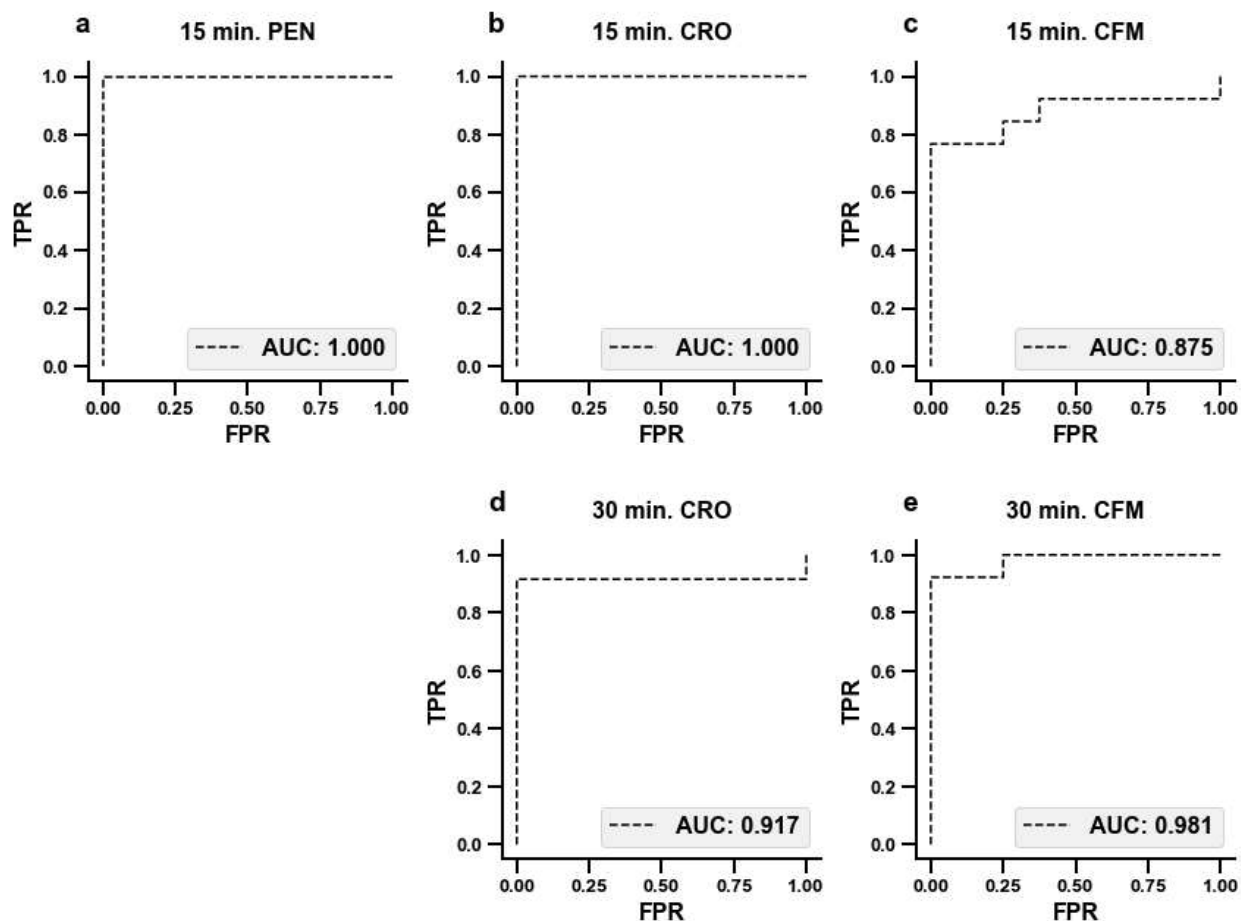


Fig 2-S4 Receiver operating characteristic (ROC) curves. ROC curves were generated from the data shown in Fig 2-4, Table 2-S4. The false positive rate (FPR) is shown on the x-axis and the true positive rate (TPR) is shown on the y-axis. The area under the curve (AUC) is shown for each plot. **(a-c)** Results of nuc-aAST after 15 min of exposure to **(a)** penicillin (PEN), **(b)** cefixime (CFM), or **(c)** ceftriaxone (CRO). **(d-e)** The nuc-aAST results after exposure to **(d)** CFM or **(e)** CRO for 30 min.

Table 2-S1. *Neisseria gonorrhoeae* isolates used in this study. Isolates were obtained from the University of Washington Neisseria Reference Laboratory (UW NRL), the Centers for Disease Control Antibiotic Resistance Isolate Bank (CDC AR Isolate Bank), and from isolates prepared by the authors from clinical urine samples obtained from consented patients at AIDS Healthcare Foundation (AHF) under IRB #18-0865. The gold standard MICs for the CDC AR Isolate bank are from the literature and all other MICs were calculated as described in the Methods. ABX: PEN = Penicillin, CRO = Ceftriaxone, CFM = Cefixime

Internal Isolate #	Source	Code or AR Bank #	Sequence Accession #	Gold Standard MIC [$\mu\text{g/mL}$]
2	UW NRL	FQ002	<i>n/a</i>	PEN (0.250), CFM (≤ 0.015), CRO (≤ 0.008)
4	UW NRL	FQ004	<i>n/a</i>	PEN (0.500), CFM (0.060), CRO (0.003)
5	UW NRL	FQ005	<i>n/a</i>	PEN (1.000), CFM (0.030), CRO (0.015)
12	UW NRL	FQ012	<i>n/a</i>	PEN (0.500), CFM (0.030), CRO (0.015)
15	UW NRL	FQ015	<i>n/a</i>	PEN (0.015), CFM (≤ 0.015), CRO (≤ 0.008)
16	UW NRL	FQ016	<i>n/a</i>	PEN (0.015), CFM (≤ 0.015), CRO (≤ 0.008)
17	UW NRL	FQ017	<i>n/a</i>	PEN (0.060), CFM (≤ 0.015), CRO (≤ 0.008)
18	UW NRL	FQ018	<i>n/a</i>	PEN (2.000), CFM (0.060), CRO (0.030)
19	UW NRL	FQ019	<i>n/a</i>	PEN (2.000), CFM (0.030), CRO (0.015)
20	UW NRL	FQ020	<i>n/a</i>	PEN (0.060), CFM (≤ 0.015), CRO (≤ 0.008)
41	UW NRL	FQ041	<i>n/a</i>	PEN (2.000), CFM (0.250), CRO (0.125)
44	UW NRL	FQ044	<i>n/a</i>	PEN (8.000), CFM (≤ 0.015), CRO (≤ 0.008)
30	CDC AR Isolate Bank	194	SAMEA3165247	PEN (1.000), CFM (1.000), CRO (0.500)
165	CDC AR Isolate Bank	165	SAMEA3165293	PEN (4.000), CFM (0.250)
166	CDC AR Isolate Bank	166	SAMEA3165270	PEN (4.000), CFM (0.250)
172	CDC AR Isolate Bank	172	SAMEA3165249	PEN (2.000), CFM (0.25)
174	CDC AR Isolate Bank	174	SAMEA3165241	PEN (4.000), CFM (0.25)
175	CDC AR Isolate Bank	175	SAMEA3165668	PEN (0.250), CFM (0.015)
176	CDC AR Isolate Bank	176	SAMEA3165296	PEN (4.000), CFM (0.250)
179	CDC AR Isolate Bank	179	SAMEA3165655	PEN (0.250), CFM (0.015)
191	CDC AR Isolate Bank	191	SAMEA3165239	PEN (8.000), CFM (0.250)
194	CDC AR Isolate Bank	194	SAMEA3165247	CFM (1.000), CRO (0.500)
78; Sample 1	AHF	N/A	<i>n/a</i>	PEN (0.250), CRO (0.004)
84; Sample 2	AHF	N/A	<i>n/a</i>	PEN (0.500), CRO (0.008)
88; Sample 3	AHF	N/A	<i>n/a</i>	PEN (64.000)
93; Sample 4	AHF	N/A	<i>n/a</i>	PEN (2.000)

Table 2-S2. Percentage lysis of *Neisseria gonorrhoeae* cells after 5 min exposure to an enhancer. Cqs are measured from qPCR as reported in main methods and the mean of the three PCR triplicates is reported in the table. Equations 3 and 4 are used to calculate the percentage lysis and the error in that calculation based on error propagation from the standard deviation of qPCR triplicates. Data are plotted in Fig 2-3 a-f; negative percentages were set to 0 for visualization, as described in Methods. Enhancers: CHAPS = zwitterionic surfactant 3-[(3-cholamidopropyl)dimethylammonio]-1-propanesulfonate at a final concentration of 10 mM; TNP = non-ionic surfactant TERGITOL NP at a final concentration of 5 mM and an HLB of 13.1; BAC = cationic surfactant benzalkonium chloride at a final concentration of 0.1%; SDS = anionic surfactant sodium dodecyl sulfate at a final concentration of 0.01%; TRIS = Tris buffer at pH 8.5; water = nuclease-free water.

Table 2-S2 is available to download at: <https://doi.org/10.1371/journal.pbio.3000651.s006>

Table 2-S3. The percentage of *Neisseria gonorrhoeae* DNA accessible after a 15-min antibiotic (ABX) exposure (1 µg/mL) followed by a 5-min exposure to an enhancer. The PCR quantitation cycle (Cq) is measured by qPCR (see Methods) and the mean of the PCR triplicates is reported. Equations 1 and 2 are used to calculate the percentage accessibility and the error in that calculation is based on the error propagation of the standard deviation of qPCR triplicates. “Treated” indicates the isolate was exposed to an antibiotic; “control” indicates no antibiotic exposure. Data are plotted in Fig 2-3g-x., negative percentages were set to 0 for visualization, as described in Methods. ABX: PEN = Penicillin, CRO = Ceftriaxone, CFM = Cefixime. Isolate categories: S = susceptible to ABX; R = resistant to ABX

Table 2-S3 is available to download at: <https://doi.org/10.1371/journal.pbio.3000651.s007>

Table 2-S4. The percentage of *Neisseria gonorrhoeae* DNA accessible after a 15- or 30-min exposure to an antibiotic (ABX) and 5 min enhancement with CHAPS. The mean percentage of accessible DNA is calculated from at least three biological replicates of that nuc-aAST condition in clinical isolates (details of individual replicates are shown in Table 2-S11 and Table 2-S12). Additionally, we report the standard error of the mean (SEM) and standard deviation (SD) of the biological replicate nuc-aASTs. Each nuc-aAST used 1µg/mL of ABX followed by 5 min of CHAPS as an accessibility “enhancer.” Data are plotted in Fig 2-4, negative percentage accessibilities were set to 0 for visualization, as described in Methods. ABX: PEN = Penicillin, CRO = Ceftriaxone, CFM = Cefixime. Isolates: S = susceptible to ABX; R = resistant to ABX

Table 2-S4 is available to download at: <https://doi.org/10.1371/journal.pbio.3000651.s008>

Table 2-S5. The results of nuc-aAST with a dLAMP readout using contrived samples with *Neisseria gonorrhoeae* (Ng) isolates and clinical urine samples positive for Ng. Contrived samples are nuc-aASTs performed with clinical Ng isolates spiked-into healthy urine; assay conditions are 15-min exposures to 1 µg/mL antibiotic (ABX) followed by 5 min exposure to the enhancer CHAPS. One of the three technical replicates from each of the six clinical urine sample nuc-aASTs (Fig 2-6d and Table 2-S6) was also run in dLAMP (Fig 2-6e and Table 2-S5). Assay conditions were fresh, clinical urine samples, run with 30-min exposures to 1 µg/mL ABX followed by 3-5 min exposure to the enhancer TNP. The concentration of the Ng 16S DNA reported in copies/µL and p-values are calculated as described in the “Statistical analysis” section of the Methods for dLAMP experiments. (Negative percentages were set to 0 for visualization, as described in Methods. In Fig 2-6e, antibiotic-susceptible and antibiotic-intermediate samples are plotted together under the category not-resistant (NR)). ABX: PEN = Penicillin, CRO = Ceftriaxone, CFM = Cefixime

Internal Isolate # or clinical sample	Clinical Sample #	Sample Type	ABX	duration of dLAMP [min]	p-value	Concentration (Control) [copies/µL]	Concentration (Treated) [copies/µL]	% Accessibility
17	n/a	contrived	PEN	7	0.044	0.95	0.29	69.15
19	n/a	contrived	PEN	7	0.935	1.77	2.21	-24.55
20	n/a	contrived	PEN	8	0.007	2.70	1.07	60.38
44	n/a	contrived	PEN	8	1.000	2.57	12.00	-367.24
84	2	clinical sample	CRO	20	0.000	46.20	20.90	54.76
84	2	clinical sample	PEN	20	0.001	46.20	30.90	33.12
88	3	clinical sample	PEN	20	0.484	5.10	4.17	18.24
93	4	clinical sample	PEN	20	1.000	35.10	43.80	-24.79
78	1	clinical sample	CRO	20	0.000	14.30	6.16	56.92
78	1	clinical sample	PEN	20	0.000	14.30	6.59	53.92
17	n/a	contrived	PEN	30	0.000	1637.97	53.23	96.75
19	n/a	contrived	PEN	30	0.967	1139.73	985.64	13.52
20	n/a	contrived	PEN	30	0.000	1486.59	19.47	98.69
44	n/a	contrived	PEN	30	1.000	1409.27	1398.56	0.76
84	2	clinical sample	CRO	30	0.000	58.71	26.58	54.72
84	2	clinical sample	PEN	30	0.008	58.70	41.90	28.62
88	3	clinical sample	PEN	30	0.732	6.50	5.67	12.77
93	4	clinical sample	PEN	30	1.000	49.40	60.10	-21.66
78	1	clinical sample	CRO	30	0.000	21.10	8.98	57.44
78	1	clinical sample	PEN	30	0.000	21.10	9.20	56.40

Table 2-S6. Nuc-aAST data for clinical urine samples and isolates from the samples. All nuc-aASTs were run with a 30-min antibiotic (ABX) exposure and a 3-5 min of TNP enhancement step. The internal isolate number and clinical sample name corresponds to the MIC values in Table 2-S1. The sample number corresponds to the clinical sample number reported in Fig 2-5d. The sample type refers to if the nuc-aAST results come from an assay run directly from the clinical urine sample or on the isolate prepared from that urine sample. Technical replicates are parallel nuc-aASTs run for each condition. The percentage accessibility is calculated from the qPCR measurements and the error is propagated according to Equations 2 and 3, as described for previous calculations. ABX: PEN = Penicillin, CRO = Ceftriaxone.

Table 2-S6 is available to download at: <https://doi.org/10.1371/journal.pbio.3000651.s010>

Table 2-S7. Nuc-aAST summary of samples and isolates from the samples. The data is summarized with the mean percentage accessibility calculated from the technical replicate nuc-aASTs (mean percentages accessibility are shown in Fig 2-5d). Additionally, the standard error of the mean (SEM) and standard deviation (SD) are reported from the technical replicate nuc-aASTs. The technical replicates in this table are only the replicates that met our criteria for inclusion as described in the Methods. ABX: PEN = Penicillin, CRO = Ceftriaxone

Table 2-S7 is available to download at: <https://doi.org/10.1371/journal.pbio.3000651.s011>

Table 2-S8. DNase I inactivation data. Data plotted in Fig 2-S1 Mean Cq is computed from qPCR triplicates. Error bars are 98% confidence intervals for three PCR replicates [55].

Sample ID	DNaseI	Duration Extraction/ Inactivation [min]	mean Cq	PCR error
A	FALSE	10	23.08	0.14
B	TRUE	10	23.24	0.12
C	TRUE	7	23.28	0.10
D	TRUE	5	23.21	0.14
E	TRUE	3	23.21	0.29
F	TRUE	2	23.25	0.02

Table 2-S9. DNA digestion of the lambda spike-in. Mean Cq is calculated from PCR triplicates and error is calculated (as described in main methods) for PCR triplicates. Percentage DNA digestion is calculated for each clinical sample from the samples with and without DNase I. The error in the PCR measurements is propagated for calculate the error bar in the percentage digestion of the spike-in DNA. Data are shown in Fig 2-S2.

Clinical Sample identifier	DNase	Sample_Cq_mean	PCR error	percent DNA digestion	error percent digestion
A	FALSE	25.35	0.001854308	n/a	
A	TRUE	31.19	0.001854308	98.26	0.0019
B	FALSE	26.11	0.000263021	n/a	
B	TRUE	30.78	0.000263021	96.07	0.0004
C	FALSE	26.70	0.000287049	n/a	
C	TRUE	32.89	0.000287049	98.63	0.0003

Table 2-S10. Percentage accessibility of DNA over time without an enhancer. S = susceptible to ABX; R = resistant to ABX. Data are plotted in Fig 2-2.

Isolate	Susceptibility	time point (min)	Cq control	Cq treated	% accessibility	% accessibility error	p-value (isolate 15)	p-value (isolate 16)
15	S	15	19.21	19.30	5.83	3.01	n/a	n/a
15	S	30	19.26	19.22	-2.57	2.60	n/a	n/a
15	S	45	19.17	19.24	4.96	3.18	n/a	n/a
15	S	60	19.09	19.26	10.91	3.46	n/a	n/a
15	S	90	18.98	19.28	18.59	1.72	n/a	n/a
15	S	120	18.77	19.34	32.79	0.54	n/a	n/a
16	S	15	19.24	19.30	4.29	2.76	n/a	n/a
16	S	30	19.24	19.16	-5.21	1.88	n/a	n/a
16	S	45	19.09	19.14	3.85	2.88	n/a	n/a
16	S	60	19.01	19.16	9.87	3.23	n/a	n/a
16	S	90	18.82	19.17	21.72	1.37	n/a	n/a
16	S	120	18.54	19.26	39.29	1.67	n/a	n/a
18	R	15	18.63	18.74	7.56	2.34	0.478	0.194
18	R	30	18.63	18.72	6.05	2.13	0.011	0.002
18	R	45	18.61	18.72	7.34	2.10	0.339	0.165
18	R	60	18.57	18.65	5.39	3.47	0.123	0.177
18	R	90	18.39	18.42	2.28	4.35	0.004	0.002
18	R	120	18.33	18.35	1.60	3.15	<.001	<.001
19	R	15	18.88	18.97	6.26	1.98	0.845	0.373
19	R	30	18.92	18.97	3.85	1.96	0.027	0.004
19	R	45	18.90	18.95	3.63	2.78	0.616	0.928
19	R	60	18.82	18.91	6.05	2.96	0.138	0.205
19	R	90	18.70	18.77	4.29	2.06	<.001	<.001
19	R	120	18.61	18.77	10.70	2.34	<.001	<.001

Table 2-S11. Each biological replicate nuc-aAST of Ng DNA accessible after a 15-min exposure to an antibiotic (ABX) and 5 min enhancement with CHAPS. Replicate numbers refer to which biological replicate experiment the data are from. The PCR quantitation cycle (Cq) is measured by qPCR (see Methods) and the mean of the PCR triplicates is reported. Equation 1 is used to calculate the percentage accessibility and equation 3 is used to calculate the percentage lysis. “Treated” indicates the isolate was exposed to an antibiotic; “control” indicates no antibiotic exposure. Data are used to calculate mean percentage accessibility for each isolate, which are plotted in Fig 2-4(a-c), Fig 2-S3, and shown in Table 2-S4. ABX: PEN = Penicillin, CRO = Ceftriaxone, CFM = Cefixime. Susceptibility: S = susceptible to ABX; R = resistant to ABX; I = intermediate MIC.

Table 2-S11 is available to download at: <https://doi.org/10.1371/journal.pbio.3000651.s015>

Table 2-S12. Each biological replicate nuc-aAST of Ng DNA accessible after a 30-min exposure to an antibiotic (ABX) and 5 min enhancement with CHAPS. Replicate numbers refer to which biological replicate experiment the data are from. The PCR quantitation cycle (Cq) is measured by qPCR (see Methods) and the mean of the PCR triplicates is reported. Equation 1 is used to calculate the percentage accessibility and equation 3 is used to calculate the percentage lysis. “Treated” indicates the isolate was exposed to an antibiotic; “control” indicates no antibiotic exposure. Data are used to calculate mean percentage accessibility for each isolate, which are plotted in Fig 2-4(d-e), Fig 2-S3, and shown in Table 2-S4. ABX: PEN = Penicillin, CRO = Ceftriaxone, CFM = Cefixime. Susceptibility: S = susceptible to ABX; R = resistant to ABX.

Table 2-S12 is available to download at: <https://doi.org/10.1371/journal.pbio.3000651.s016>

Table 2-S13. A representative subset of fluorescence values from a digital LAMP antibiotic-susceptibility test (AST) run on a susceptible *N. gonorrhoeae* isolate in the control (no antibiotic) treatment. A representative AST from one of the contrived samples using isolates was selected and the LAMP amplification curves from the first 100 positive wells are shown. These curves are plotted in Fig 2-6b. See also Table 2-S14 – Table 2-S16 for the complete dataset used in Fig 2-6b.

Table 2-S1 is available to download at: <https://doi.org/10.1371/journal.pbio.3000651.s018>

Table 2-S14. A representative subset of fluorescence values from a digital LAMP antibiotic-susceptibility test (AST) run on a susceptible *N. gonorrhoeae* isolate in the treated (penicillin) treatment. These are representative wells to show LAMP amplification curves. These curves are plotted in Fig 2-6b. A representative AST from one of the contrived samples using isolates was selected. See also Table 2-S13, Table 2-S15 – Table 2-S16 for the complete dataset used in Fig 2-6b.

Table 2-S2 is available to download at: <https://doi.org/10.1371/journal.pbio.3000651.s019>

Table 2-S15. A representative subset of fluorescence values from a digital LAMP antibiotic-susceptibility test (AST) run on a resistant *N. gonorrhoeae* isolate in the control (no antibiotic) treatment. These are representative wells to show LAMP amplification curves. These curves are plotted in Fig 2-6b. A representative AST from one of the contrived samples using isolates was selected. See also Table 2-S13 – Table 2-S14, Table 2-S16 for the complete dataset used in Fig 2-6b.

Table 2-S15 is available to download at: <https://doi.org/10.1371/journal.pbio.3000651.s020>

Table 2-S16. A representative subset of fluorescence values from a digital LAMP antibiotic-susceptibility test (AST) run on a resistant *N. gonorrhoeae* isolate in the treated (penicillin) treatment. These are representative wells to show LAMP amplification curves. These curves are plotted in Fig 2-6b. A representative AST from one of the contrived samples using isolates was selected. See also Table 2-S13 – Table 2-S15 for the complete dataset used in Fig 2-6b.

Table 2-S16 is available to download at: <https://doi.org/10.1371/journal.pbio.3000651.s021>

*Chapter 3***SARS-COV-2 VIRAL LOAD IN LONGITUDINALLY COLLECTED SALIVA AND NASAL SWABS**

Emily S. Savela*, Alexander Winnett*, Anna E. Romano*, Michael K. Porter, Natasha Shelby, Reid Akana, Jenny Ji, Matthew M. Cooper, Noah W. Schlenker, Jessica A. Reyes, Alyssa M. Carter, Jacob T. Barlow, Colten Tognazzini, Matthew Feaster, Ying-Ying Goh, Rustem F. Ismagilov. 2021. “Quantitative SARS-CoV-2 viral-load curves in paired saliva and nasal swabs inform appropriate respiratory sampling site and analytical test sensitivity required for earliest viral detection” medRxiv. doi:

<https://doi.org/10.1101/2021.04.02.21254771>

ABSTRACT

Early detection of SARS-CoV-2 infection is critical to reduce asymptomatic and pre-symptomatic transmission, curb the spread of variants by travelers, and maximize treatment efficacy. Low-sensitivity nasal-swab testing (antigen and some nucleic-acid-amplification tests) is commonly used for surveillance and symptomatic testing, but the ability of low-sensitivity nasal-swab tests to detect the earliest stages of infection has not been established. In this case-ascertained study, conducted between November 2020 and April 2021 in the greater Los Angeles County area, initially-SARS-CoV-2-negative household contacts of individuals diagnosed with COVID-19 prospectively self-collected paired anterior-nares nasal-swab and saliva samples twice daily for viral-load quantification by high-sensitivity RT-qPCR and digital-RT-PCR assays. We captured viral-load profiles from the incidence of infection for seven individuals and compared diagnostic sensitivities between respiratory sites. A combination of analytical sensitivity of tests along with sample type determine the test performance. Consistent with literature, peak viral loads were higher in nasal swabs than saliva. However, in the early days of infection, high-analytical-sensitivity testing with saliva outperformed high-analytical-sensitivity nasal swab testing during the first 3.5 days of detectable infection. For most participants, nasal swabs reached higher peak viral loads than saliva, but were undetectable or at lower loads during the first few days of infection. High-sensitivity saliva testing was most reliable for earliest detection. Our study illustrates the value of acquiring early (within hours after a negative high-sensitivity test) viral-load profiles to guide the appropriate

analytical sensitivity and respiratory site for detecting earliest infections. Such data are challenging to acquire but critical to design optimal testing strategies in the current pandemic and will be required for responding to future viral pandemics. As new variants and viruses emerge, up-to-date data on viral kinetics are necessary to adjust testing strategies for reliable early detection of infections.

Keywords: COVID-19; Saliva; Nasal swab; Diagnostics; Pre-Symptomatic; Surveillance; RT-qPCR; Longitudinal sampling; Case-ascertained; Household study; Transmission

INTRODUCTION

Early detection of SARS-CoV-2 infection is needed to reduce asymptomatic and pre-symptomatic transmission, including the introduction and spread of new viral variants from travelers. More than half of transmission events¹ occur from pre-symptomatic or asymptomatic persons. Early detection enables individuals to self-isolate sooner, reducing transmission within households and local communities, and to vulnerable populations, including individuals hospitalized for non-COVID-19 illnesses and individuals at high risk for severe disease due to multiple medical comorbidities (e.g., residents of skilled nursing or long-term-care facilities or memory-care facilities). Low-sensitivity nasal-swab tests are commonly used for SARS-CoV-2 detection and symptomatic testing.² As new variants-of-concern emerge, e.g. the Delta variant with increased transmissibility,³⁻⁵ high viral loads,^{4,6} and outbreaks with large numbers of breakthrough infections,⁷ it is clear that testing strategies (analytical sensitivity and sample type) need to be adjusted to diagnose infections earlier.

Although national vaccination efforts are reducing severe COVID-19 outcomes in the U.S., a sizable portion of the world's population is likely to remain unvaccinated due to limited vaccine availability, medical ineligibility (in the U.S., children under 12 years of age are not yet eligible), or personal preference. Thus, testing remains an important tool for preventing outbreaks among children in schools and daycare facilities (where children under age 2 cannot wear masks), which may spread to the community and increase rates of infection among high-risk and unvaccinated individuals. Tests that detect early infections are also important to prevent viral transmission in congregate settings with high-risk or unvaccinated populations, such as hospitals, college dormitories, homeless shelters, correctional facilities, summer camps for children, elementary schools, and long-term care facilities.

Beyond outbreak prevention and control, early detection of COVID-19 may also be useful for individual patient care, as high-risk patients who are identified early can be monitored and treatment initiated swiftly if it becomes appropriate. Several treatments show exclusive or increased efficacy only when given early in the infection. The advantage of earlier treatment initiation is likely due to reduction of viral replication either directly or by promotion of an early effective immune response, which prevents a later exaggerated inflammatory response.⁸ Results of the ACTT-1 trial demonstrated a survival benefit in patients for whom Remdesivir was initiated in the early stages of treatment (supplemental oxygen only), but that benefit was lost once disease progressed, and advanced respiratory support was needed.⁸⁻¹⁰ Convalescent plasma failed to show efficacy in a study where the median time to entry in the study was 8 days after symptom onset¹¹ but demonstrated protection against progression to respiratory failure when given to individuals of advanced age earlier in the course of the illness.¹² Similarly, the use of anti-SARS-CoV-2 monoclonal antibody therapy (bamlanivimab or casirivimab plus imdevimab) did not show benefit over placebo in a cohort of hospitalized patients.¹³ However, when given to outpatients with mild or moderate COVID-19, who may have otherwise progressed to hospitalization later in the course of illness, reductions in emergency room or medical visit rates and more rapid declines in viral load¹⁴⁻¹⁶ have been observed. Further, a greater effect was observed among the subgroup of patients who had not yet developed a detectable endogenous antibody response.^{8,15}

However, it is currently unclear which testing strategy can detect SARS-CoV-2 infection of circulating variants at the earliest stages. Does one need a high-sensitivity test, or would a low-sensitivity test suffice? Which sample type should one use?

Tests with high analytical sensitivity can detect low levels of molecular components of the virus (e.g. RNA or proteins), in a sample. Analytical sensitivity is described by the limit of detection (LOD) of a test (defined as the lowest concentration of the viral molecules that produces 95% or better probability of detection). The lower the LOD, the higher the analytical sensitivity of the assay. LOD of SARS-CoV-2 diagnostic tests are described in various units; the most directly comparable among tests are units that report the number of viruses (viral particles) or viral RNA copies per milliliter of sample. Viral RNA copies/mL are roughly equivalent to genome copy equivalents/mL (GCE/mL) or nucleic acid detectable units/mL (NDU/mL). These LOD values are tabulated by the U.S. Food & Drug Administration (FDA).¹⁷ High-sensitivity tests have LOD values equivalent to

$\sim 10^2$ to 10^3 copies/mL of sample, whereas low-sensitivity tests have LOD values equivalent to $\sim 10^5$ to 10^7 copies/mL. Therefore, to choose the appropriate test for reliable early detection, one needs to measure viral loads present in samples collected early in the course of infection,¹⁸ and then choose a test with an LOD below that viral load. Initial data by us¹⁹ and others^{20,21} show that, at least in some humans, SARS-CoV-2 viral load can be low (in the range of 10^3 – 10^5 copies per mL of saliva sample) early in infection, therefore only high-sensitivity tests would reliably detect infection.

Sampling site or specimen type may also be critical to early detection. Other respiratory viruses have been shown to have detection rates that vary by sampling site,²² which have occasionally been linked to viral tropism. For example, the cellular receptor for entry of MERS-CoV is expressed nearly exclusively in the lower respiratory tract, prompting recommendations for diagnostic testing of specific sample types (bronchoalveolar lavage, sputum and tracheal aspirates).²³ A previous study on SARS-CoV found high levels of viral RNA in saliva and throat wash early in the infection course (before the development of lung lesions), to suggest saliva as a promising sample type for early detection.²⁴ Although nasopharyngeal (NP) swab is often considered the gold standard for SARS-CoV-2 detection, it requires collection by a healthcare worker and is not well tolerated. Furthermore, the performance of NP swabs for early detection of current SARS-CoV-2 variants is not known. Other sample types, such as nasal (anterior-nares or mid-turbinate) swabs²⁵⁻²⁸ and saliva²⁹⁻³² are more practical, especially for repeated sampling in serial surveillance testing (also described as “screening”).

Studies comparing paired samples (collected from different locations in the respiratory tract) from the same individual are inconsistent in their findings of which sample type had the better sensitivity. Some studies concluded that nasal swabs outperform saliva/oral fluid^{27,33-36} and had higher viral loads,^{26,28,34} whereas others concluded that testing performance in different locations of the respiratory tract is similar.^{30,37-43} Some studies have observed detection of SARS-CoV-2 in saliva before nasal swabs, or in saliva but not in nasal swabs;^{21,44,45} one study of an emerging variant (B.1.616) showed poor detectability of SARS-CoV-2 in NP swabs.⁴⁶ It is not known whether NP is the best respiratory site for currently circulating variants and emerging variants.

There are several possible explanations for these inconsistencies in respiratory sampling site. Most studies comparing clinical sensitivity of different respiratory sites for SARS-CoV-2 detection

focused only on viral detection, not viral-load quantification, which is needed to infer whether detection would have been achieved by assays with different LODs. Although a few studies collected samples in RNA-stabilizing buffers,^{40,47-49} most have collected dry-swabs or saliva in sterile collection vessels;^{26-28,30,37,50-57} without an RNA-stabilizing buffer, introducing risk of viral degradation during transport and handling, which will affect detection and quantification. Most studies that compared multiple respiratory sites for SARS-CoV-2 detection selected individuals already known to be positive for SARS-CoV-2, thus missing the very earliest detectable loads and also not having context for how far along the course of infection that individual might have been. An excellent study comparing nasal swabs and saliva sampling early in the infection among adults at a university⁵⁸ suggested that high-sensitivity testing is needed for early detection; by leveraging university saliva surveillance testing and enrolling close contacts, the researchers reported longitudinal viral kinetics data from 60 participants, 3 of whom (based on our interpretation of the study) were negative in both sample types upon enrollment, allowing for definitive quantification of the earliest day(s) of infection. The thorough work done here shows both how important it is to obtain early samples, but also how difficult it is to capture samples from which to assess the earliest days of infection.

Negative samples preceding the first positive result are needed confirm with high resolution the true starting point of longitudinal measurements on viral load. In order to compare diagnostic performance at different stages of the infection, studies with longitudinal data often align the comparisons to an infection time point—typically days relative to symptom onset,^{27,30,35,47,58-64} laboratory diagnosis (i.e., first positive test result),^{27,38,59,65} or peak viral load,⁵⁸ but these measures can be highly variable among people. Misalignment of illness stage may confound comparisons of sample type sensitivity or viral loads throughout the course of infection. Despite the urgency of defining optimal diagnostic strategies to contain further outbreaks (and spread of variants-of-concern), there is a lack of quantitative data on longitudinal SARS-CoV-2 viral load in paired sample types with sample collection starting prior to earliest detectable viral loads.

To understand the required test sensitivity and the optimal sample type for earliest SARS-CoV-2 detection, we designed a case-ascertained study of household transmission with high-frequency sampling of both saliva and anterior-nares nasal swabs. Building on our earlier work,¹⁹ we enrolled individuals from Los Angeles County, California, ages 6 and older who had recently

tested positive (household index case), and their exposed household contacts at risk of infection. All participants self-collected saliva and anterior-nares nasal swabs twice daily, in the morning upon waking and before bed. Importantly, all samples were immediately placed in a guanidinium-based inactivating solution (see Methods) that preserves viral RNA. We measured the stability of RNA in this buffer over the time periods relevant to our sample processing. Samples were screened for SARS-CoV-2 *N1* and *N2* gene positivity using a high-sensitivity assay and if a transmission event was observed (a previously SARS-CoV-2 negative participant tested positive in at least one sample type), we quantified viral loads in all samples (saliva and nasal swab) prospectively collected from that participant for at least two weeks from their first positive. Quantification was performed via quantitative reverse-transcription PCR (RT-qPCR), with a subset of measurements validated by reverse-transcription droplet digital PCR (RT-ddPCR), capturing the early and full course of acute SARS-CoV-2 infection with high sensitivity.

RESULTS

First, we established and validated two independent quantitative assays to measure SARS-CoV-2 viral load: a RT-qPCR based on the assay put forth by the U.S. Centers for Disease Control and Prevention (CDC)⁶⁶ and a RT-ddPCR assay developed by Bio-Rad.⁶⁷ Both of these assays received an emergency use authorization (EUA) for qualitative, but not quantitative, detection of SARS-CoV-2. In initial testing, when combined with standard KingFisher MagMax sample preparation protocols, these assays performed well to quantify heat-inactivated SARS-CoV-2 viral particles spiked into commercially available SARS-CoV-2 negative saliva and nasal fluid from pooled donors. However, they did not provide reliable quantification when we analyzed individual saliva samples freshly collected from positive participants in this study. Carryover of materials from some of the mucus-rich samples was inhibitory, as determined by RT-ddPCR analysis of dilutions of eluted RNA (data not shown). We optimized the extraction and each quantitative assay protocol (see Methods) to obtain more reliable quantification of SARS-CoV-2 viral load. We confirmed that the LOD of the modified assay was 1,000 copies/mL or better (see Methods, Fig. 5-S1).

We cross-validated our quantification methods in two steps. First, we used commercial, heat-inactivated SARS-CoV-2 viral particles to establish calibration curves for both saliva and swab samples to convert RT-qPCR quantification cycle values (*C_q*, also referred to as cycle thresholds, *C_t*) to viral load. Input particle concentrations for each point on the curve were calculated based on

the stock quantification reported on the certificate of analysis for each lot of particles. We could not extend the calibration curve to very high viral loads because of the limited concentration of viral particle stock; so, to confirm performance at high viral loads, we quantified 42 swab and 63 saliva samples from SARS-CoV-2-positive participants with both RT-qPCR and RT-ddPCR methods. We observed excellent concordance between the calibration curve (Data in Fig. 5-S2), RT-qPCR and RT-ddPCR assays over the entire dynamic range of input concentrations (Fig. 5-1), even though RT-qPCR eluents were run as-is and RT-ddPCR eluents from high-concentration samples were significantly diluted. For nasal-swab samples, RT-ddPCR values were slightly below the RT-qPCR values, however this difference was consistent across the entire dynamic range, indicating no concentration-dependent biases like enzymatic inhibition. We chose not to adjust the calibration curve to fit RT-ddPCR values; we reported the concentrations based on the calibration curves derived from the certificate of analysis from the BEI reference material. For saliva samples, all points tightly clustered around the $x=y$ line.

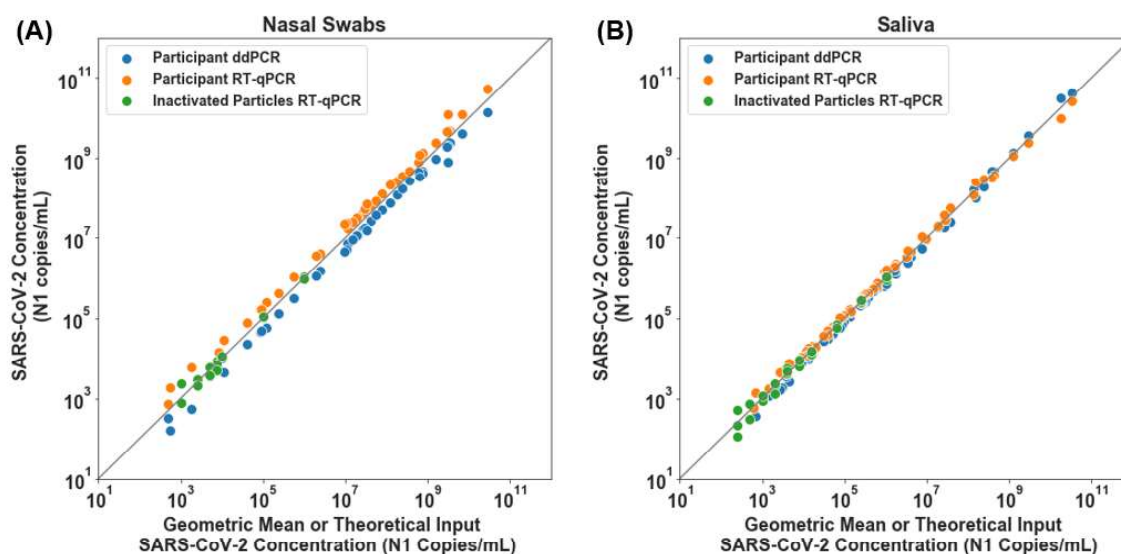


Figure 3-1. SARS-CoV-2 viral load quantification for nasal-swab (A) and saliva (B) specimens from positive participants measured with RT-ddPCR and RT-qPCR. Participant nasal swab (A) or saliva (B) SARS-CoV-2 *N1* concentration (copies/mL) per detection method, RT-ddPCR (Blue circles) and RT-qPCR (orange circles) plotted against geometric mean of RT-qPCR and RT-ddPCR viral load concentrations. A total of 42 nasal swab and 63 saliva samples from study participants were quantified with both methods. Theoretical SARS-CoV-2 concentration input represents data from calibration curves created with a dilution series of contrived samples prepared using commercial, inactivated SARS-CoV-2 particles spiked into commercially available SARS-CoV-2 negative saliva or nasal fluid pooled from human donors (green circles), extracted and detected with RT-qPCR. Grey line represents $x=y$.

Next, to quantify viral load at the earliest stage of infection, we analyzed the viral loads in the saliva and nasal swabs of participants who were negative in both sample types upon enrollment

and became positive during their participation in the study (Fig. 5-2). We extended each participant's enrollment in our study to acquire 14 days of paired saliva and nasal-swab samples starting from the first positive sample. Data in Fig. 5-2 reports the viral load concentrations as measured on the day of extraction. All samples were stored at 4 °C before extraction; time of storage varied between 0-27 days. The stability of SARS-CoV-2 RNA in nasal-swab samples was slightly lower (1 Cq loss of RNA detected after a median of 15 days) than the stability of SARS-CoV-2 RNA in saliva samples (1 Cq loss of RNA detected after a median of 51 days) (Fig. 5-S3). An assessment of how viral-load measurements in Fig. 5-2 may have been affected by time between sample collection and quantification is included in Fig. 5-S4. Given the large dynamic range of the viral loads in these samples (~24 Cq or about 10,000,000 fold), we considered stability corresponding to a 1 Cq (2 fold) loss to be adequate.

Here we report complete viral load curves in saliva and anterior-nares nasal swabs from seven individuals (Fig. 3-2). Each of these participants tested negative (ND, not detected; Fig. 3-2) in both saliva and nasal swabs upon study enrollment, ensuring that we capture the earliest days of infection. *RNase P* Cq values remained consistent throughout the collection period for both saliva and nasal swabs for most of the participants (Fig. 3-2A, B, D, F, and G), indicating observed changes in viral loads were likely not a sampling artifact but rather reflected the underlying biology of the infection. Because nasal swabs are commonly used with low-sensitivity tests, and because such tests are proposed to be utilized for SARS-CoV-2 serial surveillance testing (screening),^{68,69} we wished to compare whether low-analytical-sensitivity testing with nasal swabs could provide equivalent performance to high-analytical-sensitivity testing with saliva.^{31,52,70} We did not run any tests with low-analytical sensitivity; our quantitative viral load measurements were used to predict the performance of a test with an LOD of low-analytical sensitivity. When viral loads crossed a threshold of 1.9×10^5 copies/mL, shown as the lower bound of the green shaded region (Fig 3-2), we marked the sample with an orange triangle for nasal swabs or an orange circle for saliva samples.

In five out of seven participants, saliva testing with high analytical sensitivity would have detected SARS-CoV-2 earlier than nasal swab testing at the same sensitivity. In six out of seven participants, high-sensitivity saliva testing would have been superior for early detection of SARS-CoV-2 infection compared with inferred detection of low-sensitivity nasal-swab measurements (and equivalent for the seventh participant). In two participants, saliva viral loads never reached a

concentration of the low analytical sensitivity threshold, and these figure panels do not have an orange circle (Fig 3-2C-D).

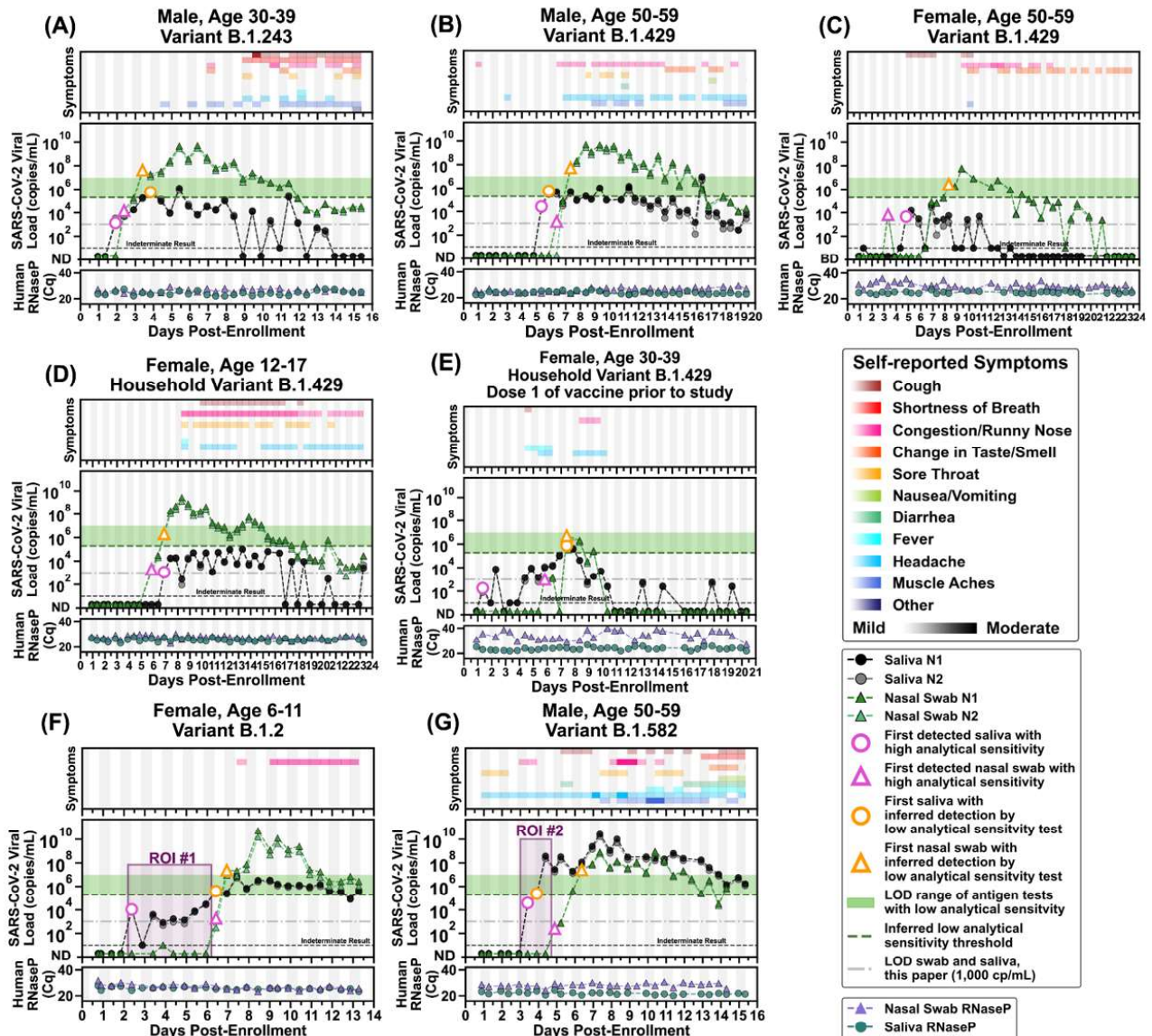


Figure 3-2. Symptoms and SARS-CoV-2 viral loads in paired saliva and nasal-swab samples of seven participants who became SARS-CoV-2 positive during study participation. (A-G) Self-reported twice-daily symptom data over the course of enrollment are shown as a top panel for each of the participants (see color-coded legend for symptom categories). Details of symptoms are included in the raw data files. Demographic data including any reported medical conditions are included in Table 3-S1. Viral loads are reported for the *N1* and *N2* genes of SARS-CoV-2 for both saliva (black and grey circles) and nasal-swab samples (dark-green and light-green triangles); ND = not detected for Cqs ≥ 40 ; Samples with an indeterminate result by the CDC RT-qPCR assay are shown along the horizontal black dashed line. (see Methods for details). The limit of detection of the assay used for high analytical sensitivity measurements is shown with a horizontal grey dashed line. The limit of detection (LOD) of the Abbott ID NOW (3.0×10^5 NDU/mL¹⁷) is indicated by the horizontal green dashed line; the range of LODs of antigen tests (horizontal green bar) are shown for reference (data are from Table S2 in ref. ¹⁹). A diagnostic test does not provide reliable detection for samples

with viral loads below its LOD. For each participant, the first detected saliva point is emphasized with a pink circle (high analytical sensitivity) and the first detected nasal swab is emphasized with a pink triangle (high analytical sensitivity). Inferred detection, when quantitative viral loads cross 3.0×10^5 copies/mL (low analytical sensitivity threshold), of the first data point that could be detected by low sensitivity measurements is emphasized with an orange circle for saliva and an orange triangle for nasal swabs. Vertical shading in grey indicates nighttime (8pm – 8am). Internal control of *RNase P* gene Cqs from the CDC primer set are provided for each sample to compare self-sampling consistency and sample integrity (failed samples, where *RNase P* Cq ≥ 40 , are not plotted). Participant gender, age range, and SARS-CoV-2 variant are given in each panel's title. Two regions of interest (ROI) are indicated by purple-shaded rectangles and discussed in the main text.

In the first participant, (Fig. 3-2A), detection occurred first in saliva at low viral load (1.3×10^3 copies/mL *NI* gene, pink circle), while the nasal swab remained negative, and days before the participant reported any symptoms. As measured, viral load in nasal-swab samples reached the level of LOD of low-sensitivity tests (orange triangle) 1.5 days after the first saliva positive samples. This same pattern of earlier detection in high-sensitivity saliva was observed in five of the other six participants: high-sensitivity saliva was 2.5 days earlier (Fig. 3-2B), 3.5 days earlier (Fig. 3-2C), 6 days earlier (Fig. 3-2E), 4.5 days earlier (Fig. 3-2F), and 2.5 days earlier (Fig. 3-2G). Even conservatively accounting for potential decreases of viral RNA in the nasal swab resulting from delays between sample collection and quantification only impact the interpretation of two points, conservatively decreasing the delay from 1.5 to 1 day for the first participant (Fig. 3-2A and Fig. 3-S4A) and from 3.5 to 3 days for the third participant (Fig. 3-2C and Fig. 3-S4C). The maximum delay in detection between saliva and nasal swab in an unvaccinated person was observed by the youngest participant in our study (see ROI#1 of Fig. 3-2F). This participant had detectable but low viral load (10^3 - 10^4) of SARS-CoV-2 RNA in saliva for 4 days while nasal swabs remained negative by high-sensitivity measurements. The nasal viral load spiked above 10^{10} copies/mL. Even after spiking to high viral load in nasal swab, her only symptoms were mild congestion/runny nose. Even with high-sensitivity nasal swab testing, only one participant tested positive in nasal swab before saliva (Fig. 3-2D). In this participant, SARS-CoV-2 RNA was detectable with a high-sensitivity nasal swab (pink triangle) 1 day before high-sensitivity saliva (pink circle). Nasal swabs reached the detection range of low-sensitivity tests (orange triangle) on the same day as the first saliva sample was detected (pink circle). For all seven participants, high-sensitivity saliva testing would have detected SARS-CoV-2 RNA either the same day or up to 6 days before viral loads in nasal swab reached the detection limits of low-sensitivity nasal swab tests. This pattern of earlier positivity but lower viral loads in saliva compared with nasal swabs was not due to RNA degradation in saliva;

when we examined the potential effect of RNA stability there was little effect on RNA concentration over time in saliva samples stored in the preservation buffer at 4 °C (Fig. 3-S3, Fig. 3-S4).

Three participants (Fig. 3-2C–E) were infected with the same variant, B.1.429 (CAL20), classified as a variant-of-concern at the time of this study. The SARS-CoV-2 variant for the participants in Fig. 3-2D and Fig. 3-2E were inferred from the sequenced sample of the household's presumed index case. Saliva viral loads for each of these participants (Fig. 3-2C-E) were low. Of note, the participants in Fig. 3-2C and 5-2E showed high *RNase P* Cq values (indicating low concentration of the human control target); and variability of *RNase P* Cq values across the nasal-swab samples suggests that inconsistent swab-sampling quality could have impacted these participants' viral load data, and should be taken into account when interpreting those data. These two participants (Fig. 3-2C and 5-2E) also had low viral load in both saliva and nasal swabs. Their viral load measurements were near the LOD of our assay, and therefore as expected, many samples from these participants had indeterminate results.

The fifth participant (Fig. 3-2E) had received one dose of the Pfizer-BioNTech COVID-19 vaccine⁷¹ 13 days prior to her first sample. As the only participant in our study who had received a vaccine dose, observations here are not powered to make conclusions about viral load due to vaccination. This participant had very low viral loads in both saliva and nasal-swab sample types and several indeterminate test results when adjacent viral load measurements were near the LOD of our assay. Peak viral loads were lower and shorter in duration compared with the other six study participants. A high-sensitivity saliva test (pink circle) detected the infection 6 days before viral loads reached the lower range of the LODs of low-sensitivity tests (orange triangle) for this participant. Recent data from individuals infected by the Delta variant suggest viral loads in breakthrough infections are not impacted by vaccination status.^{7,72}

The final participant (Fig. 3-2G) with medical history significant for obesity, reported experiencing symptoms beginning 3 days prior to enrollment, and tested negative for SARS-CoV-2 by a CLIA-lab test 2 days prior to enrollment in the study. This person would later report more diverse symptoms (including gastrointestinal symptoms) and with higher symptom-severity ratings than the other six participants. Remarkably (see ROI#2 in Fig. 3-2G), saliva viral load spiked to 3.7×10^8 viral copies/mL (*NI* gene target) while SARS-CoV-2 RNA remained undetectable in nasal

swab, even by the high-sensitivity assay used here. This contrast between high and likely infectious viral load in saliva⁷³ at the same time point as a negative nasal swab emphasizes the need for careful choice of sampling site and test sensitivity in the early stages of SARS-CoV-2 infection to minimize transmission.

Compiled data from all seven participants highlights the non-trivial interplay of anatomical sampling site, infection stage, and diagnostic test sensitivity (Fig. 3-3). Samples (either saliva or nasal swab) with SARS-CoV-2 viral loads above 3.0×10^5 cp/mL, the LOD of an example low analytical sensitivity test Abbott ID NOW, were inferred to be positive by a low analytical sensitivity test. The percentage of participants with either observed or inferred positive results at each time point (0.5-day intervals) from the first positive revealed that high-sensitivity saliva testing outperforms both high-sensitivity nasal swab testing, for the first 4.0 days, and inferred low-sensitivity nasal swab testing, for the first 5.5 days, in the earliest days of detectable infection (Fig 3-3A). If we adjust the threshold for performance to 85% of participants detected, the advantage becomes 3.5 days for high-sensitivity nasal swab testing and 4.5 days for low-sensitivity nasal swab testing. Analytical sensitivity of the test strongly impacts the overall test performance and the preferred sample type: based on viral loads in saliva, inferred positivity by low-analytical-sensitivity saliva testing was outperformed by high-sensitivity saliva and both high- and low- analytical sensitivity nasal swab testing (Fig. 3-3A).

Next, we plotted viral loads in each respiratory site starting from the first positive test (Fig. 3-3B). Paired samples for a given time point are connected with grey lines, with emphasis on paired samples where only saliva (black connecting line) or nasal swab (green connecting line) were positive. From day 0 to day 6, using high-sensitivity testing for both sample types, saliva is more frequently positive than nasal swabs, shown by bolded black lines (Fig. 3-3B). Comparison of paired samples between day 6 and day 12 both sample types show highly concordant detection. In a later time interval, between days 12 and 16, nasal swabs are more frequently positive than saliva, shown by bolded green lines (Fig. 3-3B). The median of peak viral loads is higher in nasal swabs than saliva (Fig. 3-3C), which is also consistent with literature.^{26,28,36}

Many testing strategies and decisions are based on the presence or absence of symptoms.^{2,74} We considered the positivity rate of high- or low- analytical sensitivity testing methods with each

sample type during the first ten days of test-positive infection, separating into categories of no symptoms or symptomatic if the participant reported at least one COVID-19-like symptom (Fig. 3-3D). This interval of 10 days was selected, to capture the pre-symptomatic and symptomatic phases of infection for this cohort, while avoiding samples collected during the post-symptomatic phase of infection. Regardless of symptom status or sample type, high-sensitivity testing results in considerably higher positivity frequency than low-sensitivity testing (Fig. 3-3D). For samples collected while participants were asymptomatic, high-sensitivity saliva testing was more effective (74% positivity) than nasal swabs of high- (52%) or low-sensitivity (34%) or of saliva of low-sensitivity (17%). In contrast, during symptomatic phases, which is often concurrent with peak nasal viral loads (Fig. 3-2), high-sensitivity saliva (88%) and high-sensitivity nasal swab testing (89%) have similar positivity rates. Additionally, based on our measured viral loads, low-sensitivity nasal-swab testing is predicted to perform better in symptomatic cohorts than in asymptomatic persons, consistent with how these tests were originally authorized.

These data paint a more nuanced view than “saliva is better than swab”. SARS-CoV-2 RNA is more detectable in saliva than nasal swab during the early phase of the infection (Fig 3B). However, because saliva viral loads generally remained lower than nasal swabs (Fig 3C), the inferred positivity by a low-analytical-sensitivity saliva test was outperformed by both high- and low-analytical sensitivity nasal swab (Fig 3A). This was independent of symptom status (Fig 3D). Analytical sensitivity of the test, along with sample type, strongly impacts overall performance.

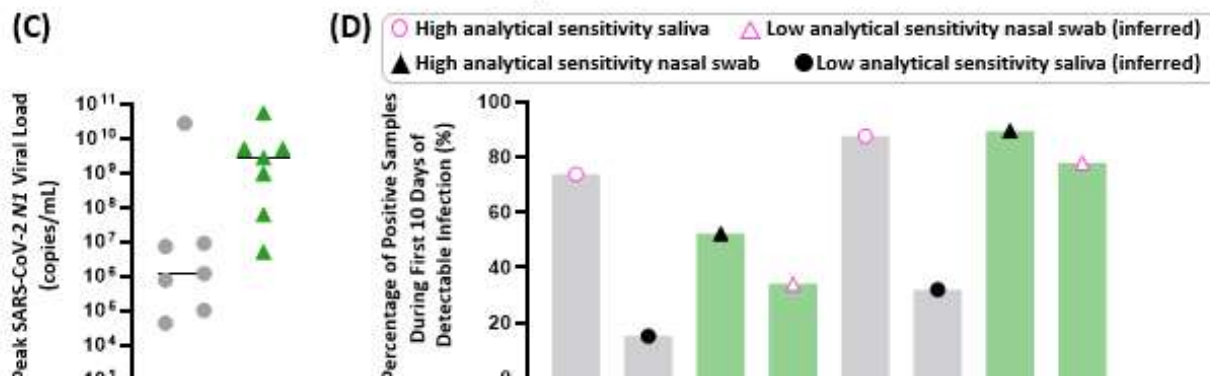
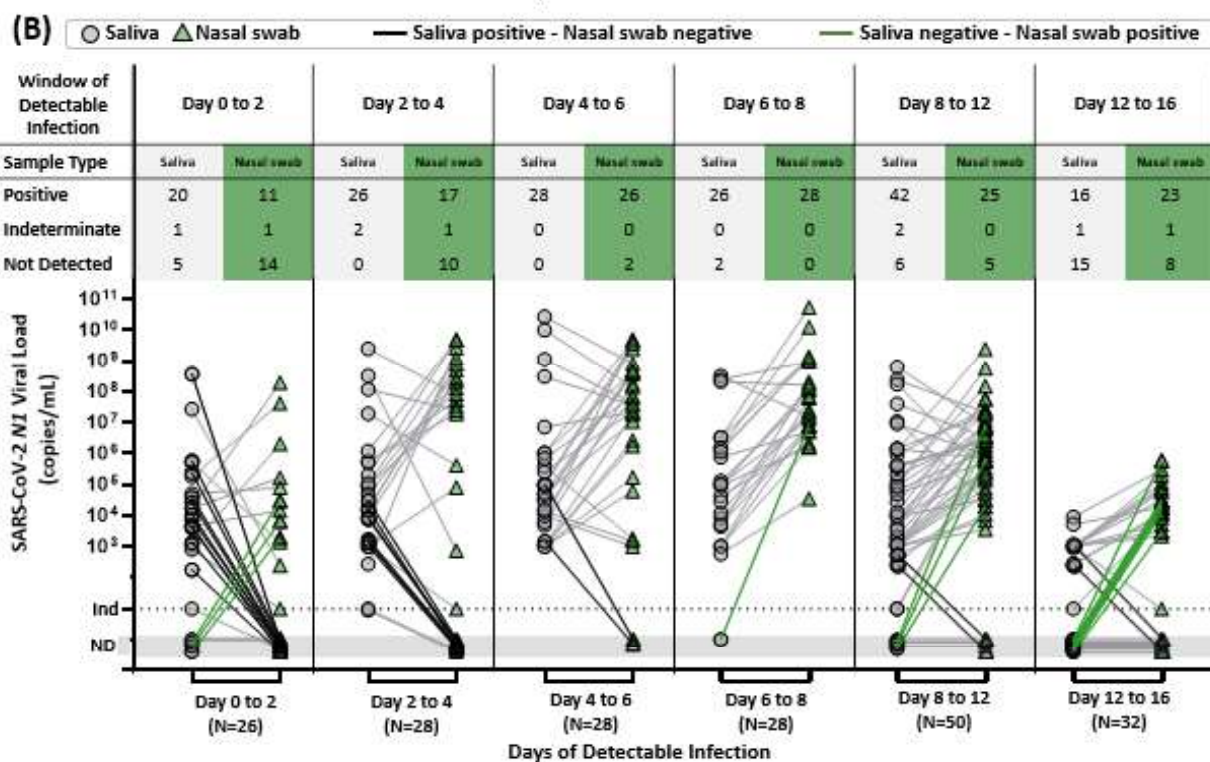
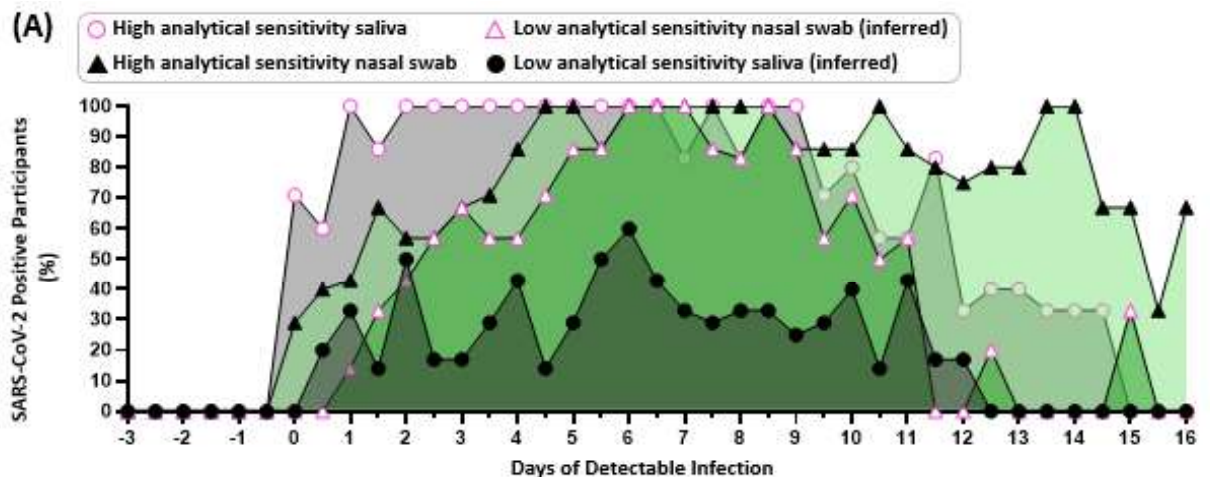


Figure 5-3. Summary of Diagnostic Insights from Study Participants who became infected with SARS-CoV-2 while enrolled in the study (A) Participant infection time courses were aligned to the first high-sensitivity (LOD of $\leq 1 \times 10^3$ copies/mL) positive result from either saliva or nasal swab sample type (day 0) and the percentage of positive tests

was calculated for each time point (0.5-day intervals) from the first positive sample. The predicted performance of low-sensitivity nasal swabs was determined using the individual SARS-CoV-2 *NI* viral load values for each participant individually shown in Fig. 3-2, or above a viral load threshold of 3.0×10^5 copies/mL, which among the most-sensitive of the low-sensitivity tests (Abbott ID NOW) we included in shaded region of Fig. 2. We show the percentage of participants who were detected by our high sensitivity saliva test (black circle) or could be inferred to be detectable by a low-sensitivity nasal swab test (green triangle) at a given timepoint. **(B)** Quantitative SARS-CoV-2 *NI* viral loads of paired samples collected during time windows of the infection (aligned to first positive result by high sensitivity testing of either sample type) are shown for saliva (grey circles) and nasal swabs (green triangles). Paired samples for a given time point are connected with grey lines, with emphasis on paired samples where only saliva (black connecting line) or nasal swab (green connecting line) were positive. ND = Not Detected, Ind = Indeterminate result. **(C)** Peak SARS-CoV-2 *NI* viral loads measured in saliva (grey circles) and nasal swab (green triangles) for each of the seven participants are shown. Horizontal black line indicates the median. **(D)** Percentage of positive test results (out of total number of tests) are shown for the first 10 days for each participant (day 0 corresponds to the first positive test result in either sample type). Saliva (grey bars) and nasal swab (green bars) are shown. Positivity was either observed (by our high sensitivity test) or inferred to be positive by viral loads above a LOD threshold of 3.0×10^5 copies/mL for low-sensitivity tests. The symptomatic category includes any sample where one or more symptom was reported at the time of sample

LIMITATIONS

Our study needs to be interpreted in the context of its limitations. First, our results capture viral load dynamics from a limited number of individuals from one region of one country with limited SARS-CoV-2 diversity. A larger study with individuals of diverse ages, genetic backgrounds, medical conditions, COVID-19 severity, and SARS-CoV-2 lineages would be ideal to provide a more nuanced and representative understanding of viral dynamics in saliva and nasal-swab samples. Second, the commercial inactivating buffer used here (Spectrum SDNA-1000) is not authorized (at the time of this writing) for the sample collection of nasal swabs. Third, we have paired data for saliva and anterior-nares nasal swabs but do not compare nasopharyngeal (NP) swabs, sputum, or other lower-respiratory specimens. We do not know whether other sampling sites, such as nasopharyngeal swabs or oropharyngeal swabs, would have provided earlier or later detection than saliva. As mentioned above, parallel sampling of multiple respiratory sites should be done as new variants emerge. Fourth, we do not have data for low-sensitivity tests or any antigen tests, and are inferring ability to pick up infections based on the quantified viral load in the participant samples and the LODs reported by the FDA for the diagnostic platforms. Fifth, our investigation of SARS-CoV-2 RNA stability in each sample type (saliva, nasal swabs) in the inactivating buffer at 4 °C during storage suggests some degradation may have occurred in some samples, and revealed subtle differences between degradation in saliva and nasal swabs (Fig. 3-S3). See Supplement for a complete analysis of RNA stability. Sixth, our samples were self-collected by participants after detailed training by our study coordinators during the study enrollment process. Samples self-collected without such training may result in lower quality specimens. Similarly, our participants were able to collect saliva samples during specific parts of their day (after waking and before going

to bed) without eating, drinking, or brushing teeth prior to collection. This protocol may not be practical in all settings and we do not know how deviations from this protocol would affect viral loads in saliva. Lastly, our samples were self-collected in a guanidinium-based inactivating and stabilizing buffer that preserves viral RNA but eliminated the opportunity to also perform viral culture.

CONCLUSIONS

By rapidly enrolling household members at high risk for contracting COVID-19 and having them self-sample and report symptoms twice daily in paired respiratory sites, we were able to observe patterns in SARS-CoV-2 viral load in the earliest days of infection. All seven participants tested negative by both sample types (saliva and nasal swabs) upon enrollment, ensuring we captured the earliest detectable SARS-CoV-2 viral load (within 12 hours) in both sample types. Our dataset helps inform diagnostic testing strategies by showing differences in viral loads in paired nasal swabs and saliva samples at high temporal resolution (twice daily) during the early days and pre-symptomatic phases of infection.

We drew five conclusions from our study:

First, choosing the correct respiratory sampling site is critical for earliest detection of SARS-CoV-2 infection. In our study, alignment of longitudinal data to the first day of positivity clearly shows the superiority of high-sensitivity saliva testing over high-sensitivity nasal swab testing for detection in the first 3.5 days of detectable infection, by conservative estimation of 85% of participants detected by each (Fig. 3-3A). Although sampling with NP swabs may be considered by some to be the gold-standard for COVID-19 testing, there are no data suggesting NP swabs are superior for earliest detection of SARS-CoV-2 infection. Furthermore, anterior-nares swabs and saliva tests have become more common than NP swabs for practical reasons. Given our data, early infection viral load dynamics in multiple sampling sites should be investigated and compared with saliva as new SARS-CoV-2 variants emerge.

Second, our data explain the conflicting results in the literature comparing the performance of testing from paired respiratory sites, with some studies showing nasal-swabs outperform saliva^{26,28,36} and others showing saliva (or oral fluid) has equivalent or better detection to nasal-swabs.^{21,30,37-45} Through longitudinal rather than cross-sectional sampling, we show the relative viral

loads in each respiratory site is a factor of infection stage (shown in time intervals in Fig. 3-3B), and the kinetics of viral load over the course of the infection may be quite distinct in each sample type for an individual (Fig. 3-2). Most studies examining paired sample types have enrolled participants after a positive test or after symptom onset; as our data show, detectable viral loads precede symptoms, in most cases (5/7 participants) by several days (Fig. 3-2). Thus, enrollment after positivity or after symptom onset is not an appropriate study design to determine the respiratory sample type in which the virus is first detectable (Fig. 3-3A, Fig. 3-S5).

Third, peak viral load measured in nasal swabs (Fig. 3-3C) is not representative of detectable viral load in the earliest days of infection (Fig. 3-3A) nor during the pre-symptomatic phase (Fig. 3-3D). Early in an infection, it is inappropriate to assume that a person is “not infectious” or “has low viral load” based on a measurement from a single sample type such as a nasal swab, given that saliva is known to carry infectious virus.⁷³ In our study, we observed a participant with very high ($>10^7$ - 10^8 copies/mL) viral load in saliva samples while the paired nasal swab was either negative (Fig. 3-2G, ROI#2) or had low ($\sim 10^3$ copies/mL) viral load (Fig. 3-2G, day after ROI#2). Quantitative SARS-CoV-2 culture from paired saliva and swab samples is still needed to understand infectiousness during the early stages of SARS-CoV-2 infection.

Fourth, using a diagnostic test with high analytical sensitivity (Fig. 3-3D), rather than a test of a particular detection method (RT-PCR, antigen, next-generation sequencing, etc.), is essential to early detection. Often the test type (e.g., RT-qPCR) is incorrectly equated with high analytical sensitivity, and some current travel and work guidelines specify a test type (e.g., RT-qPCR) rather than a particular test LOD. However, this is an invalid assumption; FDA testing¹⁷ demonstrated that sensitivity of RT-qPCR tests ranges from highly sensitive (e.g., LOD of 180 NDU/mL for PerkinElmer and 450 NDU/mL for Zymo Research) to substantially less sensitive (e.g., LOD of 180,000 NDU/mL for TaqPath COVID-19 Combo Kit and 540,000 NDU/mL for Lyra Direct SARS-CoV-2 Assay). FDA’s NDU/mL is approximately equivalent to the copy/mL scale used in this paper. The low-sensitivity end of this RT-qPCR sensitivity range (corresponding to the higher LOD values) overlaps with the range of low-sensitivity rapid isothermal nucleic-acid tests (e.g., LOD of 180,000 NDU/mL for Atila BioSystems and 300,000 NDU/mL for Abbott ID NOW tests) and approaches the analytical sensitivity range of antigen tests. Therefore, to achieve early detection, tests with high sensitivity rather than tests of a particular type should be chosen. With many strategies for

asymptomatic screening/surveillance testing in use, it is critically important to consider whether the LODs of the tests would be able to detect early infection, and to prompt actions that minimizes transmission.

Fifth, our data show the utility of combining knowledge of the appropriate respiratory site and the appropriate test analytical sensitivity for achieving earliest detection. Among our unvaccinated participants, when a high-sensitivity test was combined with saliva as a sample type, SARS-CoV-2 infection was detected up to 4.5 days before viral loads in nasal swabs reached the LODs of low-sensitivity tests (Fig. 3-2F). Although high-sensitivity saliva testing was usually able to detect earlier than nasal swabs (Fig. 3-3A, Fig. 3-S5), during the peak of the infection viral loads in nasal swabs were usually higher than in saliva (Fig. 3-3C). Furthermore, SARS-CoV-2 was detected in saliva with high-sensitivity methods when the viral loads were low (Fig. 3-2, Fig. 3-3D, Fig. 3-S5); low-sensitivity saliva tests would likely not have been able to detect these infections early. These observations support the preferred use of nasal swabs in environments where only low-sensitivity testing is available, although the performance of such testing for early detection is poor (Fig. 3-3D). These observations also show that the choice of the optimal respiratory sampling site is nuanced and depends on the phase of the infection being detected (early vs peak) and on the analytical sensitivity of the test being used with each sample type.

Our work suggests three steps to improve effectiveness of diagnostic tests in early detection and preventing transmission of SARS-CoV-2 as new variants emerge and as infections spread to additional segments of the global population: (1) Additional longitudinal studies are needed that include high-frequency collection from multiple respiratory sites using quantitative assays with high analytical sensitivity. (2) Policy makers need to use such quantitative data to revise and optimize testing, surveillance, and screening guidelines to ensure early detection of SARS-CoV-2 infections and reduction of transmission. (3) Innovation is needed to produce rapid point-of-care tests with high analytical sensitivity for a range of sample types (including saliva) at a price point to enable global distribution.

As new SARS-CoV-2 variants emerge, quantitative studies of the kinetics of early-stage viral loads must be continually updated. Importantly, such studies should be undertaken in people of a wide range of ethnicities, races, health conditions, and ages. For example, children under 12 years

of age remain ineligible for vaccination even as schools around the country reopen for in-person studies. Given the potential differences in viral kinetics between children and adults, it is critical to collect quantitative viral-load data from children to understand the most effective testing strategies for this population. Quantitative studies of viral-load dynamics must also include vaccinated persons. Breakthrough cases are often asymptomatic⁷⁵ and recent evidence suggests that vaccinated individuals may transmit infections from the new variants, including Delta.⁷ Another reason for continued monitoring of early viral kinetics is that viral evolution, including of host tropism, can markedly diminish the effectiveness of a diagnostic strategy. In one study, decreased clinical sensitivity of NP swabs was observed in SARS-CoV-2 variant B.1.616,⁴⁶ which may indicate a tropism shift of the virus into lower-respiratory compartments. Finally, quantitative data must be acquired in parallel with viral-culture data to understand the viral loads and phases of infection that are most relevant to transmission.

Early detection of infection clearly reduces community transmission, however for most of the COVID-19 pandemic, policy makers have had to develop testing strategies in the absence of quantitative data on viral kinetics from the earliest stage of infection. Testing strategies have been guided by the available viral-load data, which has come mostly from hospitalized patients, symptomatic people, and people who have tested positive with the commonly available tests; but these data cannot inform on the best strategies for *earliest* detection. Moreover, lacking such data-based guidance, diagnostic tests have been used incorrectly (with false-negative results due to using tests with insufficient sensitivity) in several scenarios, resulting in outbreaks that could have been prevented with an appropriate testing strategy.⁷⁶⁻⁸² Once armed with data on early viral-load kinetics of new and emerging variants, policy makers will be able to develop targeted testing strategies (frequency of sampling, required test sensitivity, and appropriate respiratory site) for key populations undergoing regular repeated testing, such as hospital staff and nursing-home staff. Such data would also inform optimal testing guidelines for early detection in situations where a single test is typically administered to admit a person into an environment (e.g., persons embarking on a flight or cruise, summer camps, or admission to a country) where the impact of false negatives is particularly high.

One barrier to implementing such more advanced testing strategies is availability of appropriate tests. Because the optimal sample type for early detection might be different for different populations, or might change as new variants emerge, tests with robust high analytical sensitivity

across multiple sample types are needed. Developing such tests is challenging because it requires incorporating robust sample-preparation technology to purify and concentrate pathogen nucleic acids from diverse human matrices, from upper respiratory (e.g. fluids from the nasal, nasopharyngeal, oral and oropharyngeal compartments, captured in swabs or saliva) to lower respiratory samples (e.g. sputum, tracheal aspirate, bronchoalveolar lavage). It is even more challenging to incorporate such sample-preparation technology into tests that can be broadly deployed—at very low cost—at the point of care in limited-resource settings (such as schools, homes, and businesses, and especially in the developing countries). Development of such highly sensitive, rapid, and inexpensive tests with broad sample-type compatibility is urgently needed.

We hope our data, important work by others in this area,^{20,21,58,73} and future quantitative studies of early viral-load kinetics will lead to improved testing strategies to combat the current COVID-19 pandemic. The methodology for performing such studies efficiently and quickly will likely be extendable to defining strategies for early detection of causative pathogens in subsequent pandemics.

METHODS

Refer to the Supplementary Information for detailed methods.

Participant Population

This study is an extension of our previous study examining viral load in saliva.¹⁹ Both studies were reviewed and approved by the Institutional Review Board of the California Institute of Technology, protocol #20-1026. All participants provided either written informed consent or (for minors ages 6-17) assent accompanied by parental permission, prior to enrollment. Participants were eligible if they had recently (within 7 days) been diagnosed with COVID-19 by a CLIA laboratory test, or lived with someone meeting who had. Demographic and medical information for the seven participants described here can be found in Table 3-S1.

Questionnaires and Symptom Monitoring

Acquisition of participant data was performed as described in our previous study.¹⁹ Symptoms (including those listed by the CDC⁸³) were reported by participants twice daily in parallel

with sample collection. Participants recorded any COVID-19-like symptoms (as defined by the CDC⁸³) on a symptom-tracking card or on a custom app run on REDCap.

Participants self-collected nasal-swab (1 swab) and saliva (~1.5mL) samples in the Spectrum SDNA-1000 Saliva Collection Kit (Spectrum Solutions LLC, Draper, UT, USA), which contains 1.5mL of liquid buffer, at home twice per day (after waking up and before going to bed), per manufacturer's guidelines. Of note, at the time of this writing, Spectrum devices are not approved for the collection of nasal-swab samples. Participants were instructed not to eat, drink, smoke, brush their teeth, use mouthwash, or chew gum for at least 30 min prior to donating. Prior to nasal-swab donation, participants were asked to gently blow their noses to remove debris. Participants were provided with one of the following types of sterile flocked swabs: Nest Oropharyngeal Specimen Collection Swabs (Cat. NST-202003, Stellar Scientific, Baltimore, MD, USA) Puritan HydraFlock Swab (Cat. 25-3000-H E30, Puritan, Guilford, ME, USA) or Copan USA FLOQSwab (Cat. 520CS01, VWR International, Radnor, PA, USA). Participants were instructed to swab each nostril for four complete rotations using the same swab while applying gentle pressure, then to break the tip of the swab into the Spectrum tube and securely screw on the cap. A parent or legal guardian assisted all minors with swab collection and they were instructed to wear a face covering during supervision.

Samples were stored at 4 °C and were equilibrated to room temperature before being processed with extraction protocols.

RNA Extraction and Nucleic Acid Quantification

Participant saliva and anterior-nares swab samples were extracted using the KingFisher Flex 96 instrument (ThermoFisher Scientific) with the MagMax Viral Pathogen I Nucleic Acid Isolation kit (Cat. A42352, Applied Biosystems, Waltham, MA, USA) guided by ThermoFisher technical notes for SARS-CoV-2 modification and saliva.

RT-qPCR was performed as previously described¹⁹ using the CDC 2019-Novel Coronavirus (2019-nCoV) Real-Time RT-PCR Diagnostic Panel,⁶⁶ with duplicate reactions. To establish the limit of detection (LOD) for each sample type (saliva, nasal swab), 20 contrived samples with the equivalent of 1,000 copies/mL were prepared, individually extracted as described above, and subjected to RT-qPCR, with a positive result for detection (as defined in the EUA for the CDC RT-

qPCR assay) in ≥ 19 of 20 ($\geq 95\%$) of replicates establishing the LOD (Fig. 3-S1 A,B). For quantification of viral load from RT-qPCR, a standard curve was prepared for both the saliva and nasal-swab protocols with a serial dilution of known concentration (based on the certificate of analysis, COA) of heat-inactivated SARS-CoV-2 particles (Batch 70034991, Cat. NR-52286, BEI Resources, Manassas, VA, USA) in the inactivating buffer from the Spectrum SDNA-1000 Saliva Collection Kit (Spectrum Solutions LLC, Draper, UT, USA) were prepared in triplicate for each concentration, then extracted and measured by RT-qPCR as described above. For positive samples meeting quality control Cq cutoffs based on the CDC guidelines,⁶⁶ the mean Cq of duplicate positive reactions was used for conversion to viral load using the equations shown below obtained from these calibration curves.

$$(1) \text{ Saliva } N1 \text{ gene viral load [copies/mL]} = 2^{((Cq-46.349)/-1.0357)}$$

$$(2) \text{ Saliva } N2 \text{ gene viral load [copies/mL]} = 2^{((Cq-46.374)/-1.0759)}$$

$$(3) \text{ Nasal Swab } N1 \text{ gene viral load [copies/mL]} = 2^{((Cq-48.221)/-1.0643)}$$

$$(4) \text{ Nasal Swab } N2 \text{ gene viral load [copies/mL]} = 2^{((Cq-48.330)/-1.1044)}$$

Quantification was also performed by reverse-transcription droplet digital PCR (RT-ddPCR) on elutions from both the calibration curve samples (Fig. 3-1, Fig. 3-S2) and participant samples (Fig. 3-1) using the Bio-Rad SARS-CoV-2 Droplet Digital PCR kit (Cat. 12013743, Bio-Rad). Droplets were created using the QX200 Droplet Generator (Cat #1864002, Bio-Rad), thermocycling performed on Bio-Rad C1000 and detected using the QX200 Droplet Digital PCR system (Cat. 1864001, Bio-Rad). Samples were analyzed with QuantaSoft analysis Pro 1.0.595 software following Bio-Rad's research-use only (RUO) SARS-CoV-2 guidelines.⁶⁷

Viral Sequencing

Saliva and nasal-swab samples with an *N1* gene Cq of below 26 were sent to Chan Zuckerberg Biohub for SARS-CoV-2 viral genome sequencing, a modification of Deng *et al.* (2020)⁸⁴ as described in Gorzynski *et al.* (2020).⁸⁵ Sequences were assigned pangolin lineages

described by Rambaut *et al.* (2020)⁸⁶ using Phylogenetic Assignment of Named Global outbreak LINEages software v2.3.2 (github.com/cov-lineages/pangolin). Chan Zuckerberg Biohub submitted consequence genomes to GISAID.

DATA AVAILABILITY

Data are available on CaltechDATA at <https://data.caltech.edu/records/1942>

COMPETING INTERESTS STATEMENT

RFI is a co-founder, consultant, and a director and has stock ownership of Talis Biomedical Corp. In addition, RFI is an inventor on a series of patents licensed by the University of Chicago to Bio-Rad Laboratories Inc. in the context of ddPCR.

FUNDING

This study is based on research funded in part by the Bill & Melinda Gates Foundation (INV-023124). The findings and conclusions contained within are those of the authors and do not necessarily reflect positions or policies of the Bill & Melinda Gates Foundation. This work was also funded by the Ronald and Maxine Linde Center for New Initiatives at the California Institute of Technology and the Jacobs Institute for Molecular Engineering for Medicine at the California Institute of Technology. AW is supported by a National Institutes of Health NIGMS Predoctoral Training Grant (GM008042) and a UCLA DGSOM Geffen Fellowship; MMC is supported by a Caltech Graduate Student Fellowship; and MP and JTB are each partially supported by National Institutes of Health Biotechnology Leadership Predoctoral Training Program (BLP) fellowship from Caltech's Donna and Benjamin M. Rosen Bioengineering Center (T32GM112592).

ACKNOWLEDGEMENTS

We thank Lauriane Quenee, Junie Hildebrandt, Grace Fisher-Adams, RuthAnne Bevier, Chantal D'Apuzzo, Ralph Adolphs, Victor Rivera, Steve Chapman, Gary Waters, Leonard Edwards, Gaylene Ursua, Cynthia Ramos, and Shannon Yamashita for their assistance and advice on study implementation and/or administration. We thank Jessica Leong, Jessica Slagle, Mika Walton, Angel Navarro, Daniel Brenner, and Ojas Pradhan for volunteering their time to help with this study, Si Hyung Jin for helping with a literature review, and Mary Arrastia for providing biosafety support. We thank Maira Phelps, Lienna Chan, Lucy Li, Dan Lu and Amy Kistler at the Chan Zuckerberg

Biohub for performing SARS-CoV-2 sequencing. We thank Angie Cheng, Susan Magdaleno, Christian Kis, Monica Herrera, and Zaina Lemeir for technical discussions regarding saliva extraction and ddPCR detection. We thank Jennifer Fulcher, Debika Bhattacharya and Matthew Bidwell Goetz for their ideas on potential study populations and early study design. We thank Omai Garner and David Beenhouwer for providing materials for initial nasal-swab validation. We thank Martin Hill, Alma Sanchez, Scott Kim, Debbie Noble, Nina Paddock, Whitney Harrison, Emily Holman, Isaac Turner, Vivek Desai, Luke Wade, Tom Mayell, Stu Miller, and Jennifer Howes for their support with recruitment. We thank Allison Rhines, Karen Heichman, and Dan Wattendorf for valuable discussion and guidance. Finally, we thank all the case investigators and contact tracers at the Pasadena Public Health Department and the City of Long Beach Department of Health & Human Services for their efforts in study recruitment and their work in the pandemic response.

REFERENCES

- 1 Johansson, M. A. *et al.* SARS-CoV-2 Transmission From People Without COVID-19 Symptoms. *JAMA Network Open* **4**, e2035057-e2035057 (2021).
- 2 WHO. *Recommendations for national SARS-CoV-2 testing strategies and diagnostic capacities*, <<https://apps.who.int/iris/bitstream/handle/10665/342002/WHO-2019-nCoV-lab-testing-2021.1-eng.pdf>> (2021).
- 3 Scientific Advisory Group for Emergencies (SAGE). *Consensus statement from the Scientific Pandemic Influenza Group on Modelling, Operational sub-group (SPI-M-O); 30 June 2021*, <<https://www.gov.uk/government/publications/spi-m-o-consensus-statement-on-covid-19-30-june-2021>> (2021).
- 4 Li, B. *et al.* Viral infection and transmission in a large, well-traced outbreak caused by the SARS-CoV-2 Delta variant. *medRxiv*, 2021.2007.2007.21260122, doi:10.1101/2021.07.07.21260122 (2021).
- 5 Fisman, D. N. & Tuite, A. R. Progressive Increase in Virulence of Novel SARS-CoV-2 Variants in Ontario, Canada. *medRxiv*, 2021.2007.2005.21260050, doi:10.1101/2021.07.05.21260050 (2021).
- 6 Yadav, P. D. *et al.* SARS CoV-2 variant B.1.617.1 is highly pathogenic in hamsters than B.1 variant. *bioRxiv*, 2021.2005.2005.442760, doi:10.1101/2021.05.05.442760 (2021).
- 7 Brown, C., Vostok, J., Johnson, H. *et al.* Outbreak of SARS-CoV-2 Infections, Including COVID-19 Vaccine Breakthrough Infections, Associated with Large Public Gatherings — Barnstable County, Massachusetts, July 2021. *MMWR Morb Mortal Wkly Rep* **70**, 1059-1062 (2021).

- 8 NIH. *Therapeutic Management of Adults With COVID-19*, <<https://www.covid19treatmentguidelines.nih.gov/therapeutic-management/>> (2021).
- 9 NIH. *Table 2a. Remdesivir: Selected Clinical Data*, <<https://www.covid19treatmentguidelines.nih.gov/antiviral-therapy/remdesivir/table--remdesivir-clinical-data/>> (2021).
- 10 Beigel, J. H. *et al.* Remdesivir for the Treatment of Covid-19 — Final Report. *N. Engl. J. Med.* **383**, 1813-1826, doi:10.1056/NEJMoa2007764 (2020).
- 11 Simonovich, V. A. *et al.* A Randomized Trial of Convalescent Plasma in Covid-19 Severe Pneumonia. *N. Engl. J. Med.* **384**, 619-629, doi:10.1056/NEJMoa2031304 (2020).
- 12 Libster, R. *et al.* Prevention of severe COVID-19 in the elderly by early high-titer plasma. *medRxiv*, 2020.2011.2020.20234013, doi:10.1101/2020.11.20.20234013 (2020).
- 13 Lundgren, J. D. *et al.* A Neutralizing Monoclonal Antibody for Hospitalized Patients with Covid-19. *N. Engl. J. Med.* **384**, 905-914, doi:10.1056/NEJMoa2033130 (2021).
- 14 Chen, P. *et al.* SARS-CoV-2 Neutralizing Antibody LY-CoV555 in Outpatients with Covid-19. *N. Engl. J. Med.* **384**, 229-237, doi:10.1056/NEJMoa2029849 (2021).
- 15 Weinreich, D. M. *et al.* REGN-COV2, a Neutralizing Antibody Cocktail, in Outpatients with Covid-19. *N. Engl. J. Med.* **384**, 238-251, doi:10.1056/NEJMoa2035002 (2021).
- 16 FDA. *Fact sheet for health care providers emergency use authorization (EUA) of casirivimab and imdevimab*, <<https://www.fda.gov/media/143892/download>> (2020).
- 17 FDA. *SARS-CoV-2 Reference Panel Comparative Data*, <<https://www.fda.gov/medical-devices/coronavirus-covid-19-and-medical-devices/sars-cov-2-reference-panel-comparative-data>> (2020).
- 18 Suess, T. *et al.* Comparison of Shedding Characteristics of Seasonal Influenza Virus (Sub)Types and Influenza A(H1N1)pdm09; Germany, 2007–2011. *PLoS One* **7**, e51653, doi:10.1371/journal.pone.0051653 (2012).
- 19 Winnett, A. *et al.* SARS-CoV-2 Viral Load in Saliva Rises Gradually and to Moderate Levels in Some Humans. *medRxiv*, 2020.2012.2009.20239467, doi:10.1101/2020.12.09.20239467 (2020).
- 20 Kissler, S. M. *et al.* Densely sampled viral trajectories suggest longer duration of acute infection with B.1.1.7 variant relative to non-B.1.1.7 SARS-CoV-2. *medRxiv*, 2021.2002.2016.21251535, doi:10.1101/2021.02.16.21251535 (2021).
- 21 Kissler, S. M. *et al.* Viral dynamics of SARS-CoV-2 infection and the predictive value of repeat testing. *medRxiv*, 2020.2010.2021.20217042, doi:10.1101/2020.10.21.20217042 (2020).

- 22 Kim, Y.-g. *et al.* Comparison between Saliva and Nasopharyngeal Swab Specimens for Detection of Respiratory Viruses by Multiplex Reverse Transcription-PCR. *J. Clin. Microbiol.* **55**, 226, doi:10.1128/JCM.01704-16 (2017).
- 23 WHO. *Laboratory Testing for Middle East Respiratory Syndrome Coronavirus*, <<https://apps.who.int/iris/bitstream/handle/10665/259952/WHO-MERS-LAB-15.1-Rev1-2018-eng.pdf?sequence=1>> (2018).
- 24 Wang, W. & *et al.* Detection of SARS-associated Coronavirus in Throat Wash and Saliva in Early Diagnosis. *Emerg. Infect. Dis.* **10**, 1213-1219 (2004).
- 25 Ku, C. W. *et al.* Validation of self-collected buccal swab and saliva as a diagnostic tool for COVID-19. *Int. J. Infect. Dis.* **104**, 255-261, doi:<https://doi.org/10.1016/j.ijid.2020.12.080> (2021).
- 26 Barat, B. *et al.* Pooled Saliva Specimens for SARS-CoV-2 Testing. *J. Clin. Microbiol.* **59**, e02486-02420, doi:10.1128/JCM.02486-20 (2021).
- 27 Manabe, Y. C. *et al.* Self-Collected Oral Fluid Saliva Is Insensitive Compared With Nasal-Oropharyngeal Swabs in the Detection of Severe Acute Respiratory Syndrome Coronavirus 2 in Outpatients. *Open Forum Infectious Diseases* **8**, doi:10.1093/ofid/ofaa648 (2021).
- 28 Procop, G. W. *et al.* A Direct Comparison of Enhanced Saliva to Nasopharyngeal Swab for the Detection of SARS-CoV-2 in Symptomatic Patients. *J. Clin. Microbiol.* **58**, e01946-01920, doi:10.1128/JCM.01946-20 (2020).
- 29 Al Suwaidi, H. *et al.* Saliva for molecular detection of SARS-CoV-2 in school-age children. *Clin. Microbiol. Infect.*, doi:<https://doi.org/10.1016/j.cmi.2021.02.009> (2021).
- 30 Wyllie, A. L. *et al.* Saliva or Nasopharyngeal Swab Specimens for Detection of SARS-CoV-2. *N. Engl. J. Med.* **383**, 1283-1286, doi:10.1056/NEJMc2016359 (2020).
- 31 Petrone, M. E. *et al.* Usability of saliva collection devices for SARS-CoV-2 diagnostics. *medRxiv*, 2021.2002.2001.21250946, doi:10.1101/2021.02.01.21250946 (2021).
- 32 Tan, S. H., Allicock, O., Armstrong-Hough, M. & Wyllie, A. L. Saliva as a gold-standard sample for SARS-CoV-2 detection. *The Lancet Respiratory Medicine* **9**, 562-564, doi:10.1016/S2213-2600(21)00178-8 (2021).
- 33 von Linstow, M.-L. *et al.* Saliva is inferior to nose and throat swabs for SARS-CoV-2 detection in children. *Acta Paediatr.* **n/a**, doi:<https://doi.org/10.1111/apa.16049> (2021).
- 34 Williams, E. *et al.* Saliva as a Noninvasive Specimen for Detection of SARS-CoV-2. *J. Clin. Microbiol.* **58**, e00776-00720, doi:10.1128/JCM.00776-20.
- 35 Jamal, A. J. *et al.* Sensitivity of Nasopharyngeal Swabs and Saliva for the Detection of Severe Acute Respiratory Syndrome Coronavirus 2. *Clin. Infect. Dis.* **72**, 1064-1066, doi:10.1093/cid/ciaa848 (2021).

- 36 Fernandes, P. A. d. C. *et al.* Performance of saliva as a specimen to detect SARS-CoV-2. *J. Clin. Virol.* **142**, 104913, doi:<https://doi.org/10.1016/j.jcv.2021.104913> (2021).
- 37 Hanson, K. E. *et al.* Self-Collected Anterior Nasal and Saliva Specimens versus Health Care Worker-Collected Nasopharyngeal Swabs for the Molecular Detection of SARS-CoV-2. *J. Clin. Microbiol.* **58**, doi:10.1128/jcm.01824-20 (2020).
- 38 De Santi, C. & *et al.* Concordance between PCR-based extraction-free saliva and nasopharyngeal swabs for SARS-CoV-2 testing. *HRB Open Research* **v.1**, doi:<https://doi.org/10.12688/HRBOPENRES.13353.1> (2021).
- 39 Sasaki, T. *et al.* Detection of SARS-CoV-2 RNA using RT-qPCR in nasopharyngeal swab, saliva, lingual, and buccal mucosal swab. *Jpn. J. Infect. Dis.* **advpub**, doi:10.7883/yoken.JJID.2021.091 (2021).
- 40 Kojima, N. *et al.* Self-Collected Oral Fluid and Nasal Swabs Demonstrate Comparable Sensitivity to Clinician Collected Nasopharyngeal Swabs for Covid-19 Detection. *medRxiv*, 2020.2004.2011.20062372, doi:10.1101/2020.04.11.20062372 (2020).
- 41 Tu, Y. P. *et al.* Patient-collected tongue, nasal, and mid-turbinate swabs for SARS-CoV-2 yield equivalent sensitivity to health care worker collected nasopharyngeal swabs. *medRxiv*, 2020.2004.2001.20050005, doi:10.1101/2020.04.01.20050005 (2020).
- 42 Iwasaki, S. *et al.* Comparison of SARS-CoV-2 detection in nasopharyngeal swab and saliva. *The Journal of infection* **81**, e145-e147, doi:10.1016/j.jinf.2020.05.071 (2020).
- 43 To, K. K. *et al.* Consistent detection of 2019 novel coronavirus in saliva. *Clin. Infect. Dis.*, doi:10.1093/cid/ciaa149 (2020).
- 44 Kernéis, S. *et al.* Accuracy of antigen and nucleic acid amplification testing on saliva and naopharyngeal samples for detection of SARS-CoV-2 in ambulatory care. *medRxiv*, 2021.2004.2008.21255144, doi:10.1101/2021.04.08.21255144 (2021).
- 45 Callahan, C. *et al.* Saliva Is Comparable to Nasopharyngeal Swabs for Molecular Detection of SARS-CoV-2. *medRxiv*, 2021.2004.2021.21255621, doi:10.1101/2021.04.21.21255621 (2021).
- 46 Fillatre, P. *et al.* A new SARS-CoV-2 variant poorly detected by RT-PCR on nasopharyngeal samples, with high lethality. *medRxiv*, 2021.2005.2005.21256690, doi:10.1101/2021.05.05.21256690 (2021).
- 47 Becker, D. *et al.* Saliva is less sensitive than nasopharyngeal swabs for COVID-19 detection in the community setting. *medRxiv*, 2020.2005.2011.20092338, doi:10.1101/2020.05.11.20092338 (2020).
- 48 Banada, P. *et al.* Evaluation of sample collection and transport strategies to enhance yield, accessibility, and biosafety of COVID-19 RT-PCR testing. *medRxiv*, 2021.2003.2003.21251172, doi:10.1101/2021.03.03.21251172 (2021).

- 49 Teo, A. K. J. *et al.* Saliva is more sensitive than nasopharyngeal or nasal swabs for diagnosis of asymptomatic and mild COVID-19 infection. *Sci. Rep.* **11**, 3134, doi:10.1038/s41598-021-82787-z (2021).
- 50 Dogan, O. A. *et al.* Does sampling saliva increase detection of SARS-CoV-2 by RT-PCR? Comparing saliva with oro-nasopharyngeal swabs. *J. Virol. Methods* **290**, 114049 (2021).
- 51 Landry, M. L., Criscuolo, J. & Peaper, D. R. Challenges in use of saliva for detection of SARS CoV-2 RNA in symptomatic outpatients. *Journal of clinical virology : the official publication of the Pan American Society for Clinical Virology* **130**, 104567-104567, doi:10.1016/j.jcv.2020.104567 (2020).
- 52 Smith, R. L. *et al.* Longitudinal assessment of diagnostic test performance over the course of acute SARS-CoV-2 infection. *medRxiv* (2021).
- 53 Byrne, R. L. *et al.* Saliva offers a sensitive, specific and non-invasive alternative to upper respiratory swabs for SARS-CoV-2 diagnosis. *medRxiv*, 2020.2007.2009.20149534, doi:10.1101/2020.07.09.20149534 (2020).
- 54 Bhattacharya D. *et al.* Saliva as a Potential Clinical Specimen for Diagnosis of SARS-CoV-2. *Preprints with The Lancet*, Available at SSRN: <https://ssrn.com/abstract=3696848> (2020).
- 55 Gupta, S. *et al.* SARS-CoV-2 Detection in Gingival Crevicular Fluid. *J. Dent. Res.* **100**, 187-193, doi:10.1177/0022034520970536 (2021).
- 56 Chua, G. T. *et al.* Saliva viral load better correlates with clinical and immunological profiles in children with coronavirus disease 2019. *Emerging Microbes & Infections* **10**, 235-241, doi:10.1080/22221751.2021.1878937 (2021).
- 57 Sarinoğlu, R., Guneser, D., Sengel, B. & Karahasan Yagci, A. Evaluation of different respiratory samples and saliva for the detection of SARS-CoV-2 RNA. *Marmara Medical Journal*, doi:10.5472/marumj.866658 (2021).
- 58 Ke, R. *et al.* Daily sampling of early SARS-CoV-2 infection reveals substantial heterogeneity in infectiousness. *medRxiv*, 2021.2007.2012.21260208, doi:10.1101/2021.07.12.21260208 (2021).
- 59 Han, M. & *et al.* Viral RNA Load in Mildly Symptomatic and Asymptomatic Children with COVID-19, Seoul, South Korea. *Emerg Infect Dis.* **26**, 2497-2499 (2021).
- 60 Wölfel, R. *et al.* Virological assessment of hospitalized patients with COVID-2019. *Nature* **581**, 465-469, doi:10.1038/s41586-020-2196-x (2020).
- 61 Huang, Y. *et al.* SARS-CoV-2 Viral Load in Clinical Samples from Critically Ill Patients. *Am. J. Respir. Crit. Care Med.* **201**, 1435-1438, doi:10.1164/rccm.202003-0572LE (2020).

- 62 Pan, Y., Zhang, D., Yang, P., Poon, L. L. M. & Wang, Q. Viral load of SARS-CoV-2 in clinical samples. *The Lancet Infectious Diseases* **20**, 411-412, doi:10.1016/S1473-3099(20)30113-4 (2020).
- 63 Zou, L. *et al.* SARS-CoV-2 Viral Load in Upper Respiratory Specimens of Infected Patients. *N. Engl. J. Med.* **382**, 1177-1179, doi:10.1056/NEJMc2001737 (2020).
- 64 Arons, M. M. *et al.* Presymptomatic SARS-CoV-2 Infections and Transmission in a Skilled Nursing Facility. *N. Engl. J. Med.* **382**, 2081-2090, doi:10.1056/NEJMoa2008457 (2020).
- 65 Chong, C. Y. *et al.* Saliva Is Not a Useful Diagnostic Specimen in Children With Coronavirus Disease 2019 (COVID-19). *Clin. Infect. Dis.*, doi:10.1093/cid/ciaa1376 (2020).
- 66 FDA. *CDC 2019-Novel Coronavirus (2019-nCoV) Real-Time RT-PCR Diagnostic Panel (EUA)*, <<https://www.fda.gov/media/134922/download>> (2020).
- 67 Bio-Rad. *Bio-Rad SARS-CoV-2 ddPCR Kit, Instructions for Use*, <<https://www.bio-rad.com/webroot/web/pdf/lsr/literature/10000130776.pdf>> (2020).
- 68 Larremore, D. B. *et al.* Test sensitivity is secondary to frequency and turnaround time for COVID-19 screening. *Science Advances* **7**, eabd5393, doi:10.1126/sciadv.abd5393 (2021).
- 69 Mina, M. J., Parker, R. & Larremore, D. B. Rethinking Covid-19 Test Sensitivity — A Strategy for Containment. *N. Engl. J. Med.*, doi:10.1056/NEJMp2025631 (2020).
- 70 Bloom, J. S. *et al.* Swab-Seq: A high-throughput platform for massively scaled up SARS-CoV-2 testing. *medRxiv*, 2020.2008.2004.20167874, doi:10.1101/2020.08.04.20167874 (2021).
- 71 FDA. *Pfizer-BioNTech COVID-19 Vaccine*, <<https://www.fda.gov/emergency-preparedness-and-response/coronavirus-disease-2019-covid-19/pfizer-biontech-covid-19-vaccine>> (2021).
- 72 Riemersma, K. K. *et al.* Shedding of Infectious SARS-CoV-2 Despite Vaccination when the Delta Variant is Prevalent - Wisconsin, July 2021. *medRxiv*, 2021.2007.2031.21261387, doi:10.1101/2021.07.31.21261387 (2021).
- 73 Huang, N. *et al.* SARS-CoV-2 infection of the oral cavity and saliva. *Nat. Med.*, doi:10.1038/s41591-021-01296-8 (2021).
- 74 CDC. *Overview of Testing for SARS-CoV-2 (COVID-19)*, <<https://www.cdc.gov/coronavirus/2019-ncov/hcp/testing-overview.html>> (2021).p
- 75 CDC. COVID-19 Vaccine Breakthrough Infections Reported to CDC — United States, January 1–April 30, 2021. *MMR Morb Mortal Wkly Rep* **70**, 792-793, doi:<http://dx.doi.org/10.15585/mmwr.mm7021e3> (2021).

- 76 Pray IW, Gibbons-Burgener SN, Rosenberg AZ & et al. COVID-19 Outbreak at an Overnight Summer School Retreat — Wisconsin, July–August 2020. *MMR Morb Mortal Wkly Rep* **69**, 1600-1604, doi:<http://dx.doi.org/10.15585/mmwr.mm6943a4> (2020).
- 77 Moreno, G. K. *et al.* Severe Acute Respiratory Syndrome Coronavirus 2 Transmission in Intercollegiate Athletics Not Fully Mitigated With Daily Antigen Testing. *Clin. Infect. Dis.* **73**, S45-S53, doi:10.1093/cid/ciab343 (2021).
- 78 Winichakoon, P. *et al.* Negative Nasopharyngeal and Oropharyngeal Swabs Do Not Rule Out COVID-19. *J. Clin. Microbiol.* **58**, e00297-00220, doi:10.1128/JCM.00297-20 (2020).
- 79 Schwartz, N. G. *et al.* Adolescent with COVID-19 as the Source of an Outbreak at a 3-Week Family Gathering - Four States, June-July 2020. *MMWR. Morbidity and mortality weekly report* **69**, 1457-1459, doi:10.15585/mmwr.mm6940e2 (2020).
- 80 Cao, G. *et al.* The Potential Transmission of SARS-CoV-2 from Patients with Negative RT-PCR Swab Tests to Others: Two Related Clusters of COVID-19 Outbreak. *Jpn. J. Infect. Dis.* **73**, 399-403, doi:10.7883/yoken.JJID.2020.165 (2020).
- 81 Hagan, L. M. *et al.* Mass Testing for SARS-CoV-2 in 16 Prisons and Jails - Six Jurisdictions, United States, April-May 2020. *MMWR. Morbidity and mortality weekly report* **69**, 1139-1143, doi:10.15585/mmwr.mm6933a3 (2020).
- 82 Szablewski, C. M. *et al.* SARS-CoV-2 Transmission and Infection Among Attendees of an Overnight Camp - Georgia, June 2020. *MMWR. Morbidity and mortality weekly report* **69**, 1023-1025, doi:10.15585/mmwr.mm6931e1 (2020).
- 83 CDC. Symptoms of Coronavirus. <https://www.cdc.gov/coronavirus/2019-ncov/symptoms-testing/symptoms.html> (2020).
- 84 Deng, X. *et al.* Metagenomic sequencing with spiked primer enrichment for viral diagnostics and genomic surveillance. *Nature Microbiology* **5**, 443-454, doi:10.1038/s41564-019-0637-9 (2020).
- 85 Gorzynski, J. E. *et al.* High-throughput SARS-CoV-2 and host genome sequencing from single nasopharyngeal swabs. *medRxiv*, 2020.2007.2027.20163147, doi:10.1101/2020.07.27.20163147 (2020).
- 86 Rambaut, A. *et al.* A dynamic nomenclature proposal for SARS-CoV-2 lineages to assist genomic epidemiology. *Nature Microbiology* **5**, 1403-1407, doi:10.1038/s41564-020-0770-5 (2020).
- 87 CDC. Real-Time RT-PCR Panel for Detection 2019–Novel Coronavirus. (Centers for Disease Control and Prevention, Respiratory Viruses Branch, Division of Viral Diseases, 2020).
- 88 CDC. *COVID-19: People with Certain Medical Conditions*, <<https://www.cdc.gov/coronavirus/2019-ncov/need-extra-precautions/people-with-medical-conditions.html>> (2021).

SUPPLEMENTAL INFORMATION

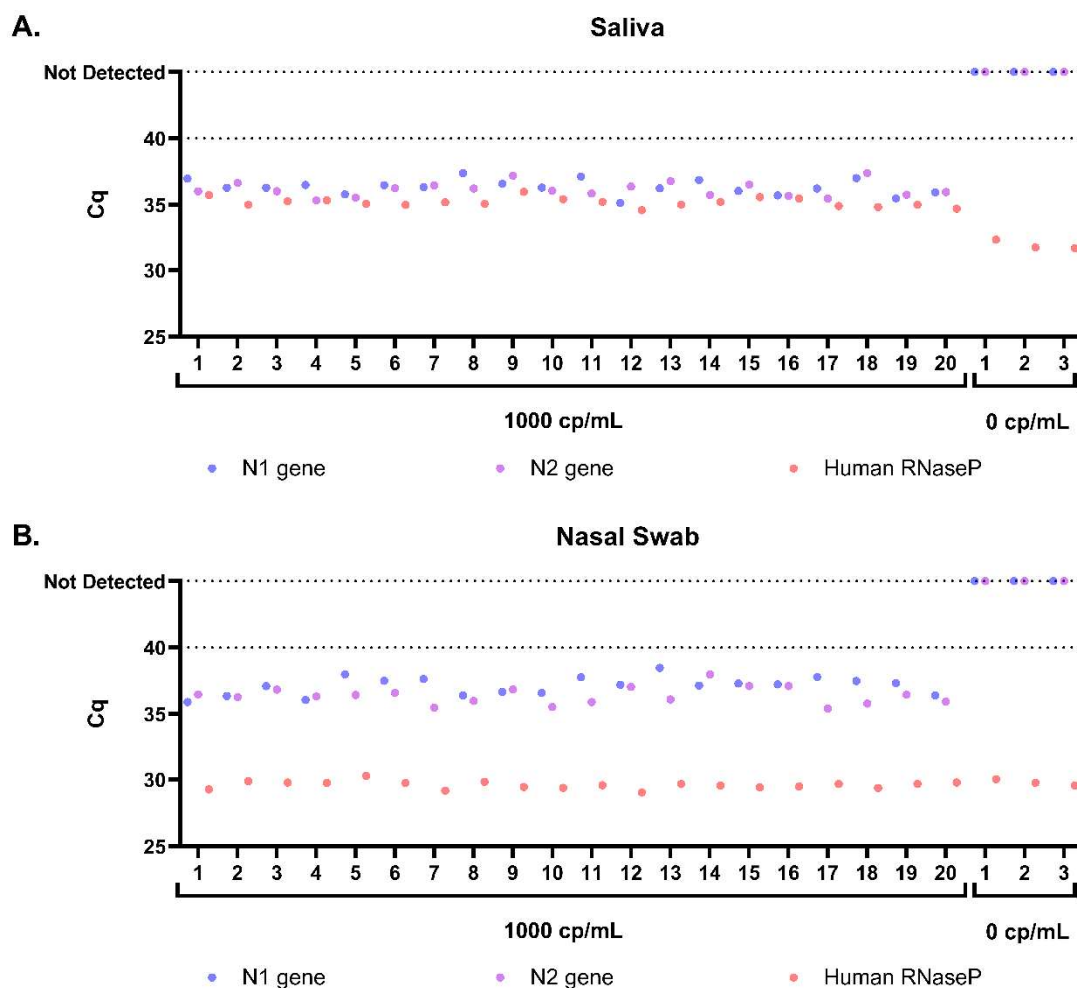


Figure 3-S1. Limit of detection of saliva and nasal-swab RT-qPCR assays used in this study. RT-qPCR quantification cycle (Cq) for SARS-CoV-2 *N1* gene (blue circle), *N2* gene (purple circle), and human *RNase P* gene (orange circle) in 20 replicates of pooled matrix spiked with 1000 copies/mL (cp/mL) heat-inactivated SARS-CoV-2 RNA and 3 replicates of pooled matrix spiked with a buffer blank for saliva (A) and nasal-swab (B) samples. Duplicate RT-qPCR reactions were performed for each extraction replicate and the averages are shown, with the following three exceptions: replicate 9 (saliva), in which the *N1* gene only amplified in 1 of the duplicate runs (*N2* in this run was positive, so per CDC EUA guidelines⁸⁷ this run was interpreted as inconclusive), replicate 10 (nasal swab) in which the *N2* gene only amplified in 1 of the duplicate runs (*N1* in this run was positive, so this run was interpreted as inconclusive), and replicate 18 (nasal swab) in which the *N1* gene only amplified in 1 of the duplicate runs (*N2* in this run was positive, so this run was also interpreted as inconclusive). None of the samples spiked at 1000 copies/mL gave a negative detection result.

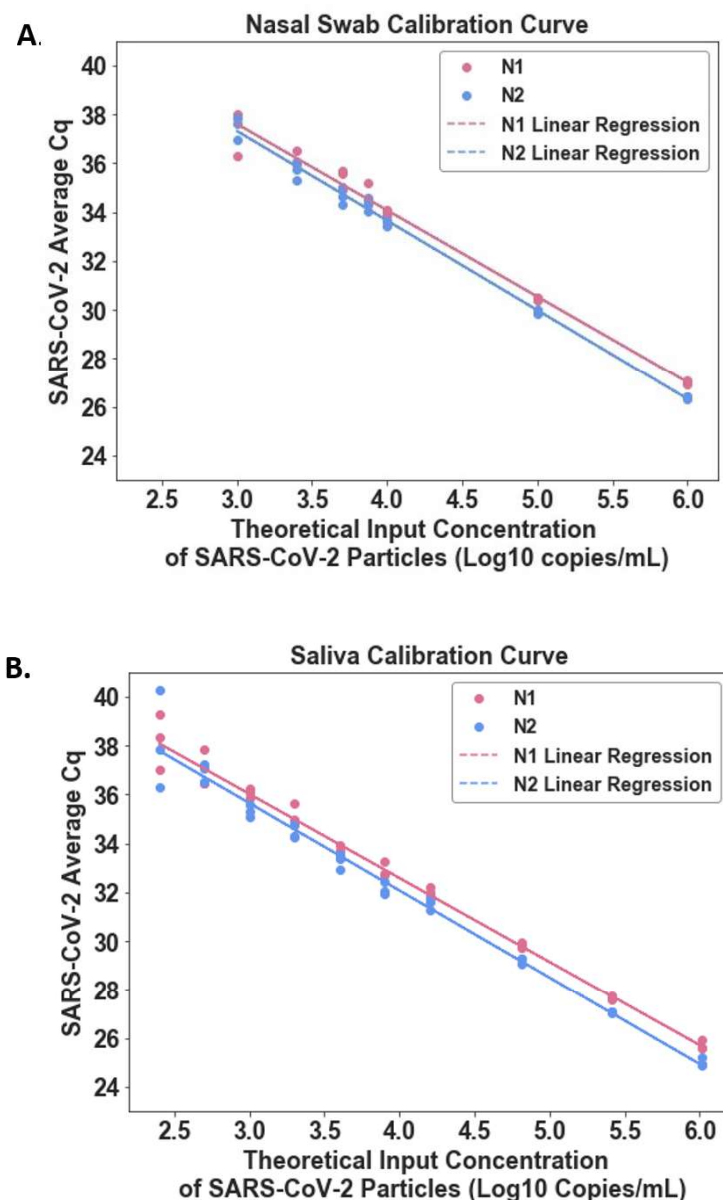


Figure 3-S2. Calibration curve of SARS-CoV-2 inactivated particles to establish viral load conversion equations. Linear regression of RT-qPCR quantification cycle (Cq) for *N1* (red circle) and *N2* (blue circles) genes at known concentrations of inactivated SARS-CoV-2 particles for saliva (A) or nasal swab (B) using this study's collection and laboratory workflows. Triplicate replicates per concentration were performed. Linear regression for *N1* represented by red line and *N2* represented by blue line. Linear regression R^2 values are 0.986 for *N1* in nasal swabs, 0.994 for *N2* in nasal swabs, 0.989 for *N1* in saliva, and 0.979 for *N2* in saliva.

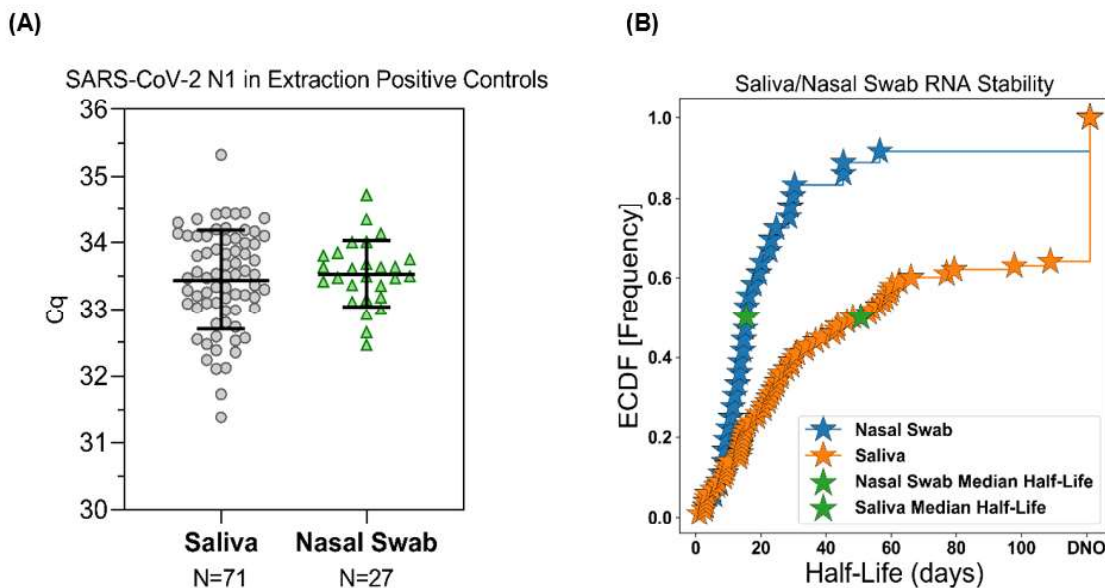


Figure 3-S3. SARS-CoV-2 RNA stability over time in Spectrum SDNA-1000 buffer at 4 °C. (A) Positive extraction control samples from 71 saliva extraction runs and 27 nasal-swab extraction runs are included to show the measurement noise in the quantification workflow. The standard deviation for the positive control measurements was 0.74 Cq for saliva and 0.49 for nasal swab. (B) Empirical cumulative distribution functions (ECDF) for the observed half-life (days) of participant saliva (orange stars) and nasal-swab (blue stars) samples in Spectrum SDNA-1000 buffer stored at 4 °C. Individual samples were extracted at multiple time points. The ECDF represents the summed probability mass function over the Cq half-lives observed. Half-life in this context refers to the time required to observe a 1 Cq increase (representing a 2-fold decrease) in RNA detected by RT-qPCR. The median point is identified with a green star for each sample, at 15.0 days for nasal swabs and 51.0 days for saliva. Of the 110 total participant saliva samples plotted in panel B, 36 samples had no evidence of degradation (DNO) under the time frame measured. Only 3 of the 36 total participant nasal-swab samples plotted in panel B had no evidence of degradation (DNO) under the time frame measured. DNO = degradation not observed, meaning that the difference in extraction Cq values of the same sample at multiple time points was within 1 standard deviation observed in replicate extraction positive controls for the respective sample type, as shown in panel A.

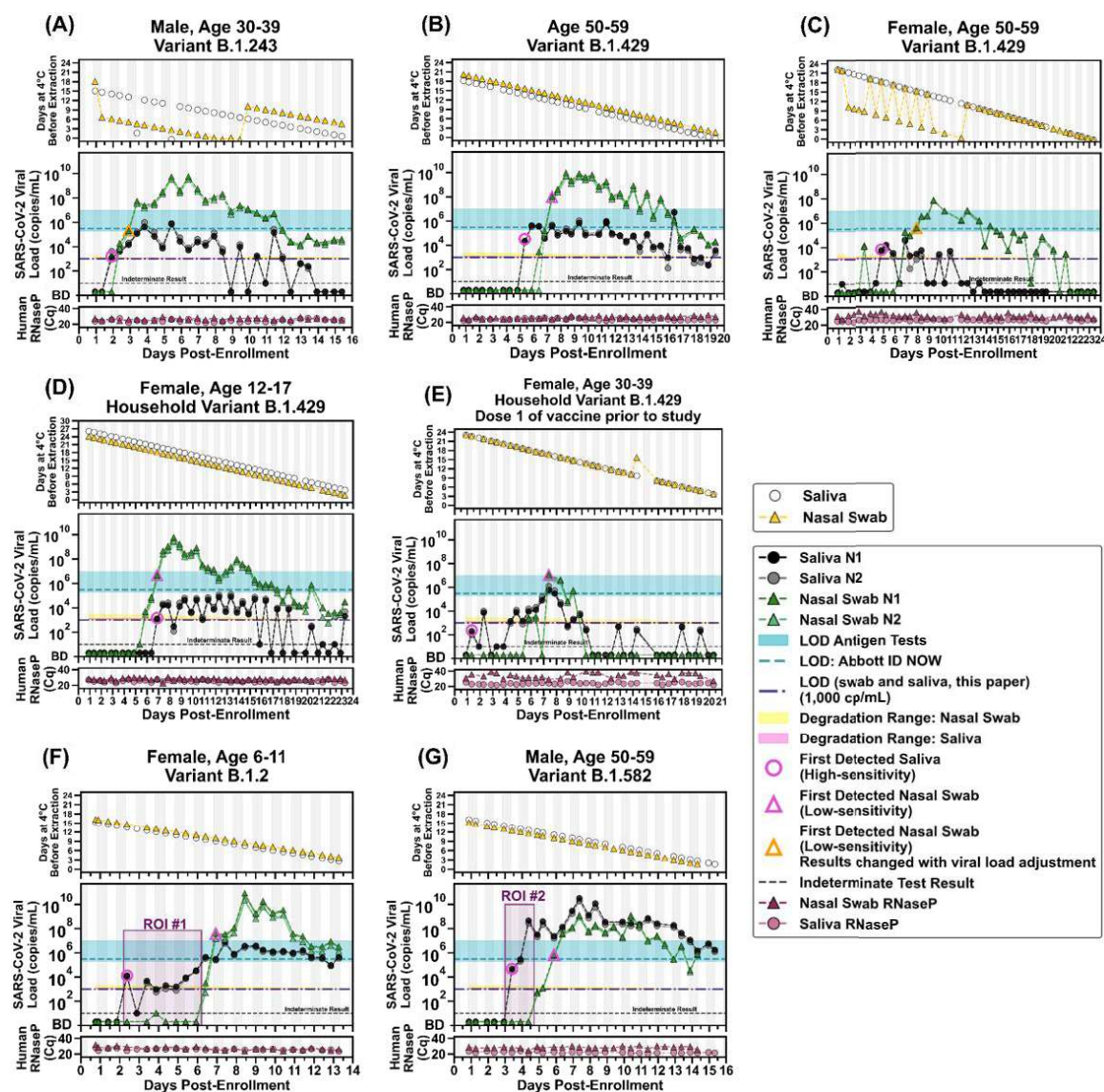


Figure 3-S4. Predicted impact of SARS-CoV-2 RNA stability on viral loads shown in Fig. 3-2. (A-G) The time [days] of sample storage at 4 °C between sample collection and RNA extraction is shown in the topmost panels. Open circles represent saliva samples and yellow triangles represent the nasal swabs. Viral load (black and grey circles) calculations are corrected for the median half-life (1 Cq decrease in RNA detected by RT-qPCR) of each sample type and the duration of storage at 4 °C before quantification (15 days for 2-fold decrease in detected RNA in nasal swabs and 51 days for 2-fold decreased in detected RNA in saliva). The degradation ranges, represented by a shaded yellow (nasal swab) or pink (saliva) region to represent how a measured value of 1,000 copies/mL may have degraded from concentrations in this range. As in Fig. 5-2, ND = not detected for Cqs ≥ 40 (see Methods for details). The limit of detection (LOD) of the saliva and nasal-swab assays used here (1,000 cp/mL) is indicated with the purple dashed line; the LOD of the Abbott ID NOW (300,000 NDU/mL¹⁷) is indicated by the horizontal green dashed line; the range of LODs of antigen tests (horizontal green bar) are shown for reference (data are from Table S2 in ref. ¹⁹). A diagnostic test does not provide reliable detection for samples with viral loads below its LOD. For each participant, the first detected saliva point is emphasized with a pink circle and their first nasal-swab point above the LOD of the ID NOW is emphasized with a pink triangle. Vertical shading in grey indicates nighttime (8pm – 8am). Internal control of *RNase P* gene Cqs from the CDC primer set are provided for each sample to compare self-sampling consistency and sample integrity (failed samples, where *RNase P* Cq ≥ 40 , are not plotted). Samples

with an indeterminate result by the CDC RT-qPCR assay are shown along the horizontal black dashed line. Participant gender, age range, and SARS-CoV-2 variant is given in each panel's title. Two regions of interest (ROI) are indicated by purple-shaded rectangles and discussed in the main text. For the two points that change interpretation with the viral load adjustment, orange triangles show which new data points become the first nasal-swab point in range of low-sensitivity tests.

Table 3-S1. Study participant demographic data. Figure 5-2 and Figure 3-S4 show viral loads and symptoms data for the seven participants for whom we observed transmission during their enrollment in the study.

	Age Range (Years)	Sex	Race; Ethnicity	Reported Medical Conditions Associated with Increased Risk of Severe COVID-19⁸⁸
Fig. 2A, Fig. S4A	30-39	Male	Other; Mexican/Mexican-American/Chicano (Salvadoran)	Diabetes
Fig. 2B, Fig. S4B	50-59	Male	Do not wish to respond; Mexican/Mexican-American/Chicano	None
Fig. 2C, Fig. S4C	50-59	Female	White; Mexican/Mexican-American/Chicano (Spanish-American from Spain)	None
Fig. 2D, Fig. S4D	12-17	Female	White; Mexican/Mexican-American/Chicano	None
Fig. 2E, Fig. S4E	30-39	Female	White; Mexican/Mexican-American/Chicano	None
Fig. 2F, Fig. S4F	6-11	Female	White; Non-Hispanic	None
Fig. 2G, Fig. S4G	50-59	Male	American Indian or Alaskan Native, White; Other Hispanic, Latinx or Spanish origin	Obesity

Supplementary Methods

Participant Population

This study is an extension of our previous study examining viral load in saliva.¹⁹ Both studies were reviewed and approved by the Institutional Review Board of the California Institute of Technology, protocol #20-1026. All participants provided either written informed consent or (for minors ages 6-17) assent accompanied by parental permission, prior to enrollment. Household index

cases were eligible for participation if they had recently (within 7 days) been diagnosed with COVID-19 by a CLIA laboratory test. Individuals were ineligible if they were hospitalized or if they were not fluent in either Spanish or English. All participant data were collected and managed using REDCap (Research Electronic Data Capture) on a server hosted at the California Institute of Technology. Demographic and medical information for the seven participants described here can be found in Table S1.

Questionnaires and Symptom Monitoring

Acquisition of participant data was performed as described in our previous study.¹⁹ Briefly, upon enrollment each participant completed an online questionnaire regarding demographics, health factors, prior COVID-19 tests, COVID-19-like symptoms since February 2020, household infection-control practices, and perceptions of COVID-19 risk. Participants also filled out a post-study questionnaire in which they documented medications taken and their interactions with each household member during their enrollment.

Information on symptoms was collected twice daily in parallel with sample collection. Participants recorded any COVID-19-like symptoms (as defined by the CDC⁸³) they were experiencing at the time of sample donation on a symptom-tracking card or on a custom app run on REDCap. Whenever possible, participants indicated the self-reported severity of each symptom. Participants were also given the opportunity to write-in additional symptoms or symptom details not otherwise listed.

Collection of Respiratory Specimens

Participants self-collected both their nasal-swab and saliva samples using the Spectrum SDNA-1000 Saliva Collection Kit (Spectrum Solutions LLC, Draper, UT, USA), which contains 1.5 mL of liquid buffer, at home twice per day (after waking up and before going to bed), per manufacturer guidelines. Of note, at the time of this writing, Spectrum devices are not approved for the collection of nasal-swab samples. Participants self-collected nasal-swab (1 swab) and saliva (~1.5mL) samples in the Spectrum SDNA-1000 Saliva Collection Kit (Spectrum Solutions LLC, Draper, UT, USA), which contains 1.5mL of liquid buffer, at home twice per day (after waking up

and before going to bed), per manufacturer's guidelines. Of note, at the time of this writing, Spectrum devices are not approved for the collection of nasal-swab samples.

Participants were instructed not to eat, drink, smoke, brush their teeth, use mouthwash, or chew gum for at least 30 min prior to donating. Prior to nasal-swab donation, participants were asked to gently blow their noses to remove debris. Participants were provided with one of the following types of sterile flocked swabs: Nest Oropharyngeal Specimen Collection Swabs (Cat. NST-202003, Stellar Scientific, Baltimore, MD, USA) Puritan HydraFlock Swab (Cat. 25-3000-H E30, Puritan, Guilford, ME, USA) or Copan USA FLOQSwab (Cat. 520CS01, VWR International, Radnor, PA, USA). Participants were instructed to swab each nostril for four complete rotations using the same swab while applying gentle pressure, then to break the tip of the swab into the Spectrum tube and securely screw on the cap. A parent or legal guardian assisted all minors with swab collection and they were instructed to wear a face covering during supervision. Tubes were labeled and packaged by the participants and transported at room temperature by a touch-free medical courier to the California Institute of Technology daily for analysis.

Upon receipt of the samples in the California Institute of Technology laboratory, each sample was inspected for quality. A sample failed quality control if the preservation buffer was not released from the Spectrum SDNA-1000 cap, or if sample tubes were leaking or otherwise unsafe to handle. Samples that failed quality control were not processed. Inactivated samples were stored at 4 °C and were equilibrated to room temperature before being processed with extraction protocols.

RNA Extraction Protocols

Participant saliva and anterior-nares swab samples were extracted using the KingFisher Flex 96 instrument (ThermoFisher Scientific) with the MagMax Viral Pathogen I Nucleic Acid Isolation kit (Cat. A42352, Applied Biosystems, Waltham, MA, USA) guided by ThermoFisher technical notes for SARS-CoV-2 modification and saliva. Each extraction batch, depending on the sample type being extracted, contained a contrived SARS-CoV-2 negative control sample containing either 225 μ L of Spectrum buffer mixed with 225 μ L of commercial pooled human saliva (Lee Bio 991-05-P-PreC) or 240 μ L of Spectrum buffer with 10 μ L of pooled commercial nasal fluid (Lee Bio 991-13-P-PreC); a contrived SARS-CoV-2 positive control sample was also included in each

extraction batch, with the formulations above, but with the Spectrum buffer spiked with 7,500 genomic copy equivalents/mL of heat-inactivated SARS-CoV-2 particles (BEI NR-52286).

Saliva and anterior-nares swab samples were prepared for purification by transferring 550 μ l (for saliva) or 250 μ l (for nasal swab) of each sample from its corresponding Spectrum buffer tube into a 1.5 mL lo-bind Eppendorf tube containing 10 μ l (for saliva) or 5 μ l (for nasal swab) of proteinase K. To maximize recovery of RNA off swabs, prior to transfer, pipet mixing was performed 5-7 times near the swab in the Spectrum tube before aliquoting into an Eppendorf tube. Saliva samples were vortexed for 30 sec in the Eppendorf tube. Samples were incubated at 65 °C for 10 min, then centrifuged at 13,000 x g for 1 min. Aliquots of 400 μ l (for saliva) or 200 μ l (for nasal swab) were transferred into a KingFisher 96 deep well plate (Cat. 95040450, ThermoFisher Scientific) and processed following KingFisher protocols MVP_400ul_3washes.bdz (for saliva) or MVP_200ul_2washes.bdz (for nasal swab). Ethanol washes were performed with 80% ethanol. Both sample types were eluted into 100 μ l of MagMax viral pathogen elution buffer.

RT-qPCR

Quantification of SARS-CoV-2 was performed as previously described.¹⁹ Briefly, the CDC⁶⁶ SARS-CoV-2 *N1* and *N2* gene primers and probes with an internal control targeting *RNase P* gene primer and probe were run in a multiplex RT-qPCR reaction using TaqPath 1-Step Rt-qPCR Mastermix (Cat. A15299, ThermoFisher Scientific). Reactions were run in duplicate on a CFX96 Real-Time Instrument (Bio-Rad Laboratories, Hercules, CA, USA).

RT-ddPCR

Reverse-transcription droplet digital PCR (RT-ddPCR) was performed using the Bio-Rad SARS-CoV-2 Droplet Digital PCR kit (Cat. 12013743, Bio-Rad). Swab samples were processed following the manufacturer's RUO protocol with 5.5 μ l template per 22 μ l reaction. A total of 42 participant nasal-swab samples were characterized by RT-ddPCR. Modifications were made for saliva samples by reducing the template addition to 2.75 μ l per 22 μ l reaction. A total of 63 participant saliva samples were characterized by RT-ddPCR. Prior to adding template, samples were diluted into digital range using nuclease-free water. Droplets were created using the QX200 Droplet Generator (Cat #1864002, Bio-Rad), thermocycling performed on Bio-Rad C1000 and detected

using the QX200 Droplet Digital PCR system (Cat. 1864001, Bio-Rad). Samples were analyzed with QuantaSoft analysis Pro 1.0.595 software following Bio-Rad's RUO SARS-CoV-2 guidelines.⁶⁷

Viral Load Standard Curves

A standard curve was prepared for both the saliva and nasal-swab protocols. Samples were prepared with known concentrations (based on the certificate of analysis, COA) of heat-inactivated SARS-CoV-2 particles (Batch 70034991, Cat. NR-52286, BEI Resources, Manassas, VA, USA) in the inactivating buffer from the Spectrum SDNA-1000 Saliva Collection Kit (Spectrum Solutions LLC, Draper, UT, USA). To prepare the samples for the saliva protocol (Fig. S2A) a dilution curve of heat-inactivated SARS-CoV-2 particles (Batch 70034991, Cat no. NR-52286, BEI) in the Spectrum device inactivation buffer at concentrations of 0 copies/mL, 1,000 copies/mL, 2,000 copies/mL, 4,000 copies/mL, 8,000 copies/mL, 16,000 copies/mL, 64,000 copies/mL, 256,000 copies/mL, 1,020,000 copies/mL, and 4,100,000 copies/mL. Samples were made by mixing 620 μ L of each concentration of the dilution series with 620 μ L of healthy pooled human saliva (Cat, 991-05-P, Lee Biosolutions, Maryland Heights, MO, USA). Triplicate extractions were performed according to the saliva RNA extraction protocol. Each extraction was run in triplicate qPCR reactions and single RT-ddPCR reactions.

To prepare the samples for the nasal-swab RNA extraction protocol (Fig. S2B) we created dilution curves for each sample type (saliva and nasal swab) and each target (*N1* and *N2* genes) using heat-inactivated SARS-CoV-2 particles (Batch 70034991, Cat no. NR-52286, BEI) in the Spectrum inactivation buffer. We ran a dilution series of commercial quantified stock (3.75×10^8 GE/mL) in a 10-fold dilution series from 1×10^6 to 1×10^4 copies/mL with finer resolution down to our LOD at 1×10^3 copies/mL. To each dilution we added 32 μ L of healthy human nasal fluid (Cat No 991-13-P-PreC, Lee Biosolutions) to 768 μ L of each dilution for a total volume of 800 μ L. Triplicate extractions were performed according to the nasal-swab RNA extraction protocol (described above). Each extraction was run in triplicate qPCR reactions and single RT-ddPCR reactions.

Equations from the calibration curves are below. These calibration curves are used to convert the C_q values obtained by RT-qPCR to viral load in each participant sample. For saliva, viral load is a calculation of viral copies/mL in the saliva corrected for dilution with the Spectrum buffer. We assumed that participants donate saliva to the fill line, matching the 1:1 dilution in Spectrum buffer

recreated when preparing contrived samples for the saliva calibration curve. For nasal swabs, viral load is a calculation of the concentration of viral copies/mL released from the swab into the 1.5 mL of inactivating buffer (which is a similar volume as the 1-3 mL of viral transport media typically used for sample collection). Concentrations higher than 1,000,000 copies/mL could not be characterized due to a limitation of the available stock concentration of commercial inactivated SARS-CoV-2. To validate linear conversion was acceptable at concentrations higher than 1,000,000 copies/mL, we compared RT-ddPCR and RT-qPCR quantification on some participant samples (Fig. 5-1).

$$(1) \text{ Saliva N1 gene viral load [copies/mL]} = 2^{((Cq-46.349)/-1.0357)}$$

$$(2) \text{ Saliva N2 gene viral load [copies/mL]} = 2^{((Cq-46.374)/-1.0759)}$$

$$(3) \text{ Nasal Swab N1 gene viral load [copies/mL]} = 2^{((Cq-48.221)/-1.0643)}$$

$$(4) \text{ Nasal Swab N2 gene viral load [copies/mL]} = 2^{((Cq-48.330)/-1.1044)}$$

Establishment of Limit of Detection

Results of the calibration curve (Fig. 5-S2 A,B) demonstrated 3 of 3 replicates detected at 1,000 copies/mL saliva (for saliva) and 1,000 copies/mL buffer (for nasal swabs). For each sample type (saliva, nasal swab), 20 contrived samples with the equivalent of 1,000 copies/mL were prepared as described above, individually extracted as described above, and subjected to RT-qPCR as described above. The LOD for each sample type through the workflow was considered established if a positive result for detection (as defined in the EUA for the CDC RT-qPCR assay) was obtained for ≥ 19 of 20 ($\geq 95\%$) of replicates at the input concentration (Fig. 5-S1 A,B).

Three of three replicate sample extractions included in the calibration curves for both contrived nasal-swab samples and contrived saliva samples spiked with heat-inactivated SARS-CoV-2 particles at a concentration of 1,000 copies/mL were detected by RT-qPCR, prompting testing of additional 20 replicates of each sample type spiked at that concentration, individually extracted, and tested by RT-qPCR to establishment of the LOD for our RT-qPCR assay. For both sample types (saliva and nasal swabs), 20 of 20 replicates were positive for SARS-CoV-2 (Fig. 5-

S1 A,B), establishing 1,000 copies/mL of saliva and 1,000 copies/mL of swab buffer as the high-sensitivity LOD for our RT-qPCR assays.

Data Analysis

Before we converted Cq values to viral load, we used Cq cutoffs based on the CDC guidelines⁶⁶ to exclude from the viral-load plots any points that were indeterminate or fails, and any samples whose RNase P Cq values ≥ 40 . Because we ran duplicate RT-qPCR reactions, the mean Cq of positive reactions was used for conversion to viral load.

RNAseq

Saliva and nasal-swab samples below *NI* Cq of 26 were sent to Chan Zuckerberg Biohub for SARS-CoV-2 viral genome sequencing, a modification of Deng et al. (2020)⁸⁴ as described in Gorzynski et al. (2020).⁸⁵ Sequences were assigned pangolin lineages described by Rambaut *et al.* (2020)⁸⁶ using Phylogenetic Assignment of Named Global outbreak LINEages software v2.3.2 (github.com/cov-lineages/pangolin). Consequences viral genomes were submitted to GISAID by Chan Zuckerberg Biohub, see data availability section for accession id details.

SARS-CoV-2 RNA Stability at 4 °C

As described above, each extraction batch included a contrived sample spiked with SARS-CoV-2 heat-inactivated particles. For all available saliva or nasal-swab extraction batches, the Cq value of the SARS-CoV-2 *NI* gene in the contrived SARS-CoV-2 positive extraction control was collected. The standard deviation of these measurements was calculated and used to establish a threshold for expected noise between repeat extractions of the same sample. To assess samples for evidence of SARS-CoV-2 RNA degradation, any participant sample that had more than one extraction replicate performed were analyzed. Samples where the difference in Cq values between the extractions was less than the threshold of expected noise between replicate extractions were defined as degradation not observed, (DNO). For samples where the difference was above this threshold, the time for 1 Cq increase (2-fold decrease) in RNA detected by RT-qPCR is described by the term half-life, which was calculated according to Equation 5, below:

$$(5) t_{1/2} = \frac{-\ln 2}{k}$$

Where “k” is defined as the slope of the linear regression of the natural logarithm of the viral load vs. extraction date (relative to sample collection date). Empirical cumulative distribution functions (ECDF) were calculated using the statsmodels Python package. Confidence intervals were constructed using 2500 bootstrap trials. The median over the entire dataset (saliva or swab) was used as a point estimate of RNA half-life.

Calculations that predict the impact of storage time at 4 °C and RNA stability on viral load are calculated according to Equation 6, below.

$$(6) y_{adj} = y_{deg} 2^{\frac{\Delta t}{t_{1/2}}}$$

Where y_{adj} is defined as the adjusted viral load, y_{deg} is defined as the viral load before adjustment for degradation (as calculated by Equations 1-4), and $t_{1/2}$ is defined as the RNA half-life, shown in Equation 5.

APPENDIX A: POLYMERASE-ACCESSIBILITY ANTIBIOTIC SUSCEPTIBILITY TEST FOR CARBAPENEM-RESISTANT ENTEROBACTERIACEAE

Nathan G. Schoepp, Eric J. Liaw, Alexander Winnett, Emily S. Savela, Omai B. Garner, and Rustem F. Ismagilov. 2020. “Differential DNA Accessibility to Polymerase during Nucleic Acid Amplification Enables 30-minute phenotypic β -lactam Antibiotic Susceptibility testing of Carbapenem-resistant Enterobacteriaceae.” *PLoS Biology*. 18(3):e3000652. doi: 10.1371/journal.pbio.3000652.

ABSTRACT

The rise in carbapenem-resistant Enterobacteriaceae (CRE) infections has created a global health emergency, underlining the critical need to develop faster diagnostics to treat swiftly and correctly. Although rapid pathogen-identification tests are being developed, gold-standard antibiotic susceptibility testing (AST) remains unacceptably slow (1–2 days) and innovative approaches for rapid phenotypic ASTs for CREs are urgently needed. Motivated by this need, in this manuscript we tested the hypothesis that upon treatment with β -lactam antibiotics, susceptible Enterobacteriaceae isolates would become sufficiently permeabilized, making some of their DNA accessible to added polymerase and primers. Further, we hypothesized that this accessible DNA would be detectable directly by isothermal amplification methods that do not fully lyse bacterial cells. We build on these results to develop the pol-aAST (polymerase-accessibility AST), a new phenotypic approach for β -lactams, the major antibiotic class for Gram-negative infections. We test isolates of the three causative pathogens of CRE infections using ceftriaxone, ertapenem, and meropenem, and demonstrate agreement with gold-standard AST. Importantly, pol-aAST correctly categorized resistant isolates that are undetectable by current genotypic methods (negative for β -lactamase genes or lacking predictive genotypes). We also test contrived and clinical urine samples. We show that the pol-aAST can be performed in 30 min sample-to-answer using contrived urine samples, and has the potential to be performed directly on clinical urine specimens.

INTRODUCTION

The evolution and global spread of carbapenem-resistant Enterobacteriaceae (CRE) threatens to disrupt modern healthcare systems, which rely heavily on β -lactams (especially carbapenems, the last-resort treatments) to control bacterial infections [1-3]. Mortality rates for CRE infections are as high as 30–49% [4-6], and thus the global emergence and spread of CRE infections represents a public health emergency [7-9]. The CDC places CRE in its highest (“urgent”) category of antimicrobial-resistant pathogen threats [8,10] and the World Health Organization (WHO) labels CRE as a critical-priority pathogen [7]. *Escherichia coli*, *Klebsiella pneumoniae*, and *Enterobacter* spp. compose the majority of CRE infections, and are the most commonly monitored Enterobacteriaceae [8,11-13].

To halt the further spread of CRE, patients need to be treated swiftly and correctly at the point of care (POC); however, there is no fast and general method for determining antibiotic susceptibility [14-16]. The current clinical workflow for treatment of bacterial infections consists of an identification (ID) step followed by an antibiotic susceptibility test (AST). Although progress is being made to develop faster ID tests [17-19] and a rapid 20-min ID test is on the horizon [20-22], the gold-standard for AST remains a culture-based workflow using broth or agar dilution that requires 1–2 days and is thus far too slow [23,24]. Because AST results are so delayed, health care providers usually treat empirically, leading to inappropriate prescriptions and even life-threatening outcomes, [25] and the further spread of resistance. To improve treatment and promote antibiotic stewardship, healthcare providers need a rapid phenotypic AST [26-29].

ASTs are either genotypic or phenotypic. Genotypic tests predict resistance by measuring the presence of genes known to be involved in resistance. Genotypic tests can be fast [30], but often have limited clinical utility because they target defined mechanisms of resistance. For example, rapid genotypic methods to detect Gram-negative β -lactamase genes have been developed [31-34], but these tests only detect one of the many known β -lactamase classes, and still require 30–40 min (estimated from described methods). Similarly, the commercial Cepheid Xpert® Carba-R assay, which detects five β -lactamase gene families, and was shown to detect 50% of resistant isolates and took 88 min [35]. Moreover, although Carba-R is FDA-approved, its utility in treatment scenarios is limited

(i.e., negative results are not actionable) so when prescribing antibiotics, it must be used in conjunction with a phenotypic AST [36,37]. Rapid methods for measuring the activity of specific β -lactamases also exist [38-42]. However, these tests only detect one mechanism of resistance, and sample-to-answer times have not been reported.

Phenotypic ASTs are ideal because they measure susceptibility directly by exposing the sample to antibiotics (ABX) and measuring the target organism's response. The gold-standard AST (broth microdilution [23,24]) is a phenotypic test. Most phenotypic tests require the growth of viable organisms isolated from patient samples, a process that requires days and is thus too slow for the POC. Innovative, faster phenotypic tests for β -lactams were developed based on *in situ* nucleic-acid staining or fluorescence measurements [43-45], flow cytometry [46], microscopy [47-49], optical density [50,51], and mass spectrometry [52]. However, the majority of the currently proposed methods still require 60–180 min ABX-exposure steps in addition to the time needed to perform the assay, and no method has emerged that requires short (~15 min) ABX exposure, short (~15 min) assay time, and does not require excessively complex or delicate instrumentation so the method can be deployed at the POC.

Rapid phenotypic methods based on quantification of nucleic acids (NAs) have shown great promise for a rapid POC AST due to the speed, specificity, and robustness of NA detection [53-58]. There is an additional advantage to using NA quantification as a readout of the bacterial response to antibiotic: because rapid pathogen identification (ID) from clinical samples is commonly performed via NA analysis, it would likely be easier to integrate NA-based phenotypic AST into a combined ID/AST workflow performed from the same clinical sample. Additionally, the use of NA-based methods provides molecular specificity towards the target pathogen, which is important in clinical samples that can contain multiple organisms. For ABX that directly or indirectly impact NA replication on short time scales, we have demonstrated that the quantification of DNA [59,60] or RNA [61] can be used to rapidly (30 min) and reliably determine susceptibility to nitrofurantoin and/or ciprofloxacin. Subsequent efforts have targeted the β -lactam class (the most widely prescribed class of ABX [1,2]) using these methods [62]. However, because β -lactams do not directly impact NA replication on short time scales, this direct translation of the existing

NA-based technique required a two-hour antibiotic exposure, which is not sufficiently rapid for POC. For a POC AST to impact management of CRE infections, it must (i) determine susceptibility to β -lactams, including carbapenems; (ii) it must be rapid (< 30 min sample-to-answer) [63,64]; and (iii) it must be phenotypic [26,27]. As discussed below, rapid pathogen ID technologies are becoming available and therefore pathogen ID is not the focus of this work.

Here, we hypothesized that a new NA-based approach could be used to develop a rapid phenotypic AST for multiple β -lactams. We hypothesized that upon treatment with β -lactam antibiotics, susceptible Enterobacteriaceae isolates would become sufficiently permeabilized so some of their DNA would become accessible to added polymerase and primers. Further, we hypothesized that this accessible DNA would be detectable directly by isothermal amplification methods that do not fully lyse bacterial cells. To differentiate between resistant and susceptible organisms, rather than measuring how total NA concentration is impacted by ABX exposure (as in previous NA-based ASTs), we hypothesized that we could measure the accessibility of NAs to polymerase following a short ABX exposure. Here we test these hypotheses and use them to design a new AST method, termed pol-aAST (polymerase-accessibility AST). To validate the method, we performed 82 ASTs using clinical isolates of three major CRE pathogens exposed to each of three commonly prescribed β -lactams for Gram-negative infections: ceftriaxone (CRO), ertapenem (ETP), and meropenem (MEM). To further demonstrate that this method has potential to be used clinically, in POC-relevant timescales, we (i) performed timed sample-to-answer experiments using contrived urine samples to ensure the whole assay can be performed in < 30 min, and (ii) we performed a pilot study on clinical urine samples from patients with urinary tract infections (UTI).

RESULTS

The pol-aAST relies on differential accessibility of nucleic acids to polymerases as a result of ABX exposure. In this manuscript, we define differential accessibility to polymerase as a difference in the measured rate of amplification between control and ABX-treated samples. In the first step of pol-aAST, a single sample is split into control and treated aliquots of equal volume, and the treated aliquot is exposed to a β -lactam. ABX-exposure

is a critical step in any phenotypic AST because phenotypic tests measure the response of bacteria to ABX. If the bacteria in the sample are resistant, we hypothesized that no differences in NA amplification will be observed between control and treated aliquots. If the bacteria are susceptible, we hypothesized that ABX treatment would lead to a compromised peptidoglycan cell wall (Fig A-1a) and partial release of NAs (Fig A-1b). We hypothesized that both the compromised cell wall and partial release of NAs would increase the accessibility of NAs to polymerase in a treated ABX-susceptible aliquot. In the second step of pol-aAST, control and treated aliquots are exposed to polymerase in amplification conditions (Fig A-1c) and the rate of amplification is measured.

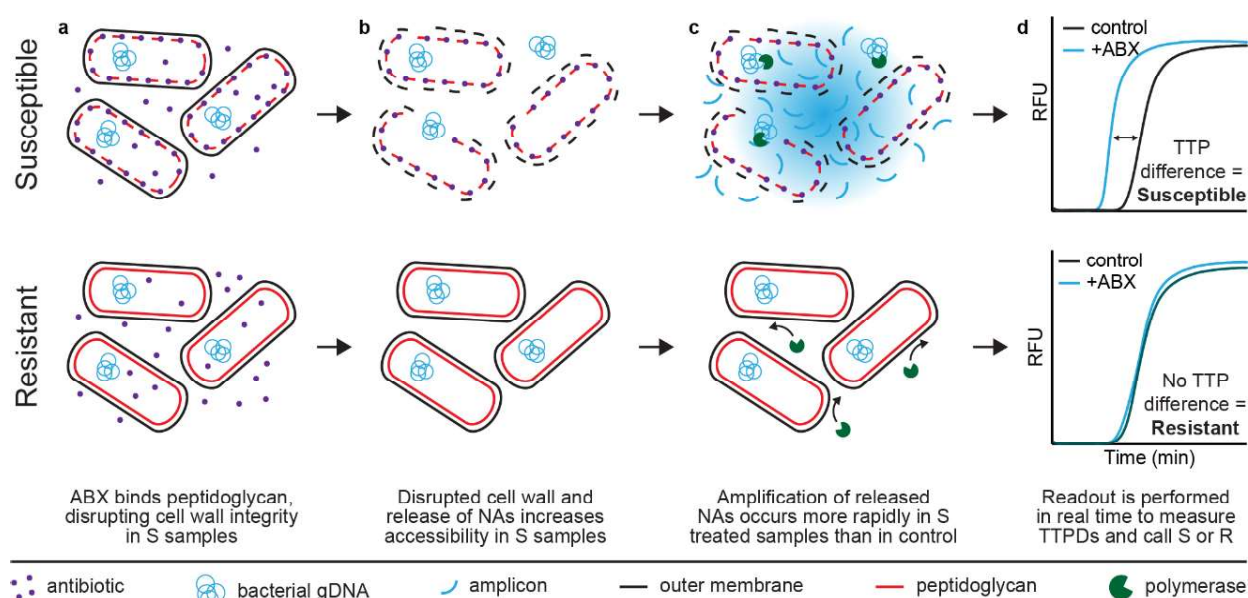


Fig A-1. Overview of the polymerase-accessibility AST (pol-aAST) shown for susceptible (S) and resistant (R) samples exposed to β -lactams. (a) Treated aliquots are exposed to a β -lactam. In susceptible samples, β -lactams compromise cell wall integrity. (b) Nucleic acids (NAs) are released from compromised cells, increasing NA accessibility to polymerase. (c) Released NAs in the susceptible treated aliquot amplify faster than NAs from intact cells in the control aliquot, resulting in a difference in time-to-positive. No difference in amplification between control and treated aliquots is observed in resistant samples. (d) Time-to-positive difference (TTPD) between control and treated aliquots is used to assess susceptibility.

To successfully differentiate susceptible and resistant samples, ideal amplification conditions must i) not fully lyse cells, ii) enhance alterations (damage) to the cell wall caused by exposure to β -lactams, and iii) increase NA release only from ABX-damaged cells. The rate of amplification is dependent on the concentration of polymerase-accessible NA. In susceptible samples, more NAs are released in the treated aliquot, leading to faster amplification in susceptible treated aliquots (Fig B-1d) relative to the controls. Resistant

samples are not affected by the ABX, so control and treated aliquots have similar NA release and time-to-positive. In these samples, the low concentration of naturally occurring extracellular DNA is ultimately amplified, but at a slower rate. Amplification rate in an isothermal amplification reaction is quantified by measuring the time-to-positive (TTP), the time it takes the reaction fluorescence to reach a predetermined threshold. We found that using pol-aAST, isolates susceptible to the β -lactam being tested show increased accessibility of NAs to polymerase, manifesting in an earlier TTP relative to the control. The TTPs of any two samples, such as the control and treated aliquots, can be compared to generate a TTP difference value (TTPD), which can then be used to determine susceptibility by comparing to a susceptibility threshold. Here we use the DNA polymerase *Bst* 3.0 under loop-mediated isothermal amplification (LAMP) conditions.

We hypothesized that the chemical environment in which amplification occurs would significantly impact the result of pol-aAST, and that for pol-aAST to differentiate susceptible and resistant samples, amplification conditions should not be fully lysing. To test this, we performed pol-aAST using LAMP, and quantitative PCR (qPCR) (Fig A-2). LAMP is performed at a single temperature (70 °C), which we hypothesized would not be fully lysing, whereas qPCR is a thermocycled amplification technique reaching a maximum temperature of 95 °C, which we hypothesized would be fully lysing. Indeed, we observed that pol-aAST was successful in differentiating susceptible and resistant isolates when performed using LAMP, but not when performed using qPCR (Fig A-2). We tested qPCR with a total of two susceptible and two resistant isolates, none of which showed a statistically significant difference in C_q between control and treated samples. When using LAMP, detectable differences were observed between control and treated aliquots when using isolates susceptible to the target β -lactam (TTPD = 1.02 min). Additionally, the presence of cells not lysed during LAMP is evidenced by the shorter TTPs seen when an aliquot of the same sample is lysed using an extraction buffer prior to performing LAMP (see Fig A-5). These differences confirm that choice of amplification chemistry is critical to the success of pol-aAST, and are consistent with previous work evaluating thermal lysis [65].

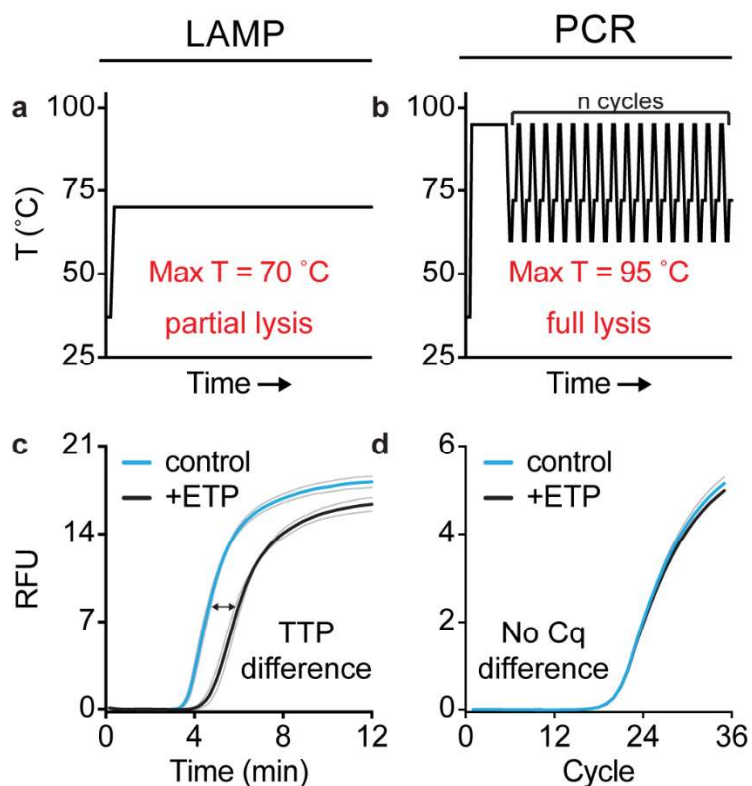


Fig A-2. The pol-aAST requires non-lytic amplification conditions. (a–b) Thermal profiles of LAMP and PCR. (c–d) LAMP and PCR amplification curves for a susceptible *E. coli* isolate exposed to ertapenem (ETP) for 15 min. Blue and black lines are the average of triplicate samples. Grey lines represent standard deviation of triplicates. A difference in time-to-positive (TTP) for control and treated aliquots is observed for susceptible isolates when quantifying nucleic acids using LAMP, but not PCR. Raw data are provided in Table A3-5.

To investigate the mechanism of pol-aAST, we performed experiments to separate free NAs from NAs contained within structurally intact cells or associated with cell debris. Susceptible and resistant clinical isolates were exposed to β -lactams for 15 min, then filtered through 0.2 μ M filters to remove cells from free NAs. NAs in the sample and eluate were then quantified using droplet digital PCR (ddPCR). We observed that following exposure to β -lactams, susceptible isolates treated with β -lactams released a significantly larger percentage of DNA than resistant samples (Fig A-3). The amount of DNA released depended on the ABX being tested. Exposure to meropenem resulted in an average of 21% of DNA being released from susceptible isolates, with a slightly smaller average percent (15%) released as a result of exposure to ertapenem. Interestingly, susceptible samples only released an average of 6% of DNA when exposed to CRO, demonstrating that NA release is dependent on choice of ABX and not, e.g., a universal stress response. These results also

demonstrate that the magnitude of the effect of a β -lactam on cell wall integrity can be measured and is different depending on the ABX used, even on short exposure time scales.

To validate the pol-aAST method, we first performed 82 ASTs using 12 clinical isolates of *Escherichia coli* (*Ec*), 8 clinical isolates of *Klebsiella pneumoniae* (*Kp*), and 9 clinical isolates of two species of *Enterobacter* (*Ebs*) and the β -lactams CRO, ETP, and MEM. The set included isolates from each genus that were susceptible and isolates that were resistant to each of the three antibiotics. In addition to isolates obtained from the UCLA Clinical Microbiology Laboratory (see Methods), those tested included *Ec* and *Kp* isolates from the Centers for Disease Control (CDC) Enterobacteriaceae Carbapenem Breakpoint panel [66], as well as all available *Enterobacter* spp. isolates from the same panel. All samples were amplified using quantitative LAMP and categorical agreement was compared to gold-standard broth microdilution AST. Two approaches for determining susceptibility were investigated in all pol-aASTs performed.

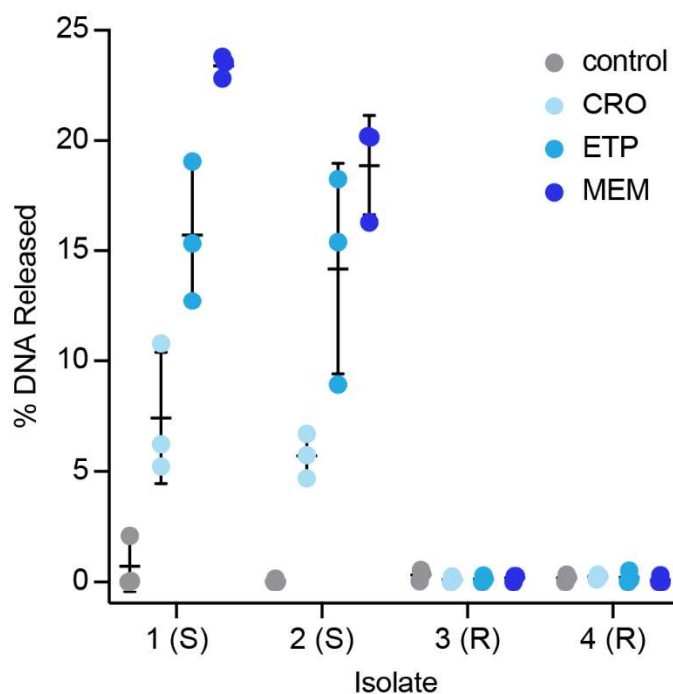


Fig A-3. Percentage of DNA released following antibiotic exposure. Two susceptible (S) and two resistant (R) *E. coli* isolates were exposed to no antibiotic (control), ceftriaxone (CRO), ertapenem (ETP), or meropenem (MEM) for 15 min before filtering to separate intact cells from extracellular DNA. Experiments were performed in triplicate for all isolate/antibiotic combinations. Each point represents a single experiment; lines represent the average and standard deviation of replicate experiments. Raw data are provided in Table A3-6.

The first approach we investigated was to compare the difference in TTP values of the control and treated aliquots in each pol-aAST. This difference was defined as $TTPD_{CT}$ (Fig A-4a). Using the $TTPD_{CT}$ method, we obtained 100% categorical agreement with gold-standard AST for all antibiotics tested with *Ec* (Fig A-4b), *Kp* (Fig A-4c), and *Ebs* (Fig A-4d) isolates, even with resistant isolates for which the genotypic tests fail to correctly predict the resistance phenotype (red points in Fig A-4). The values of $TTPD_{CT}$ were well-separated between susceptible and resistant isolates in all CRE-ABX combinations. Note that the threshold values separating $TTPD_{CT}$ of susceptible and resistant isolates depend on the antibiotic used (e.g. CRO gives a smaller response and therefore requires a lower threshold), as well as the pathogen tested (e.g. *K. pneumoniae* gives stronger response and requires a higher threshold). The area under the curve (AUC) of the receiver operating characteristic (ROC) curve was 1.00 for all isolates and antibiotics tested. There were no errors relative to gold-standard AST when determining susceptibility by $TTPD_{CT}$.

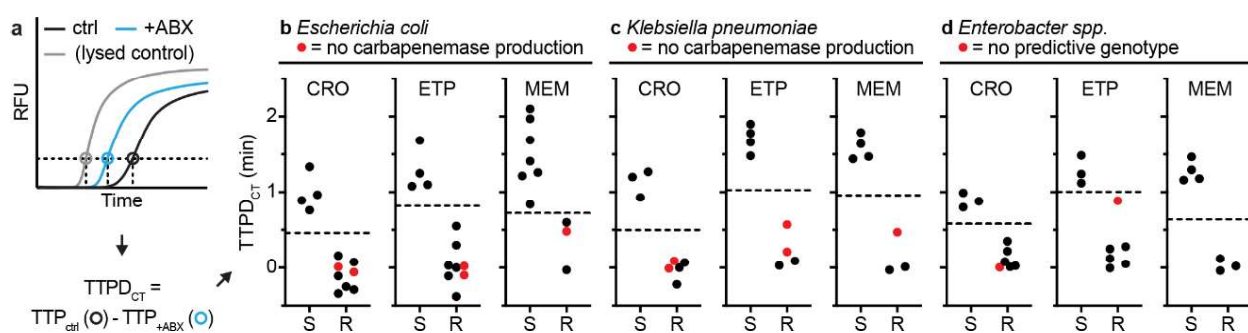


Fig A-4. Validation of the pol-aAST method using control (ctrl) and antibiotic-treated (+ABX) aliquots. (a) Example calculation of time-to-positive difference (TTPD) between control and treated aliquots ($TTPD_{CT}$). The TTP (in min) of the control and treated aliquots are used to calculate $TTPD_{CT}$. (b–d) The pol-aAST results using *Escherichia coli* (b) *Klebsiella pneumoniae* (c), and *Enterobacter* spp. (d) isolates exposed to ceftriaxone (CRO), ertapenem (ETP), and meropenem (MEM) for 15 min. Red points represent isolates with either no detectable carbapenemase genes (*Ec* and *Kp* isolates) according to a published genotypic assay [67] and commercial assay [68], or no predictive genotype (*Ebs* isolates) according to the whole genome sequencing by the CDC [66]. S/R thresholds (dashed lines) were set halfway between the lowest susceptible (S) and the highest resistant (R) $TTPD_{CT}$ values. Raw data are provided in Table A-S3.

The second approach we investigated was to compare the difference in TTP values of a fully lysed aliquot and the antibiotic-treated aliquot in each pol-aAST. The fully lysed aliquot was created by extracting NA from the ABX-treated sample using a single-step, LAMP-compatible extraction buffer. This difference was defined as $TTPD_{LT}$ (Fig A-5a). It is important to note that $TTPD_{LT}$ only requires an ABX-treated sample during the

exposure step (the method does not require the use of a no-ABX control during exposure), meaning the original sample does not have to be split prior to exposure. Again, the thresholds were defined individually for each antibiotic and pathogen. Using the $TTPD_{LT}$ method, we obtained 100% categorical agreement with gold-standard AST for all antibiotics tested only with *Ec* (Fig A-5b) and *Kp* (Fig A-5c) isolates, and with resistant isolates for which the genotypic tests fail to correctly predict the resistance phenotype (red points in Fig A-5). When testing *Ebs* (Fig A-5d) isolates, we observed two errors in which an isolate classified as CRO-resistant was called as susceptible, resulting in an overall categorical agreement of 88%. Because of these errors, the AUC for *Ebs* isolates tested with CRO was 0.94. Aside from these errors, susceptible and resistant isolates were well separated in all cases, with AUC = 1.000 for all antibiotics tested with *Ec* and *Kp*. Although we observed two errors, using the $TTPD_{LT}$ metric still gave excellent agreement with gold-standard AST and required no splitting of the sample prior to exposure.

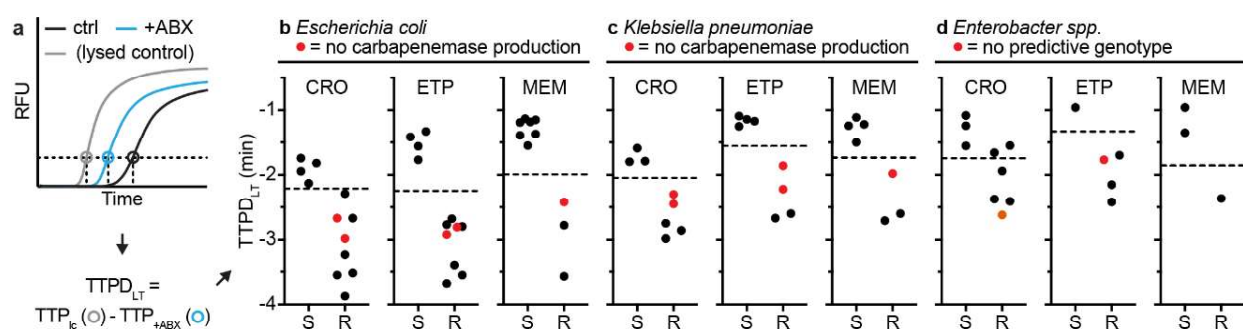


Fig A-5. Validation of the pol-aAST method using lysed control (lc) and antibiotic-treated (+ABX) aliquots. (a) Example calculation of time-to-positive difference (TTPD) between the lysed-control and antibiotic-treated aliquots ($TTPD_{LT}$). The TTP (in min) in the lysed-control and antibiotic-treated aliquots are used to calculate $TTPD_{LT}$ (b–d) The pol-aAST results using *Escherichia coli* (b) *Klebsiella pneumoniae* (c), and *Enterobacter spp.* (d) isolates exposed to ceftriaxone (CRO), ertapenem (ETP), and meropenem (MEM) for 15 min. Red points represent isolates with either no detectable carbapenemase genes (*Ec* and *Kp* isolates) according to a published genotypic assay [67] and commercial assay [68], or no predictive genotype (*Ebs* isolates) according to the CDC [66]. S/R thresholds (dashed lines) were set halfway between the lowest susceptible (S) and the highest resistant (R) $TTPD_{LT}$ values except in the case of *Enterobacter spp.* treated with CRO (see text). Raw data are provided in Table A-S3.

To demonstrate one of the major differences between pol-aAST, a phenotypic method, and existing genotypic methods, we challenged the assay with five previously characterized isolates that had either i) no detectable β -lactamase genes or ii) lacked any genotypic signature predictive of β -lactam resistance. We tested two *Ec* and two *Kp* isolates

with no detectable β -lactamase genes as measured by both a published genotypic assay designed to screen for six β -lactamase gene families [67], as well as the Cepheid Xpert® Carba-R test (a commercial, FDA-approved genotypic assay designed to screen for five β -lactamase gene families) [68]. These four isolates did not test positive in either assay because they lack the genes these assays screen for, despite being resistant (as determined by gold-standard broth microdilution). These four tested isolates were resistant to CRO and ETP, and one isolate from each genus was also resistant to MEM. Additionally, we tested a single resistant *Ebs* isolate from the CDC Enterobacteriaceae Carbapenem Breakpoint Panel (AR-Bank #0007). Whole genome sequencing of this isolate (performed by the CDC) revealed no known resistance markers [66], meaning the mechanism of resistance was uncharacterized. The pol-aAST performed excellently in all cases, and all 5 isolates were correctly categorized as resistant (Figs. A-4, A-5, red points).

To investigate the sample-to-answer time of the pol-aAST, we performed timed experiments using contrived urine samples (Fig A-6). Sample-to-answer time is a critical metric for any assay designed to be used at the point of care (POC), but is often not reported at all, even for methods claiming to be rapid. In timed experiments, we i) reduced the exposure time from 15 to 13 min to ensure all handling could be performed during the 15 min aliquoted for exposure, and ii) used an automated data-analysis spreadsheet to provide a susceptibility call as soon as the LAMP reactions reached a pre-determined threshold (indicating successful amplification). At the start of pol-aAST, a timer was started which ran for the duration of the experiment and was stopped once a susceptibility call had been made. The susceptibility of four isolates to ETP was tested simultaneously (Fig A-6a). The pol-aAST consists of only three simple handling steps (Fig A-6b-d), which allowed us to perform pol-aAST in a total time of just 29.5 min, with results in agreement with gold-standard AST (Fig A-6e).

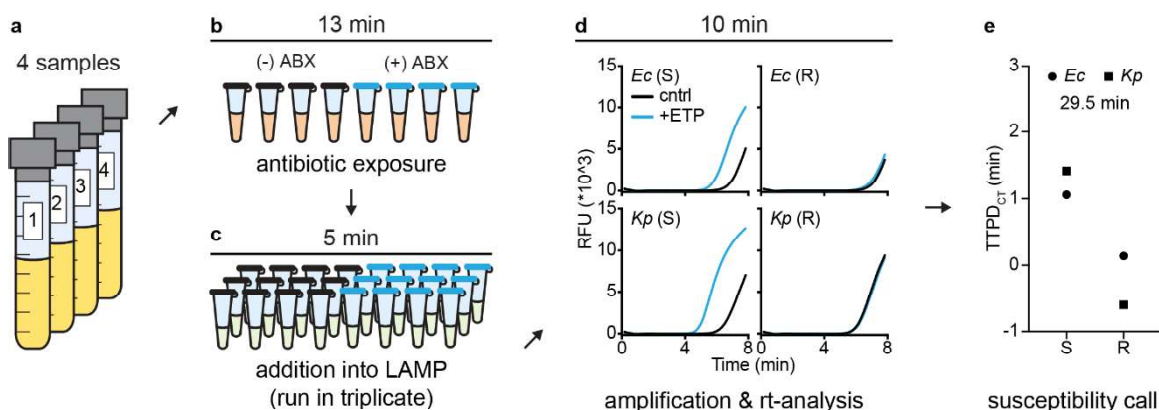


Fig A-6. Timed sample-to-answer pol-aAST using contrived urine samples spiked with either *E. coli* (*Ec*) or *Klebsiella pneumoniae* (*Kp*). (a) Because minimal sample handling is required for pol-aAST, all four contrived urine samples were run in parallel. (b) Urine samples were split into control and antibiotic-treated aliquots and incubated at 37 °C for 13 min. A timer was started immediately after sample splitting. (c) All samples were added to pre-made LAMP mix and run in technical triplicate. (d) Samples were amplified using LAMP and the fluorescence of reactions was monitored in real-time. Once total fluorescence passed a pre-determined threshold (indicating successful amplification), reactions were stopped and TTP values ported into an automated data-analysis spreadsheet. The timer was stopped as soon as the spreadsheet gave susceptibility calls. (e) Comparison of susceptibility calls with gold-standard AST categorization. Total assay time was 29.5 min. Raw data are provided in Table A-S3.

We next ran the pol-aAST on clinical urine samples from patients diagnosed with UTI. These samples were confirmed to be Enterobacteriaceae-positive UTI by the UCLA Clinical Microbiology Laboratory (CML) and the pol-aASTs were run 3–5 d post-collection. Initial experiments running the pol-aAST directly on clinical urine samples revealed an insufficient response to ABX in some samples. Because we analyzed urine samples that had been stored in a chemical preservative (see Methods) for 3–5 days after collection, some variation in the response to ABX was expected. However, we wished to test whether the delays in the response were indeed due to the phenotypic state of bacteria in these archived samples, and not due to the intrinsic biology of the bacterial strains in these samples. To test, we obtained 25 clinical urine specimens that exhibited an expected heterogeneity, as indicated by the wide range of urinalysis findings (see S2 Table); pH ranged from <5 to 8, specific gravities from <1.005 to >1.060 (above and below the ranges detected in standard urinalysis), protein of up to 2+, and the presence of ketones and bilirubin, as well as red blood cells, leukocytes, and squamous epithelial cells. Two of the samples were polymicrobial. To ensure a response from bacteria in these specimens, we added a 30 min pre-incubation step of urine with media and increased the duration of ABX exposure to 45 min (see Methods). We did not optimize these conditions and did not attempt to identify the shortest

possible incubation or exposure time. Eight samples were tested for ampicillin (AMP) susceptibility and 17 samples were tested for ETP susceptibility. Prior to testing clinical samples using AMP, we tested five *E. coli* isolates using AMP (S1 Fig). Despite the heterogeneity in the urine matrix and the likely nutrient-deprived condition of the bacteria in the urine samples, pol-aAST experiments yielded clean separation between AMP sensitive and resistant *E. coli*. Additionally, we were able to observe a response to ETP in 14 of 17 ETP-S urine samples tested. Overall, we obtained 100% categorical agreement for determination of AMP susceptibility (4/4 susceptible, and 4/4 resistant, Fig A-7), and observed a response indicating susceptibility to ETP in 14 of 17 (82.4%) confirmed-susceptible samples (Fig A-7), including the two polymicrobial samples. None of the samples received for testing by the pol-aAST method were ETP-resistant.

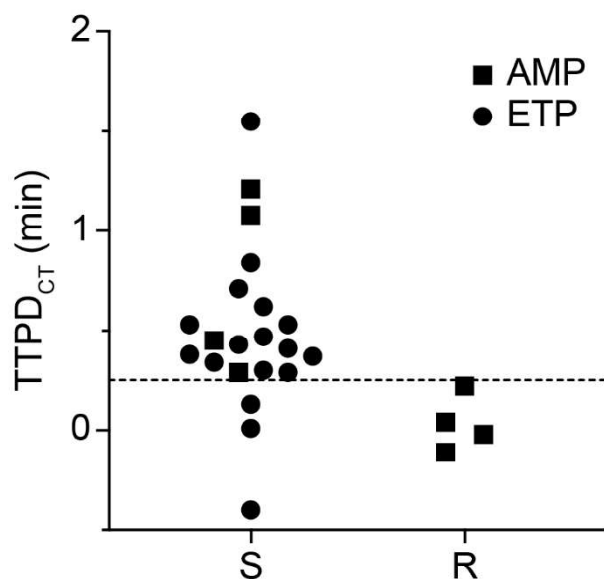


Fig A-7. Pilot testing of pol-aAST with clinical UTI samples with a modified protocol (see Methods and Discussion). TTPD_{CT} values for ampicillin (AMP) and ertapenem (ETP) susceptibility obtained by pol-aAST, with clinical UTI samples containing *E. coli*. Each point represents the TTPD_{CT} value for one clinical sample tested once by pol-aAST (S2 and S4 Tables). LAMP was performed in technical triplicate, see S4 Table for values and statistical details.

DISCUSSION

The pol-aAST method enables rapid, organism-specific measurement of susceptibility to β -lactams—the most important class of ABX for Gram-negative infections—thus providing the critically missing piece needed to develop a POC AST for this global health threat. The genera of isolates and the β -lactams used in this proof-of-concept study were intentionally chosen: *E. coli* (*Ec*), *K. pneumoniae* (*Kp*), and the

Enterobacter species *E. aerogenes* and *E. cloacae* (collectively *Ebs*), are responsible for the majority of CRE infections globally [8,11-13] (in some areas of the U.S. *Kp* is responsible for up to 90% of CRE infections [5]). It is for this reason that *Ec*, *Kp*, and *Ebs* together make up the majority of isolates in the CDC's Enterobacteriaceae Carbapenem Breakpoint panel, a collection of isolates designed specifically to challenge carbapenem-susceptibility tests in Enterobacteriaceae [66]. CRO, used broadly for a variety of infections because of its broad coverage and tolerability, was chosen as a representative third-generation cephalosporin. Similarly, ETP and MEM were chosen as clinically representative carbapenems [69]. When testing clinical samples, AMP was chosen because of its high resistance prevalence, and thus the availability of resistant samples (55.8% of clinical urine samples received by the UCLA CML are AMP-resistant [70]). We chose ETP as a representative carbapenem.

The pol-aAST has two important requirements: i) amplification conditions that are not fully lytic and ii) release of NAs only from cells that are susceptible to the β -lactam to which they are exposed. If cells fully lyse, as they do in PCR, there is no difference in amplification between control and treated aliquots in susceptible isolates (Fig A-2). It is only under partial-lysis conditions, as in LAMP, that cell integrity is preserved long enough to yield a substantial TTP difference. Cell integrity, and rate and degree of lysis, will also depend on the identity of the organism, as well as its growth rate. In partial-lysis conditions, most NAs are still protected inside cells in the control aliquot, whereas a significant portion of NAs are released and start amplifying immediately in the treated aliquot. We know from previous work [60] that the speed of an optimized bulk LAMP reaction makes it difficult to linearly correlate TTP and NA concentration, unless very sensitive real-time measurements are made. Based on the magnitude of the differences in TTP observed here and the results measuring NA release (Fig A-3), we suspect that both the state of NA (inside intact cells vs. inside or outside damaged cells) and the differences in concentration of free NA contribute to the TTP differences observed. Cell-wall defects and damage are also likely to increase the penetration of amplification reagents into DNA trapped inside the remains of susceptible treated cells especially under the elevated temperature of the amplification reaction. We chose LAMP because we have shown previously that it is a

rapid and specific isothermal amplification chemistry [60]. However, other non-lytic isothermal amplification chemistries could also be investigated. Additionally, DNA release (Fig A-3) could be measured to determine susceptibility using PCR if combined with a filtration step; we have not evaluated the pros and cons of this approach in this paper. Lastly, alternative or modified accessibility-based AST approaches will likely need to be developed for different organisms, as we have done for *Neisseria gonorrhoeae* [71].

To demonstrate the flexibility of the pol-aAST method and the simplicity of the workflow, we investigated two approaches for determining susceptibility. The first, measuring TTPD_{CT}, gave 100% categorical agreement and uses a standard ABX-exposure step wherein one aliquot serves as the control and the other aliquot is exposed to an ABX. The second, measuring TTPD_{LT}, differs in that only a single aliquot of the original sample is used during the ABX-exposure step. After exposure, this aliquot is compared with a fully lysed control aliquot, which could be extracted at any point during the assay. Using only a single aliquot of the original sample during exposure reduces the challenges of fluid handling and metering, which will be valuable when developing fully-integrated devices. When using a control and treated aliquot, both aliquots must have precisely metered volumes, and the heating required during exposure must be performed on both aliquots. Both methods showed excellent categorical agreement with gold-standard broth microdilution, and the choice of approach will be dictated by future device architecture.

To illustrate the value of phenotypic approaches, we evaluated pol-aAST using isolates that tested negative for β -lactamase genes and isolates that lack a predictive genotype (e.g. no β -lactamase production, no modified porins, no modified penicillin-binding proteins), based on published and commercial genotypic assays [67], and CDC classification based on the ResFinder database [72], respectively. The ABX-susceptibility of isolates lacking beta-lactamases cannot be detected by current, FDA-approved genotypic methods, yet bacteria that do not produce beta-lactamases can comprise 11–71% of CRE infections[4,73,74]. Using pol-aAST, all five of these isolates were correctly categorized as resistant.

Sample-to-answer time directly reflects the speed of diagnostics in practice, and is a major factor in how likely a diagnostic is to be adopted. In general, the shorter the sample-to-answer time, the more valuable the test is, and the more feasible for use at the POC. With urine as the contrived sample matrix, pol-aAST was able to be completed in < 30 min. This time scale is on par both with suggested time-frames for rapid POC diagnostics [63,64], and measured times of patient visits [75]. Additionally, because urine involves relatively simple sample-handling steps, we were able to perform four ASTs in parallel when testing contrived samples. The ability to run several samples in parallel demonstrates the potential to multiplex multiple antibiotics, which will be important for the next steps, including the design of integrated devices.

We have demonstrated direct testing of 25 clinical UTI samples using the pol-aAST with changes to the workflow (see Methods). However, even with the heterogeneity of clinical urine specimens (see urinalysis in Table A-S2), including two polymicrobial samples that were correctly classified as ETP-S, the pol-aAST demonstrated good agreement with gold-standard broth dilution. The ability to handle polymicrobial samples was predictable based on the molecular specificity of NA-based methods. We expect this work to set the foundation for future improvements when using clinical samples.

The pol-aAST method demonstrates a rapid NA-based phenotypic AST for β -lactams and CREs. As with any academic report of an innovative diagnostic technology development, this work has limitations in the breadth of its scope and level of technological maturity. The following work would further extend the clinical applicability of this study, and will be necessary for translation into a system suitable for regulatory approval and clinical use. First, the pol-aAST needs to be further developed and evaluated with fresh clinical urine samples from patients; here we have used chemically preserved samples that were 3-5 d old, which likely decreased the response time of bacteria to ABX. We expect fresh clinical samples to show more rapid and consistent responses; this hypothesis remains to be tested. We note that many state-of-the-art phenotypic AST methods are initially published without validation of performance directly on clinical samples, e.g. a recent breakthrough demonstrating phenotypic AST on isolates and on blood cultures [58]. Urine is a relevant matrix for a CRE diagnostic because UTI can be the majority cause of cases

of CRE morbidity [76], and because of the large number of hospital-acquired infections that involve catheters or other long-term indwelling medical devices [11], where CRE infections cause major problems. Second, to expand the scope of this approach, other sample types such as blood and blood cultures should be tested (in combination with appropriate pathogen-isolation and pathogen-enrichment technologies). Third, only categorical (S/R) agreement with the gold-standard method was tested here. While in the majority of cases a rapid categorical AST is clinically actionable, testing samples with a range of minimum inhibitory concentrations (MIC), including those with intermediate resistance, would further broaden the scope of the method. Fourth, we have not tested pol-aAST against heteroresistant samples. However, these are more common in Gram-positive organisms [77] and are not common in Gram-negative organisms. Fifth, the pol-aAST chemistry should be integrated with microfluidic devices so the AST can be performed directly on clinical samples with minimal user intervention. Sixth, the performance of these integrated devices will need to be evaluated in pre-clinical and clinical studies.

We emphasize that the specific pol-aAST described in this paper, just like other innovative rapid ASTs [60,78-81], is not intended to be the sole test to guide treatment. Even though pol-aAST is based on detection of pathogen-specific nucleic acids and can therefore provide pathogen ID, we anticipate that in a clinical workflow pol-aAST would be performed after a separate rapid pathogen ID step [17,18,20]. This ID step would then allow an unambiguous choice of the appropriate rapid AST. Furthermore, pol-aAST would likely be combined with rapid AST for other antibiotics, such as fluoroquinolones that can be used to treat CRE infections. AST methods that rely on similar underlying chemistries are more likely to be successfully integrated together. Isothermal amplification of pathogen-specific nucleic acids appears to be a promising approach for AST and we have already shown how rapid fluoroquinolone AST can be performed in 30 min using digital LAMP [60]. Integration of pol-aAST with these complementary methods and translation to a distributable diagnostic will enable: i) improved antibiotic stewardship by reducing empiric use of carbapenems for Enterobacteriaceae, ii) improved patient outcomes by detecting CRE infections for which carbapenems would be ineffective, and iii) more cost-effective surveillance of CRE outbreaks.

We envision that exploratory and mechanistic research inspired by pol-aAST will lead to a new generation of AST diagnostics. Additional mechanistic studies, such as those involving visualizing bacterial response to antibiotics [82,83], would clarify the effects of different ABX on the responses measured in pol-aAST for different pathogens. To evaluate whether pol-aAST can be broadened beyond CREs and β -lactams, these studies would include organisms with cell envelopes that differ from Enterobacteriaceae (e.g., Gram-positives), and other antimicrobials that affect the cell envelope, such as antimicrobial peptides [84] or vancomycin. It would also be desirable to evaluate pol-aAST with more amplification chemistries, including modified LAMP assays [85,86] and other isothermal chemistries [87-89], such as recombinase polymerase amplification (RPA), that are actively being developed and can be performed at lower temperatures. Ultimately, this new generation of AST diagnostics will be integrated with the rapid ID methods being developed [17,18,20] and with future rapid NA-based AST methods for additional ABX and pathogens. For example, we have developed the nuc-aAST [71], which measures accessibility of DNA to nucleases and was used to perform a rapid test of antibiotic susceptibility on the fastidious organism *Neisseria gonorrhoeae*. In contrast to the pol-aAST, the nuc-aAST enhances antibiotic-induced damage using surfactants after the ABX exposure step, and performs full cell lysis. Ultimately, to address the broad diversity of antibiotic-resistant pathogens, it is clear that integrated, multiplexed POC devices that incorporate multiple rapid phenotypic AST methods are needed. Innovative methods based on antibiotic-induced accessibility of nucleic acids to enzymes are promising for generating such ASTs for multiple antibiotics and pathogens in an approach that is intrinsically compatible with other rapid AST methods [60] and with rapid pathogen ID [17,18,21,22].

METHODS

Ethics statement

Remnant urine samples from patients with confirmed UTI were received by UCLA CML and released to the Caltech researchers under UCLA IRB #19-001098. The UCLA IRB waived the requirement for informed consent/assent/parent permission under 45 CFR 46.116(d) for the entire study. No identifying information was obtained by the Caltech team and the research was determined to be exempt by Caltech IRB (applications #18-0858 and #19-0909).

Study Design

The objective of this study was to develop a rapid phenotypic AST for β -lactams based on DNA accessibility to polymerase for use with Enterobacteriaceae. To calculate the sample size necessary to validate the method (Fig A-4, A-5), the methods and Equation 5 from Banoo et al. [90] were used as described previously [60]. Namely, we suspected that the specificity and sensitivity of the nuc-aAST method would be 95% with a desired margin of error of $\pm 10\%$. Under these conditions, 18.2 (or 19) samples must be tested with the nuc-aAST method and compared to the gold standard. We performed 36 ASTs with isolates susceptible to the ABX being tested, and 46 ASTs with isolates resistant to the ABX being tested.

Isolates, growth conditions, and antibiotic exposure conditions

We obtained 25 de-identified clinical isolates from the UCLA Clinical Microbiology Laboratory (CML) and the CDC's Enterobacteriaceae Carbapenem Breakpoint panel [66]. In the case of isolates obtained from the UCLA CML, MICs were determined as described previously [59]. Genotypic testing of the two *Ec* and two *Kp* isolates selected for their lack of known β -lactamase genes was performed by UCLA CML using a previously published assay [67] and separately at the Keck School of Medicine of USC using the FDA-approved Cepheid Xpert® Carba-R test. Whole genome sequencing of the single *Ebs* isolate selected for its lack of known resistance genes was performed by the CDC [66]. All isolates were stored as glycerol stocks at $-80\text{ }^{\circ}\text{C}$. Glycerol stocks were streaked onto Trypticase Soy Agar with 5% sheep's blood (Becton Dickinson, Franklin Lakes, NJ, USA) and grown overnight at $37\text{ }^{\circ}\text{C}$ or resuspended directly in liquid media. Prior to experiments, a small clump of cells was resuspended from plates or glycerol stocks in 2 mL Brain Heart Infusion Broth (BHI, Becton Dickinson) at $37\text{ }^{\circ}\text{C} + 5\% \text{CO}_2$ with 500 rpm shaking for 2 to 4 h until visibly turbid. OD_{600} of the cultures was then measured, and working cultures prepared at an OD_{600} of 0.01–0.07 and grown for 50 – 145 min at $37\text{ }^{\circ}\text{C} + 5\% \text{CO}_2$ with 500 rpm. Working cultures were then diluted 10X into control and treated aliquots for antibiotic exposure. For validation experiments, antibiotic exposure was performed in 100 μL volumes consisting of 80 μL Mueller Hinton II Broth (Becton Dickinson), 5 μL nuclease-free H_2O (NF- H_2O), 5 μL 20X antibiotic stock solution, and 10 μL of working culture. In control aliquots, antibiotic stock solution was replaced with NF- H_2O . For filtration experiments, antibiotic exposure was performed in 100 μL volumes consisting of 65 μL Mueller Hinton II Broth

(Becton Dickinson), 21 μL nuclease-free H_2O (NF- H_2O), 4 μL 25X antibiotic stock solution, and 10 μL of working culture. In control aliquots, antibiotic stock solution was replaced with NF- H_2O .

Antibiotic stocks

Ceftriaxone disodium salt hemi(heptahydrate) (Sigma, St. Louis, MO, USA), ertapenem sodium salt (Research Products International, Prospect, IL, USA), and meropenem trihydrate (TCI, Portland, OR, USA) were used to create 1.0 mg/mL antibiotic stock solutions in NF- H_2O based on manufacturer reported purity, aliquoted, and stored at $-80\text{ }^\circ\text{C}$. Ampicillin sodium salt (Sigma, St. Louis, MO, USA) was used to create 10.0 mg/mL antibiotic stock solutions in NF- H_2O based on manufacturer reported purity, aliquoted, and stored at $-80\text{ }^\circ\text{C}$. Aliquots were only thawed and used once on the days of experiments.

Comparison of amplification methods

In order to compare amplification using LAMP and PCR, *E. coli* isolates were exposed to 0.5 $\mu\text{g}/\text{mL}$ ertapenem for 15 min. Samples were then transferred directly into either PCR or LAMP mix on ice. Amplification was started immediately. Quantitative PCR (qPCR) was performed on a Roche LightCycler 96 using SsoFast EvaGreen Supermix (BioRad, Hercules, CA, USA). 10 μL reactions were used. 10% of the final reaction volume was template. Published primers targeting the 23S rRNA genes of Enterobacteriaceae were used [91] at a final concentration of 500 nM. Cycling conditions consisted of 3.0 min at $95\text{ }^\circ\text{C}$, followed by 35 cycles of $95\text{ }^\circ\text{C}$ for 10 sec, $60\text{ }^\circ\text{C}$ for 10 sec, and $72\text{ }^\circ\text{C}$ for 15 sec. Fluorescence was measured using the SYBR Green channel after each $72\text{ }^\circ\text{C}$ extension step. LAMP was performed on a BioRad CFX96 using the following conditions: 10 μL reaction volume containing 1X Isothermal Reaction Buffer II (NEB), 5 mM MgSO_4 (NEB), 1.4 mM dNTPs (NEB), 320 U/mL *Bst* 3.0 (NEB), and 2 μM Syto-9 (Thermo Fisher). 10% of the reaction volume was template. Primer sequences (designed to target the 23S rRNA genes of Enterobacteriaceae) and concentrations have been described previously [60]. Cycling conditions consisted of 2.0 min at $12\text{ }^\circ\text{C}$ (while lid was heating), followed by 120 cycles of $70\text{ }^\circ\text{C}$ for 10 sec. Fluorescence was measured using the SYBR Green channel

every 10 sec (after each cycle). We also ran an analogous LAMP reaction in the absence of Tween-20 (which is normally present in Isothermal Reaction Buffer II; NEB), to test for a potential difference in lysis efficiency, however the resulting reaction rates were substantially lower than when Tween-20 was included.

Filtration experiments

Filtration experiments were performed using *E. coli* isolates exposed to 0.5 µg/mL ETP for 15 min. Immediately following exposure, cultures were passed through 0.22 µm, 1.5 mL cellulose acetate centrifuge tube filters (Corning Costar Spin-X, Corning, NY, USA). DNA retention by the filters was < 7% when measured by quantifying purified Lambda phage DNA (NEB) before and after filtration. Quantification was performed using ddPCR (QX200, BioRad). In filtration experiments, 50 µL of sample was added to the filter and centrifuged for 4 min at 1000 rcf. DNA was extracted from both the feed and filtrate using QuickExtract DNA Extraction Solution (Lucigen, Middleton, WI, USA). Samples were diluted 10X into extraction buffer and extracted according to manufacturer instructions. The concentration of the single copy *E. coli uidA* gene was then quantified in the feed and filtrate extractions. The percentage of *E. coli* DNA in the filtrate was calculated as the filtrate concentration divided by the feed concentration. Droplet digital PCR (ddPCR) was performed using QX200 ddPCR Supermix for EvaGreen (BioRad); 10% of the final reaction volume was template. Published primers targeting the *uidA* gene in *E. coli* were used[92] at a final concentration of 500 nM. Cycling conditions consisted of 5.0 min at 95 °C, followed by 40 cycles of 95 °C for 30 sec, 60 °C for 30 sec, and 72 °C for 30 sec., with final dye stabilization steps of 4 °C for 5.0 min followed by 90 °C for 5.0 min.

pol-aAST validation with clinical isolates

For pol-aAST validation experiments, *E. coli* and *Enterobacter* spp. isolates were exposed to either 2.0 µg/mL ceftriaxone (CRO), 0.5 µg/mL ertapenem (ETP), or 1.0 µg/mL meropenem (MEM). *K. pneumoniae* isolates were exposed to either 2.0 µg/mL CRO, 1.0 µg/mL ETP, or 1.0 µg/mL MEM. Some isolates were run multiple times on different days. If this was the case, the average TTPD_{CT} and TTPD_{LT} are reported for that isolate. All isolates were exposed to ABXs for 15 min in 100 µL reaction volumes in 200 µL PCR tube strips. After 15 min of ABX exposure, 10 µL of samples were transferred as template to

LAMP reaction mix (as described above) on ice in technical triplicate. Amplification was immediately started.

Timed sample-to-answer using contrived urine samples

Timed sample to answer experiments were performed in the same fashion as pol-aAST validation experiments, except with the following modifications. Following initial growth and measurement of OD, isolates were resuspended in fresh, never-frozen, pooled human urine from healthy donors (Lee BioSciences). Additionally, a timer was started as soon as samples were added to the ABX exposure conditions. *Escherichia coli* (*Ec*) and *Klebsiella pneumoniae* (*Kp*) isolates were exposed to 0.5 and 1.0 $\mu\text{g/mL}$ ETP (respectively) for 13 min. 13 min was chosen to ensure all handling steps could be completed within the first 15 min of the assay. Amplification was performed until all reactions reached a fluorescence value of 1000 relative fluorescent units (RFU) or greater. Amplification was then stopped, and TTP values copied into a spreadsheet pre-populated with formulas to automatically output susceptibility calls. The timer was stopped once a susceptibility call had been determined.

Testing of pol-aAST with clinical samples

UCLA CML performed urinalysis, confirmation of urinary tract infection, pathogen isolation and identification, and subsequent gold-standard AST using broth microdilution. Gold-standard AST results were sent to Caltech researchers on the same day samples were received. Enterobacteriaceae-positive samples were shipped at ambient temperature to Caltech in BD Vacutainer Plus C&S preservative tubes (Becton Dickinson, Cat. 364951) containing a boric acid preservative. The pol-aAST experiments were performed directly on these samples within 3–5 d of their collection at UCLA. Urine samples were first warmed up to 37 °C without shaking for 30 min, to approximate temperature of freshly collected urine. Then, 30 μL of urine was diluted into 70 μL of Cation-adjusted Mueller Hinton II Broth (MHB, BD) containing 0.1% Tween-20 (Teknova) and placed at 37 °C with shaking at 750 rpm for 3 min. Samples were then centrifuged at 5000 rcf for 2 min. The supernatant was removed, and the sample resuspended in 100 μL of MHB. Samples were then incubated for 30 min at 37 °C with 750 rpm shaking. ABX exposure was performed in a final volume of 100 μL , after transfer of 20 μL of incubated sample to 80 μL of the exposure condition: 75 μL of MHB and 5 μL of 20X ABX stock solution in NF-H₂O for treated aliquots, or 75 μL of MHB with

5 μL of NF-H₂O alone for control aliquots. For measurement of ETP susceptibility, the exposure condition contained a final concentration of 1 $\mu\text{g}/\text{mL}$ of ETP. Aliquots were incubated at 37 °C with shaking for 20 min. For measurement of AMP susceptibility, the ABX-exposure condition contained a final concentration of 16 $\mu\text{g}/\text{mL}$ of AMP, and aliquots were incubated at 37 °C with shaking for 45 min. The control and treated aliquots were subjected to a set of dilutions to account for variable bacterial load of the samples and resolution within the working range of the LAMP reaction. Following dilution, 1 μL of the control and treated aliquots was added to each LAMP reaction well. There were three technical replicates (3 LAMP reaction wells) for each condition (control and treated). We measured the time-to-positive (TTP) for the reactions at each dilution, and then selected the dilution that yielded a control TTP value later than 4.7 min. The TTP results from this dilution were used to calculate TTPD_{CT} (and determine susceptibility). Samples with a $\text{TTPD}_{\text{CT}} > 0.25$ min were considered susceptible, while samples with $\text{TTPD}_{\text{CT}} \leq 0.25$ min were considered resistant. The susceptibility determination of the pol-aAST method was then compared to the gold-standard culture results obtained by the UCLA CML to measure assay performance.

Statistical analysis

Significance referenced in the text for Fig A-2 were calculated using GraphPad Prism 8.0 software from an unpaired, two-tailed t-test comparing the averages of three replicate C_q values of each control sample to each treated sample. A significance value of 0.02 was used for statistical significance. All percent release values (Fig A-3) and TTPD values (Figs 3-4 – 3-6) were calculated using Microsoft Excel. Data were plotted using GraphPad Prism 8.0 software. Thresholds for determining susceptibility in TTPD_{CT} and TTPD_{LT} plots were set halfway between the lowest S and highest R values for each organism/ABX combination. For preliminary tests with clinical samples, we defined a TTPD_{CT} of above 0.25 min for a susceptible determination; this value would be further defined in a subsequent larger-scale clinical trial.

REFERENCES

1. Van Boeckel TP, Gandra S, Ashok A, Caudron Q, Grenfell BT, Levin SA, et al. Global antibiotic consumption 2000 to 2010: an analysis of national pharmaceutical sales data. *Lancet Infect Dis.* 2014;14(8):742-50. doi: 10.1016/s1473-3099(14)70780-7.
2. Versporten A, Zarb P, Caniaux I, Gros MF, Drapier N, Miller M, et al. Antimicrobial consumption and resistance in adult hospital inpatients in 53 countries: results of an internet-

- based global point prevalence survey. *Lancet Global Health*. 2018;6(6):e619-e29. doi: 10.1016/S2214-109X(18)30186-4.
3. Magill SS, Edwards JR, Beldavs ZG, Dumyati G, Janelle SJ, Kainer MA, et al. Prevalence of antimicrobial use in US acute care hospitals, May-September 2011. *JAMA*. 2014;312(14):1438-46. doi: 10.1001/jama.2014.12923.
 4. Zhang Y, Wang Q, Yin Y, Chen H, Jin L, Gu B, et al. Epidemiology of Carbapenem-Resistant Enterobacteriaceae Infections: Report from the China CRE Network. *Antimicrob Agents Chemother*. 2018;62(2):e01882-17. doi: 10.1128/AAC.01882-17.
 5. Satlin MJ, Chen L, Patel G, Gomez-Simmonds A, Weston G, Kim AC, et al. Multicenter Clinical and Molecular Epidemiological Analysis of Bacteremia Due to Carbapenem-Resistant Enterobacteriaceae (CRE) in the CRE Epicenter of the United States. *Antimicrob Agents Chemother*. 2017;61(4):e02349-16. doi: 10.1128/AAC.02349-16.
 6. Iovleva A, Doi Y. Carbapenem-Resistant Enterobacteriaceae. *Clin Lab Med*. 2017;37(2):303-15. doi: 10.1016/j.cll.2017.01.005.
 7. WHO. Global Priority List of Antibiotic-resistant Bacteria to Guide Research, Discovery, and Development of New Antibiotics 2017 [December 3, 2018]. Available from: <https://www.who.int/medicines/publications/global-priority-list-antibiotic-resistant-bacteria/en/>.
 8. CDC. Antibiotic Resistance Threats in the United States 2013 [December 3, 2018]. Available from: <https://www.cdc.gov/drugresistance/pdf/ar-threats-2013-508.pdf>.
 9. Gelband H, Miller-Petrie M, Pant S, Levinson SGJ, Barter D, Laxminarayan AWR. State of the World's Antibiotics 2015. Available from: https://cddep.org/publications/state_worlds_antibiotics_2015/.
 10. CDC. Antibiotic/Antimicrobial Resistance: Biggest Threats and Data 2019 [April 2019]. Available from: https://www.cdc.gov/drugresistance/biggest_threats.html.
 11. Guh AY, Bulens SN, Mu Y, Jacob JT, Reno J, Scott J, et al. Epidemiology of Carbapenem-Resistant Enterobacteriaceae in 7 US Communities, 2012-2013. *JAMA*. 2015;314(14):1479-87. doi: 10.1001/jama.2015.12480.
 12. Cerqueira GC, Earl AM, Ernst CM, Grad YH, Dekker JP, Feldgarden M, et al. Multi-institute analysis of carbapenem resistance reveals remarkable diversity, unexplained mechanisms, and limited clonal outbreaks. *Proc Natl Acad Sci U S A*. 2017;114(5):1135-40. doi: 10.1073/pnas.1616248114.
 13. Weiner LM, Webb AK, Limbago B, Dudeck MA, Patel J, Kallen AJ, et al. Antimicrobial-Resistant Pathogens Associated With Healthcare-Associated Infections: Summary of Data Reported to the National Healthcare Safety Network at the Centers for Disease Control and Prevention, 2011–2014. *Infect Control Hosp Epidemiol*. 2016;37(11):1288-301. doi: 10.1017/ice.2016.174.

14. White House. National Action Plan for Combating Antibiotic-Resistant Bacteria 2015 [December 3, 2018]. Available from: https://obamawhitehouse.archives.gov/sites/default/files/docs/national_action_plan_for_combating_antibiotic-resistant_bacteria.pdf.
15. WHO. Global Action Plan on Antimicrobial Resistance 2015 [December 3, 2018]. Available from: <https://www.who.int/antimicrobial-resistance/global-action-plan/en/>.
16. O'Neill J. Tackling Drug-Resistant Infections Globally: Final Report and Recommendations. Review on Antimicrobial Resistance [Internet]. 2016 12/01/2016. Available from: <https://amr-review.org/Publications.html>.
17. Renner LD, Zan J, Hu LI, Martinez M, Resto PJ, Siegel AC, et al. Detection of ESKAPE Bacterial Pathogens at the Point of Care Using Isothermal DNA-Based Assays in a Portable Degas-Actuated Microfluidic Diagnostic Assay Platform. *Appl Environ Microbiol*. 2017;83(4). doi: 10.1128/aem.02449-16.
18. Poritz MA, Blaschke AJ, Byington CL, Meyers L, Nilsson K, Jones DE, et al. FilmArray, an automated nested multiplex PCR system for multi-pathogen detection: development and application to respiratory tract infection. *PLoS One*. 2011;6(10):e26047. doi: 10.1371/journal.pone.0026047.
19. Gootenberg JS, Abudayyeh OO, Kellner MJ, Joung J, Collins JJ, Zhang F. Multiplexed and portable nucleic acid detection platform with Cas13, Cas12a, and Csm6. *Science*. 2018;360(6387):439-44. doi: 10.1126/science.aaq0179.
20. Phaneuf CR, Mangadu B, Piccini ME, Singh AK, Koh CY. Rapid, Portable, Multiplexed Detection of Bacterial Pathogens Directly from Clinical Sample Matrices. *Biosensors*. 2016;6(4):E49. doi: 10.3390/bios6040049.
21. Ahn H, Batule BS, Seok Y, Kim MG. Single-Step Recombinase Polymerase Amplification Assay Based on a Paper Chip for Simultaneous Detection of Multiple Foodborne Pathogens. *Anal Chem*. 2018;90(17):10211-6. doi: 10.1021/acs.analchem.8b01309.
22. Raja B, Goux HJ, Marapadaga A, Rajagopalan S, Kourentzi K, Willson RC. Development of a panel of recombinase polymerase amplification assays for detection of common bacterial urinary tract infection pathogens. *J Appl Microbiol*. 2017;123(2):544-55. doi: 10.1111/jam.13493.
23. CLSI. M07-A10; Methods for Dilution Antimicrobial Susceptibility Testing for Bacteria That Grow Aerobically; Approved Standard-Tenth Edition: Clinical and Laboratory Standards Institute; 2015.
24. Jorgensen JH, Ferraro MJ. Antimicrobial susceptibility testing: a review of general principles and contemporary practices. *Clin Infect Dis*. 2009;49(11):1749-55. doi: 10.1086/647952.
25. Blank S, Daskalakis DC. *Neisseria gonorrhoeae* - Rising Infection Rates, Dwindling Treatment Options. *N Engl J Med*. 2018;379(19):1795-7. doi: 10.1056/NEJMp1812269.

26. Piddock LJ. Assess drug-resistance phenotypes, not just genotypes. *Nat Microbiol*. 2016;1(8):16120. doi: 10.1038/nmicrobiol.2016.120.
27. Bard J, Lee F. Why can't we just use PCR? The role of genotypic versus phenotypic testing for antimicrobial resistance testing. *Clin Microbiol Newsl*. 2018;40(11):87-95. doi: <https://doi.org/10.1016/j.clinmicnews.2018.05.003>.
28. van Belkum A, Bachmann TT, Lüdke G, Lisby JG, Kahlmeter G, Mohess A, et al. Developmental roadmap for antimicrobial susceptibility testing systems. *Nature Reviews Microbiology*. 2018. doi: 10.1038/s41579-018-0098-9.
29. WHO. No time to wait: Securing the future from drug-resistant infections Report to the Secretary-General of the United Nations; 2019.
30. Kostic T, Ellis M, Williams MR, Stedtfeld TM, Kaneene JB, Stedtfeld RD, et al. Thirty-minute screening of antibiotic resistance genes in bacterial isolates with minimal sample preparation in static self-dispensing 64 and 384 assay cards. *Appl Microbiol Biotechnol*. 2015;99(18):7711-22. doi: 10.1007/s00253-015-6774-z.
31. Kalsi S, Valiadi M, Tsaloglou MN, Parry-Jones L, Jacobs A, Watson R, et al. Rapid and sensitive detection of antibiotic resistance on a programmable digital microfluidic platform. *Lab Chip*. 2015;15(14):3065-75. doi: 10.1039/c5lc00462d.
32. Nakano R, Nakano A, Ishii Y, Ubagai T, Kikuchi-Ueda T, Kikuchi H, et al. Rapid detection of the *Klebsiella pneumoniae* carbapenemase (KPC) gene by loop-mediated isothermal amplification (LAMP). *J Infect Chemother*. 2015;21(3):202-6. doi: 10.1016/j.jiac.2014.11.010.
33. Mu X, Nakano R, Nakano A, Ubagai T, Kikuchi-Ueda T, Tansho-Nagakawa S, et al. Loop-mediated isothermal amplification: Rapid and sensitive detection of the antibiotic resistance gene ISAbal-blaOXA-51-like in *Acinetobacter baumannii*. *J Microbiol Methods*. 2016;121:36-40. doi: 10.1016/j.mimet.2015.12.011.
34. Hu C, Kalsi S, Zeimpekis I, Sun K, Ashburn P, Turner C, et al. Ultra-fast electronic detection of antimicrobial resistance genes using isothermal amplification and Thin Film Transistor sensors. *Biosens Bioelectron*. 2017;96:281-7. doi: 10.1016/j.bios.2017.05.016.
35. Cortegiani A, Russotto V, Graziano G, Geraci D, Saporito L, Cocorullo G, et al. Use of Cepheid Xpert Carba-R(R) for Rapid Detection of Carbapenemase-Producing Bacteria in Abdominal Septic Patients Admitted to Intensive Care Unit. *PLoS One*. 2016;11(8):e0160643. doi: 10.1371/journal.pone.0160643.
36. Biofire. The BioFire FilmArray 2019 [March 8, 2019]. Available from: <https://www.biofire.com/products/filmarray/>.
37. Shawar R. 510(k) Premarket Notification for K160901 Cepheid Xpert Carba-R Assay. Silver Spring, MD: USA Food and Drug Administration, Department of Health and Human Services; 2016.

38. Lasserre C, De Saint Martin L, Cuzon G, Bogaerts P, Lamar E, Glupczynski Y, et al. Efficient Detection of Carbapenemase Activity in Enterobacteriaceae by Matrix-Assisted Laser Desorption Ionization-Time of Flight Mass Spectrometry in Less Than 30 Minutes. *J Clin Microbiol.* 2015;53(7):2163-71. doi: 10.1128/JCM.03467-14.
39. Bogaerts P, Yunus S, Massart M, Huang TD, Glupczynski Y. Evaluation of the BYG Carba Test, a New Electrochemical Assay for Rapid Laboratory Detection of Carbapenemase-Producing Enterobacteriaceae. *J Clin Microbiol.* 2016;54(2):349-58. doi: 10.1128/JCM.02404-15.
40. Robinson AM, Medlicott NJ, Ussher JE. The rapid detection of cefotaxime-resistant Enterobacteriaceae by HPLC. *Future Sci OA.* 2016;2(4):FSO142. doi: 10.4155/fsoa-2016-0042.
41. Bernabeu S, Dortet L, Naas T. Evaluation of the beta-CARBA test, a colorimetric test for the rapid detection of carbapenemase activity in Gram-negative bacilli. *J Antimicrob Chemother.* 2017;72(6):1646-58. doi: 10.1093/jac/dkx061.
42. Zhang Y, Lei JE, He Y, Yang J, Wang W, Wasey A, et al. Label-Free Visualization of Carbapenemase Activity in Living Bacteria. *Angew Chem Int Ed Engl.* 2018;57(52):17120-4. doi: 10.1002/anie.201810834.
43. Santiso R, Tamayo M, Gosalvez J, Bou G, Fernandez Mdel C, Fernandez JL. A rapid in situ procedure for determination of bacterial susceptibility or resistance to antibiotics that inhibit peptidoglycan biosynthesis. *BMC Microbiol.* 2011;11:191. doi: 10.1186/1471-2180-11-191.
44. Bou G, Otero FM, Santiso R, Tamayo M, Fernandez Mdel C, Tomas M, et al. Fast assessment of resistance to carbapenems and ciprofloxacin of clinical strains of *Acinetobacter baumannii*. *J Clin Microbiol.* 2012;50(11):3609-13. doi: 10.1128/JCM.01675-12.
45. Park K, Jeong J, Yi SY, Lee WS, Shin YB. FRET probe-based antibacterial susceptibility testing (F-AST) by detection of bacterial nucleases released by antibiotic-induced lysis. *Biosensors Bioelectron.* 2019. doi: 10.1016/j.bios.2019.01.033.
46. Faria-Ramos I, Espinar MJ, Rocha R, Santos-Antunes J, Rodrigues AG, Canton R, et al. A novel flow cytometric assay for rapid detection of extended-spectrum beta-lactamases. *Clin Microbiol Infect.* 2013;19(1):E8-E15. doi: 10.1111/j.1469-0691.2012.03986.x.
47. Burnham CA, Frobel RA, Herrera ML, Wickes BL. Rapid ertapenem susceptibility testing and *Klebsiella pneumoniae* carbapenemase phenotype detection in *Klebsiella pneumoniae* isolates by use of automated microscopy of immobilized live bacterial cells. *J Clin Microbiol.* 2014;52(3):982-6. doi: 10.1128/JCM.03255-13.
48. Su IH, Ko WC, Shih CH, Yeh FH, Sun YN, Chen JC, et al. A dielectrophoresis system for testing antimicrobial susceptibility of Gram-negative bacteria to beta-lactam antibiotics. *Anal Chem.* 2017. doi: 10.1021/acs.analchem.7b00220.

49. Kang W, Sarkar S, Lin ZS, McKenney S, Konry T. Ultrafast Parallelized Microfluidic Platform for Antimicrobial Susceptibility Testing of Gram Positive and Negative Bacteria. *Anal Chem*. 2019;91(9):6242-9. doi: 10.1021/acs.analchem.9b00939.
50. Cansizoglu MF, Tamer YT, Farid M, Koh AY, Toprak E. Rapid ultrasensitive detection platform for antimicrobial susceptibility testing. *PLoS Biol*. 2019;17(5):e3000291. doi: 10.1371/journal.pbio.3000291.
51. Mo M, Yang Y, Zhang F, Jing W, Iriya R, Popovich J, et al. Rapid Antimicrobial Susceptibility Testing of Patient Urine Samples Using Large Volume Free-Solution Light Scattering Microscopy. *Anal Chem*. 2019;91(15):10164-71. doi: 10.1021/acs.analchem.9b02174.
52. Lange C, Schubert S, Jung J, Kostrzewa M, Sparbier K. Quantitative matrix-assisted laser desorption ionization-time of flight mass spectrometry for rapid resistance detection. *J Clin Microbiol*. 2014;52(12):4155-62. doi: 10.1128/jcm.01872-14.
53. Rolain JM, Mallet MN, Fournier PE, Raoult D. Real-time PCR for universal antibiotic susceptibility testing. *J Antimicrob Chemother*. 2004;54(2):538-41. doi: 10.1093/jac/dkh324.
54. Mach KE, Mohan R, Baron EJ, Shih MC, Gau V, Wong PK, et al. A biosensor platform for rapid antimicrobial susceptibility testing directly from clinical samples. *J Urol*. 2011;185(1):148-53. doi: 10.1016/j.juro.2010.09.022.
55. Halford C, Gonzalez R, Campuzano S, Hu B, Babbitt JT, Liu J, et al. Rapid antimicrobial susceptibility testing by sensitive detection of precursor rRNA using a novel electrochemical biosensing platform. *Antimicrob Agents Chemother*. 2013;57(2):936-43. doi: 10.1128/AAC.00615-12.
56. Mezger A, Gullberg E, Goransson J, Zorzet A, Herthnek D, Tano E, et al. A general method for rapid determination of antibiotic susceptibility and species in bacterial infections. *J Clin Microbiol*. 2015;53(2):425-32. doi: 10.1128/JCM.02434-14.
57. Barczak AK, Gomez JE, Kaufmann BB, Hinson ER, Cosimi L, Borowsky ML, et al. RNA signatures allow rapid identification of pathogens and antibiotic susceptibilities. *Proc Natl Acad Sci U S A*. 2012;109(16):6217-22. doi: 10.1073/pnas.1119540109.
58. Bhattacharyya RP, Bandyopadhyay N, Ma P, Son SS, Liu J, He LL, et al. Simultaneous detection of genotype and phenotype enables rapid and accurate antibiotic susceptibility determination. *Nat Med*. 2019;25(12):1858-64. doi: 10.1038/s41591-019-0650-9.
59. Schoepp NG, Khorosheva EM, Schlappi TS, Curtis MS, Humphries RM, Hindler JA, et al. Digital Quantification of DNA Replication and Chromosome Segregation Enables Determination of Antimicrobial Susceptibility after only 15 Minutes of Antibiotic Exposure. *Angew Chem Int Ed Engl*. 2016;55(33):9557-61. doi: 10.1002/anie.201602763.
60. Schoepp NG, Schlappi TS, Curtis MS, Butkovich SS, Miller S, Humphries RM, et al. Rapid pathogen-specific phenotypic antibiotic susceptibility testing using digital LAMP quantification in clinical samples. *Sci Transl Med*. 2017;9(410). doi: 10.1126/scitranslmed.aal3693.

61. Khazaei T, Barlow JT, Schoepp NG, Ismagilov RF. RNA markers enable phenotypic test of antibiotic susceptibility in *Neisseria gonorrhoeae* after 10 minutes of ciprofloxacin exposure. *Sci Rep*. 2018;8(1). doi: 10.1038/s41598-018-29707-w.
62. Ota Y, Furuhashi K, Nanba T, Yamanaka K, Ishikawa J, Nagura O, et al. A rapid and simple detection method for phenotypic antimicrobial resistance in *Escherichia coli* by loop-mediated isothermal amplification. *J Med Microbiol*. 2019. doi: 10.1099/jmm.0.000903.
63. Marston HD, Dixon DM, Knisely JM, Palmore TN, Fauci AS. Antimicrobial Resistance. *JAMA*. 2016;316(11):1193-204. doi: 10.1001/jama.2016.11764.
64. Hicks JM, Haeckel R, Price CP, Lewandrowski K, Wu AHB. Recommendations and opinions for the use of point-of-care testing for hospitals and primary care: summary of a 1999 symposium. *Clin Chim Acta*. 2001;303(1-2):1-17. doi: Doi 10.1016/S0009-8981(00)00400-9.
65. Valiadi M, Kalsi S, Jones IGF, Turner C, Sutton JM, Morgan H. Simple and rapid sample preparation system for the molecular detection of antibiotic resistant pathogens in human urine. *Biomed Microdevices*. 2016;18(1). doi: 10.1007/s10544-016-0031-9.
66. CDC. Enterobacteriaceae Carbapenem Breakpoint Panel 2015 [cited 2018 November 20, 2018]. Available from: <https://www.cdc.gov/ARIsolateBank/Panel/PanelDetail?ID=7>.
67. Pollett S, Miller S, Hindler J, Uslan D, Carvalho M, Humphries RM. Phenotypic and molecular characteristics of carbapenem-resistant Enterobacteriaceae in a health care system in Los Angeles, California, from 2011 to 2013. *J Clin Microbiol*. 2014;52(11):4003-9. doi: 10.1128/JCM.01397-14.
68. Cepheid. Xpert® Carba-R 2018 [cited 2018 November 26, 2018]. Available from: <http://www.cepheid.com/us/cepheid-solutions/clinical-ivd-tests/healthcare-associated-infections/xpert-carba-r>.
69. Hawkey PM, Livermore DM. Carbapenem antibiotics for serious infections. *BMJ*. 2012;344:e3236. doi: 10.1136/bmj.e3236.
70. UCLA Health System. Antimicrobial Susceptibility Summary 2019; 2019. Available from: https://www.asp.mednet.ucla.edu/files/view/AMIC_2017.pdf.
71. Savelle ES, Schoepp NG, Cooper MM, Rolando JC, Klausner JD, Soge OO, et al. Measurement of DNA Accessibility in *Neisseria gonorrhoeae* Exposed to Beta-lactams Accelerates Phenotypic Antibiotic Susceptibility Testing. *PLoS Biol*. 2020.
72. Zankari E, Hasman H, Cosentino S, Vestergaard M, Rasmussen S, Lund O, et al. Identification of acquired antimicrobial resistance genes. *J Antimicrob Chemother*. 2012;67(11):2640-4. doi: 10.1093/jac/dks261.
73. Chang YY, Chuang YC, Siu LK, Wu TL, Lin JC, Lu PL, et al. Clinical features of patients with carbapenem nonsusceptible *Klebsiella pneumoniae* and *Escherichia coli* in intensive care

- units: a nationwide multicenter study in Taiwan. *J Microbiol Immunol Infect.* 2015;48(2):219-25. doi: 10.1016/j.jmii.2014.05.010.
74. Tamma PD, Goodman KE, Harris AD, Tekle T, Roberts A, Taiwo A, et al. Comparing the Outcomes of Patients With Carbapenemase-Producing and Non-Carbapenemase-Producing Carbapenem-Resistant Enterobacteriaceae Bacteremia. *Clin Infect Dis.* 2017;64(3):257-64. doi: 10.1093/cid/ciw741.
75. Rui P, Okeyode T. National Ambulatory Care Survey: 2015 State and National Summary Tables 2015 [December 3, 2018]. Available from: https://www.cdc.gov/nchs/data/ahcd/namcs_summary/2015_namcs_web_tables.pdf.
76. Braykov NP, Eber MR, Klein EY, Morgan DJ, Laxminarayan R. Trends in resistance to carbapenems and third-generation cephalosporins among clinical isolates of *Klebsiella pneumoniae* in the United States, 1999-2010. *Infect Control Hosp Epidemiol.* 2013;34(3):259-68. doi: 10.1086/669523.
77. Musta AC, Riederer K, Shemes S, Chase P, Jose J, Johnson LB, et al. Vancomycin MIC plus heteroresistance and outcome of methicillin-resistant *Staphylococcus aureus* bacteremia: trends over 11 years. *J Clin Microbiol.* 2009;47(6):1640-4. doi: 10.1128/jcm.02135-08.
78. Baltekin O, Boucharin A, Tano E, Andersson DI, Elf J. Antibiotic susceptibility testing in less than 30 min using direct single-cell imaging. *Proc Natl Acad Sci U S A.* 2017;114(34):9170-5. doi: 10.1073/pnas.1708558114.
79. Choi J, Yoo J, Lee M, Kim EG, Lee JS, Lee S, et al. A rapid antimicrobial susceptibility test based on single-cell morphological analysis. *Sci Transl Med.* 2014;6(267):267ra174-267ra174. doi: 10.1126/scitranslmed.3009650
80. Etayash H, Khan MF, Kaur K, Thundat T. Microfluidic cantilever detects bacteria and measures their susceptibility to antibiotics in small confined volumes. *Nat Commun.* 2016;7:12947. doi: 10.1038/ncomms12947.
81. Longo G, Alonso-Sarduy L, Rio LM, Bizzini A, Trampuz A, Notz J, et al. Rapid detection of bacterial resistance to antibiotics using AFM cantilevers as nanomechanical sensors. *Nat Nanotechnol.* 2013;8(7):522-6. doi: 10.1038/nnano.2013.120.
82. Pidgeon SE, Pires MM. Vancomycin-Dependent Response in Live Drug-Resistant Bacteria by Metabolic Labeling. *Angew Chem Int Ed Engl.* 2017;56(30):8839-43. doi: 10.1002/anie.201704851.
83. Stone MRL, Butler MS, Phetsang W, Cooper MA, Blaskovich MAT. Fluorescent Antibiotics: New Research Tools to Fight Antibiotic Resistance. *Trends Biotechnol.* 2018. doi: 10.1016/j.tibtech.2018.01.004.
84. Deshayes S, Xian W, Schmidt NW, Kordbacheh S, Lieng J, Wang J, et al. Designing Hybrid Antibiotic Peptide Conjugates To Cross Bacterial Membranes. *Bioconjug Chem.* 2017;28(3):793-804. doi: 10.1021/acs.bioconjchem.6b00725.

85. Phillips EA, Moehling TJ, Bhadra S, Ellington AD, Linnes JC. Strand Displacement Probes Combined with Isothermal Nucleic Acid Amplification for Instrument-Free Detection from Complex Samples. *Anal Chem*. 2018;90(11):6580-6. doi: 10.1021/acs.analchem.8b00269.
86. Cai S, Jung C, Bhadra S, Ellington AD. Phosphorothioated Primers Lead to Loop-Mediated Isothermal Amplification at Low Temperatures. *Anal Chem*. 2018;90(14):8290-4. doi: 10.1021/acs.analchem.8b02062.
87. Daher RK, Stewart G, Boissinot M, Bergeron MG. Recombinase Polymerase Amplification for Diagnostic Applications. *Clin Chem*. 2016;62(7):947-58. doi: 10.1373/clinchem.2015.245829.
88. Toley BJ, Covelli I, Belousov Y, Ramachandran S, Kline E, Scarr N, et al. Isothermal strand displacement amplification (iSDA): a rapid and sensitive method of nucleic acid amplification for point-of-care diagnosis. *Analyst*. 2015;140(22):7540-9. doi: 10.1039/c5an01632k.
89. Reid MS, Le XC, Zhang H. Exponential Isothermal Amplification of Nucleic Acids and Assays for Proteins, Cells, Small Molecules, and Enzyme Activities: An EXPAR Example. *Angew Chem Int Ed Engl*. 2018;57(37):11856-66. doi: 10.1002/anie.201712217.
90. Banoo S, Bell D, Bossuyt P, Herring A, Mabey D, Poole F, et al. Evaluation of diagnostic tests for infectious diseases: general principles. *Nat Rev Microbiol*. 2006;4(9 Suppl):S21-31. doi: 10.1038/nrmicro1523.
91. Matsuda K, Tsuji H, Asahara T, Kado Y, Nomoto K. Sensitive quantitative detection of commensal bacteria by rRNA-targeted reverse transcription-PCR. *Appl Environ Microbiol*. 2007;73(1):32-9. doi: 10.1128/aem.01224-06.
92. Chern EC, Siefring S, Paar J, Doolittle M, Haugland RA. Comparison of quantitative PCR assays for *Escherichia coli* targeting ribosomal RNA and single copy genes. *Lett Appl Microbiol*. 2011;52(3):298-306. doi: 10.1111/j.1472-765X.2010.03001.x.

ACKNOWLEDGEMENTS

We thank Sukantha Chandrasekaran, Shelley Miller, Romney Humphries, Marisol Trejo, Catherine Le, and Lyna Chheang at the UCLA Clinical Microbiology Laboratory for providing isolates and clinical urine samples and for discussion of gold-standard practices. We thank Jennifer Dien Bard at the Keck School of Medicine of USC for performing Cepheid Xpert® Carba-R tests. We also thank Natasha Shelby for help with writing and editing this manuscript.

SUPPLEMENTARY MATERIALS

Supplementary Tables and Figures

Any table that is longer than 1 page has a link to download from the Supporting Information section of the published paper.

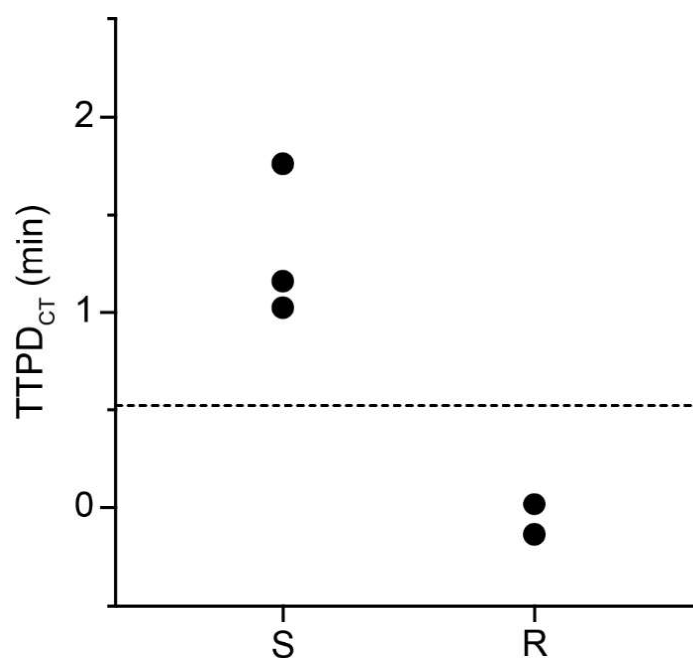


Fig A-S1. Validation of pol-aAST TTPD_{CT} method using ampicillin. *E. coli* isolates were exposed to 16 µg/mL ampicillin (AMP) for 15 min. Threshold was set halfway between the lowest susceptible (S) and highest resistant (R) TTPD_{CT} value. Data are in Table 3-S3.

Table A-S1. Clinical isolates used in this study. Isolates were obtained from the UCLA Clinical Microbiology Laboratory (CML) and the CDC's Enterobacteriaceae Carbapenem Breakpoint panel. The minimum inhibitory concentration (MIC) of each isolate (based on broth microdilution performed by UCLA CML) are provided.

Table A-S1 is available to download at <https://doi.org/10.1371/journal.pbio.3000652.s001>

Table A-S2. Clinical urine samples from patients with urinary tract infections (UTI) used in this study. Clinical samples were obtained from the UCLA Clinical Microbiology Laboratory (CML). MICs based on broth microdilution performed by UCLA CML are provided along with urinalysis results.

Table A-S2 is available to download at <https://doi.org/10.1371/journal.pbio.3000652.s002>

Table A-S3. Raw data and calculated error for all pol-aASTs performed using clinical isolates. Cqs and time-to-positives (TTPs) are provided.

Table A-S3 is available to download at <https://doi.org/10.1371/journal.pbio.3000652.s003>

Table A-S4. Raw data and calculated error for all pol-aASTs performed using clinical UTI samples. Cqs and time-to-positives (TTPs) are provided.

Table A-S4 is available to download at <https://doi.org/10.1371/journal.pbio.3000652.s004>

Table A-S5. Raw data for amplification curves shown in Fig 2. Technical triplicate values are provided for control and treated (0.50 µg/mL ETP) samples run using LAMP and PCR. Grey lines in Fig 2 represent standard deviation of the triplicate samples calculated using Graphpad Prism.

Table A-S5 is available to download at <https://doi.org/10.1371/journal.pbio.3000652.s005>

Table A-S6. Raw data for percentage of DNA release shown in Fig 3. Negative percentage release values were set to zero before averaging. Averages and standard deviations of each isolate/antibiotic combination were calculated using Graphpad Prism.

Table A-S6 is available to download at <https://doi.org/10.1371/journal.pbio.3000652.s006>

APPENDIX B: QUANTIFICATION OF SARS-COV-2 VIRAL LOAD IN LONGITUDINALLY COLLECTED SALIVA SAMPLES

Alexander Winnett*, Matthew M. Cooper*, Natasha Shelby*, Anna E. Romano, Jessica A. Reyes, Jenny Ji, Michael K. Porter, Emily S. Savelle, Jacob T. Barlow, Reid Akana, Colten Tognazzini, Matthew Feaster, Ying-Ying Goh, Rustem F. Ismagilov. 2020. "SARS-CoV-2 Viral Load in Saliva Rises Gradually and to Moderate Levels in Some Humans." medRxiv. <https://doi.org/10.1101/2020.12.09.20239467>

ONE SENTENCE SUMMARY

In some human infections and variant(s), SARS-CoV-2 viral load can rise slowly (over days) and remain near the limit of detection of rapid, low-sensitivity tests.

ABSTRACT

Transmission of SARS-CoV-2 in community settings often occurs before symptom onset, therefore testing strategies that can reliably detect people in the early phase of infection are urgently needed. Early detection of SARS-CoV-2 infection is especially critical to protect vulnerable populations who require frequent interactions with caretakers. Rapid COVID-19 tests have been proposed as an attractive strategy for surveillance, however a limitation of most rapid tests is their low sensitivity. Low-sensitivity tests are comparable to high sensitivity tests in detecting early infections when two assumptions are met: (1) viral load rises quickly (within hours) after infection and (2) viral load reaches and sustains high levels ($>10^5$ – 10^6 RNA copies/mL). However, there are no human data testing these assumptions. In this study, conducted in October 2020 in the greater Los Angeles area, we document a case of presymptomatic household transmission from a healthy young adult to a sibling and a parent. Participants prospectively provided twice-daily saliva samples. Samples were analyzed by RT-qPCR and RT-ddPCR and we measured the complete viral load profiles throughout the course of infection of the sibling and parent. This study provides evidence that in at least some human cases of SARS-CoV-2, viral load rises slowly (over days, not hours) and not to such high levels to be detectable reliably by any low-sensitivity test. Additional viral load profiles from different samples types across a broad demographic must be obtained to describe the

early phase of infection and determine which testing strategies will be most effective for identifying SARS-CoV-2 infection before transmission can occur.

INTRODUCTION

As of early December 2020, nearly one year after the first COVID-19 outbreak in Wuhan, China, there have been more than 65 million cases and 1.5 million deaths globally.¹ Transmission of SARS-CoV-2 in community settings often occurs before symptom onset,^{2,3} putting at great risk people who require frequent interactions with caregivers, such as residents of nursing homes. Better strategies for using the available COVID-19 diagnostic tests are critically needed to decrease overall transmission, thereby reducing transmission to these vulnerable populations.⁴

Transmission from asymptomatic or presymptomatic individuals is considered the Achilles' Heel of COVID-19 infection control.³ In a recent epidemiologic investigation of 183 confirmed COVID-19 cases in Wanzhou, China, about 76% of transmissions occurred from individuals without symptoms (either asymptomatic or presymptomatic).⁵ Numerous transmission events originating from individuals without symptoms have been documented in a variety of locations, such as dinner parties,⁶ skilled nursing facilities,^{2,7} correctional facilities,⁸ sporting events,^{9,10} religious ceremonies,⁶ and spring break trips.¹¹

The importance of effective testing strategies to quell transmission from individuals without symptoms is underscored by an outbreak at an overnight camp in Wisconsin¹² where a 9th grade student developed symptoms the day after arrival, prompting quarantine of 11 close contacts. All 11 contacts were asymptomatic and released from quarantine after receiving negative rapid antigen test results. However, 6 of the 11 went on to develop symptoms, and an outbreak ensued, with more than 100 additional individuals (a total of 3/4 of camp attendees) infected. In contrast, a more successful containment of an outbreak was documented in a skilled nursing facility in Los Angeles, where serial surveillance PCR testing was initiated immediately after three residents became symptomatic and tested positive.¹³ PCR results prompted isolation of 14 infected individuals without symptoms, which limited the outbreak to a total of only 19 out of 99 residents over the course of two weeks. These cases demonstrate the value of testing strategies that can detect and isolate infected individuals in the early phase in the infection, reducing the potential for

transmission to others during the elicitation window (the period when a person is infectious but not isolating).¹⁴

More than 200 *in vitro* diagnostics have received Emergency Use Authorization (EUA) from the U.S. Food and Drug Administration for identification of acute SARS-CoV-2 infection.¹⁵ These tests have a wide range of sensitivities. The most sensitive tests, with limits of detection (LOD) of 10^2 - 10^3 RNA copies/mL, include the RT-qPCR assays. These tests typically involve more intensive sample-preparation methods to extract and purify RNA and most are run in centralized laboratories (with a few exceptions of point-of-care tests that integrate rigorous sample preparation and RNA detection^{15,16}). At the other extreme are the low-sensitivity tests (LODs of $\sim 10^5$ - 10^7 RNA copies/mL), such as antigen tests or molecular tests that do not perform rigorous sample preparation. These tests offer tangible advantages, such as being fast (rapid antigen tests yield results in minutes), less expensive to manufacture, and can be deployable outside of laboratories.

Rapid, low-sensitivity tests are clearly a valuable part of the overall infection control strategy; however, the use of such tests as a strategy for diagnosing infected persons at the early phase of infection is controversial. The U.S. Food & Drug Administration (FDA) has authorized such tests for use in symptomatic populations. Data in several reports suggest that such tests may miss presymptomatic and asymptomatic individuals early in the infection.^{12,17} However, logical arguments have also been made,^{18,19} in favor of widely deploying surveillance tests with “analytic sensitivities vastly inferior to those of benchmark tests.”¹⁸

Low-sensitivity tests will be equally effective to high-sensitivity tests at minimizing transmission if the following two assumptions about the early phase of SARS-CoV-2 infection hold true: (i) viral load increases rapidly, by orders of magnitude within hours, and (ii) viral load reaches and sustains high levels during the infectious window, such that a rapid low-sensitivity test would have a similar ability to detect early-phase infections compared with high-sensitivity tests. These two assumptions have not been tested in humans. Viral load at the early phases of SARS-CoV-2 infection remains a knowledge gap necessary to inform the use of testing resources to effectively minimize transmission. To fill this knowledge gap, and inform selection of diagnostic tests appropriate for identifying infections in the earliest phases, requires studies that

monitor SARS-CoV-2 viral load with high temporal resolution (beginning at the incidence of infection) and in a large, diverse cohort of individuals.

We are conducting a case-ascertained observational study in which community members recently diagnosed with COVID-19 and their SARS-CoV-2-presumed-negative household contacts prospectively provide twice-daily saliva samples. We are quantifying absolute SARS-CoV-2 RNA viral load from these saliva samples using RT-qPCR and RT digital droplet PCR (RT-ddPCR) assays. This article documents preliminary results from the study, with the complete SARS-Cov-2 viral load profiles from two cases of observed household transmission.

METHODS

Participant Population

This study was reviewed and approved by the Institutional Review Board of the California Institute of Technology, protocol #20-1026. All participants provided written informed consent prior to participation. Individuals ages 6 and older were eligible for participation if they lived within the jurisdiction of a partnering public health department and were recently (within 7 days) diagnosed with COVID-19 by a CLIA laboratory test or were currently living in a shared residence with at least one person who was recently (within 7 days) diagnosed with COVID-19 by a CLIA laboratory test. The exclusion criteria for the study included physical or cognitive impairments that would affect the ability to provide informed consent, or to safely self-collect and return samples. In addition, participants must not have been hospitalized, and they must be fluent in either Spanish or English. Individuals without laboratory confirmed COVID-19 but with symptoms of respiratory illness in the 14 days preceding screening for enrollment were not eligible. Study data were collected and managed using REDCap (Research Electronic Data Capture) hosted at the California Institute of Technology.

Symptom Monitoring

Participants in the study completed a questionnaire upon enrollment to provide information on demographics, health factors, COVID-19 diagnosis history, COVID-19-like symptoms since February 2020, household infection-control practices and perceptions of COVID-19 risk. Additionally, participants recorded any COVID-19-like symptoms (as defined by the U.S. Centers

for Disease Control²⁰) that they were experiencing on a symptom-tracking card at least once per day. Participants also filled out an additional questionnaire at the conclusion of the study to document behaviors and interactions with household members during their enrollment.

Collection of Respiratory Specimens

Participants self-collected saliva samples using the Spectrum SDNA-1000 Saliva Collection Kit (Spectrum Solutions LLC, Draper, UT, USA) at home twice per day (after waking up and before going to bed), following the manufacturer's guidelines. Participants were instructed not to eat, drink, smoke, brush their teeth, use mouthwash, or chew gum for at least 30 min prior to donating. These tubes were labelled and packaged by the participants and transported at room temperature by a medical courier to the California Institute of Technology daily for analysis.

Nucleic Acid Extraction

An aliquot of 400 μL from each saliva sample in Spectrum buffer was manually extracted using the MagMAX Viral/Pathogen Nucleic Acid Isolation Extraction Kit (Cat. A42352, Thermo Fisher Scientific) and eluted in 100 μL . Positive extraction controls and negative extraction controls were included in every extraction batch: Positive extraction controls were prepared by combining 200 μL commercial pooled human saliva (Cat. 991-05-P, Lee Bioscience) with 200 μL SARS-CoV-2 heat inactivated particles (Cat. NR-52286, BEI Resources) at a concentration equivalent to 7500 genomic equivalent units/mL, mixed with the buffer from the Spectrum SDNA-1000 Saliva Collection Device. Negative extraction controls were prepared by combining 200 μL commercial pooled human saliva and 200 μL Spectrum buffer. Spectrum buffer contained components that inactivate the virus and stabilize the RNA, facilitating the study.

Quantification of Viral Load by RT-qPCR

An aliquot of 5 μL of eluent was input into duplicate 20 μL RT-qPCR reactions (Cat. A15299, TaqPath 1-Step RT-qPCR Master Mix, CG) with multiplex primers and probes from Integrated DNA Technologies (Coralville, IA, USA) targeting SARS-CoV-2 N1 (Cat. 10006821, 10006822, 10006823) and N2 (Cat. 10006824, 10006825, 10007050), and human RNase P (Cat. 10006827, 10006828, 10007061). Positive and negative reaction controls were included on every plate: Templates for positive control reactions contained 4 copies per μL of SARS-CoV-2 genomic

RNA from nCoV 2019-nCoV/USA-WA1/2020 (Cat. NR-52281, BEI) in 5 μ L of nuclease-free water (Cat. AM9932, ThermoFisher Scientific), and negative reaction controls contained only nuclease-free water. Reactions were run on a CFX96 Real-time PCR System (Bio-Rad Laboratories) according to the amplification protocol defined in the CDC 2019-Novel Coronavirus (2019-nCoV) Real-Time RT-PCR Diagnostic Panel, with Ct determination by auto-thresholding each target channel. Ct values were converted to viral load relative to the resulting value of known input of SARS-CoV-2 heat-inactivated particles in the positive extraction control. The conversion was done across all qPCR samples, using the average Ct values of the positive control for the two SARS-CoV-2 gene targets (N1 and N2; each 32.50 and N=11) after auto-thresholding on cycles 10-45.

Quantification of Viral Load by RT-ddPCR

An aliquot of 5.5 μ L from a dilution of the eluent (samples were diluted to be within the range required for ddPCR) was input into 22 μ L reactions of the Bio-Rad SARS-CoV-2 ddPCR Kit (Cat. 12013743, BioRad Laboratories) for multiplex quantification of SARS-CoV-2 N1 and N2 targets, and human RNase P targets. Droplets were generated on a QX200 droplet generator (#1864002, Bio-Rad Laboratories) and measured using a QX200 Droplet Digital PCR System (#1864001, Bio-Rad Laboratories), with analysis using QuantaSoft Analysis Software.

Conversion of Ct Values to Viral Load

RT-qPCR Ct values from our assay were converted to viral load (copies/mL) using the following equation:

$$Viral\ Load = 7500 * (2^{32.50-Ct})$$

Both the CLIA Laboratory and the laboratory analysis in Kissler et al.²¹ utilized similar assays to ours, and therefore we assumed this same equation could be used to estimate viral load from Ct values from those sources.

Sequencing

Extracted RNA from samples taken from the early, peak, and late infection stages of each of the three individuals infected with SARS-CoV-2 was sequenced by the Chan Zuckerberg

Biohub (San Francisco, CA, USA). All sequences, throughout infection, and across household contacts, were found to be identical.

RESULTS AND DISCUSSION

We report a case of SARS-CoV-2 transmission in a household of four individuals, who we refer to as Parent-1, Parent-2, Sibling-1, and Sibling-2 (Table B-S1). Sibling-1 (who reported recent close contact with someone infected with SARS-CoV-2) and Sibling-2 returned home together from out-of-state and were CLIA-lab RT-qPCR tested for COVID-19 the next day. The following day, Sibling-2's specimen resulted negative, and Sibling-1's specimen resulted positive, prompting Sibling-1 to isolate and all household members to quarantine. Within hours of receiving Sibling-1's positive-test result, they were enrolled in the study. Parent-2 remained SARS-CoV-2-negative in all samples. Parent-1 and Sibling-2 were SARS-CoV-2-negative upon enrollment and became continuously positive starting ~36 hours after enrollment. Viral sequencing determined that the SARS-CoV-2 in samples from Sibling-1, Parent-1 and Sibling-2 shared identical sequences to each other, highly supportive of household transmission.

All nucleic acid measurements from saliva samples included human RNase P target measurements (Figure 4-S2) as an indicator of sample quality to confirm that viral load dynamics were not an artifact of sample collection. RNase P Ct values were consistent across samples from each participant: during the early phase of infection (from enrollment to just beyond peak viral load, up to day 8 of enrollment), the 15 samples from Parent-1 had an average RNase P Ct value of 27.28 (± 1.12 SD), and the 15 samples from Sibling-2 had an average Ct value of 24.51 (± 1.31 SD). Also, a pattern of lower RNase P Ct values (more human material) in morning samples than evening samples is occasionally discernable, although this pattern does not appear to dominate viral load signal.

RT-qPCR and RT-ddPCR measurements of viral load from saliva samples provided by the three infected individuals (Figure 4-1) offer three insights. (i) Presymptomatic viral loads in some humans can rise over the course of days not hours, which is slower than expected.^{18,22} This slow rise increases the utility of sensitive tests (such as PCR) to enable earlier detection and isolation of infected individuals before their viral load increases to a presumably more infectious level. Sibling-2's viral load rose slowly—within PCR detection range—for 3 days until viral load

reached the limit of detection (LOD) for rapid tests. This slow rise also makes it more dangerous to assume that most persons with low viral load will not become infectious¹⁹ and therefore do not need to self-isolate: Sibling-2 produced 6 positive samples in the 10^3 - 10^5 copies/mL range presymptomatically before peaking at $\sim 10^7$ copies/mL. (ii) Peak viral load does not always rise above the LOD of rapid, low-sensitivity tests, as expected.^{18,22} Of 88 positive SARS-CoV-2 samples, only one sample was well above the LOD range of rapid tests. Furthermore, in Sibling-1, the logical source of the two infections, neither the CLIA-lab test nor our testing detected viral loads above 10^7 copies/mL during the presumed period of household transmission. (iii) The LOD of a test can affect how early in infection we can diagnose an infected person, and how consistently we can detect early-phase infections. Of the 52 positive samples from the first 10 days of the study, 33 were near or above the LOD of the more sensitive rapid test (ID NOW, as determined by the FDA) whereas only 3 were near or above the least sensitive LOD of 9.3×10^6 copies/mL (Table B-S2). Importantly, there were several days during the presymptomatic period that Parent-1 and Sibling-2 were detected by RT-qPCR, but may not have been reliably detected by many low-sensitivity tests.

The insights from this study are also supported by analysis of data by Kissler et al.,²¹ reporting longitudinal (but less frequent) testing of anterior nares and oropharyngeal swabs from individuals associated with the National Basketball Association (Figure 4-S1). In Kissler et al.²¹, viral loads rose slowly (for up to 5 days in some individuals) between the first PCR positive test to the LOD of rapid tests. Few of these samples ever reached viral loads well above the LODs of most rapid antigen tests (Table B-S2). Low-sensitivity tests have a role in the COVID-19 testing strategies, but our limited data from this study and data from Kissler et al.²¹ demonstrate clearly that for at least some individuals, low-sensitivity tests will likely be unable to reliably diagnose SARS-CoV-2 infection during the early phase of infection. Our limited data are consistent with the use of low-sensitivity tests for point-of-care confirmation of suspected COVID-19 in symptomatic individuals, as authorized by the FDA, but not for universal surveillance testing of asymptomatic individuals, as has been proposed.^{18,19,22}

Additional studies are urgently needed to address several limitations of this work. High-frequency viral load measurements from the incidence of infection must be observed in a larger, diverse pool of participants to infer the distribution of viral load profiles in human SARS-CoV-2

infection. SARS-CoV-2 lineages should be determined with viral RNA sequencing to understand differences in viral load with emerging and circulating variants. Both saliva and nasal swabs have been proposed as sample types for rapid, low-sensitivity tests; however, the LOD of these tests is better defined in nasal swabs. Our study only analyzed saliva; although saliva has been demonstrated to be a more sensitive sample type than nasopharyngeal swab by some studies,²³ other studies have arrived at the opposite conclusion.^{24,25} The details of saliva collection, sample stabilization, preanalytical handling, sample-preparation protocols, and timing of sampling may play a role in the apparent sensitivity measured in different sample types. No previous study has directly compared saliva with other sample types during the early phase of SARS-CoV-2 infection. Quantitative comparisons of multiple respiratory sample types (including nasal, oropharyngeal, and nasopharyngeal swabs) at the same time points are needed to clarify viral load profiles in different respiratory specimen types. Lastly, to understand the relationship between viral load and infectiousness, direct comparisons of RNA viral load to culturable virus titer across the entire course of infection are needed. Data to address these limitations are needed to inform optimal testing strategies to reduce SARS-CoV-2 transmission.

Understanding the kinetics of viral load from the incidence of infection and throughout the infectious period for a broad demographic will have implications on SARS-CoV-2 testing policies, including policies around travel. For example, several states require recent negative test results for out-of-state visitors prior to arrival. Although some states acknowledge the risk of false negative results by low-sensitivity tests and require PCR confirmation,^{19,26} others do not specify the type of negative test result required for arrival.²⁷ If rapid low-sensitivity tests are used, they would risk missing presymptomatic individuals before they rise to their highest (and presumably most infectious) viral load. Such false negative tests have the potential to create a costly false sense of security; individuals who may have been recently exposed and receive a negative result from a low-sensitivity test may be more likely—compared to individuals who did not get a test—to come into contact with other members of the community, including the most vulnerable populations.

All tests have value when used properly and within the right strategy, and we anticipate that these preliminary results will stimulate studies, with larger sample sizes and more SARS-CoV-2 variants, that will provide a better understanding of SARS-CoV-2 viral load in the early stages of infection and lead to the development of effective testing strategies.

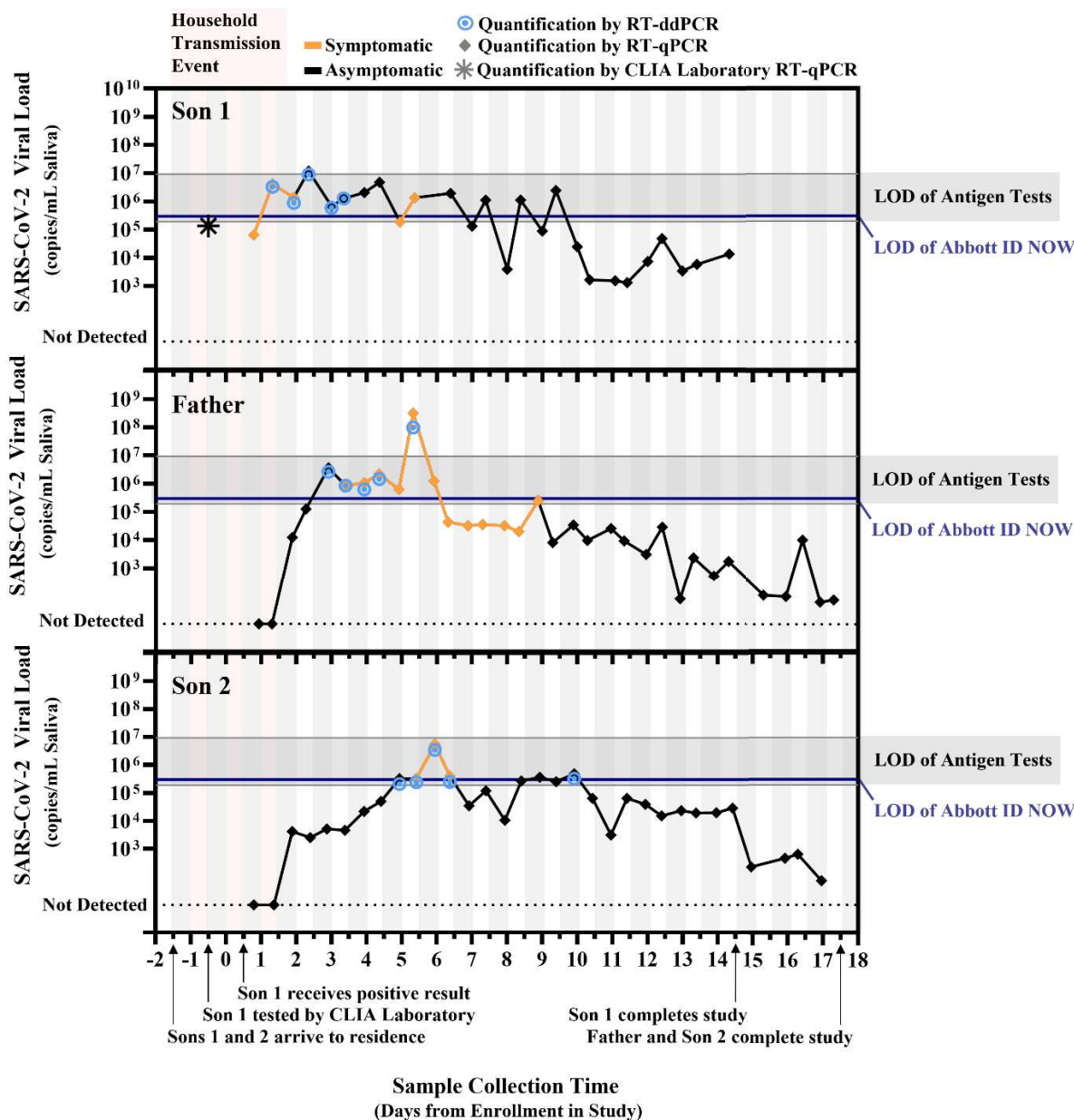


Fig B-1. Quantified SARS-CoV-2 saliva viral load after transmission between household contacts relative to detection limits of rapid tests. SARS-CoV-2 viral load over time for “Sibling-1” (the household index case), as well as “Parent-1” and “Sibling-2.” All three viral sequences were identical. Star indicates the viral load estimated from the cycle threshold (Ct) result from the commercial CLIA laboratory test used to diagnose Sibling-1. Diamonds indicate conversion from N1 target cycle threshold values obtained by RT-qPCR to SARS-CoV-2 viral load. Bullseyes indicate viral load obtained by single-molecule RT droplet digital PCR (RT-ddPCR). Black lines represent periods when participants reported no symptoms; orange lines indicate periods when participants reported at least one symptom. Vertical bars indicate the before noon (white) and after noon (grey) periods of each day. Pink shading indicates the presumed period of the household transmission events. Horizontal blue lines depict the limit of detection (LOD) of the Abbott ID NOW (3×10^5 copies/mL) for upper respiratory specimens from U.S. FDA SARS-CoV-2 Reference Panel Comparative testing data. Horizontal grey bars depict the range of LODs estimated for commercial antigen tests for upper respiratory specimens (1.90×10^5 copies/mL to 9.33×10^6 copies/mL; see Table B-S2).

DATA AVAILABILITY

Raw Ct values and calculated viral loads are available at CaltechDATA, <https://data.caltech.edu/records/1702>

COMPETING INTERESTS STATEMENT

The authors report grants from the Bill & Melinda Gates Foundation (to RFI) and the Jacobs Institute for Molecular Engineering for Medicine (to RFI), as well as a Caltech graduate fellowship (to MMC), two National Institutes of Health Biotechnology Leadership Pre-doctoral Training Program (BLP) fellowships (to MKP and JTB) from Caltech's Donna and Benjamin M. Rosen Bioengineering Center (T32GM112592), and a National Institutes of Health NIGMS Predoctoral Training Grant (GM008042) (to AW) during the course of the study. Dr. Ismagilov is a co-founder, consultant, and a director and has stock ownership and received personal fees from Talis Biomedical Corp., outside the submitted work. In addition, Dr. Ismagilov is an inventor on a series of patents licensed to Bio-Rad Laboratories Inc. in the context of ddPCR, with royalties paid.

FUNDING

This study is based on research funded in part by the Bill & Melinda Gates Foundation. The findings and conclusions contained within are those of the authors and do not necessarily reflect positions or policies of the Bill & Melinda Gates Foundation. This work was also funded by the Jacobs Institute for Molecular Engineering for Medicine. AW is supported by an NIH NIGMS Predoctoral Training Grant (GM008042); MMC is supported by a Caltech Graduate Student Fellowship; and MP and JTB are each partially supported by National Institutes of Health Biotechnology Leadership Pre-doctoral Training Program (BLP) fellowships from Caltech's Donna and Benjamin M. Rosen Bioengineering Center (T32GM112592).

ACKNOWLEDGEMENTS

We thank Lauriane Quenee, Junie Hildebrandt, Grace Fisher-Adams, RuthAnne Bevier, Chantal D'Apuzzo, Ralph Adolphs, Victor Rivera, Steve Chapman, Gary Waters, Leonard Edwards, and Shannon Yamashita for their assistance and advice on study implementation or administration. We thank Jessica Leong, Jessica Slagle, and Angel Navarro for volunteering their time to help with this study. We thank Kissler et al. for making their data publicly available to the community. We thank Maira Phelps, Lienna Chan, Lucy Li and Amy Kistler at the Chan Zuckerberg Biohub for performing SARS-CoV-2 sequencing. We thank Jennifer Fulcher, Debika

Bhattacharya and Matthew Bidwell Goetz for their ideas on potential study populations and early study design. We thank Martin Hill, Alma Sanchez, Scott Kim, Debbie Noble, Nina Paddock, Whitney Harrison, and Stu Miller for their support with recruitment. We thank Allison Rhines, Karen Heichman, and Dan Wattendorf for valuable discussion and guidance. Finally, we thank all the Pasadena Public Health Department case investigators and contact tracers for their efforts in study recruitment and their work in the pandemic response.

REFERENCES

- 1 CSSE. *COVID-19 Dashboard by the Center for Systems Science and Engineering (CSSE) at Johns Hopkins University (JHU)*, <https://gisanddata.maps.arcgis.com/apps/opsdashboard/index.html#/bda7594740fd40299423467b48e9ecf6> (2020).
- 2 Arons, M. M. *et al.* Presymptomatic SARS-CoV-2 Infections and Transmission in a Skilled Nursing Facility. *New England Journal of Medicine* **382**, 2081-2090, doi:10.1056/NEJMoa2008457 (2020).
- 3 Gandhi, M., Yokoe, D. S. & Havlir, D. V. Asymptomatic Transmission, the Achilles' Heel of Current Strategies to Control Covid-19. *New England Journal of Medicine* **382**, 2158-2160, doi:10.1056/NEJMe2009758 (2020).
- 4 Richmond, C. S., Sabin, A. P., Jobe, D. A., Lovrich, S. D. & Kenny, P. A. SARS-CoV-2 sequencing reveals rapid transmission from college student clusters resulting in morbidity and deaths in vulnerable populations. *medRxiv*, doi:10.1101/2020.10.12.20210294 (2020).
- 5 Shi, Q. *et al.* Effective control of SARS-CoV-2 transmission in Wanzhou, China. *Nature Medicine*, doi:10.1038/s41591-020-01178-5 (2020).
- 6 Wei WE *et al.* Presymptomatic Transmission of SARS-CoV-2 — Singapore, January 23–March 16, 2020. *MMWR. Morbidity and mortality weekly report* **69**, 411–415, doi:<http://dx.doi.org/10.15585/mmwr.mm6914e1> (2020).
- 7 Kimball A, Hatfield KM, Arons M & et al. Asymptomatic and Presymptomatic SARS-CoV-2 Infections in Residents of a Long-Term Care Skilled Nursing Facility — King County, Washington, March 2020. *MMWR. Morbidity and mortality weekly report* **69**, doi:<http://dx.doi.org/10.15585/mmwr.mm6913e1> (2020).
- 8 Pringle JC, Leikauskas J, Ransom-Kelley S & et al. COVID-19 in a Correctional Facility Employee Following Multiple Brief Exposures to Persons with COVID-19 — Vermont, July–August 2020. *MMWR. Morbidity and mortality weekly report* **69**, 1569–1570, doi:<http://dx.doi.org/10.15585/mmwr.mm6943e1> (2020).
- 9 Atrubin D, Wiese M & Bohinc B. An Outbreak of COVID-19 Associated with a Recreational Hockey Game — Florida, June 2020. *MMWR. Morbidity and mortality weekly report* **69**, 1492–1493, doi:<http://dx.doi.org/10.15585/mmwr.mm6941a4> (2020).

- 10 Teran RA, Ghinai I, Gretsche S & et al. COVID-19 Outbreak Among a University's Men's and Women's Soccer Teams — Chicago, Illinois, July–August 2020. *MMWR. Morbidity and mortality weekly report* **69**, 1591–1594, doi:<http://dx.doi.org/10.15585/mmwr.mm6943e5> (2020).
- 11 Lewis M, Sanchez R, Auerbach S & et al. COVID-19 Outbreak Among College Students After a Spring Break Trip to Mexico — Austin, Texas, March 26–April 5, 2020. *MMWR. Morbidity and mortality weekly report* **69**, 830–835, doi:<http://dx.doi.org/10.15585/mmwr.mm6926e1> (2020).
- 12 Pray IW, Gibbons-Burgener SN, Rosenberg AZ & et al. COVID-19 Outbreak at an Overnight Summer School Retreat — Wisconsin, July–August 2020. *MMR Morbidity and mortality weekly report* **69**, 1600–1604, doi:<http://dx.doi.org/10.15585/mmwr.mm6943a4> (2020).
- 13 Dora AV, Winnett A, Jatt LP & et al. Universal and Serial Laboratory Testing for SARS-CoV-2 at a Long-Term Care Skilled Nursing Facility for Veterans — Los Angeles, California, 2020. *MMWR. Morbidity and mortality weekly report* **69**, 651–655, doi:<http://dx.doi.org/10.15585/mmwr.mm6921e1> (2020).
- 14 CDC. Investigating a COVID-19 Case. (2020). <https://www.cdc.gov/coronavirus/2019-ncov/php/contact-tracing/contact-tracing-plan/investigating-covid-19-case.html>
- 15 FDA. *Emergency Use Authorization (EUA) information, and list of all current EUAs*, <https://www.fda.gov/emergency-preparedness-and-response/mcm-legal-regulatory-and-policy-framework/emergency-use-authorization#2019-ncov> (2020).
- 16 Smithgall, M. C., Scherberkova, I., Whittier, S. & Green, D. A. Comparison of Cepheid Xpert Xpress and Abbott ID Now to Roche cobas for the Rapid Detection of SARS-CoV-2. *Journal of Clinical Virology* **128**, 104428, doi:<https://doi.org/10.1016/j.jcv.2020.104428> (2020).
- 17 Torres, I., Poujois, S., Albert, E., Colomina, J. & Navarro, D. Real-life evaluation of a rapid antigen test (Panbio COVID-19 Ag Rapid Test Device) for SARS-CoV-2 detection in asymptomatic close contacts of COVID-19 patients. *medRxiv*, doi:10.1101/2020.12.01.20241562 (2020).
- 18 Mina, M. J., Parker, R. & Larremore, D. B. Rethinking Covid-19 Test Sensitivity — A Strategy for Containment. *New England Journal of Medicine*, doi:10.1056/NEJMp2025631 (2020).
- 19 New York Times. *Thinking of Traveling in the U.S.? Check Which States Have Travel Restrictions*, <https://www.nytimes.com/2020/07/10/travel/state-travel-restrictions.html> (2020).
- 20 CDC. Symptoms of Coronavirus. https://www.cdc.gov/coronavirus/2019-ncov/symptoms-testing/symptoms.html?CDC_AA_refVal (2020).
- 21 Kissler, S. M. *et al.* Viral dynamics of SARS-CoV-2 infection and the predictive value of repeat testing. *medRxiv*, 2020.2010.2021.20217042, doi:10.1101/2020.10.21.20217042 (2020).

- 22 Larremore, D. B. *et al.* Test sensitivity is secondary to frequency and turnaround time for COVID-19 screening. *Science Advances*, eabd5393, doi:10.1126/sciadv.abd5393 (2020).
- 23 Wyllie, A. L. *et al.* Saliva or Nasopharyngeal Swab Specimens for Detection of SARS-CoV-2. *New England Journal of Medicine* **383**, 1283-1286, doi:10.1056/NEJMc2016359 (2020).
- 24 Schwob, J. M. *et al.* Antigen rapid tests, nasopharyngeal PCR and saliva PCR to detect SARS-CoV-2: a prospective comparative clinical trial. *medRxiv*, 2020.2011.2023.20237057, doi:10.1101/2020.11.23.20237057 (2020).
- 25 Becker, D. *et al.* Saliva is less sensitive than nasopharyngeal swabs for COVID-19 detection in the community setting. *medRxiv*, doi:10.1101/2020.05.11.20092338 (2020).
- 26 Mass.gov. *Information on the Outbreak of Coronavirus Disease 2019 (COVID-19) : COVID-19 Travel Order*, <https://www.mass.gov/info-details/covid-19-travel-order> (2020).
- 27 DC Health. *Coronavirus (COVID-19) Situational Update: Thursday, Nov. 5, 2020*. https://coronavirus.dc.gov/sites/default/files/dc/sites/coronavirus/release_content/attachments/Situational-Update-Presentation_11-05-20.pdf (2020).

SUPPLEMENTAL INFORMATION

Table B-S1. Pertinent Demographic and Health Information for Study Participants.

	Household Members			
	Parent-1	Parent-2	Sibling-1	Sibling-2
Age Range (Years)	50-60	50-60	18-25	18-25
Race, Ethnicity	White, Non-Hispanic	White, Non-Hispanic	White, Non-Hispanic	White, Non-Hispanic
Self-Described Health Status	“Excellent”	“Excellent”	“Excellent”	“Excellent”
Reported Medical Conditions	None	None	None	None

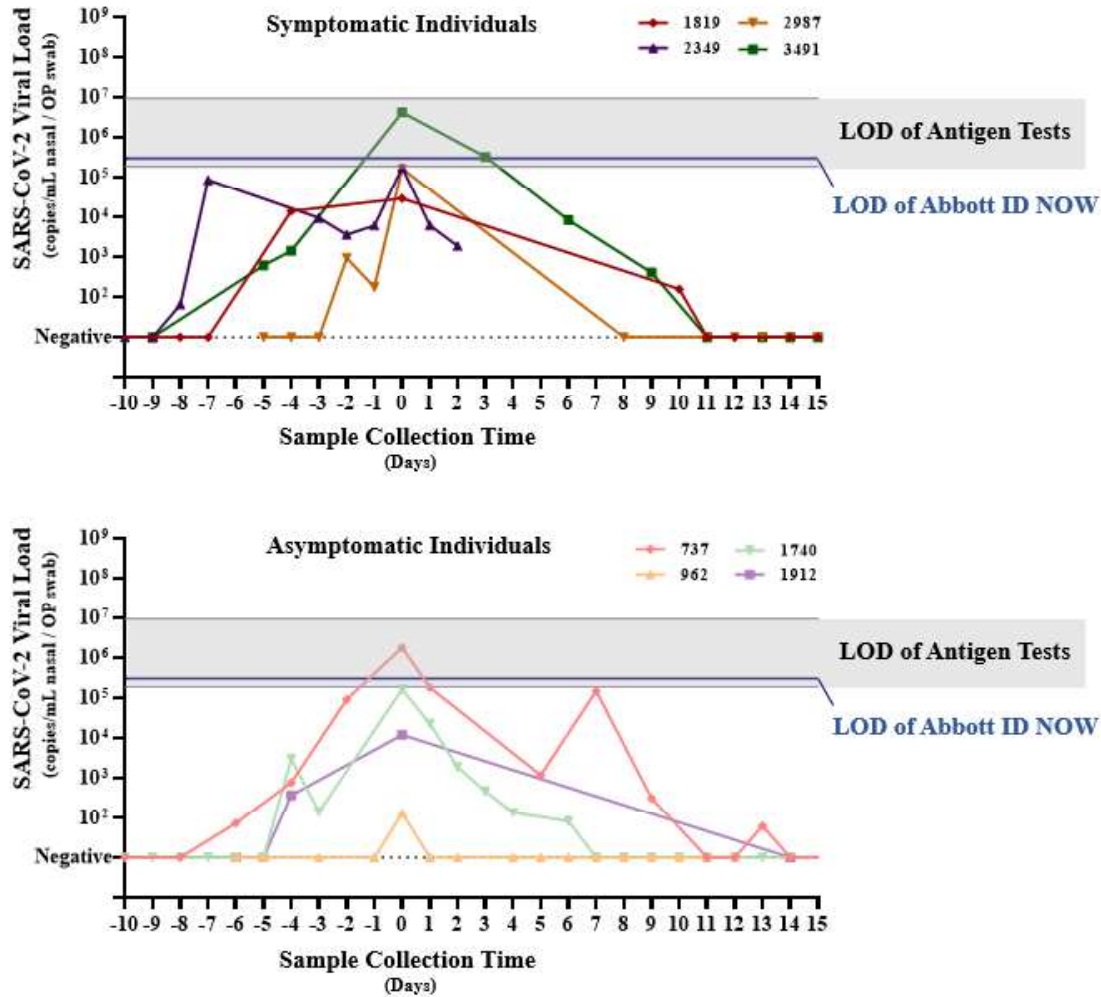


Fig B-S1. Re-analysis of Select Data from Kissler et al. (2020).¹ Cycle threshold values from the eight individuals who had at least 3 measurements from anterior nares and oropharyngeal (OP) swabs during the pre-peak period of infection were converted to viral load and replotted. Viral loads are plotted with peak viral load assigned to Day 0. A) Viral load profiles of individuals who became symptomatic and B) Viral load profiles of individuals who did not report symptoms. Horizontal blue line on each plot depicts the limit of detection (LOD) of Abbott ID NOW (3×10^5 copies/mL from U.S. FDA SARS-CoV-2 Reference Panel Comparative testing data).² Horizontal grey bar depicts the range of LODs for commercial antigen tests (1.90×10^5 copies/mL to 9.33×10^6 copies/mL; see Table B-S2).

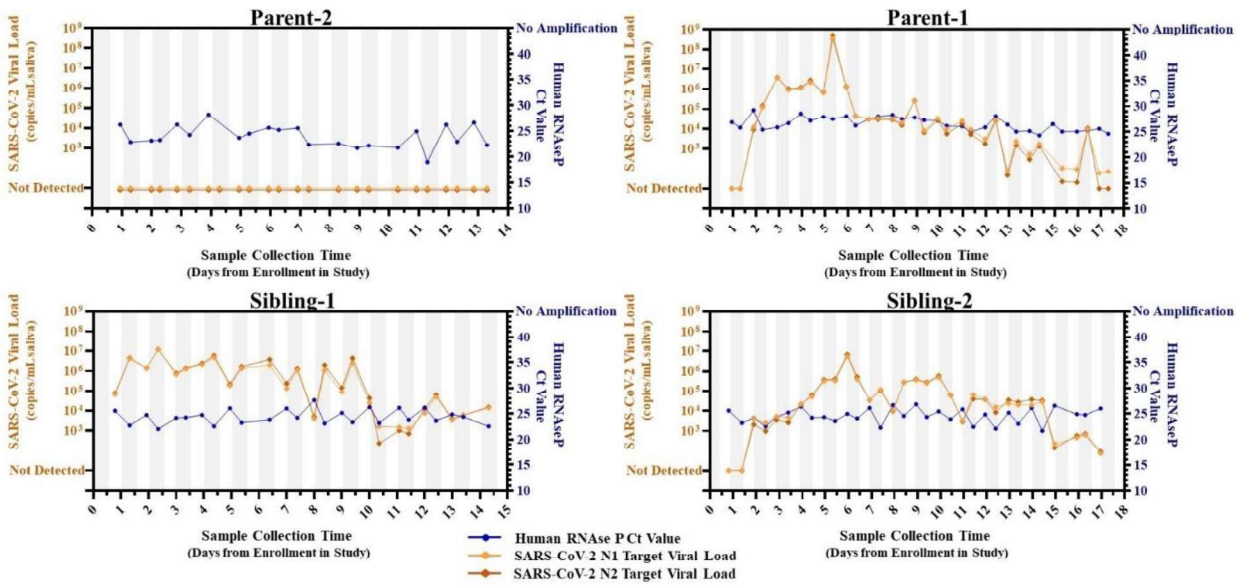


Fig B-S2. Human RNase P Ct values and SARS-CoV-2 viral load measurements from RT-qPCR for all household contacts.

Table B-S2. Summary of Reported Limits of Detection (LOD) for Rapid Point of Care SARS-CoV-2 Antigen Tests. Information on limit of detection was collected from instructions for use (IFU) and from published literature that reported LOD in units of copies/mL or could be unambiguously converted to copies/mL.

<u>Company</u>	<u>Product</u>	<u>Limit of Detection (copies/mL)</u>	<u>Reference</u>	<u>Explanation</u>
Quidel	Sofia SARS Antigen FIA	6.0x10 ⁶	Arnaout et al. ³	Estimated from US FDA Emergency Use Authorization Instructions For Use
		1.36x10 ⁶		In the US FDA Emergency Use Authorization Instructions For Use, the Limit of Detection is reported as Tissue Culture Infectious Dose 50 (TCID50). Pollack et al. determine a conversion from TCID50 per volume to mass of antigen, and mass of antigen per volume to RNA copies per volume.
BD	Veritor™ Plus System for rapid COVID-19 (SARS-CoV-2) Test	8.07x10 ⁵	Pollack et al. ⁴	
Lumira Dx	COVID-19 SARS-CoV-2 Antigen Test	1.9x10 ⁵	Instructions for Use ⁵	Estimated from US FDA Emergency Use Authorization Instructions For Use. The Limit of Detection is reported as TCID50 per volume. The lot of virus from BEI that was used for testing is reported in the IFU, and the certificate of analysis for that lot provides conversion from the TCID50 value to RNA copies per volume.
Abbott	PANBIO™ COVID-19 Ag Rapid Test Device	7.94x10 ⁵	Albert et al. ⁶	Albert et al report the results of samples tested by RT-qPCR (converted to viral load) and the stated POC antigen test to define the Limit of Detection.
		3.55x10 ⁶	Corman et al. ⁷	Corman et al. report the results of samples tested by RT-qPCR (converted to viral load) and the stated POC antigen test to define the Limit of Detection. Two tests with particularly poor analytical limit of detection (RapidGEN Biocredit COVID-19 Ag Test, LOD = 1.58x10 ¹⁰ and Coris Bioconcept COVID 19 Ag Respi-Strip, LOD=2.88x10 ⁷) were excluded from this table as not representative.

Supplemental References

- 1 Kissler, S. M. *et al.* Viral dynamics of SARS-CoV-2 infection and the predictive value of repeat testing. *medRxiv*, 2020.2010.2021.20217042, doi:10.1101/2020.10.21.20217042 (2020).
- 2 FDA. SARS-CoV-2 Reference Panel Comparative Data. <https://www.fda.gov/medical-devices/coronavirus-covid-19-and-medical-devices/sars-cov-2-reference-panel-comparative-data> (2020).
- 3 Arnaout, R. *et al.* SARS-CoV2 Testing: The limit of detection matters. *bioRxiv*, doi:10.1101/2020.06.02.131144 (2020).
- 4 Pollock, N. R. *et al.* Correlation of SARS-CoV-2 nucleocapsid antigen and RNA concentrations in nasopharyngeal samples from children and adults using an ultrasensitive and quantitative antigen assay. *medRxiv*, 2020.2011.2010.20227371, doi:10.1101/2020.11.10.20227371 (2020).
- 5 FDA. LumiraDx: SARS-CoV-2 Ag Test (Instructions for Use). <https://www.fda.gov/media/141304/download> (2020).
- 6 Torres, I., Poujois, S., Albert, E., Colomina, J. & Navarro, D. Real-life evaluation of a rapid antigen test (Panbio COVID-19 Ag Rapid Test Device) for SARS-CoV-2 detection in asymptomatic close contacts of COVID-19 patients. *medRxiv*, 2020.2012.2001.20241562, doi:10.1101/2020.12.01.20241562 (2020).
- 7 Corman, V. M. *et al.* Comparison of seven commercial SARS-CoV-2 rapid point-of-care antigen tests. *medRxiv*, 2020.2011.2012.20230292, doi:10.1101/2020.11.12.20230292 (2020).

APPENDIX C: ABBREVIATIONS

aAST	accessibility AST
ABX	antibiotic, antibiotics
AST	antimicrobial susceptibility test/testing, antibiotic susceptibility test/testing
AHF	AIDS Healthcare Foundation
AIDS	acquired immunodeficiency syndrome
AMP	ampicillin (antibiotic)
AR	antibiotic resistant, antibiotic resistance
AUC	area under the curve
BAC	benzalkonium chloride (cationic surfactant)
BIL	bilirubin (urinalysis)
BLO	blood (urinalysis)
CaCl ₂	calcium chloride
Cat	catalog
CDC	Centers for Disease Control and Prevention
CHAPS	3-[(3-Cholamidopropyl)dimethylammonio]-1-propanesulfonate hydrate (zwitterionic surfactant)
CIP	ciprofloxacin (antibiotic)
CLSI	Clinical and Laboratory Standards Institute
CFM	cefixime (antibiotic)
CFM-S	cefixime-susceptible
CFM-R	cefixime-resistant
CFU	colony-forming unit
CLIA	Clinical Laboratory Improvement Amendments
CML	clinical microbiology laboratory
COVID-19	coronavirus disease 2019

cp/ μ L	copies/microliter (concentration)
cp/mL	copies/milliliter (concentration)
Cq	quantification cycle (qPCR), same as Ct
CRE	carbapenem-resistant Enterobacteriaceae
CRO	ceftriaxone (antibiotic)
CRO-S	ceftriaxone-susceptible
CRO-R	ceftriaxone-resistant
Ct	cycle threshold (qPCR), same as Cq
Da	dalton (unit of mass)
dLAMP	digital loop-mediated isothermal amplification, digital LAMP
DMSO	dimethyl sulfoxide
DNA	deoxyribonucleic acid
DNase	deoxyribonuclease
DNO	no evidence of degradation
dPCR	digital polymerase chain reaction, digital PCR (ddPCR is droplet digital PCR)
<i>Ec</i>	<i>Escherichia coli</i>
ECDF	empirical cumulative distribution function
<i>Ebs</i>	<i>Enterobacter spp. (E. aerogenes, E. cloacae)</i>
ETP	ertapenem (antibiotic)
ETP-S	ertapenem-susceptible
EUA	emergency use authorization
EUCAST	European Committee on Antimicrobial Susceptibility Testing
FDA	U.S. Food and Drug Administration
FPR	false positive rate
GCE/mL	genome/genomic copies equivalent per milliliter (concentration)
gDNA	genomic DNA
GLU	glucose (urinalysis)
GWM	Graver-Wade Medium
HLB	hydrophilic-lipophilic balance

hr,h	hour (unit of time)
ID	identification
IFU	instructions for use
IRB	Institutional Review Board
kDa	kilodalton (unit of mass)
KET	ketone (urinalysis)
<i>Kp</i>	<i>Klebsiella pneumoniae</i>
LAMP	loop-mediated isothermal amplification
LEU	leukocyte esterase (urinalysis)
LOD	limit of detection, limits of detection
MATLAB	matrix laboratory (programming language)
MERS-CoV	Middle East Respiratory Syndrome Coronavirus
MEM	meropenem (antibiotic)
MHB	Meuller Hinton II Broth
mg/mL	milligram per milliliter (concentration)
MIC	minimum inhibitory concentration
min	minute (unit of time)
mL	milliliter (unit of volume)
mOsm/kg	milliosmoles per kilogram (unit of osmotic pressure)
MTM	Modified Thayer-Martin (agar)
n	number
NA	nucleic acid
NAAT	nucleic acid amplification test(s)
NDU/mL	nucleic acid detectable units per milliliter (concentration)
NaHCO ₃	sodium bicarbonate
NF-H ₂ O	nuclease-free water
NG, Ng	<i>Neisseria gonorrhoeae</i>
NIT	nitrite (urinalysis)
nM	nanomolar (concentration)
NR	not-resistant [to antibiotic]

nuc-aAST	nuclease-accessibility AST
OM	outer membrane
PCR	polymerase chain reaction
PEN	penicillin (antibiotic)
PEN-R	penicillin-resistant
PEN-S	penicillin-susceptible
PG	peptidoglycan
POC	point of care
pol-aAST	polymerase-accessibility AST
PPHD	Pasadena Public Health Department
PRO	protein (urinalysis)
QC	quality control
R	resistant [to antibiotic]
REDCap	Research Electronic Data Capture (software)
RFU	Relative Fluorescence Units
RNA	ribonucleic acid
RNase P	Ribonuclease P (human gene)
ROC	receiver operating characteristic
ROI	region of interest
RT	reverse-transcription, reverse transcriptase
RT-ddPCR	reverse transcription droplet digital PCR
RT-qPCR	quantitative reverse transcription PCR
RT-PCR	reverse-transcription PCR
S	susceptible [to antibiotic]
SARS-CoV-2	severe acute respiratory syndrome coronavirus 2
SD	standard deviation
sec	second(s) (unit of time)
SEM	standard error of the mean
SDS	sodium dodecyl sulfate (anionic surfactant)
SG	specific gravity (urinalysis)

SOP	standard operating procedure
STI	sexually transmitted infection
T	temperature
TNP	tergitol-NP (surfactant)
TPR	true positive rate
Tris	Tris(Hydroxymethyl)aminomethane
TTP	time-to-positive
TTPD	time-to-positive difference
TTPD _{CT}	time-to-positive difference between control and treated
TTPD _{LT}	time-to-positive difference between fully lysed and treated
UCLA	University of California, Los Angeles
USC	University of Southern California
μg/mL	microgram per milliliter (concentration)
μL	microliter (unit of volume)
μM	micromolar (concentration)
UTI	urinary tract infection
qLAMP	quantitative loop-mediated isothermal amplification, quantitative LAMP, real-time LAMP
WHO	World Health Organization